SULFUR NITROGEN HETEROCYCLES AS CHARGE TRANSFER MATERIALS

by

KATHRYN ELVIA PREUSS

A thesis

presented to the University of Waterloo

in fulfillment of the

thesis requirement for the degree of

Doctor of Philosophy

in

Chemistry

Waterloo, Ontario, Canada, 2000

The University of Waterloo requires the signatures of all persons using or photocopying this thesis. Please sign below, and give address and date.

ABSTRACT

SULFUR NITROGEN HETEROCYCLES AS

CHARGE TRANSFER MATERIALS

Kathryn Elvia Preuss

University of Waterloo, 2000

Supervisor:

Prof. Richard T. Oakley

A variety of compounds based on either 1,5,2,4,6,8-dithiatetrazocine or 1,2,3-dithiazolyl have been prepared, isolated, and characterized by single crystal X-ray crystallography. Where appropriate, the redox properties of these materials have been studied by cyclic voltammetry and the conductivities and magnetic susceptibilities have been measured. Those compounds with an open shell ground state have been further characterized by electron paramagnetic resonance. Theoretical investigations of several species have been carried out using density functional theory (B3LYP) computational methods on a 6-31G** basis set. The results have been interpreted in the context of designing novel charge transfer acceptors, charge transfer donors, and neutral radical conductors.

Although hydroquinone-like 3,7-diaryl-1,5,2,4,6,8-dithiatetrazocine derivatives can be prepared and isolated, chemical oxidation does not generate a species in which there is a quinone-like bond length alternation. For example, the reaction of 3,7-bis(2-bromothiophene)-1,5,2,4,6,8-dithiatetrazocine with tetracyanoethylene oxide oxidizes only one of the two thienyl groups. The crystal structure of the product 3-(2-bromothiophene)-7-(2,3-bis(dicyanomethylene)thiophene)-1,5,2,4,6,8-dithiatetrazocine has been determined. The experimental results militate against the use of 1,5,2,4,6,8-dithiatetrazocine derivatives as charge transfer acceptors.

When two 1,2,3-dithiazoles are ring-fused to a central phenyl ring such that the nitrogens of the two heterocycles are *para*- to one another, a stable radical cation oxidation state can be isolated. Charge transfer salts with 1:1, 2:1, and 3:2 cation-to-anion stoichiometric ratios have been characterized by X-ray crystallography. While the 1:1 and 2:1 salts show relatively low conductivities ($\sigma \approx 10^{-5}$ S cm^{-1}), the conductivities measured for the 3:2 salts are significantly higher ($\sigma \approx 10^{-2}$ - 10 S cm^{-1}).

The ring-fused benzo-bis(1,2,3-dithiazole) in which the nitrogens of the two heterocycles are *meta*- to one another also has an accessible, stable radical cation oxidation state. The pyridine analog of this species, however, has a remarkably high proton affinity, complicating the isolation of the free base and its oxidized radical cation. When protonated, the closed shell cation salt can be easily isolated. The crystal structure of 4-chloro-1-imidopyridine[2,3-*d*:6,5-*d*']-bis(1,2,3-dithiazolylium) hexafluoroantimonate has been determined. Cyclic voltammetry studies show that the stable neutral radical oxidation state of this species is accessible by electroreduction. Upon further electroreduction to the radical anion, proton shifting occurs. The narrow electrochemical window between the anion/neutral redox pair and the neutral/cation redox pair suggests that this compound may have properties favourable for the design of a neutral radical conductor.

Bis(1,2,3-dithiazole)s need not be ring-fused to a central aryl ring. Several compounds in which the two heterocycles are bridged *via* the carbon C5 have been characterized. These include three closed shell species and a species with a triplet ground state. Of the three closed shell compounds, two have stable radical cation oxidation states. Charge transfer salts of these have been characterized by X-ray diffraction. The diradical species has been isolated and identified by electron paramagnetic resonance. In addition, the analogous 4-chloro-5-(2,3,4,5,6-pentafluorophenyl)-1,2,3-dithiazolyl has been characterized by X-ray crystallography. This is the first simple 1,2,3-dithiazolyl isolated and characterized in the solid state.

ACKNOWLEDGEMENTS

There are many people that have helped, guided, and worked with me during these nearly five years, all of whom I owe a heart felt thanks. The most important of these is, of course, my advisor, Professor Richard T. Oakley. Under his supervision, I have learned a tremendous amount of technical skill and academic knowledge. His enthusiasm for the research and his friendship with his students creates a productive and enjoyable atmosphere in which scholarship and accomplishment flourish. He is both a good scientist and a good human being. Thank you very much, Rich, for all that you have taught me.

Many others have shared the lab with me over the years, making my studies that much more interesting and enjoyable. I would like to thank Dr. Rob Reed, Prof. Noel George, Prof. Craig MacKinnon, and Greg Patenaude, all of whom have moved on since I worked with them at the University of Guelph. I would also like to thank Hongzhou Zhang, Leanne Beer, Dan Myles, and James Mingie, with whom I am currently enjoying working at the University of Waterloo. The friendship and encouragement of each one was invaluable.

The members of my supervisory committee, Prof. John Goddard, Prof. Adrian Schwan, and Prof. Linda Nazar, have been kind and most helpful throughout. I am very grateful for the time they have devoted to me and the advice they have bestowed upon me over the years.

Much of the research presented within this thesis could not have been accomplished without the assistance of a number of other researchers and technicians. The groups of Prof. Robert C. Haddon and of Prof. A. Wally Cordes deserve a special thanks in this respect. Furthermore, I am indebted to Mr. Yves Savoret, without who's glass blowing skills my research would have been significantly restricted. I should also like to thank Dr. Nicolas Taylor for his friendship and tutoring in the techniques of X-ray crystallography. Finally, the technicians and

secretaries of the chemistry departments of both the University of Guelph and the University of Waterloo have proven to be not only friendly and kind, but efficient and knowledgeable. They, too, deserve thanks since nothing would get done without them.

I would especially like to thank my mother, father, and brother. Without my family, I could not have accomplished any of this.

Table of Contents

List of Captioned Figures

List of Tables

List of Uncaptioned (Numbered Only) Figures

Figures are numbered separately in each chapter. The roman numeral prefix in the figure label corresponds to the chapter in which the figure appears (*e.g.*, a figure appearing in Chapter 4 is labeled with the prefix **IV-**). Those figures that appear in more than one chapter are listed here more than once.

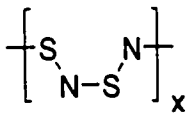

I-1

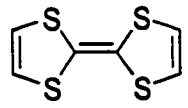

I-2

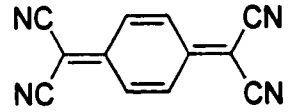

I-3

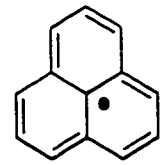

I-4

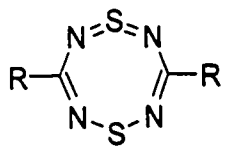

I-5

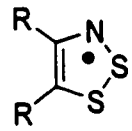

I-6

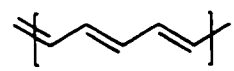

I-7

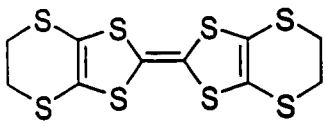

I-8

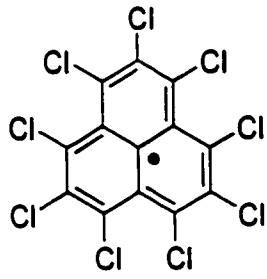

I-9

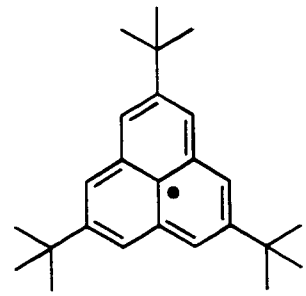

I-10

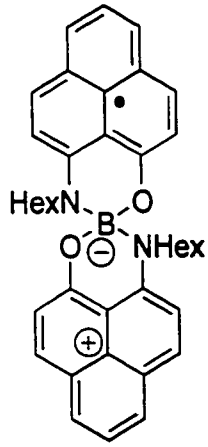

I-11

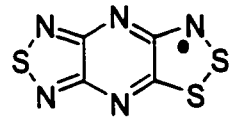

I-12

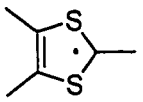

I-13

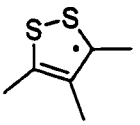

I-14

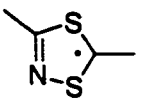

I-15

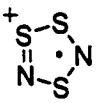

I-16

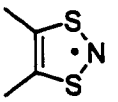

I-17

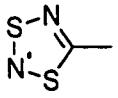

I-18

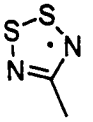

I-19

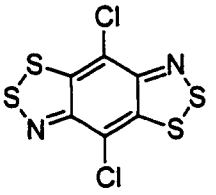

I-20

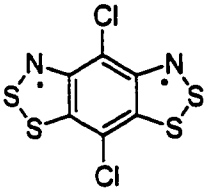

I-21

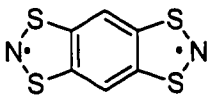

I-22

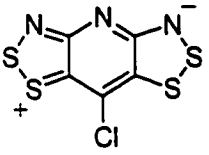

I-23

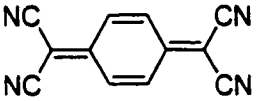

II-1

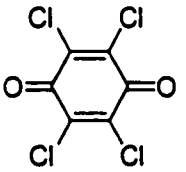

II-2

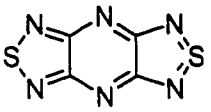

II-3

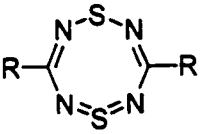

II-4

a) R = H

b) R = Ph

c) R = $N(Me)_2$

d) R = 4-CH_3O-C_6H_4

e) R = 4-$C_2H_5O(CO)$-C_6H_4

f) R = *t*-Bu

g) R =

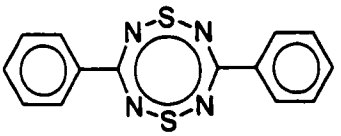

II-4b

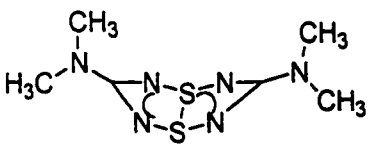

II-4c

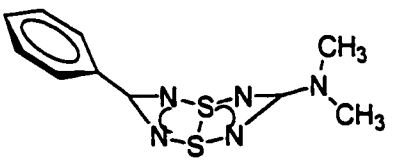

II-4h

II-5

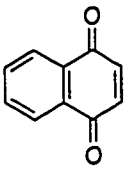

II-6

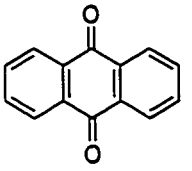

II-7

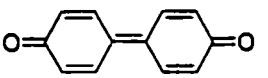

II-8

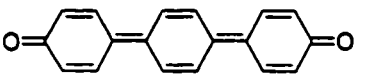

II-9

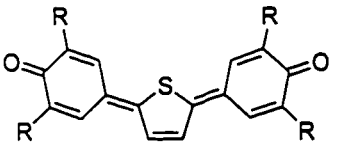

II-10

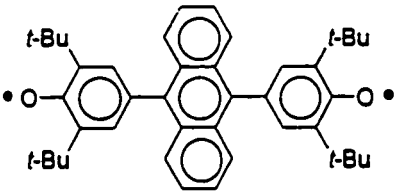

II-11

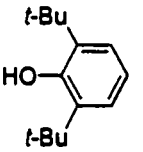

II-12

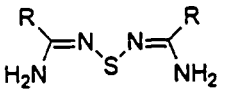

II-13

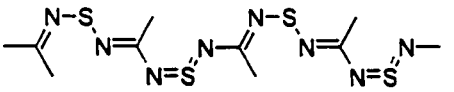

II-14

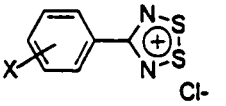

II-15

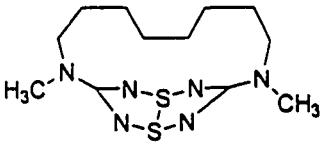

II-16

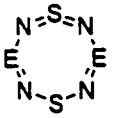

II-17

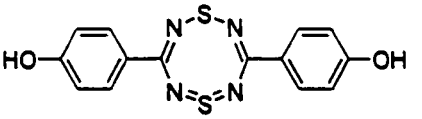

II-18

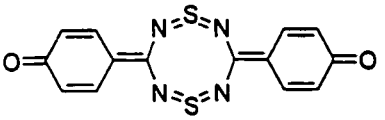

II-19

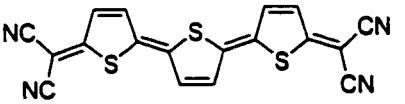

II-20

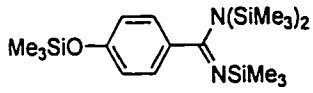

II-21

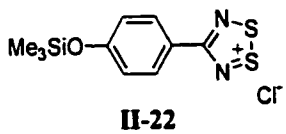

II-22

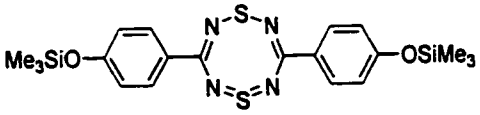

II-23

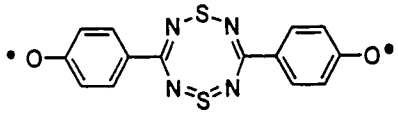

II-24

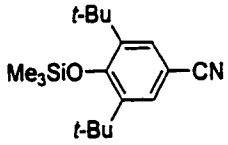

II-25

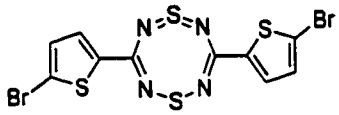

II-26

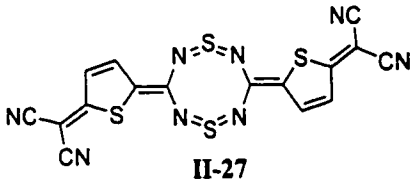

II-27

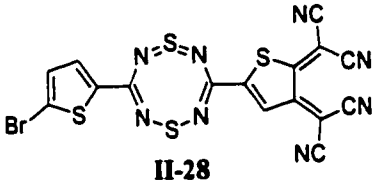

II-28

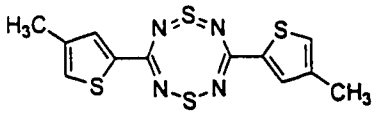

II-29

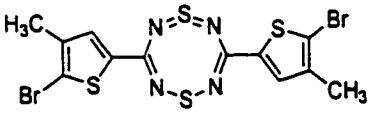

II-30

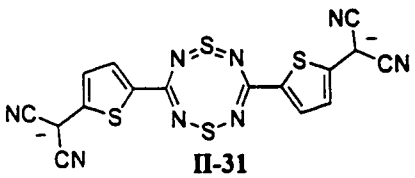

II-31

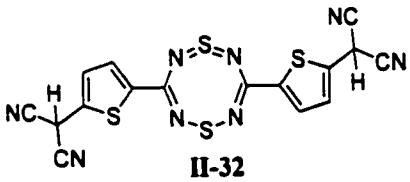

II-32

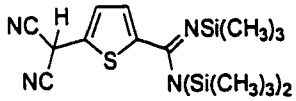

II-33

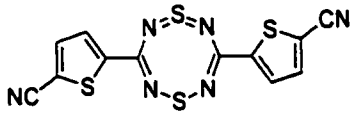

II-34

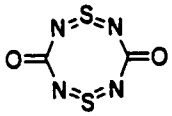

II-35

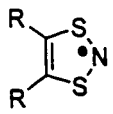

III-1
a) R = H

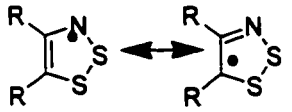

III-2
a) R = H
b) R = Cl

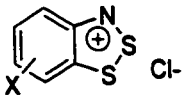

III-3

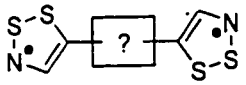

III-4a

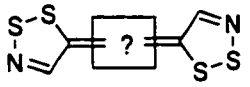

III-4b

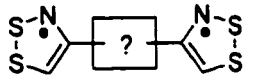

III-5

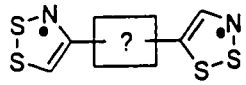

III-6a

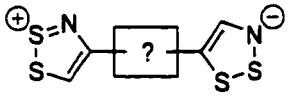

III-6b

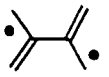

III-7

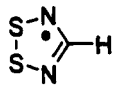

III-8

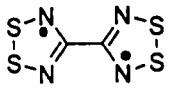

III-9

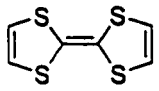

III-10

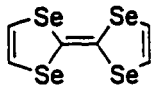

III-11

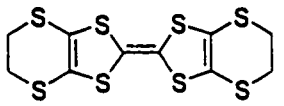

III-12

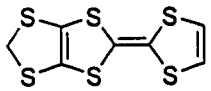

III-13

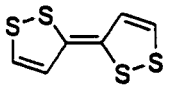

III-14

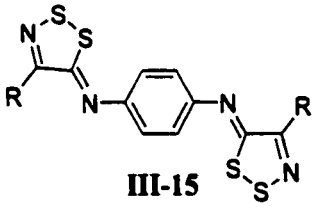

III-15
a) R = H
b) R = Cl

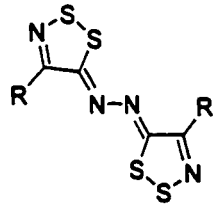

III-16
a) R = H
b) R = Cl

III-17
a) R = H
b) R = Cl

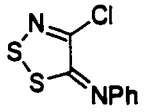

III-18

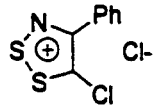

III-19

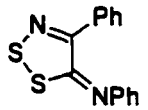

III-20

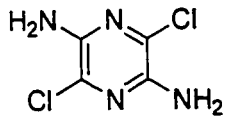

III-21

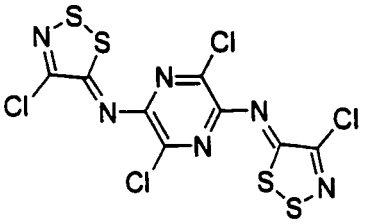

III-22

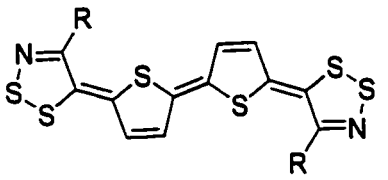

III-23

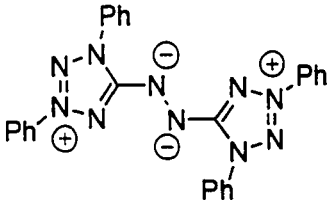

III-24

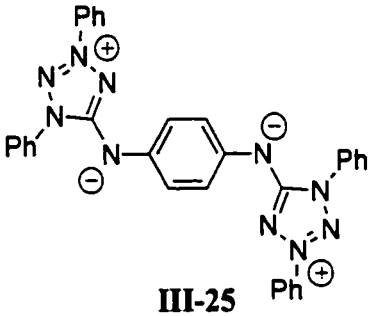

III-25

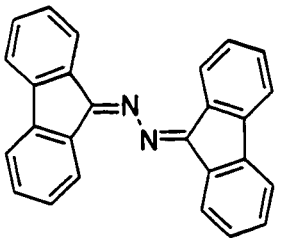

III-26

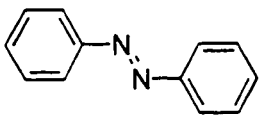

III-27

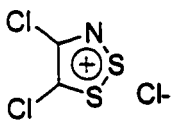

IV-1

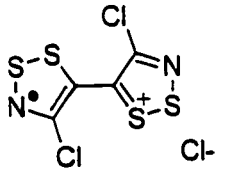

[IV-2][Cl]

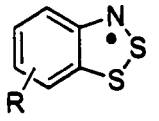

IV-3

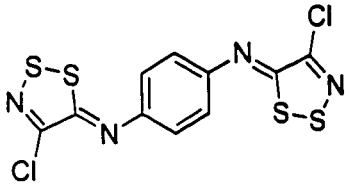

IV-4

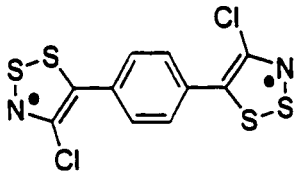

IV-5

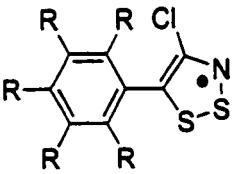

IV-6
a) R = F
b) R = H

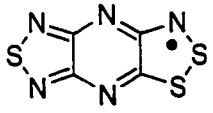

IV-7

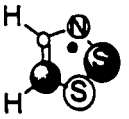

V-1

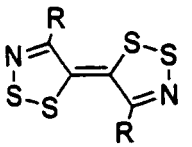

V-2, R=H
V-2a, R=Cl

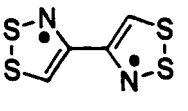

V-3

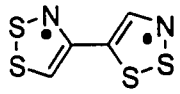

V-4a

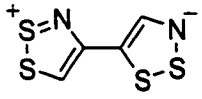

V-4b

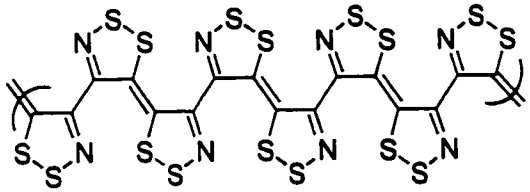

V-5

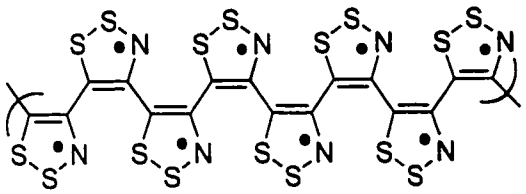

V-6a

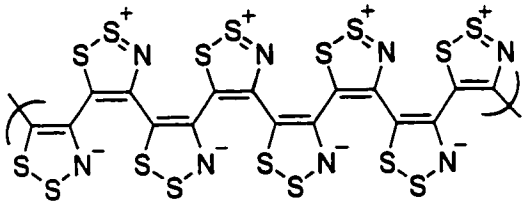

V-6b

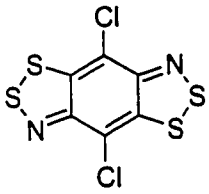

V-7

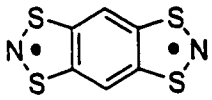

V-8

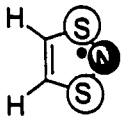

V-9

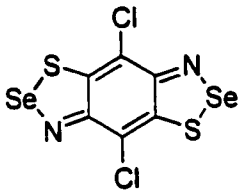

V-10

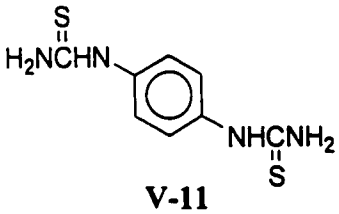

V-11

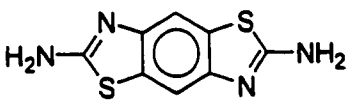

V-12

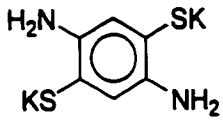

V-13

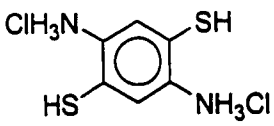

V-14

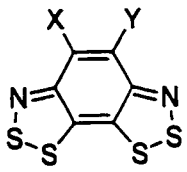

V-15

a, X = H, Y = H
b, X = H, Y = Cl
c, X = Cl Y = Cl

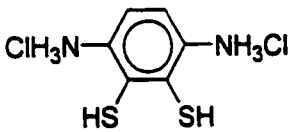

V-16

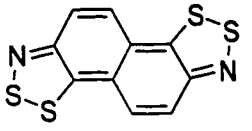

V-17

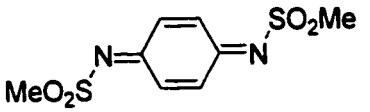

V-18

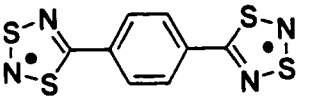

V-19

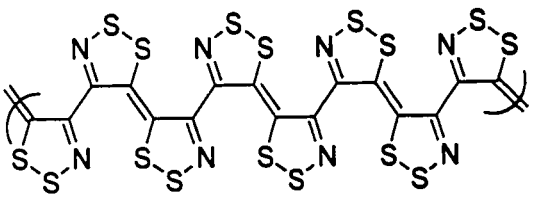

VI-1

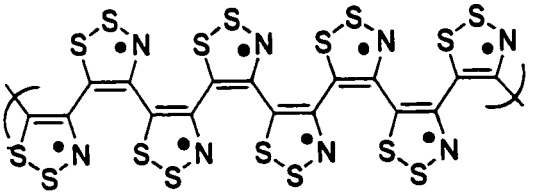

VI-2a

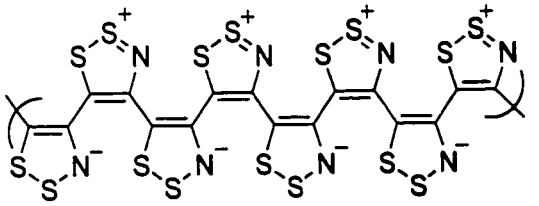

VI-2b

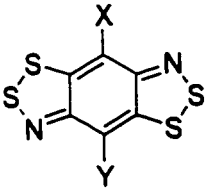

VI-3
a) X=Y=H
b) X=Cl, Y=H
c) X=Y=Cl

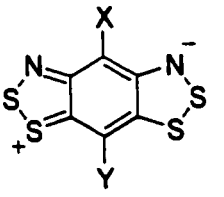

VI-4
a) X=Y=H
b) X=Cl, Y=H
c) X=Y=Cl

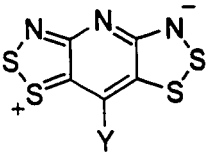

VI-5
a) Y=H
b) Y=Cl

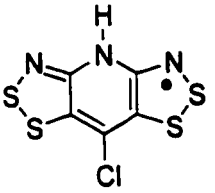

VI-6

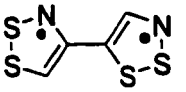

VI-7a

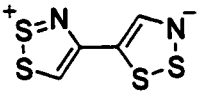

VI-7b

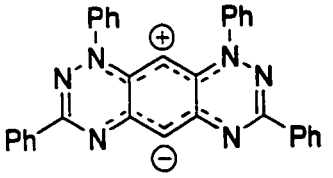

VI-8

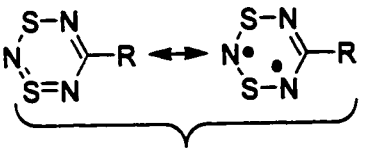

VI-9
a) R = H
b) R = Ph

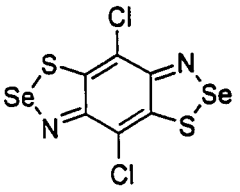

VI-10

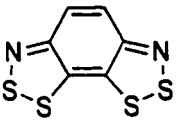

VI-11

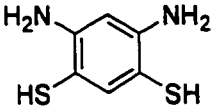

VI-12

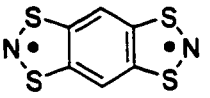

VI-13

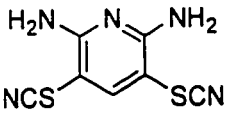

VI-14

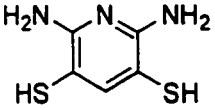

VI-15

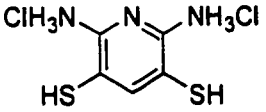

VI-16

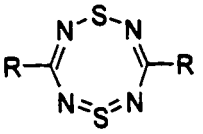

VI-17

VI-18

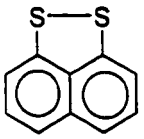

VI-19

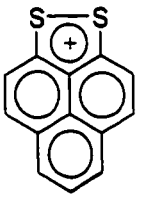

VI-20

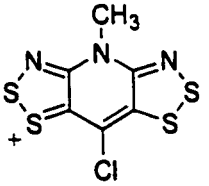

VI-21

Chapter 1 Introduction

1.1 Introduction and Scope

In the course of the last four decades, new classes of conducting materials have sparked interest within the chemistry and physics research communities. It is unlikely that traditional metallic conducting and semiconducting materials, such as copper and doped silicon, will be universally replaced by the new polymeric and molecular materials. However, many of these new compounds may find unique applications as components in low-cost data storage,[1, 2] nano-circuitry,[3] and mechanically flexible electronic devices.[4] Equally important, in the pursuit of molecular materials, is the insight gained into the nature of conduction within these new materials and the requirements necessary to successfully design a conducting polymer or molecular solid. Thus, while the majority of the materials reported may never find an appropriate application, the research provides the required knowledge base.

There is a large field of research that focuses on the design of conducting polymers. This encompasses organic materials, such as polyacetylene,[5] a variety of organometallics (*e.g.*, metallophthalocyanines[6]), and heteroatomic materials, such as $(SN)_x$ (**I-1**).[7,8,9] Discussion of these compounds throughout this thesis is limited to the case in which a specific polymer provides a good example of some conceptual point or is directly related to a particular molecular material.

Research in the area of molecular materials is equally diverse. Semiconducting and metallic materials include oligomers (*e.g.*, hexathiophene[10, 11, 12]), charge transfer (CT) salts,[13] such as the well-known tetrathiafulvalene-tetracyanoquinone[14,15,16] ([TTF][TCNQ]) pair (**I-2** and **I-3** respectively), and thin films of C_{60}.[17,18] Some of these materials, such as certain salts of C_{60},[19] have been shown to possess superconducting properties at low temperatures.

The great majority of molecular conducting materials are closed shell species that rely on electron transfer for the generation of charge carriers. There are comparatively few examples of

single-component metallic conducting molecular materials currently in existence. These were first suggested by Haddon[20] in the form of the organic neutral radical **I-4**.

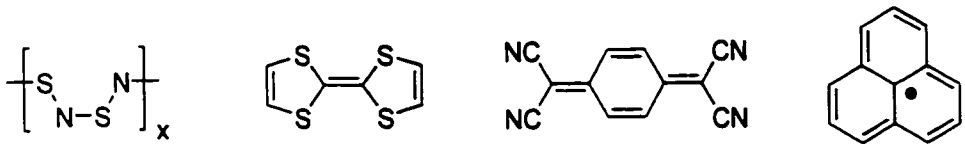

I-1 **I-2** **I-3** **I-4**

Figure 1.1 A sample of some important polymeric and molecular conductors.

The scope of this thesis comprises the synthesis and characterization of a number of sulfur- and nitrogen-containing (SN) heterocycles designed to have a potential use as molecular conductors. This chapter serves as a general introduction to the research presented throughout this thesis and provides the background necessary for the understanding of the various projects in terms of their relevance and importance in the study of molecular conductors. In the second chapter, a variety of compounds containing the 1,5,2,4,6,8-dithiatetrazocine ring (**I-5**) are presented with the intent of determining their applicability as an acceptor material in CT salts. The results were largely discouraging, consequently Chapter 2 can be set apart, somewhat, from the remainder of the work presented herein. The balance of the thesis (Chapters 3 to 6) focuses on materials that are based on the 1,2,3-dithiazole (DTA) heterocycle (**I-6**). A range of closed shell bridged bis(1,2,3-DTA)s is explored in Chapter 3, with the goal of designing new CT donor molecules. A neutral radical material based on an open shell bridged bis(1,2,3-DTA) is presented in Chapter 4. The key difference between the closed shell bis(1,2,3-DTA)s discussed in Chapter 3 and the open shell example introduced in Chapter 4 is the nature of the bridging ligand. Futhermore, it is shown that a simple neutral radical 1,2,3-DTA can be stablized in the solid state, given a judicious choice of substituent. Chapters 5 and 6 address bis(1,2,3-DTA)s that are fused

to a central aromatic ring. In the former, the materials have quinoid closed shell ground states with accessible radical cation oxidation states. Thus, they are considered in terms of their application as CT donors. In the latter chapter, the 1,2,3-DTA rings are fused to the central ring in such a manner as to negate a quinoid closed shell ground state. The result is the generation of compounds which possess an open shell configuration and a charge separated configuration very close in energy. Ongoing investigation of one of these materials suggests that protonation (or alkylation) of the rings leads to novel cationic systems with promising electrochemical properties. The ultimate goal of this continuing project is the creation of a new class of neutral radical conductor (NRC).

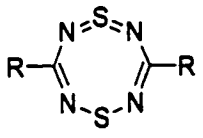

I-5

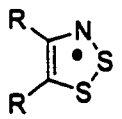

I-6

Figure 1.2 Generic 1,5,2,4,6,8-dithiatetrazocine and 1,2,3-dithiazole rings.

1.2 Overview

In the presentation of our quest for novel conducting materials, a number of key principles must be addressed. A brief discussion of band theory, from a chemist's perspective, is introduced in this chapter. Included is a band description of semiconductors, metallic conductors, Mott insulators, and charge density wave (CDW) driven distortions. This is followed by a cursory survey of notable contributions to charge transfer (CT) salts and radical ion conductors (RIC)s, uncharged open-shell molecules as neutral radical conductors (NRC)s, and a brief account of relevant sulfur-nitrogen heterocycles. Further theory appropriate to this dissertation includes some points concerning the electronic structures of diradicals and a qualitative description of the computational methods employed herein.

1.3 Principles of Band Theory

In order to understand band theory from a chemist's perspective, it is helpful to start from a model representative of a molecule (*i.e.*, with finite size) and then extend this to an infinite system more closely akin to an array of atoms or molecules in a crystal lattice. For further simplification, the initial model need only be one-dimensional.

Consider a particle on a ring of periodic potential, and let this potential, at every periodic point, be equivalent (*i.e.*, $V_{(\theta)} = V_{(\theta+2\pi n)}$). Let the potential between points be zero. This relatively unsophisticated model, shown in **Figure 1.3**, is a useful depiction of a carbon-based aromatic ring, wherein the particle is an electron and the periodic points of potential are atoms (*e.g.*, for benzene, $n = 6$).

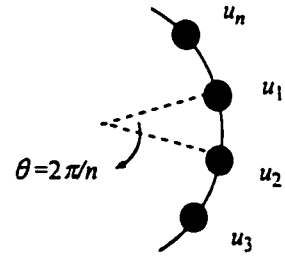

Figure 1.3 A particle on a ring of periodic potential: n is the number of potential points (atoms) on the ring, u_m is the potential at each point m, ($m = 1, 2, ..., n$).

For the system described above, the Schrödinger equation, $\mathcal{H}\Psi = E\Psi$, can be written as

$$\frac{-h^2}{8\pi^2 I}\frac{\partial^2}{\partial^2\theta}\Psi + V_{(\theta)}\Psi = E\Psi \qquad \textbf{Equation 1.1}$$

where I is the product of the mass of the particle and the square of the radius of the ring. The n-fold symmetry requires that

$$\psi_{(\theta)}^*\psi_{(\theta)} = \psi_{(\theta+2\pi n)}^*\psi_{(\theta+2\pi n)} = c^*\psi_{(\theta)}^* c\psi_{(\theta)} \qquad \textbf{Equation 1.2}$$

where c is a phase factor and $c^*c = 1$. Furthermore, because an n-fold rotation restores the system to its original state, $c^n = 1$, or

$$c = \sqrt[n]{1} = \exp(2\pi ij/n) \qquad j = (0, 1, ..., n\text{-}1) \qquad \textbf{Equation 1.3}$$

This is equivalent to saying that there are n solutions to $\sqrt[n]{1}$. For n equals 2, there are two solutions ($j = 0, 1$), or $\sqrt[2]{1} = \pm 1$.

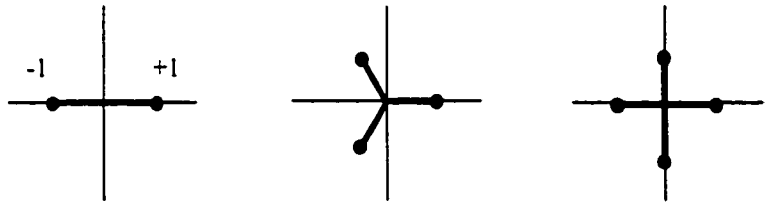

Figure 1.4 Pictorial description of results for $n = 2$, 3, and 4.

Since $\psi = (c_1u_1 + c_2u_2 + ...)$, the general solution for the wavefunction ψ_j is given by

$$\psi_j = \frac{1}{\sqrt{n}} \sum_{m=1}^{n} \exp\left(\frac{2\pi ijm}{n}\right) u_m \qquad \textbf{Equation 1.4}$$

Equation 1.4 is known as a Bloch function. It can be used, for example, to determine the wavefunctions of an aromatic ring such as benzene. These are pure angular momentum states (*i.e.*, moving waves), the sums and differences of which yield standing waves which are the familiar molecular orbitals of benzene (**Figure 1.5**).

To derive the energies of these normalized orbitals, it is not necessary to normalize **Equation 1.5** again.

$$E_j = \int \psi_j^* H \psi_j \, d\tau \qquad \textbf{Equation 1.5}$$

At the simple Hückel level, interactions further removed than the nearest neighbor need not be considered. Therefore only three terms in ψ_j^* are non-zero.

$$E_j = \frac{1}{n}\sum_{m=1}^{n}\left[\int\left[\exp\left(\frac{-2\pi ij(m-1)}{n}\right)\right]u_{m-1}\,H\left[\exp\left(\frac{2\pi ijm}{n}\right)\right]u_m d\tau\right. \qquad \textbf{Equation 1.6}$$
$$+ \int\left[\exp\left(\frac{-2\pi ij(m)}{n}\right)\right]u_m H\left[\exp\left(\frac{2\pi ijm}{n}\right)\right]u_m d\tau$$
$$\left. + \int\left[\exp\left(\frac{-2\pi ij(m+1)}{n}\right)\right]u_{m+1} H\left[\exp\left(\frac{2\pi ijm}{n}\right)\right]u_m d\tau\right]$$

If we define the resonance integral, β, as

$$\beta = \int u_{m-1} H u_m \, d\tau \qquad \textbf{Equation 1.7}$$
$$= \int u_{m+1} H u_m \, d\tau$$

and the coulomb parameter, α, as

$$\alpha = \int u_m H u_m \, d\tau \qquad \textbf{Equation 1.8}$$

then the energy can be rewritten as **Equation 1.9**. Thus far, the quantum number j has been defined as $j = (0, 1, ..., n\text{-}1)$. It is valuable to recognize that, within this model, the point u_m where $m = n$ is the same point as that designated by $m = -1$. Consequently, j may equally be defined as $j = (0, \pm 1, \pm 2, ..., \pm n/2)$.

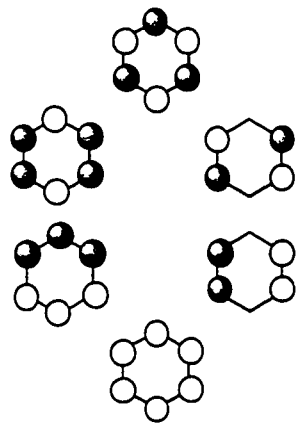

Figure 1.5 The simple HMOs of benzene.

$$E_j = \alpha + 2\beta\cos(2\pi j/n)$$

Equation 1.9 Energies of the simple HMOs.

The maximum value of any cosine function is unity. Therefore, no matter how many atoms n appear in the ring, the energy levels are confined to values between $\alpha \pm 2\beta$. This is shown schematically in **Figure 1.6** for n = 3, 4, 5, 6, and some arbitrarily large but finite value.

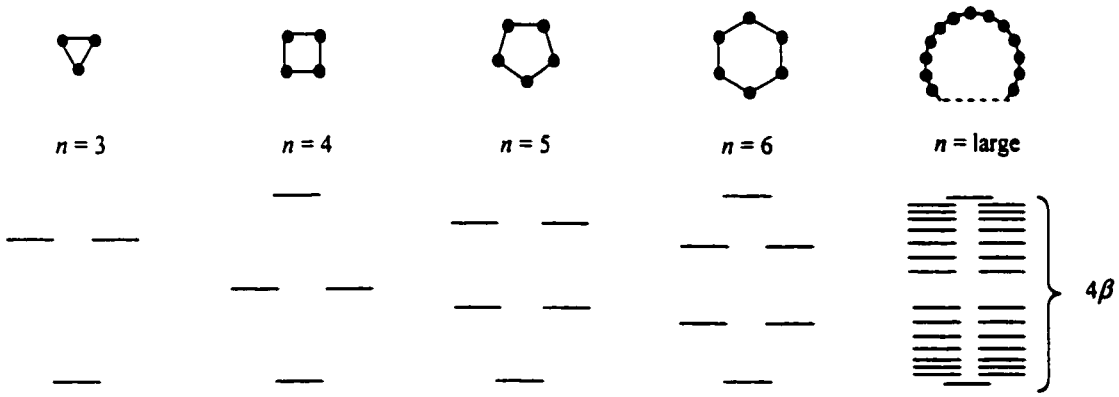

Figure 1.6 The maximum energy dispersion for this model is 4β.

It can easily be seen that as n increases, the energy difference between MOs decreases and, in the limit of $n \rightarrow \infty$, a continuum, or band, of crystal orbitals with a width of 4β is produced. Approaching this limit, the ring becomes very large such that its curvature approaches zero. Thus,

the finite ring has become a good model for a one-dimensional chain of infinite length, *i.e.*, a one-dimensional crystal.

This shift from a large but finite ring to an infinite chain does not much change the model or the equations already presented, other than that it requires a redefinition of the periodic potential sites (atoms) in terms of a distance from some arbitrary origin.

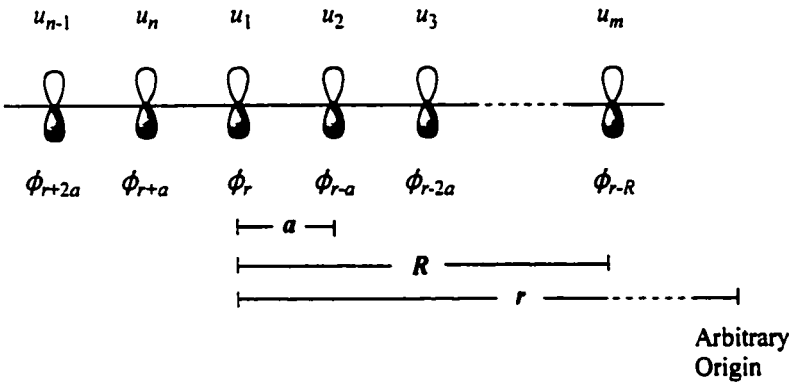

Figure 1.7 Redefining the periodic potential positions in terms of distance from some arbitrary origin. $\boldsymbol{R} = \boldsymbol{ma}$.

From the Bloch theorem in **Equation 1.4** for the finite ring model, it is now possible to redefine the exponential term

$$2\pi ijm/n = i\,(2\pi/a)(j/n)\,ma = ikR \qquad \textbf{Equation 1.10}$$

Notice that while $\boldsymbol{R}$ is a vector in the $\boldsymbol{a}$ direction, $\boldsymbol{k}$ both encompasses the quantum number j and has units of reciprocal distance ($\boldsymbol{a}^{-1}$). We can also put a restriction on the possible values of $\boldsymbol{k}$. Since $j = (0, \pm1, \pm2, ..., \pm n/2)$, and from **Equation 1.10**, $\boldsymbol{k} = (2\pi/a)(j/n)$, the values of $\boldsymbol{k}$ must be quantized and must fall between $-\pi/a$ and $+\pi/a$. Furthermore, due to symmetry, only the values of $\boldsymbol{k} = (0 \ldots \pi/a)$ are unique and need be cited (values of $\boldsymbol{k} = (0 \ldots -\pi/a)$ are the same as their positive counterparts). Finally it is prudent to recognize that although $\boldsymbol{k}$ is a quantum number with

n values, n is infinitely large which leads to a continuum of energy states.

We have noted that $\boldsymbol{k}$ has units of reciprocal distance acquired from the $\boldsymbol{a}^{-1}$ term. This term also imparts a directionality, thus $\boldsymbol{k}$ is properly a wave vector in reciprocal space. This is meaningful in terms of a crystal lattice structure. Any point within the first Brillouin zone† can be located by a vector $\boldsymbol{k}$. The wavefunction and energy equations can now be restated as follows:

$$\psi_k = \frac{1}{\sqrt{n}} \sum_{m=1}^{n} \exp(ikma)\phi_{(r-ma)} \qquad \textbf{Equation 1.11}$$

$$E_k = \alpha + 2\beta\cos(ka) \qquad \textbf{Equation 1.12}$$

In order to represent the information that these equations provide in an easily accessible manner, it is common to map the energy over the $\boldsymbol{k} = (0 \ldots \pi/\boldsymbol{a})$ continuum. These convenient graphs, called dispersion curves, display the variations in energy for several potential functions over the same $\boldsymbol{k}$ space continuum. For example, a theoretical infinite chain of atoms, each of which has an s orbital, a p_y orbital and a p_z orbital, has a set of dispersion curves like those shown in **Figure 1.8**. At ($\boldsymbol{k} = 0$), all the atomic orbitals are of the same phase, making the $\sigma_{(s)}$ crystal orbital (CO) and the $\pi_{(Py)}$ CO completely bonding but the $\sigma_{(Pz)}$ CO completely antibonding. At ($\boldsymbol{k} = \pi/\boldsymbol{a}$), there is a phase alternation at every atomic site in the chain reversing the bonding properties of these COs.

---

† The first Brillouin zone is a reciprocal lattice cell constructed from a Wigner-Seitz primitive cell by shifting the origin such that it is located at the center. It has the shape of a polyhedron with sets of parallel faces.

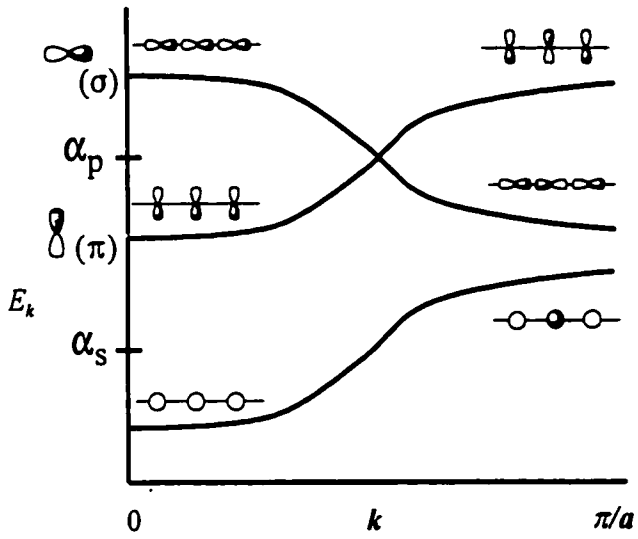

Figure 1.8 Dispersion curves for a theoretical atomic chain.

In a crystalline solid, there is an approximately continuous set of n states along the dispersion curve. The density of states (DOS) is defined as the number of states in a small energy increment ∂E. Where the slope of the dispersion curve is steep, the DOS along the line of the curve is less than at points where the slope is small. The DOS is illustrated by taking the first derivative of the dispersion curve and plotting the inverse of this against the energy (**Figure 1.9**).

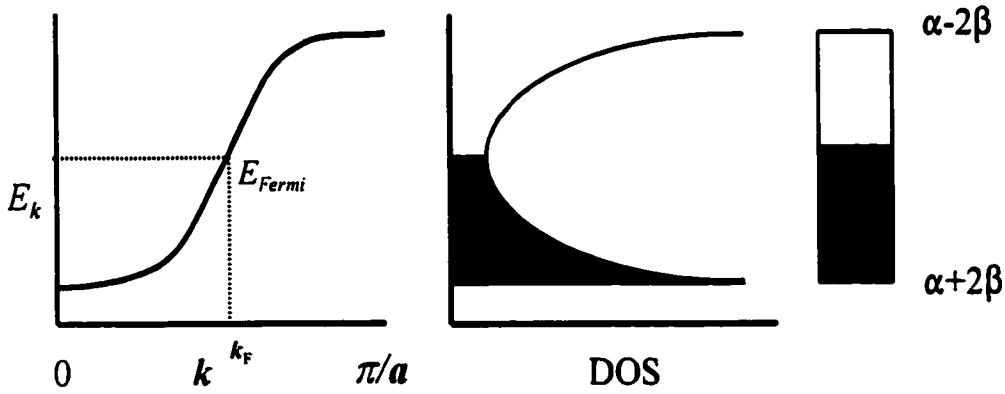

Figure 1.9 Dispersion curve, density of states (DOS), and block representation of a 1D energy band. The level of filling reflects one electron per site.

Block drawings are often shown to represent bands in a solid state structure. In fact, these are derived from the DOS schemes. A steep slope in the dispersion curve leads to a small (narrow) DOS and a large band width.

1.3.1 Metals, Semiconductors and Insulators

Electronic conduction properties of solid state materials are often described in terms of their band structures. A metallic conductor, one in which the conductivity increases with a decrease in temperature, is illustrated as a partially-filled band. The Fermi level[†] is found somewhere within the band rather than within a band gap. The occupying electrons are able to move relatively freely within the band, needing no activation energy to induce conduction. The conductivity, σ, (**Equation 1.13**) is dominated by the large, and effectively constant, number of charge carriers, n. The decrease in conductivity observed upon an increase in temperature is a result of electron - phonon interactions, *i.e.*, interactions with the lattice vibrations, that effectively decrease the carrier mobility, μ.

$\sigma = n|e|\mu$ where e is the charge **Equation 1.13**

Insulators and semiconductors are both characterized by completely filled bands (and higher lying empty bands). The significant difference between the two is the distance between the highest lying filled band and the lowest lying empty band, known as the band gap. A semiconducting material has a small band gap, ($E_{gap} << kT$, where k is the Boltzmann constant and T is the temperature). A band gap on the order of kT or larger, and the compound is nominally an

---

[†] The Fermi level in a metal is the highest filled state. The Fermi energy is the energy at the Fermi level. In reality, there is a thermal distribution at the Fermi level (not shown herein).

insulator. In contrast to a metallic conductor, a semiconductor displays an increase in conductivity with an increase in temperature. In order to permit conduction, an activation energy proportional to the width of the band gap is required such that electrons from the valence (filled) band are promoted to the conduction (empty) band. Thus, the conductivity, σ, is largely governed by the number of charge carriers, n, which is generally small. The small changes in mobility, μ, are obscured by the large changes in n.

Many of the semiconductors currently employed in the electronics industry are doped. A silicon matrix doped with arsenic is known as an n-doped semiconductor since As carries one more electron than does Si. This introduces a (very narrow) occupied band closer to the existing silicon conduction band, effectively narrowing the band gap. Conversely, doping silicon with aluminum introduces "holes" in the matrix creating a p-type semiconductor. This is synonymous with interposing an empty energy level close to the highest lying filled silicon band. The new empty band is very narrow and serves mainly as a reservoir for electrons excited from the band below. The conduction mechanism is best described in terms of the new "holes" created in the valence band.

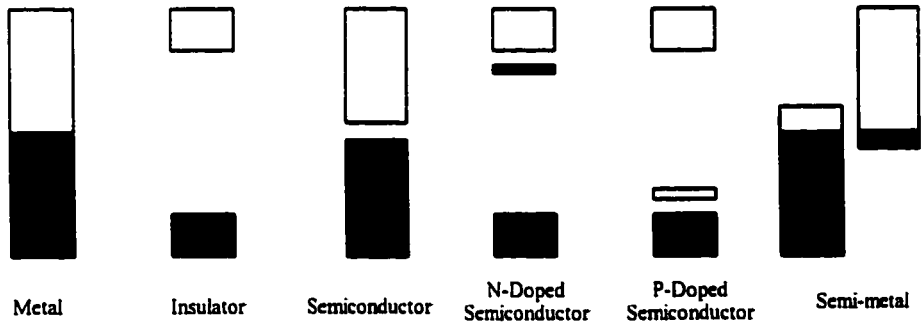

Figure 1.10 Band structure representations of a metal, an insulator, a semiconductor, doped semiconductors, and a semi-metal.

Finally, a semi-metal is a zero-gap semiconductor.[21] For instance, a material that achieves two partially filled bands as a result of partial electron transfer between the overlapping bands of two components (*e.g.*, [TTF][TCNQ]).[15] The HOMO of the donor component must be higher in energy than the LUMO of the acceptor in order for this charge transfer to occur.

1.3.2 Conductivity in Metals

It has previously been noted that, in the free-electron model shown in **Figure 1.9**, for every filled state with momentum *k*, there is a filled state with equal and opposite momentum -*k*. As a result, in the absence of an electric field, there is no net current. The application of an electric field to this model has the effect of raising the energy levels of the *k* states and lowering those of the -*k* states. In the case that the band is partially filled, a net current is generated by the flow of charge carriers from the higher lying *k* states to the lower -*k* energy levels. If the band is filled, no net flow of carriers is possible since there are no empty energy levels to receive the electrons from the higher lying *k* states.

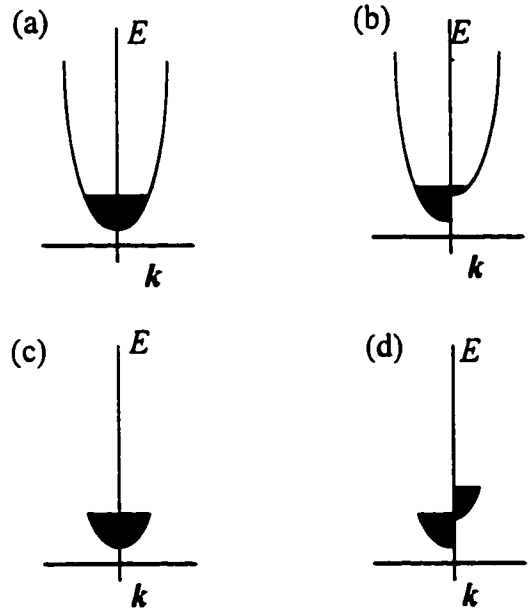

Figure 1.11 The dispersion curves of a metal and an insulator upon application of an electric field.

1.3.3 Charge Density Waves (CDWs) and Peierls Distortion

There are many organic conducting materials for which a quasi-one-dimensional model, such as that discussed thus far, is valid. These tend to suffer from an instability closely akin to the well-known Jahn-Teller distortion. This instability is readily demonstrated by a thought experiment. A hypothetical model is established consisting of a chain of evenly spaced hydrogen atoms. The atoms are in close enough proximity that overlap of the 1s orbitals occurs generating a half-filled band. This describes a metallic conductor. However, it is well known that this system is more stable with an alternate shortening and lengthening in bond distances, the limit of which is the generation of individual H_2 molecules. It is worth noting that, although hydrogen does exist as a gas consisting of H_2 molecules at standard temperature and pressure, at high pressure (> 4 Mbar), it forms a structure that is the three dimensional equivalent of the equidistant chain with metallic conducting properties.[22]

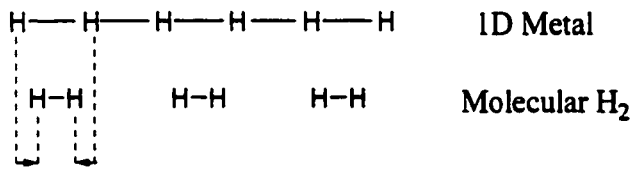

Figure 1.12 One-dimensional metallic hydrogen array *vs.* elemental hydrogen.

Peierls[23] showed that any partially filled one dimensional system is unstable as a regular array and will distort, an effect known as the Peierls, or charge density wave (CDW) driven, distortion. For a system, like metallic hydrogen, in which there is one unpaired electron per site (*i.e.*, the band filling level is 0.5), the distortion is manifested as alternating bond distances (or dimerization). While the half-filled band model is convenient, it is not unique. *Any* degree of partial filling in a one dimensional system has an associated CDW, a repeating pattern of alternating

regions of higher and lower charge density within the lattice. Consequently, all partially filled one dimensional systems are subject to a Peierls distortion.

This CDW-driven instability can be demonstrated, using the half-filled band model, at the Hückel level. The first step is to observe the change in the dispersion curve upon a redefinition of the lattice constant in the regular infinite chain of periodic potentials (atoms). Until this point, the unit cell of this array is defined as having a length a (giving $k = -\pi/a \ldots \pi/a$) and as containing only one atom. Redefining the unit cell as $2a$ yields $k = (-\pi/2a \ldots \pi/2a)$. Notice that since k is a vector in reciprocal space, a doubling of the lattice constant causes a halving of k. In effect, this causes a "folding" of the dispersion curve.

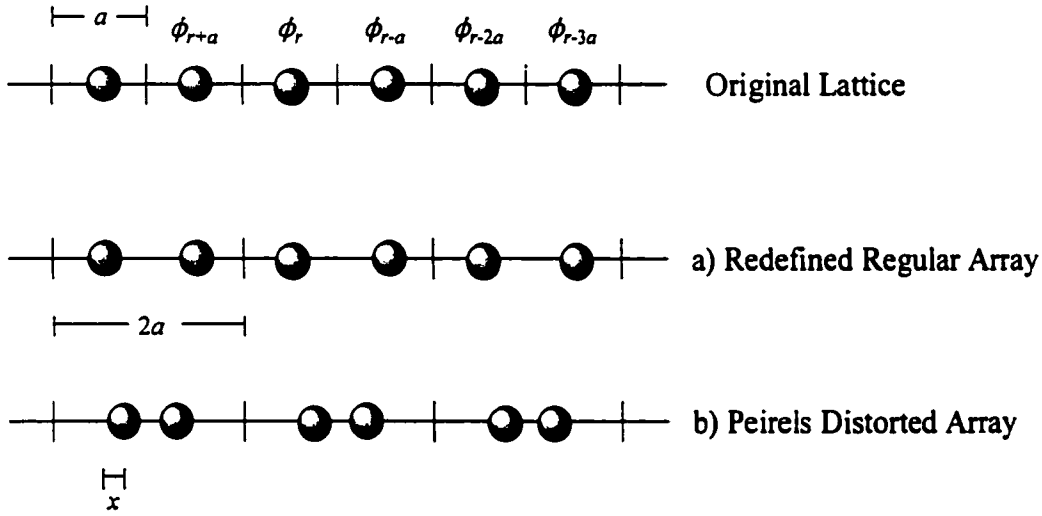

Figure 1.13 Redefining the lattice constant for (a) a regular array followed by (b) a Peirels distortion.

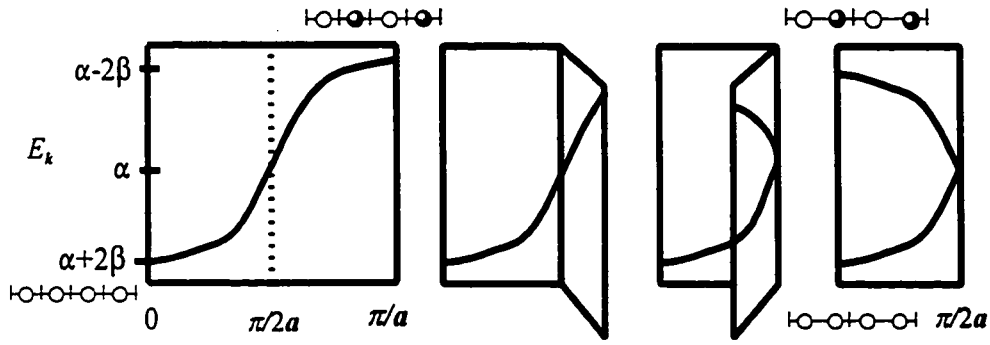

Figure 1.14 Folding of the dispersion curve upon doubling of the lattice constant of a regular *undistorted* array.

The band model now describes two bands that have no band gap between them. This is effectively the same as a continuous band and the redefinition has not altered the prediction of a metallic (or more properly, a semi-metallic) conductor in the case of a half-filled band.

The next step is to introduce the instability into the model (**Figure 1.13b**), by displacing one of the atoms in every cell by an amount x. This distortion introduces two different interaction integrals, β_1 and β_2, that are dependent upon x. For $|\beta_1| > |\beta_2|$, the energy limits are

$$k = 0, \qquad E = \alpha \pm (\beta_1 + \beta_2) \qquad \textbf{Equation 1.14}$$

$$k = \pi/2a, \qquad E = \alpha \pm (\beta_1 - \beta_2)$$

This effectively creates a band gap as shown by the plot of the dispersion curves.

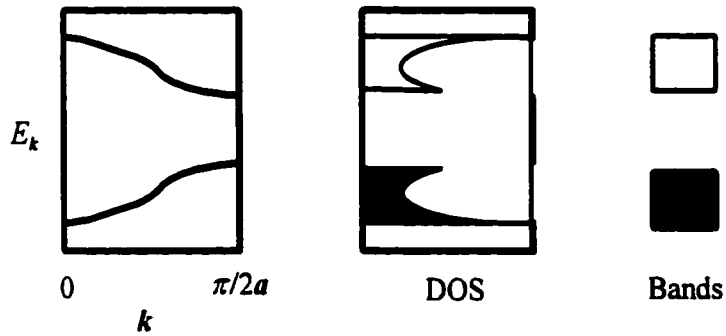

Figure 1.15 Dispersion curves, DOS, and band representation of Peierls distorted chain.

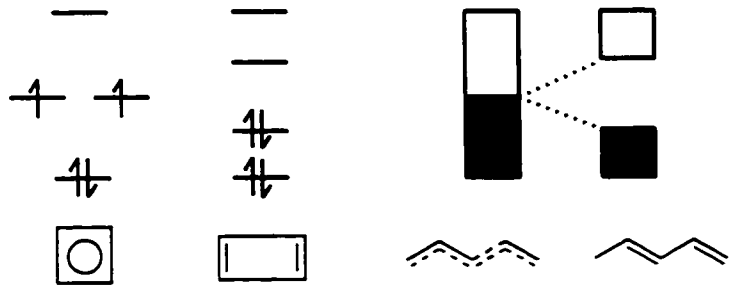

I-7

Figure 1.16 Analogy between Jahn-Teller stabilization of cyclobutadiene and Peierls distortion of polyacetylene.

Peierls distortions will always occur in a partially filled one dimensional system. Some examples include polyacetylene (**I-7**), which experiences bond alternation,[5] elemental hydrogen (H_2), and the 1:1 salt [TTF][Br] which crystallizes as $(TTF)_2^{2+}$ dimers.[24] These are all one-dimensional systems with half-filled bands.

It is important to recognize that all 1D systems are subject to a CDW-driven distortion. However, there do exist one dimensional systems, such as [TTF][TCNQ], that *appear* to be unaffected by this type of distortion. In truth, while a CDW can be determined for any partially filled one-dimensional array, the onset of a Peierls distortion is temperature dependent. [TTF][TCNQ] is undistorted under STP conditions and does not succumb to a Peierls distortion until a temperature of 58 K, for reasons associated with the degree of band filling.

In stacked molecular materials, such as [TTF][Br], every molecule in the stack is a radical cation, and a half filled band is expected. This material undergoes a CDW driven distortion resulting in dimerization under STP conditions. When neutral molecules are introduced into the stack (*e.g.*, $[TTF][Br]_{0.7}$), the band levels are no longer half filled and a new CDW is formed, with a periodicity that is not commensurate with a simple dimerization process, but rather with some larger superlattice. The difference in conductivity measured at room temperature for [TTF][Br] and $[TTF][Br]_{0.7}$ is discussed further in **Section 1.4 (Radical Ion Conductors and Charge**

Transfer Salts).

Although the complex has a 1:1 stoichiometry, the TTF stack in [TTF][TCNQ] is another example in which radical cations are interspersed with neutral molecules. Only partial charge transfer occurs between the donor and the acceptor, resulting in a band filling of approximately 0.7 - 0.75 (*i.e.*, an average transfer of 0.5 - 0.6 of an electron per TTF molecule). A CDW driven distortion is still possible, however the energy gained from the distortion is less than that gained in the half filled band case. As a result, the distortion is not observed under STP conditions.

Whether or not a Peierls distortion is observed can be explained in terms of the extent of nesting[25] in the Fermi surface. The Fermi surface can be described as the junction between filled and empty energy levels in a partially filled band. For a system with filled bands, there is no Fermi surface, so this concept applies only to metals. More precisely, the Fermi surface is a constant energy plot, in reciprocal (***k***) space, of the highest occupied energy levels at T = 0 K. If large parts of the Fermi surface may be translated by a unique vector ***q*** such that they are superimposable on other parts of the surface, the Fermi surface is said to be strongly nested. In other words, many levels in the ***k*** space continuum will be stabilized by the same distortion.

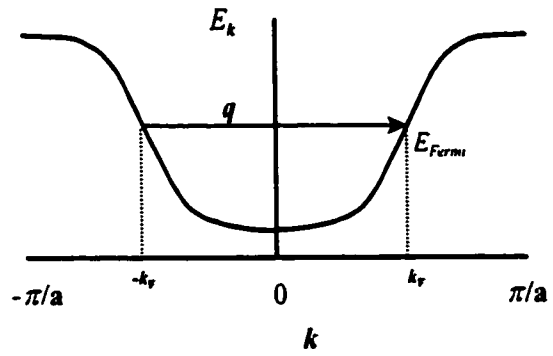

Figure 1.17 Fermi surface of a 1D system is simply two points, $+k_F$ and $-k_F$.

In a one dimensional system, the Fermi surface is simply a set of points, $\pm k_F$ (**Figure 1.17**). The unique vector by which these two points can be translated is therefore $q = 2k_F$. Since the value of k_F is determined by the extent of band filling, with a maximum occurring at $k_F = \pi/2a = a^*/2$, this is equivalent to $q = \varrho a^*/2$, where ϱ is the average number of carriers per lattice site. For a half filled band, $\varrho = 1$ and $q = (\frac{1}{2})a^*$. Similarly, for a one dimensional system in which there is only partial charge transfer, 75 % for example, $\varrho = 0.75$ and $q = (3/8)a^*$.

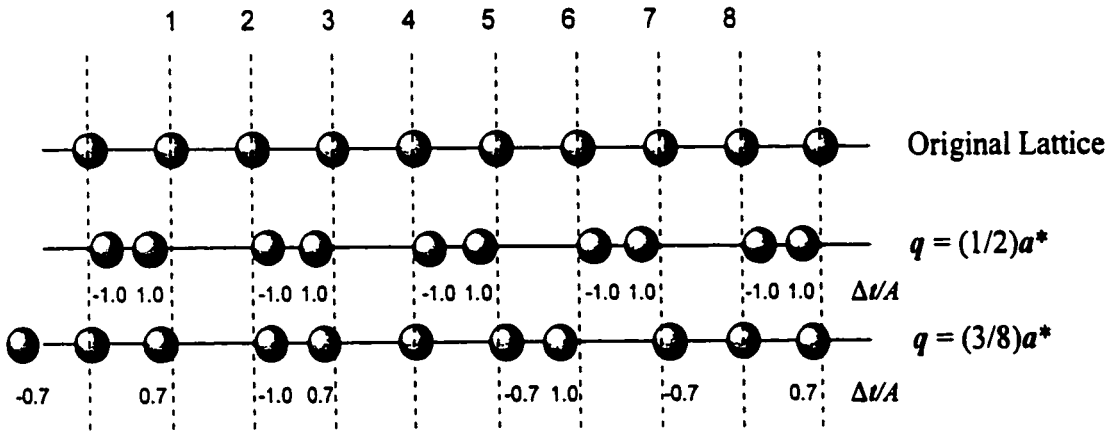

Figure 1.18 CDW-driven distortions for a one-dimensional lattice with (a) $q = (\frac{1}{2})a^*$ and (b) $q = (3/8)a^*$. The periodic lattice displacements are given by $\Delta t/A$, where the value of the weighting factor A is a function of the CDW. The phase factor ϕ has been set to $\pi/2$ for (a) and to zero for (b).

It is possible to construct a model whereby the appearance of the CDW-driven distortion can be predicted given the extent of partial band filling. Given that the undistorted one-dimensional molecular array is described by a regular intermolecular separation a (in the a direction), the one dimensional translational vector of a molecule can be described by $t = la$, where ($l = 1, 2, 3, ...$). In the presence of a harmonic modulation in the a direction, with a wavevector q, the molecular displacements (Δt) caused by the CDW-driven distortion are given by **Equation 1.15** (where A is the amplitude and ϕ is the phase).

$$\Delta t = A \sin (q \cdot t + \phi) \qquad \textbf{Equation 1.15}$$

The results for $q = (½)a^*$ and for $q = (3/8)a^*$ are shown schematically in **Figure 1.18**. In the case that $q = (3/8)a^*$, the function is periodic over $(8/3)a$, but only commensurate with the original lattice over eight lattice repeats.

In non-one-dimensional systems, there may not necessarily be a unique vector q whereby every point of the Fermi surface can be translated to some other point on the Fermi surface. Consequently, a distortion that stabilizes some energy levels may destabilize others. For this reason, Peierls distortions are largely restricted to one-dimensional arrays.

There are examples of non-one-dimensional structures that succumb to a Peierls instability. The group 15 elements, for example, distort away from a simple cubic structure because the electronic structure is effectively that of three almost independent one-dimensional systems.[25] The Fermi surface is a cube rather than a sphere.

Equally, there are examples of "one-dimensional" systems that are predicted to be distorted from electron count consideration, but are stabilized by inter-chain interactions. $(SN)_x$ is such a system.[26] When two chains of $(SN)_x$ are brought together, sulfur-sulfur contacts between the chains lead to a splitting of the partially filled bands. In essence, these two new bands are representative of the bonding and antibonding interactions between the chains. To a first approximation, the Fermi energy level does not change, but the fractional occupancy of the two bands now deviates from 0.5. Thus, the Fermi surface of the less-than-half occupied band has become more spherical and the Fermi surface of the more-than-half filled band can be described as a cube with concave edges. The degree of nesting in both has decreased. When this increased dimensionality is considered in the solid state (*i.e.*, for an infinite number of chains) the result is a Fermi surface that is weakly nested. Consequently, there is no distortion for which a significant

increase in stability results.

It has been noted that, in the one-dimensional cases in which a Peierls instability is predicted, the onset of this distortion is dependent on both temperature and pressure. The driving forces behind this distortion arise from the highest occupied energy levels. Resisting this distortion are the "elastic forces" from the underlying electronic structure (σ bond compression, for example). Bonds between atoms or molecules are often modeled as springs. Using this analogy, and applying Hooke's law to determine the potential energy (V) of the system, it is easy to see that the minimum energy for this model is at a displacement of $\Delta a = 0$. This gives some insight into why crystals (regular arrays) exist at all. It is the underlying "stiffness" of the lattice that the CDW must overcome in order to introduce a distortion.

$V = k(a + \Delta a)^2 + k(a - \Delta a)^2$ Hooke's law; k = force constant **Equation 1.16**

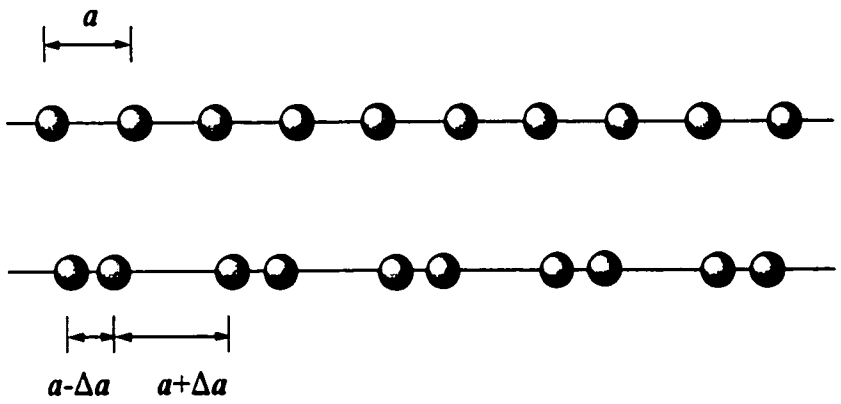

Figure 1.19 Displacement in the spring model of a one-dimensional molecular array.

Unaccounted for in any of the previous models is the interatomic (or intermolecular) repulsion. The repulsion is stronger in the asymmetric (distorted) array since it is proportional to the square of the interatomic separation. Consequently, as pressure is applied to the system and

a becomes smaller, the repulsive interaction dominates and the symmetric array eventually becomes more stable, reversing the Peierls distortion.

1.3.4 Mott-Hubbard Transitions and the Hopping Model of Conduction

There is a second scenario involving an array of radicals, such as hydrogen atoms, in which the formation of a metallic conducting structure is prevented. In a model in which unpaired electrons are each isolated on individual atoms (or molecules), electrical conduction must occur by movement of an electron from one atom site to the next. This is called the Hopping Model of conduction. When an electron hops from one site to a neighboring site, it experiences a repulsion from the electron that already resides there. This Coulombic barrier (U) is equivalent the net energy required to remove an electron from one radical site and to add an electron to another radical site. Thus, U can be approximated by the gas phase disproportionation enthalpy, ΔH_{disp}. For a neutral radical, this is the difference between the ionization potential and the electron affinity. In the case of a radical cation, this is the difference between the first and the second ionization potentials. **Figure 1.20** shows a neutral radical R as an example.

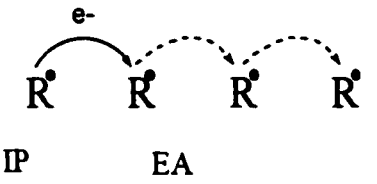

Figure 1.20 Coulombic repulsion in the Hopping model of conduction.

When the radicals are physically far removed from one another, the overlap integral, β, will be small and it can be expected that the Coulombic barrier to conduction, U, will prevent metallic behaviour. As the interatomic separation is decreased, β increases and the Coulombic repulsion

to bandwidth ratio ($\kappa = |U/4\beta|$) decreases to the point where a half-filled energy band best describes the system. This insulator-to-metal transition is the Mott-Hubbard transition. This is illustrated in **Figure 1.21**[27] where the lower energy (IP) is the energy of the singly occupied orbitals and the upper energy (EA) is the energy of an extra electron added to the solid, to give a doubly occupied orbital. The gap†, equal to U, represents the energy required to excite an electron into another orbital.

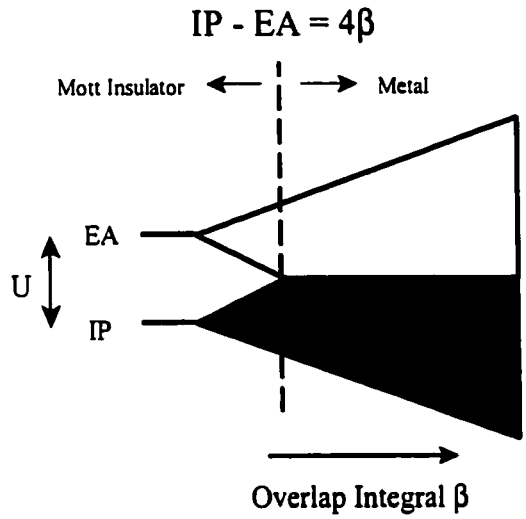

Figure 1.21 Hubbard sub-bands as a function of bandwidth, 4β.

It is important to note that the overall contribution to Coulombic repulsion, U, will be greatest for a system, like that depicted in **Figure 1.20**, in which there is an unpaired electron at every lattice site. This is equivalent to a half-filled band. The introduction of closed shell species into the lattice results in sites onto which a charge carrier may move without significant Coulombic repulsion. Thus, a Mott-Hubbard transition is rendered less likely in a system with bands in which the fractional filling is not 0.5.

---

† This gap is *not* the same as the gap which occurs in band theory, but is a consequence of electron repulsion.

1.4 Radical Ion Conductors and Charge Transfer Salts

The majority of organic compounds are insulators, characterized by extremely low electrical conductivity ($\sigma < 10^{-10}$ S cm^{-1} at RT). There are, however, a number of classes of organic materials that exhibit significantly higher conductivities. Most common among these materials are radical ion conductors (RICs) and charge transfer (CT) salts.

Charge transfer (CT) salts are solid state materials comprised of two molecular components, a π-molecular electron donor (D) and a π-molecular electron acceptor (A). Co-crystallization of these two components results in the oxidation of the donor and the reduction of the acceptor, by electron transfer (DA and $D^{+\cdot}A^{-\cdot}$). This redox process is limited to the case in which the frontier molecular orbitals of the two components are compatible (*i.e.*, the donor HOMO is close in energy to the acceptor LUMO). Complete electron transfer is not necessary and, in fact, may be unfavourable. The degree of electron transfer is largely dictated by the ionization potential of the donor, the reduction potential of the acceptor, and the electrostatic Coulomb interactions binding the resulting ionic material.

Of the many known CT materials, [TTF][TCNQ][15] is perhaps the most widely recognized example of a salt exhibiting high conductivity (10^4 S cm^{-1} near 60 K). It is composed of 1,1'3,3'-tetrathiafulvalene (**I-2**) donors and tetracyano-*p*-quinodimethane (**I-3**) acceptors in a 1:1 stoichiometric ratio. These planar molecules are represented as blocks in **Figure 1.22** where it can be seen that they crystallize as separate π stacks of **I-2** and **I-3**. Although the plane of the individual molecules is not at right angles to the stacking direction, as might be suggested by an idealized stacking model, the intermolecular π overlap remains intact and this material is an organic semi-metal.[28]

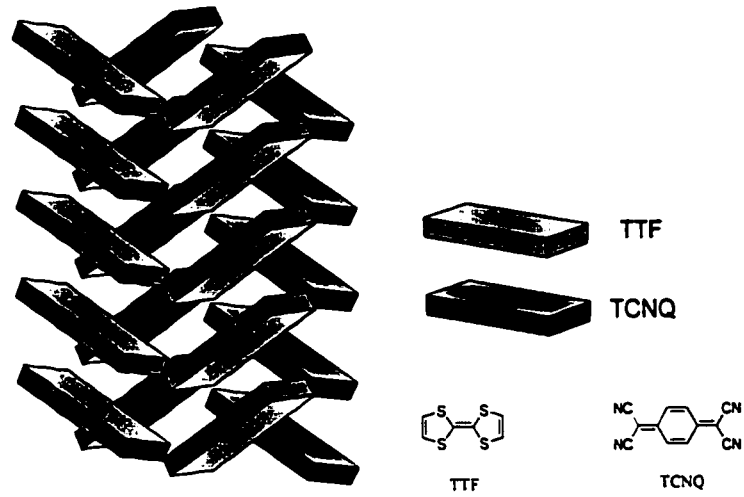

Figure 1.22 A graphic representation of the [TTF][TCNQ] crystal structure.

Radical ion conductors, RICs, are characterized by the incorporation of a simple inorganic counterion in lieu of the acceptor (or donor) component. The oxidation of a strong π-molecular donor (D) or the reduction of a strong π-molecular acceptor (A) potentially forms a highly conductive radical ion salt ($D^{+\cdot}X^{-}$ and $X^{+}A^{-\cdot}$). Examples of such RICs include the donor-based $[TTF][Br]_{0.7}$ and the acceptor-based $[Et_3NH][TCNQ]_2$ (conductivities are both on the order of 10^2 S cm^{-1}).[28,29] Bechgaard salts[30] are a large subclass of RIC in which BEDT-TTF (**I-8**) is the donor component, $[BEDT\text{-}TTF]_2[X]$, [31] (X = $GaCl_4$, $FeCl_4$, *etc.*). Conduction occurs only through the radical cation of the donor molecule (or the radical anion, $A^{-\cdot}$) and the simple counterion serves strictly as a charge balance and a means of oxidation or reduction.

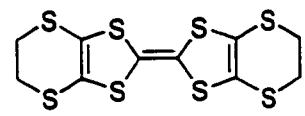

I-8

Figure 1.23 A Bechgaard salt donor, **I-8**.

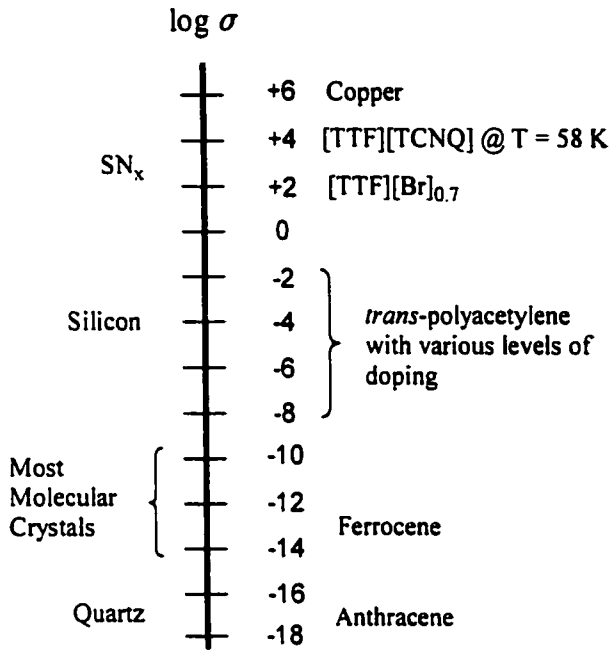

Figure 1.24 Conductivities of some common materials.

A graphic comparison of the conductivities of a variety of materials is given in **Figure 1.24**. From this diagram it can readily be seen where, in the conductivity scale, known RICs and CT salts lie in relation to other common conductors, semiconductors, and insulators.

In order for a CT salt or a RIC to exhibit conducting properties, a number of criteria must be met. Most important is that charge transfer must occur such that either or both components achieve a radical ion oxidation state. However, it has been observed that complete charge transfer greatly diminishes the conductivity of the salt, therefore incomplete or partial charge transfer is desirable. Both TTF and TCNQ, for example, possess a stable radical ion oxidation state. However, when co-crystallized as [TTF][TCNQ], the extent of charge transfer is only 0.5 - 0.6 of one electron.[16] In the case that complete electron transfer occurs in the solid, a significant amount of electrostatic repulsion can be expected between like molecules within a stack. Thus

partial transfer acts to stabilize the crystal structure by minimizing intra-stack repulsion interactions. Furthermore, partial charge transfer lowers the effective on-site electron-electron repulsion in both the donor and acceptor stacks, thereby enhancing electron mobility in the stacking direction (the main direction of conduction). By contrast, in the complete transfer model, moving an electron from one molecular site to the next leads to a larger number of energetically expensive doubly charged states.

A clear example of the superior conductivity of a salt involving partial charge transfer over one in which complete transfer occurs is the difference in conductivity between TTF oxidized with a deficit of bromine and TTF fully oxidized electrochemically in the presence of a bromide salt. The latter yields a 1:1 bromide salt, [TTF][Br], and is *13 orders of magnitude less* conductive than the $[TTF][Br]_{0.7}$ salt generated by partial oxidation.[16] By contrast, the 1:1 stoichiometry of [TTF][TCNQ] allows for partial charge transfer owing to the relative ionization potential of the donor and electron affinity of the acceptor.[32, 33]

The spatial orientation of the donor and acceptor radical ions within the material is crucial. In general, there must be some kind of intermolecular interaction available such that conduction is possible. This is commonly accomplished through intermolecular π- π overlap. In the majority of known CT salts, both conductive and insulating, the donor and acceptor molecules are arranged in stacks. The mode of stacking adopted by the crystal structure is critical to the conductive properties of the solid. In mixed stacks, donors (D) and acceptors (A) are stacked co-facially in an alternating pattern (... -D-A-D-A- ...). Generally, such an arrangement cannot be highly conductive as it prevents the formation of partially filled crystal orbitals (bands).[†] In order for the CT salt to exhibit high conductivity, the solid state structure must consist of segregated stacks of donors (... -D-D-D-D- ...) and acceptors (... -A-A-A-A- ...).[34]

[†] This is assuming that there are no appreciable lateral contacts between like molecules.

It is commonly acknowledged that segregated stacks may be formed by default in those cases where the D-A overlap is "particularly weak".[34] It is uncertain what is meant quantitatively by "particularly weak", however qualitatively, a weak D-A overlap can be designed in one of two ways. The first is to choose donor and acceptor molecules that are very different in shape (*e.g.*, RICs involving simple alkali metal salts or halide salts with planar, highly conjugated organics). In the case that both the donor and acceptor are planar, segregated stacks are formed when the frontier orbitals have the opposite symmetry with respect to inversion. [TTF][TCNQ] conforms to this rule and crystallizes in separate donor stacks (intermolecular TTF separation is 3.47 Å) and acceptor stacks (intermolecular TCNQ separation is 3.17 Å).[16] By contrast, TMPD (*N,N,N′,N′*-tetramethyl-*p*-phenylenediamine) has the same symmetry as both TCNQ and chloranil, and salts with either acceptor crystallize as mixed stacks.[34]

While these two criteria in particular are necessary for the generation of a partially-filled band, other properties are also required. The radical ions must have a sufficiently low barrier to conduction that the intermolecular overlap does indeed result in a band structure as opposed to a Mott insulating type material. This is often achieved by designing the component such that its frontier orbitals are spread over a relatively large molecular area. This avoids the trapping of the unpaired electron on one or two atoms. Furthermore, dimerization of the radicals in a Peierls-type distortion must be avoided. While the charge on the radical ions works in favour of preventing this instability, it is not unknown among CT salts.[24] One design method for further discouraging this distortion is to increase the dimensionality of the material through lateral contacts. While the protons or other groups on peripheral carbons impede the formation of these contacts, heavy chalcogens, such as sulfur and selenium, facilitate lateral contacts. The prime example of a CT component with three-dimensional contacts is C_{60}.[19]

Much of the early literature indiscriminately refers to organic CT salts with high

conductivities as organic metals. This designation is not strictly accurate since none of these materials possess a single partially filled energy band. CT salts are either semiconductors (or insulators, depending on the size of the band gap) or semi-metals.

There are several characteristic electrical, optical, and magnetic properties that differ between metals, semi-metals, and semiconductors. High conductivity alone is insufficient to characterize a material as being metallic. However, the temperature dependence of conductivity is important. Typically, the conductivity of a metal increases with a decrease in temperature, whereas the conductivity of a semiconductor decreases. In the case of [TTF][TCNQ], a metal-like increase in conductivity with decreasing temperature is observed down to a certain temperature. At this point, known as the metal-insulator transition temperature (T_{MI}), a CWD-driven instability begins to set in and a maximum conductivity is reached ($\sigma_{max,58K}$ *ca.* 10^4 S cm^{-1}).[16] Below this temperature, the conductivity drops sharply. CT compounds such as [NMP][TCNQ] (NMP = *N*-methylphenazinium) and $[TTF][SCN]_{0.54}$ also show a slight increase in conductivity with decreasing temperature followed by a metal-insulator transition. The great difference between these two compounds and [TTF][TCNQ] is the *slope* of the curvature of the temperature *vs.* conductivity plot above T_{MI}. In the case of [TTF][TCNQ], this slope is positive, creating a cusp at T_{MI} and identifying the compound as a semi-metal.[28] By contrast, for *N*-methylphenazinium tetracyanoquinodimethanide ([NMP][TCNQ])[35] and $[TTF][SCN]_{0.54}$ the slope is negative. These latter materials are part of a large class of semiconducting CT compounds that exhibit a strongly temperature-dependent charge-carrier mobility.

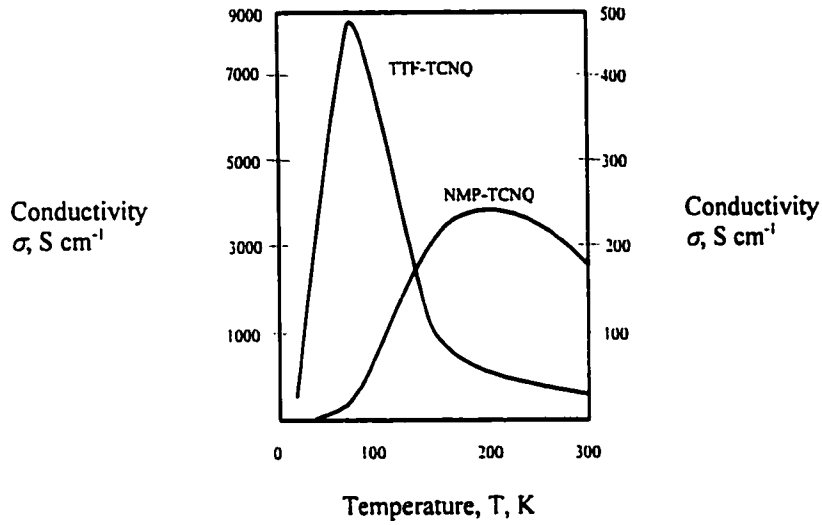

Figure 1.25 Schematic representation of temperature dependence of dc conductivity of TTF-TCNQ and NMP-TCNQ.[28, 33]

It is worth noting that a metallic state is characterized not only by electrical conductivity, but by certain optical and magnetic properties. Metals exhibit a specific frequency dependence of reflectivity, known as a Drude edge. If the Drude edge is within the visible region, a metallic luster is observed. For [TTF][TCNQ], the Drude edge is in the infrared region and the compound appears black.[28] Additionally, metals can be characterized by their nearly temperature-independent Pauli paramagnetism.[28]

1.5 Neutral Radical Conductors (NRC)s

Radical ion conductors, RICs, and CT salts rely on charge transfer in order to create a partially filled band. Thus, by their nature RICs and CT salts are either semi-metals or semiconductors, starting with a filled valence band from the donor compound and an empty conduction band of the acceptor. By contrast, a material designed solely from stable neutral radicals may be capable of exhibiting metallic conduction. These one-component molecular conductors are not to be confused with the single-component donor-acceptor systems in which

one part of the molecule acts as an electron donor and another as the acceptor.[36]

While charge transfer is not necessary in the design of an NRC, all the other criteria that describe RICs and CT salts apply equally to NRCs. In the case that each of these criteria are met, a half-filled band is the result, thereby allowing metallic conduction. In the case that the material undergoes Peierls distortion or there is a Mott-type breakdown in the band structure, it is still possible that conduction occurs upon the application of some activation energy. The NRC would then be a semiconductor.

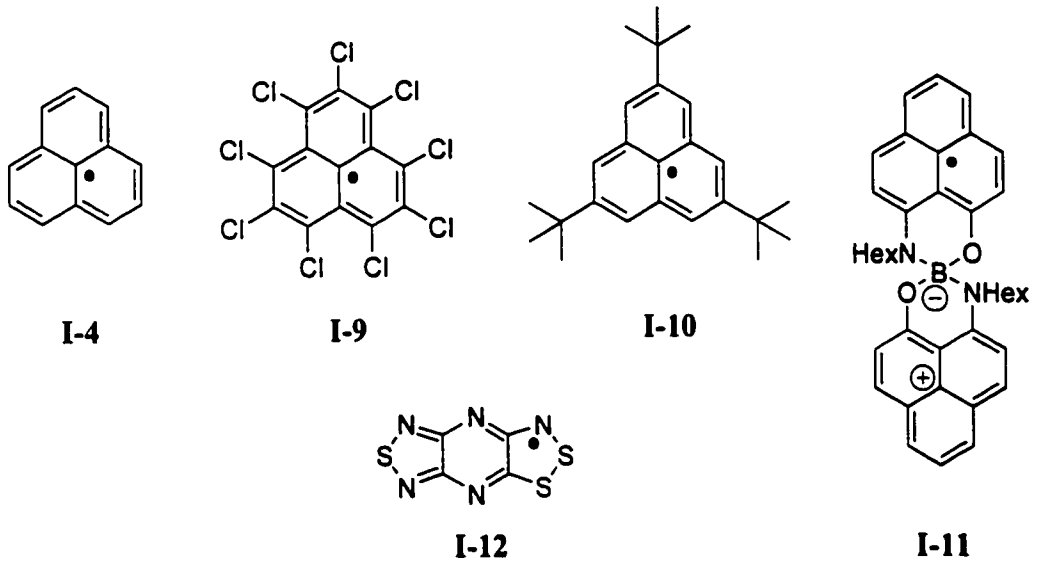

I-4 **I-9** **I-10** **I-12** **I-11**

Figure 1.26 Stable neutral radicals intended for use as NRCs.

Haddon,[20] in 1975, first suggested the design of a molecular NRC in terms of the experimentally unknown odd alternate hydrocarbon, **I-4**. While **I-4** itself has never yet been isolated in the solid state, it has been characterized by ESR. The chlorinated derivative, **I-9**, has been characterized in the solid state and appears to be a Mott insulator with no close contacts between the stacked molecules. Furthermore, **I-9** is not strictly planar, its edges appearing "ruffled" with the chlorine atoms positioned above and below the molecular plane in an alternating

pattern, presumably due to steric congestion.[37] The crystal structure of the *tris*(*t*-butyl) substituted compound **I-10** has recently been reported.[38] This compound undergoes a cofacial π bonded dimerization in the solid state, with one molecule rotated at 60° from the other. There appears to be no interaction between dimers, subsequently the material is an insulator.

Interestingly, the crystal structure and conductive properties of **I-11** were recently reported.[39] The geometry of this molecule is such that planar stacking is not possible, however, the solid state material appears to be a semiconductor, exhibiting a notable degree of conductivity at high temperature.

There are currently no molecular NRCs that display metallic conducting properties (technically, atomic compounds such as elemental sodium are metallic NRCs). The Oakley group has, for some time, been focusing on heteroatomic neutral radicals as possible NRCs. **I-12**, is the result of recent work by fellow members of the Oakley group.[40] It is the first material in which the unpaired electrons have been shown to participate in the conduction mechanism. Although **I-12** is a semi-conductor with only 2 % of the electrons unpaired at any one time (under STP conditions), it has been shown that the increase in Curie spins with increasing temperature is coincident with the increase in conductivity.

1.6 A Brief History of Sulfur-Nitrogen Heterocycles as Conducting Materials

The research contained within this thesis is part of a much larger ongoing project undertaken by the Oakley group. For a number of years, our goal has been to design, isolate and characterize novel SN heterocycles, possibly exhibiting conducting properties.

The history of SN heterocycles as conducting materials rightly begins with the discovery of the metallic conducting (and low temperature superconducting) properties of the polythiazyl $(SN)_x$ (**I-1**). This material is currently the only known metallic polymer that does not require

charge transfer in order to generate carriers. The unsaturated -S=N- repeat unit, of which $(SN)_x$ is composed, is a 3 π electron system with one unpaired electron located in a π^* orbital. The solid state structure of this polymer is a partially filled metallic band. Inter-chain sulfur interactions act to increase the dimensionality of the solid and negate the existence of a CDW-driven distortion.

In addition to the unique conductivity properities, the high electronegativity of $(SN)_x$ has been shown to lead to several enhancements in device efficiencies (*e.g.*, used as a barrier electrode in ZnS junctions, it increases the quantum efficiency of the blue-emission by a factor of 100 compared to gold; it increases the efficiency of GaAs solar cells by up to 35 %).[9] Furthermore, it is remarkably inert, showing stability to air, moisture, and acidic media. The synthesis of this material, however, poses difficulties on the industrial scale. These include the explosive nature of the S_4N_4 starting material and the intermediate S_2N_2 and rate of polymerization (on the order of weeks).

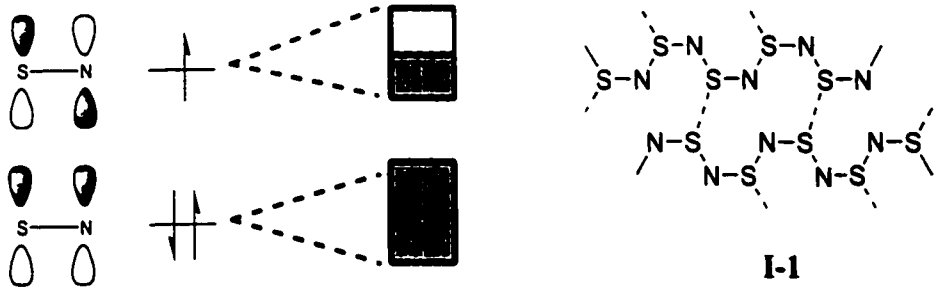

I-1

Figure 1.27 (a) The FMO manifold of the -S=N- radical and its relationship to the band structure of one-dimensional $(SN)_x$. (b) Inter-chain contacts in $(SN)_x$.

While many of the original polymeric and molecular conducting materials were primarily carbon-based species, the discovery of the properties of $(SN)_x$ prompted the design of materials that include the -S=N- unit. The incorporation of nitrogen and sulfur (and / or selenium) into the carbon frameworks leads to many new possibilities in terms of design. For example, one major

difficulty faced in the design of a carbon-based radical systems is the tendency toward irreversible dimerization through a C - C σ bond. This can often be overcome by the incorporation of a number of sulfur and nitrogen atoms. If the spin density is drawn away from the carbons and onto the heteroatoms, the tendency toward C - C dimer formation is significantly decreased. While dimerization may still occur through sulfur π contacts, increasing the number of S - S contacts within the dimer spreads the dimerizing electron pair over more bonds and acts to increase the separation distance and subsequently the "extent" of dimerization (the no-bond rule).

Further advantages of the SN heterocycles over carbon-based systems include reducing the need for peripheral hydrogens (or halogens) and thereby decreasing the steric hindrances to intermolecular overlap in all directions. The larger atomic radii of heavy chalcogens, such as sulfur and selenium, facilitate increased intermolecular overlap both within a π stack and laterally between π stacks. Again, this acts to stabilize the material against dimerization as well as decreasing the anisotropy of the system.

Finally, the incorporation of different atoms greatly increases the number of possible structural combinations available. Several possibilities for the design of a radical five-membered ring are shown in **Figure 1.28**.

Many of these heterocycles have been incorporated into the design of well-known molecular materials. For example, 1,3-DT (**I-13**) is the fundamental unit of TTF, and 1,2-DT (**I-14**) has been employed to create a TTF variant.[41] 1,3,2,4-DTDA (**I-18**) and 1,2,3,5-DTDA (**I-19**) have both been extensively investigated as a building block for radical and diradical materials. However, of the SN heterocycles presented here, only 1,3,2-DTA (**I-17**) and 1,2,3-DTA (**I-6**) are capable of substitution by fusing a ring to the two adjacent carbon sites. This aspect of the nature of these two DTAs lends them a certain flexibility in terms of material design.

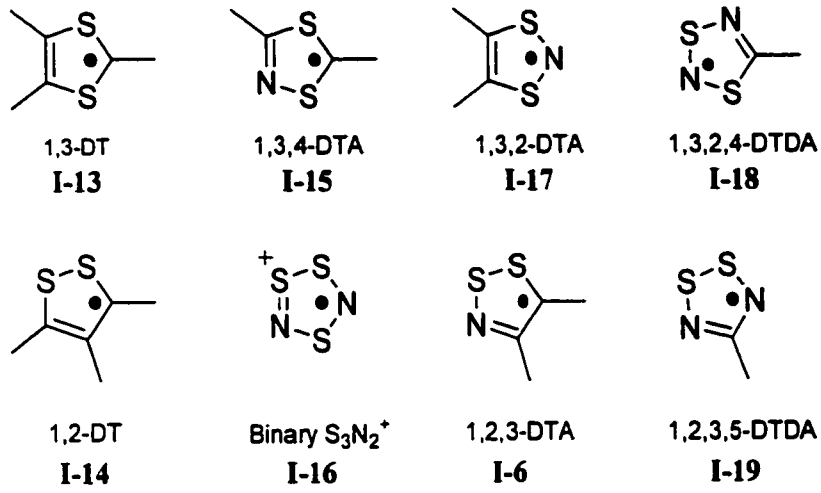

Figure 1.28 Known and theoretical five-membered radical heterocyclic rings.

Our current investigations focus solely on 1,2,3-DTA (**I-6**) as it has a number of advantages over 1,3,2-DTA (**I-17**). Primarily, the spin density in **I-17** is situated over the SNS linkage. Thus materials based on **I-17**, whether ring-fused or not, are likely to be radicals with the unpaired electron concentrated on the SNS unit. Conversely, in **I-6**, some spin density resides on one of the two carbon atoms. This allows for a much wider range in the freedom of design. Ring-fused species can be created such that the spin density is distributed over the entire molecule, improving the stability of the radical and possibly lowering the Coulombic barrier to conduction.[†] Both ring-fused and independently substituted species analogous to the closed shell TTF donor design are possible. Finally, independently substituted radicals similar to the DTDA materials are also feasible.

1.7 Diradical, Zwitterionic, and Neutral Closed Shell Configurations

Much of the work presented in this thesis (Chapters 3 to 6) focuses on molecular systems

[†] The IP-EA value of **I-12** is smaller than that of its 1,3,2-based counterpart.

that contain two 1,2,3-DTA rings. The nature of the interaction between the two unpaired electrons originating from the heterocycles of a bis(1,2,3-DTA) system is an important consideration. Both open shell and closed shell electronic configurations are possible for the neutral oxidation state. These electronic configurations are expected to give rise to significantly different bulk material properties. For example, a diradical material might be considered in terms of an NRC design. Furthermore, there exists the possibility of a single electron oxidation to a stable radical cation state. Consequently, these materials hold potential value as RIC donors.

The discussion concerning the nature of the electronic interaction between the two dithiazole rings of a bis(1,2,3-DTA) can be generalized by a two-electrons-in-two-orbitals (2-in-2) model. Given two molecular orbitals and two electrons, there are six different ways of arranging them while still obeying the Pauli exclusion principle, *i.e.*, there are six microstates.

$$N_m = \frac{n!}{e!(n-e)!} \qquad \textbf{Equation 1.17}$$

where N_m is the number of microstates, n is the number of available orbital sites (*i.e.*, twice the number of orbitals) and e is the number of electrons. In the case of two electrons and two orbitals, or four orbital sites, N_m is calculated to be six.

Two limiting cases can be envisaged for such 2-in-2 systems. The first is exemplified by the H_2 molecule, in which there is a large energy difference between the two orbitals in question. The second can be illustrated by O_2, in which the two relevant orbitals are degenerate. These models are representative of the two extremes of a continuum, from the case in which the orbital energy difference is significantly greater than the electron pairing energy to the case in which the orbital energy difference is zero.

In the H_2 model, two singly occupied 1s orbitals are brought into close proximity such that

orbital mixing occurs. Two molecular orbitals (MO) are created, one in-phase (bonding) at lower energy and one out-of-phase (antibonding) at higher energy. The ground state will be a singlet constructed of two electrons of opposite spins occupying the lowest lying MO. For H_2 under standard temperature and pressure conditions, this is indeed the case. The spin pairing energy is considerably less than the energy difference between the MO levels, therefore the lowest energy configuration is a closed shell singlet. However, there are five other possible states represented figuratively in **Figure 1.29**. These consist of three degenerate triplet states in which the electrons occupy separate orbitals in such a way as their spins do not cancel one another, one singlet state in which the spins of the electrons in the two orbitals do cancel out, and one singlet in which the electrons are paired in the higher lying MO.

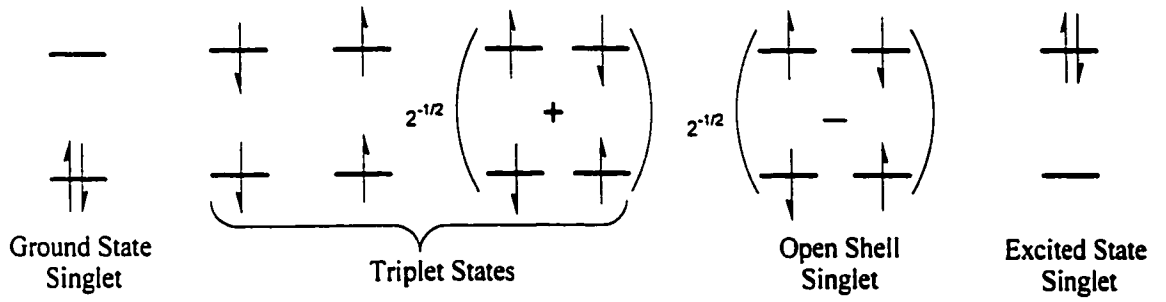

Figure 1.29 The six possible microstates for an H_2 molecule.

The 2-in-2 model could equally describe a simple diradical such as dioxygen (O_2). Again there are six microstates divided into a triplet set and three singlets. The two relevant orbitals are degenerate orthogonal antibonding π molecular orbitals which we shall designate π_x^* and π_y^* (where the z direction is the molecule axis.)

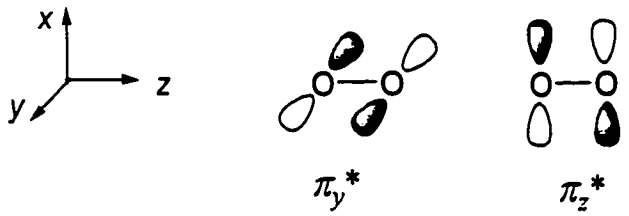

Figure 1.30 Real molecular orbitals of O_2 (adapted from Salem[42]).

In order to generate the six microstates, we must first construct two orbitals based on the sum and difference of the real orbitals π_x^* and π_y^*. This is akin to constructing the bonding and antibonding orbitals of H_2 from the 1s orbitals of each hydrogen atom. In this case, however, the resulting orbitals must be imaginary and cannot be represented as orbitals in real space. They are the equivalent of moving waves, sums and differences of which will generate real space standing waves that can be illustrated in a qualitative manner. The six microstates of O_2 are represented in **Figure 1.31**.

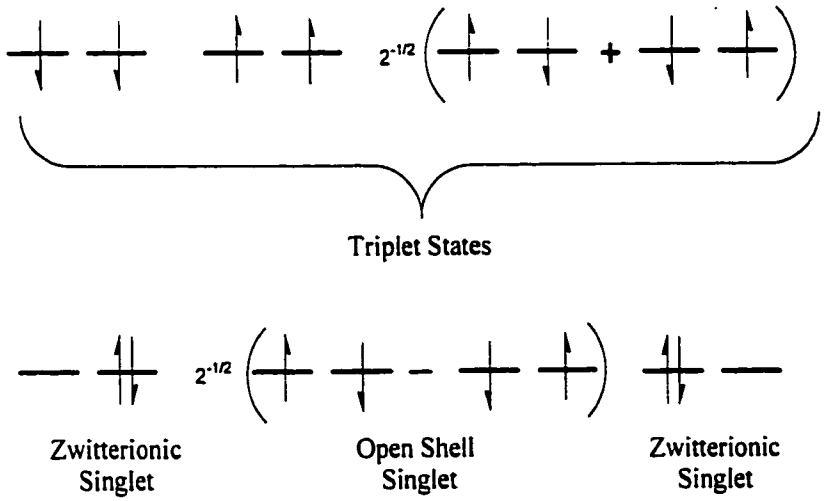

Figure 1.31 Figurative representation of the six microstates of O_2.

1.8 Quantum Calculations

Much of this project is centered around synthetic studies to determine the electron configurations of a variety of bis(1,2,3-DTA) systems. The use of computational methods presents another possible means of treating a problem concerning the electronic structure of a compound. While this thesis in no way claims to be a formal computational study of the molecular systems discussed herein, we have employed molecular modeling, using the Gaussian 98 for Windows (G98W) package, to guide our research and support our conclusions. In order to place the results of these computations in context, a brief and largely qualitative overview of these methods is appropriate.

1.8.1 Computational Methods[43]

We have made use of two main classes of calculation; semiempirical and density functional theory (DTF). The semiempirical methods include extended Hückel molecular orbital (EHMO) theory and modified neglect of differential overlap (MNDO) theory. EHMO has provided a language for the discussion of orbital interactions throughout this thesis. The use of MNDO is restricted to the calculations using the G98W package and has been employed in order to quickly obtain an appropriate input geometry (*i.e.*, a rough estimate of bond lengths and bond angles) for calculations using DFT.

Semi-empirical methods seek to approximate the Schrödinger equation by using parameters derived from experimental data. They are most meaningful when employed on the molecular ground state systems for which they are designed. Since most such methods are well-characterized and well-parameterized for small organics, it is foreseeable that they might deal poorly with systems that differ substantially from that format.

Ab initio methods, in general, do not use experimental parameters. Their computations are

based solely on the laws of quantum mechanics (*i.e.*, first principles). There is a large variety of methods currently in use, however this discussion is intended only to familiarize the reader with the computational approaches employed within our research. Therefore, only DFT is discussed herein.

Density functional theory (DFT) is an *ab initio* method which models electron correlation via general functionals[†] of the electron density. In practice, self-consistent DFT calculations are performed iteratively. We have employed DFT using the hybrid B3LYP functional as provided in the G98W suite of programs. These calculations have afforded reasonable and reliable estimates of molecular properties; notably spin densities, ionization potentials, and electron affinities. Furthermore, they have allowed us to compare the properties of known compounds with those of similar, but experimentally unknown, compounds.

1.8.2 Basis Sets

The computational model determines the form of the Hamiltonian-like operator in the Schrödinger equation but does not dictate the form of the wavefunction. This is accomplished by a choice of basis set, or function in which the molecular orbitals are expanded. In practice, any one of a number of basis sets can be applied to a chosen model.

Minimal basis sets use fixed-size atomic-type orbitals. The STO-3G basis set, for example, uses three primitive gaussian functions (GTOs) per basis function in order to approximate a Slater-type orbital (STO). It is worth noting that while STOs are a more accurate representation than the same number of GTOs, they are computationally much less convenient to use. Since an STO can be fit by a linear combination of GTOs, it is computationally preferable to use a large number of GTOs rather than a smaller number of STOs.

[†] A functional is a function of a function.

The first way that a basis set can be made larger, and thereby more realistic, is to increase the number of basis functions per atom. These so-called split-valence basis sets include 3-21G and 6-31G. They have two or more basis functions of different size for each valence orbital. The variational procedure can allow for modifications in the molecular orbital size through the weighting of one or the other basis function.

Polarized basis sets further improve the realism of the atomic orbitals by allowing a change in orbital shape. This is accomplished by adding orbitals with angular momentum beyond that which is required for the ground state. For example, in the 6-31G** (also known as the 6-31G(d,p) basis set), *p* functions are added to the hydrogen atoms and *d* functions are added to the heavier atoms such as carbon.

There are a variety of larger basis sets, each with characteristics designed mainly to improve the results for specific types of atoms or molecules. Diffuse functions (*e.g.*, 6-31++G*) use large-size (*i.e.*, small orbital exponent) *s*- and *p*- type functions to allow orbitals to occupy a larger region of space. This can be important for systems with electrons relatively far from the nucleus, for example weakly bound anions. There are also combinations of effective core potentials and valence basis sets (*e.g.*, LANL2DZ) generally employed for molecules containing post-third row elements. For heavy elements, the core potentials are usually fit to relativistic atomic orbitals thus introducing some relativistic effects into the calculation.

Although a larger basis set generally yields a more accurate calculation, it is accompanied by a computational time and memory penalty. In making the choice as to which basis sets we would use for our calculations, we weighed the computational costs versus the accuracy gained by increasing basis set size and determined that, for our purposes, the 6-31G** was sufficient.

References for Chapter 1

1. Dodabalapur, A.; Katz, H. E.; Torsi, L.; Haddon, R. C.; *Science*, **1995**, *269*, 1560.
2. Meyer, W. H.; *Synth. Metals*, **1985**, *10*, 255.
3. Sailor, M. J.; Curtis, C. L.; *Adv. Mater.*, **1994**, *6*, 688.
4. Garnier, F.; Hajlaoui, R.; Yassar, A.; Srivastava, P.; *Science*, **1994**, *265*, 1684.
5. Friend, R. H.; Burroughes, J. H.; *Faraday Discuss. Chem. Soc.*, **1989**, *88*, 213.
6. Bao, Z.; Lovinger, A.; Brown, J.; *J. Am. Chem. Soc.*, **1998**, *120*, 207.
7. Burt, F. P.; *J. Chem. Soc.*, **1910**, *97*, 1171.
8. Cohen, M. J.; Garito, A. F.; Heeger, A. J.; MacDiarmid, A. G.; Mikulski, C. M.; Saran, M. S.; Kleppinger, J.; *J. Am. Chem. Soc.*, **1976**, *98*, 3844.
9. Rawson, J. M.; Longridge, J. J.; *Chem. Soc. Rev.*, **1997**, 53.
10. Taliani, C.; Blinov, L. M.; *Adv. Mater.*, **1996**, *8*, 353.
11. Wu, M. W.; Conwell, E. M.; *Chem. Phys. Lett.*, **1997**, *266*, 363.
12. Katz, H. E.; *J. Mater. Chem.*, **1997**, *7*, 369.
13. Bryce, M. R.; *Chem. Soc. Rev.*, **1991**, *20*, 355.
14. Ferraris, J.; Cowan, D. O.; Walatka, Jr., V.; Perlstein, J. H.; *J. Am. Chem. Soc.*, **1973**, *95*, 948.
15. Phillips, T. E.; Kistenmacher, T. J.; Ferraris, J. P.; Cowan, D. O.; *J. C. S. Chem. Commun.*, **1973**, 471.
16. Engler, E. M.; *Chemtech*, **1976**, 274.
17. Haddon, R. C.; Hebard, A. F..; Rosseinsky, M. J.; Murphy, D. W.; Duclos, S. J.; Lyons, K. B.; Miller, B.; Rosamilia, J. M.; Fleming, R. M.; Kortan, A. R.; Glarum, S. H.; Makhija, A. V.; Muller, A. J.; Eick, R. H.; Zahurak, S. M.; Tycko, R.; Dabbagh, G.; Thiel, F. A.;

Nature, **1991**, *350*, 321.

18. Haddon, R. C.; Perel, A. S.; Morris, R. C.; Palstra, T. T. M.; Hebard, A. F; *Appl. Phys. Lett.*, **1995**, *67*, 121.

19. Fleming, R. M.; Ramirez, A. P.; Rosseinsky, M. J.; Murphy, D. W.; Haddon, R. C.; Zahurak, S. M.; Makhija, A. V.; *Nature*, **1991**, *352*, 787.

20. a) Haddon, R. C.; *Nature*, **1975**, *256*, 394. b) Haddon, R. C.; *Aust. J. Chem.*, **1975**, *28*, 2343.

21. Burdett, J. K.; *Chemical Bonding in Solids*, Oxford University Press, N. Y., **1995**, 39.

22. (a) Wigner, E.; Huntington, H. B.; *J. Chem. Phys.*, **1935**, *3*, 764. b) Barbee, III, T. W.; García, A.; Cohen, M. L; *Phys. Chem. Rev.*, **1989**, *62*, 1150. c) Kaxiras, E.; Broughton, J.; Hemley, R. J.; *Phys. Chem. Rev.*, **1991**, *67*, 1138.

23. Peierls, R. E.; *Quantum Theory of Solids*, Oxford University Press, N. Y., **1955**.

24. Burdett, J. K.; *Chemical Bonding in Solids*, Oxford University Press, N. Y., **1995**, 51.

25. Burdett, J. K.; *Chemical Bonding in Solids*, Oxford University Press, N. Y., **1995**, 78 and 157.

26. Burdett, J. K.; *Chemical Bonding in Solids*, Oxford University Press, N. Y., **1995**, 81.

27. Cox, P. A.; *The Electronic Structure and Chemistry of Solids*, Oxford University Press, N. Y., **1987**,137.

28. Miller, J. S.; *Ann. N. Y. Acad. Sci.*, **1978**, *313*, 25.

29. Torrance, J. B.; *Accounts of Chem. Res.*, **1979**, *12*, 79.

30. a) Bechgaard, K.; Jacobsen, C. S.; Mortensen, K.; Pedersen, H. J.; Thorup, N.; *Solid State Comm.*, **1980**, *33*, 1119. b) Jacobsen, C. S.; Mortensen, K.; Thorup, N.; Tanner, D. B.; Weger, M.; Bechgaard, K.; *Chem. Scr.*, **1981**, *17*, 103. c) Torrance, J. B.; Pedersen, H. J.; Bechgaard, K.; *Phys. Rev. Lett.*, **1982**, *49*, 881. d) Bechgaard, K.; Carneiro, K.; Eg, O.;

Olsen, M.; Rasmussen, F. B.; *Mol. Cryst. Liq. Cryst.*, **1982**, *79*, 271. e) Guy, D. R. P.; Boebinger, G. S.; Marseglia, E. A.; Friend, R. H.; Bechgaard, K.; *J. Phys. C: Solid State Phys.*, **1983**, *16*, 691.

31. Kurmoo, M.; Day, P.; Guionneau, P.; Bravic, G.; Chasseau, D.; Ducasse, L.; Allan, M. L.; Marsden, I. D.; Friend, R. H.; *Inorg. Chem.*, **1996**, *35*, 4719.

32. Torrance, J. B.; Mayerle, J. J.; Lee, V. Y.; Bechgaard, K.; *J. Am. Chem. Soc.*, **1979**, *101*, 4747.

33. Torrance, J. B.; *Ann. N. Y. Acad. Sci.*, **1978**, *313*, 210.

34. Torrance, J. B.; from an article in *Molecular Metals*, Hatfield, W. E., Ed.; Plenum Press, NY, **1979**, 7.

35. Fritchie, C. J., Jr.; *Acta Cryst.*, **1966**, *20*, 892.

36. Yamashita, Y.; Tomura, M.; *J. Mater. Chem.*, **1998**, *8*, 1933.

37. Personal communication with Prof. R. C. Haddon, 03/2000.

38. Goto, K.; Kubo, T.; Yamamoto, K.; Nakasuji, K.; Sato, K.; Shiomi, D.; Takui, T.; Kubota, M.; Kobayashi, T.; Yakusi, K.; Ouyang, J.; *J. Am. Chem. Soc.*, **1999**, *121*, 1619.

39. Chi, X.; Itkis, M. E.; Patrick, B. O.; Barclay, T. M.; Reed, R. W.; Oakley, R. T.; Cordes, A. W.; Haddon, R. C.; *J. Am. Chem. Soc.*, **1999**, *121*, 10395.

40. Barclay, T. M.; Cordes, A. W.; Haddon, R. C.; Itkis, M. E.; Oakley, R. T.; Reed, R. W.; Zhang, H.; *J. Am. Chem. Soc.*, **1999**, *121*, 969.

41. (a) Behringer, H.; Meinetsberger, E.; *Tetrahedron Lett.*, **1975**, *40*, 3473. (b) Behringer, H.; Meinetsberger, E.; *Liebigs Ann. Chem.*, **1981**, 1928.

42. Salem, L.; *Electrons in Chemical Reactions: First Principles*, John Wiley & Sons, New York, **1982**, pp. 69-72.

43. Foresman, J. B.; Frisch, Æ.; *Exploring Chemistry with Electronic Structure Methods, Second Ed.*, Gaussian, Inc., Pittsburgh, PA, **1996**.

Chapter 2 Exploration of New Heterocyclic Electron Acceptors

2.1 Introduction

The majority of this thesis focuses on the design of new electron donors in CT salts for RICs and novel neutral radical molecular materials with prospective uses as NRCs. This chapter, however, stands apart in that the impetus leading to the research herein is the exploration of novel electron acceptors. While the literature surrounding the study of CT salts is replete with examples of variations on the classic TTF electron donor structure,[1, 2, 3] it is only relatively recently that a significant proportion of the research has been directed towards broadening the scope of possible acceptor design.[4, 5, 6] This is due, in large part, to the recognition that the conductivity in most CT salts occurs exclusively through interactions between the donor radical cations.[7] The class of CT materials known as Bechgaard salts[8, 9] goes as far as replacing the acceptor (*eg.* **II-1**) with a simple, closed shell counteranion such that the magnetic and conductive properties of the resulting material must arise solely from interactions between the radical cations of the incorporated donor molecules. Highly conductive acceptor-based versions of the Bechgaard design are currently emerging in the literature.[10] These involve an acceptor molecule, with a stable radical anion oxidation state, crystallized in a 2:1 ratio with a simple cation.

The more widely known acceptor materials are usually designed around a quinoid framework. Popular examples include TCNQ (**II-1**) and chloranil (**II-2**).[4] Heterocyclic systems such as **II-3** are also known to have accessible stable radical anion oxidation states and therefore may be capable of acting as a CT electron acceptor.[11] The most widely recognized non-quinoid electron acceptor is C_{60}.[12] Thin films of this fullerene have been shown to possess semi-conducting properties whereby electron transport (as opposed to hole transport) is responsible for the conductivity.

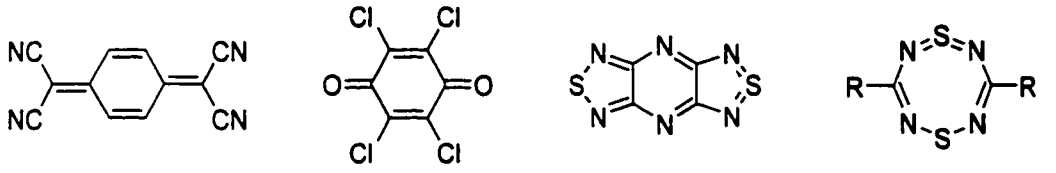

II-1 II-2 II-3 II-4

Figure 2.1 Examples of three known electron acceptors and the proposed building block for another type of molecular acceptor, **II-4**.

This chapter is devoted to the discussion of 1,5-dithia-2,4,6,8-tetrazocine (**II-4**) derivatives and our attempts at designing a novel electron acceptor incorporating this heterocycle. The key to this investigation lies in answering the question: "Can the planar, aromatic **II-4** heterocycle be oxidized such that the resulting electronic structure is best described as a quinoid formulation?"

2.1.1 Quinones

Hydroquinones can be defined as aromatic compounds that have hydroxyl and/or amino groups *ortho* or *para* to each other.[13] The two-electron oxidation of a hydroquinone (*i.e.*, the removal of two hydrogens) generates a quinone. These compounds first gained attention in two ways: as pigments, such as henna, and as drugs (various plants containing quinones, such as rhubarb, have been used as purgatives for thousands of years.)[14] Today, quinones are no less important as modern vat dyes[15†] and as antitumor agents,[16] as well as having applications as semiconductors,[17] photographic materials, pleochroic dyes in liquid crystal displays,[18] and artificial photosynthetic systems.[19,20]

Quinones can be thought of as two-stage Wurster type redox systems, meaning that they

---

† "Vat dye: A class of insoluble dyes applied by first reducing them to derivatives that are soluble in dilute alkali. In this condition they have a great attraction for certain fibres, such as cotton. The solution is applied to the material and the insoluble dye is regenerated in the fibres by atmospheric oxidation. Indigo and indanthrene are examples." - *The Facts on File Dictionary of Chemistry*, John Daintith, Ph.D. Ed., Facts on File, N. Y., **1988**.

have end groups, involved in the redox reaction, that are located outside a cyclic π system that has aromatic character in the reduced form. The two-stage reduction of a quinone gives first a radical anion and then a dianion, both of which have aromatic character. Cyclic voltammetry is commonly used to characterize the redox behaviour of such systems. The presence of a radical anion, known as a semiquinone, after the first reduction step is verifiable by EPR spectroscopy. Furthermore, the two stage mutual interconversion between a quinone and its respective dianion can be readily monitored by ultraviolet spectrophotometry as both species are highly conjugated.

The redox behaviour of the simple 1,4-benzoquinone (**II-5**) has been studied extensively. One of the findings of interest is that the electrochemical behaviour of this system in aprotic solvents differs greatly from what it is in protic solvents. The quinone electrode does not function reversibly in aprotic solvents, and the general two-step reduction is as follows:

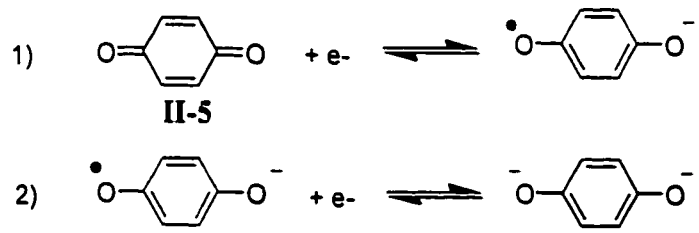

Figure 2.2 The two-step redox process of benzoquinone in an aprotic solvent.

With the addition of a proton donor, the second step shifts to a more positive potential, eventually merging with the first to produce the reversible two electron process observed in aqueous systems. In solvents such as DMF, CH_3CN, and DMSO, the fully reduced species, known as the hydroquinone, does not exhibit oxidation waves in the polarogram in a potential range corresponding to the reduction waves of the quinone. This observation suggests[21] that the radical that is formed when the hydroquinone undergoes a one-electron oxidation dimerizes and that this

dimer subsequently decomposes to form one molecule of quinone and one of hydroquinone, *i.e.*, it undergoes a disproportionation reaction.

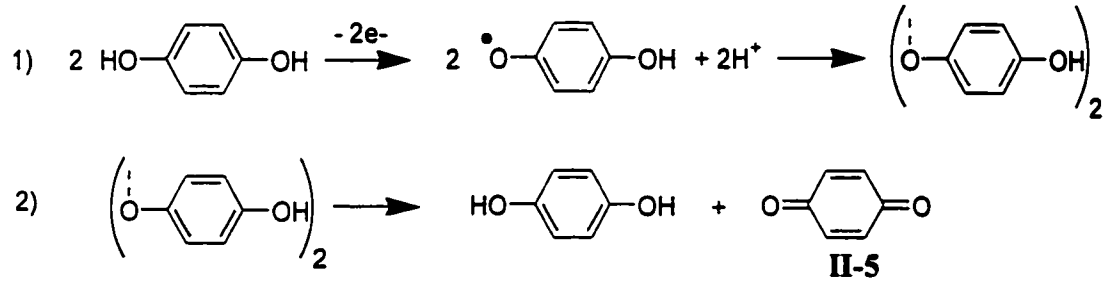

Figure 2.3 The quinone/hydroquinone redox process in non-aqueous polar solvents.

The ability of quinones to undergo reduction to the semiquinone augers well for their use as electron acceptors. Upon reduction, the incoming electron enters the LUMO of the quinone, a low-lying π^* type orbital. The lower the LUMO, the higher is the expected electron affinity and the greater is the ease of reduction. As with most substituted aromatic compounds, the introduction of electron-withdrawing groups to 1,4-benzoquinone (**II-5**) increases the electron affinity. Conversely, alkyl substitution generally leads to a decrease of electron affinity.

1,4-Benzoquinone (**II-5**) has a very large positive electron affinity (+48.4 kcal mol^{-1}).[22,†,††] This is due in great part to the presence of two highly electronegative oxygen atoms. While the unpaired electron of the semiquinone occupies the molecular π^* LUMO and is thus delocalized over the entire π system, the negative charge is largely located at the two oxygen atoms.[23] One consequence of the localization of charge in the radical anion is a decrease of electron affinity upon

---

† Note that for electron affinity, a release of energy is considered to be a positive value. This convention runs counter to most energy conventions. Orchin, M.; Kaplan, F.; Macomber, R. S.; Wilson, R. M.; Zimmer, H.; *The Vocabulary of Organic Chemistry*, John Wiley & Sons, N.Y., **1980.**

†† Compare this with -26 kcal mol^{-1} for benzene in the gas phase. (a) McClelland, B. J.; *J. Chem. Phys.*, **1967**, *46*, 4158.(b) Nenner, I.; Schulz, G. J.; *J. Chem. Phys.*, **1975**, *62*, 1747.

expansion of the π system from benzoquinone (**II-5**) to naphthoquinone (**II-6**) to anthroquinone (**II-7**). This trend is the opposite of that of the electron affinities of benzene, naphthalene, and anthracene, which increase in this order as the negative charge in the radical anions can be spread out over the entire molecule.

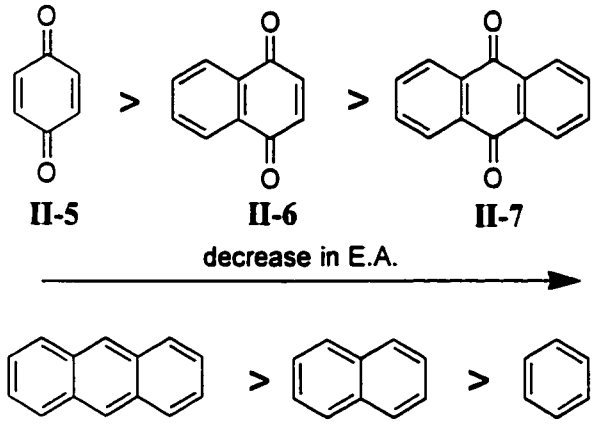

Figure 2.4 Electron affinity trends in quinones and their hydrocarbon counterparts.

2.1.2 Other Quinoid Structures

Extended quinones are those quinones which bear the quinonoid carbonyl groups in different rings. The simplest example of an extended quinone is diphenoquinone (**II-8**). As compared with 1,4-benzoquinone (**II-5**), diphenoquinone (**II-8**) shows a decrease in the degree of bond fixation. The degree of conjugation between the two rings is similar to biphenyl.[14,24]

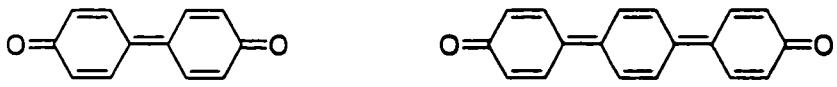

II-8 **II-9**

Figure 2.5 Diphenoquinone and the unknown triphenoquinone.

Like quinones, diphenoquinones are generally strong electron acceptors capable of being reduced to semiquinone radicals and then to diphenols. The ion-radical salts of diphenoquinones

have been found to be organic conductors.[25] An extended π system is an asset in the design of conducting materials as it stabilizes the radical oxidation state. This increase in the stability of extended quinones is important. The next logical step in extending the quinonoid system would be to make triphenoquinone (**II-9**). This, however, has never been accomplished. In order to oxidize the parent triphenohydroquinone, the aromatic stabilization energy of three benzene rings must be overcome.

In order to extend the diphenoquinone (**II-8**) system to include a third ring, a less aromatic heterocycle, such as thiophene, may be employed instead of benzene (compare the resonance energy of benzene at 36 kcal mol^{-1} to that of thiophene at 29 kcal mol^{-1}).[26] The resulting three-ring 2,5-bis(4-oxo-2,5-cyclohexadien-1-ylidene)-2,5-dihydrothiophene (**II-10**) exhibits the expected reversible two-step redox behaviour.[27]

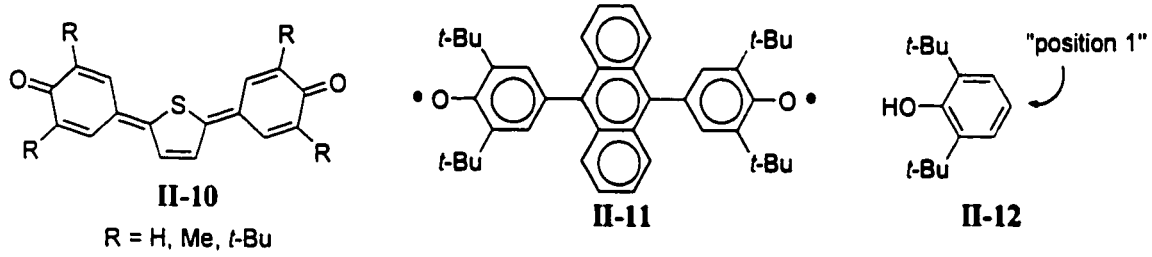

Figure 2.6 Known triphenoquinone analogues.

Another possible triphenoquinone analogue, in which the central benzene ring is replaced by anthracene, has been prepared by West and Jorgensen.[28] In this case, however, the structure of the oxidized species is reported as a diradical (**II-11**) rather than as a quinone, with an ESR spectrum as proof.

In the synthesis of **II-11**, as with many extended quinone systems, substituents at the 3- and 5- positions of the outermost benzene ring may be necessary. *tert*-Butyl groups are commonly

used as a steric "block" to prevent reaction at these positions. This promotes reaction at the 1-position when substituting the **II-12** group onto the central ring and inhibits side reactions of the addition type when oxidizing the hydroquinone to the quinone. Substituents can also be used to increase the solubility of these compounds and in some cases to facilitate identification by ^{1}H and ^{13}C NMR. However, large substituent groups have certain drawbacks. If the compound is intended for use in materials, a large *tert*-butyl group will increase the stacking space between molecules and thus decrease any desirable intermolecular interactions, precluding semiconduction.

2.1.3 Dithiatetrazocines

2.1.3.1 Discovery of a New Ring System

The discovery, in the mid-1970s, of the metallic and superconducting properties of the $(SN)_x$ polymer[29] prompted a great deal of research into thiazyl linkages (-S=N-). The Woodward group[30] was among the research teams investigating the possible synthesis of organic conductors based on the $(SN)_x$ model. Linear polymers **II-14** seemed promising candidates for conductivity. One suggested synthesis of these polymers was via intermediates such as **II-13**, and it was proposed that these intermediates should be the product of a reaction between two equivalents of an amidine and one of sulfur chloride.

However, the reaction of amidine with sulfur chloride does not produce **II-14**. Instead, an interesting, novel heterocycle has been isolated in low yield. This was the birth of the 1,5,2,4,6,8-dithiatetrazocine ring system **II-4**.

When benzamidine is used as the reagent amidine, the product **II-4b** is found to have a planar central heterocyclic ring, with the two phenyl rings distorted out of its plane by only 9.7°. All the S-N bond lengths are equal with an average observed S-N distance of 1.5645(60) Å.

Similarily, all the C-N bond lengths are found to be equal at 1.323(4) Å. This structural evidence is compatible with a delocalized, aromatic 10 π electron system.

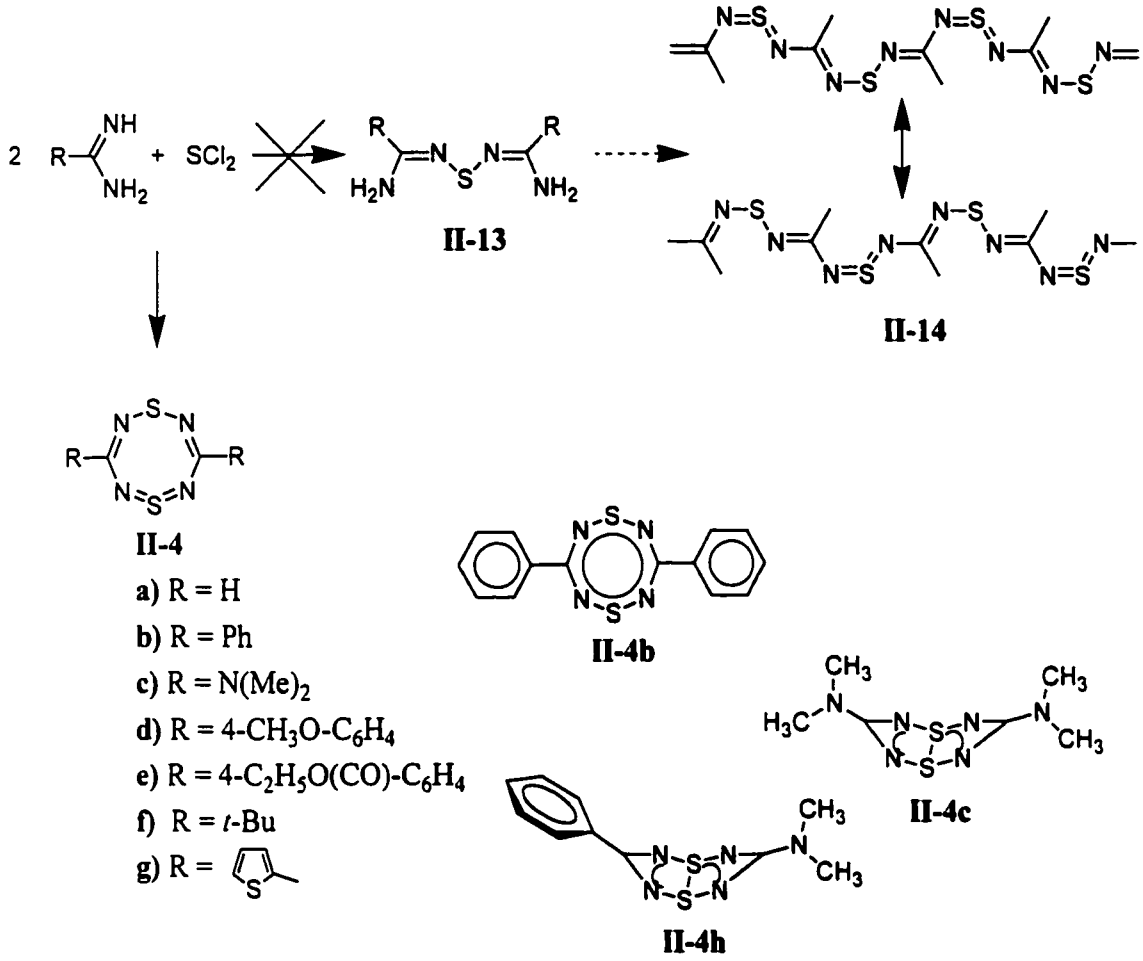

Figure 2.7 Attempted synthesis of $(SN)_x$ -type intermediates affords **II-4**.

Woodward *et al.*[30] attempted, unsuccessfully, to make the parent 1,5,2,4,6,8-dithiatetrazocine (**II-4a**, R=H) but did manage to make the dimethylamino substituted 3,7-bis(dimethylamino)-1,5-dithia-2,4,6,8-tetrazocine **II-4c** in relatively good yield. To their surprise, this compound was found to be very different from the phenyl-substituted derivative. To begin with, the ultraviolet spectrum of **II-4b** shows absorption maxima at 409, 318, 306.5, 294.5, 281,

and 271.5 nm whereas **II-4c** shows only a maximum at 229 nm in its ultraviolet spectrum. In contrast to the planar structure of **II-4b**, the crystal structure analysis of **II-4c** reveals it to be bent at the sulfur atoms into two planes at an angle of approximately 101°. All the S-N bond lengths are equal, although at 1.605 Å they are longer than those in **II-4b**. The C-N bond lengths too are equal, including the bond between the dithiatetrazocine ring carbons and the dimethylamino substituents. At 1.348 Å, these are again longer than those in **II-4b**.

Another remarkable structural feature of **II-4c** is the short S-S distance (2.428 Å) between the sulfur atoms across the ring. Although this is not in the range of the disulfide bond in, for example, S_8 (2.07 Å in the gas phase)[31], it is much shorter than the sum of two van der Waals radii for sulfur (3.6 Å)[32] indicating at least partial bonding between the sulfur atoms.

Woodward *et al.*[30] explored the thermal and chemical stability of the **II-4b** compound in an effort to come up with a general idea of its properties. They found that it is remarkably heat-stable, decomposing to benzonitrile only after prolonged heating, neat, at 220-240° C. **II-4b** is easily oxidized with KOH or HCl in aqueous dioxane, but not with *meta*-chloroperbenzoic acid in boiling methylene chloride. It is also unreactive toward *substoichiometric* amounts of several nucleophiles (benzylamine, lithium benzothiazolyl-2-mercaptide, sodium hexamethyldisilazane, butyllithium) in nonpolar solvents (benzene, toluene, and xylene.) Finally, neither **II-4b** nor **II-4c** show any basic properties when titrated with $HClO_4$ in AcOH-C_6H_5Cl. In the case of **II-4c**, this indicates partial delocalization of the free electron pairs on the dimethylamino substituents into the dithiatetrazocine ring system.

2.1.3.2 Synthetic Studies of Dithiatetrazocines

In order to further the study of this novel **II-4**, Woodward *et al.*[30] deemed it important to synthesize **II-4** with various substituents other than the original phenyl and dimethylamino groups

and thus develop a pattern of substituent effects. They reported the synthesis of the 3,7-bis(*para*-methoxy)phenyl- **II-4d** and the 3,7-bis(*para*-ethoxycarbonyl)phenyl- **II-4e** substituted compounds, both of which are planar with ultraviolet spectra that closely resemble that of the 3,7- diphenyl-derivative, **II-4b**.

In the last twenty years, other derivatives of **II-4**, with various substituents, have been characterized. Gleiter *et al.* reported[33] the synthesis of the 3,7-di-*tert*-butyl derivative **II-4f** which they have found to exist in the 10π electron planar arrangement. The aromatic nature of this compound, and that of the original diphenyl substituted **II-4b**, was later investigated by magnetic circular dichroism.[34] The MCD spectra of the two compounds show a high molar ellipticity characteristic of the ring current of a strongly aromatic system.

In 1989, Amin and Rees[35] prepared 3,7-di(2-thienyl)-1,5,2,4,6,8-dithiatetrazocine **II-4g** as the minor product of a reaction between 2-thienylamidine and sulfur dichloride in the presence of DBU. The long wavelength absorption pattern of this compound's ultraviolet spectrum indicates that it, too, exists in the 10 π planar structure. Attempts to oxidize the thiophene rings with MCPBA and N_2O_4 with the intent of obtaining the parent ring **II-4a** were unsuccessful. In the same paper, Amin and Rees reported the synthesis of the first unsymmetrically substituted dithiatetrazocine **II-4h**. The complete lack of long wavelength absorptions in the ultraviolet spectrum of this unsymmetrically substituted compound indicates that one dimethylamino substituent is sufficient to buckle the dithiatetrazocine ring into the folded conformation.

One important advancement since the initial discovery of the **II-4** systems is the development of two high yield synthetic routes to the planar aryl substituted 10 π **II-4** by Boeré *et al.* in 1993.[36] The first route (**Figure 2.8**) involves a reaction of triphenylantimony with the diaminodithiadiazolium salt **II-15** in the presence of O_2 to give **II-4** product in 40-60% yield. In the second, the same chloride salts are reacted with silylated amidines $XC_6H_4C(NSiMe_3)N(SiMe_3)_2$

in a 1:1 molar ratio affording a 18-65% product yield. Both methods were used to synthesize **II-4b(i-vi)**. Neither method, however, successfully generated 3,7-di-*tert*-butyl-1,5,2,4,6,8-dithiatetrazocine **II-4f**.

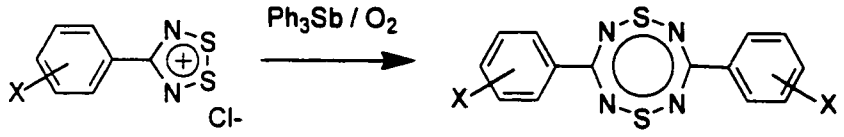

II-15 **II-4b**

i) X = H
ii) X = 4-CH_3
iii) X = 4-CH_3O
iv) X = 4-Cl
v) X = 4-CF_3
vi) X = 3-CF_3

Figure 2.8 High yield synthetic route to aryl **II-4**.

An interesting experiment was reported by Pascal, Jr. in 1993[37] in order to address the question: "Do the bent dithiatetrazocines retain any aromatic character, and, in particular, a ring current?" A cyclophane **II-16** containing the dithiatetrazocine ring was prepared and isolated and the ^{1}H NMR spectrum of the compound was recorded. The chemical shifts of the six internal methylene groups of the bridging chain were found to be in the 0.9-1.6 ppm range providing no evidence of a ring current in these bent systems.

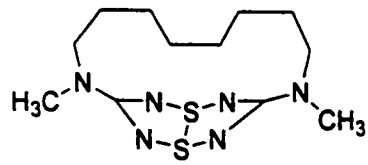

II-16

Figure 2.9 Cyclophane containing dithiatetrazocine.

In 1994, Pascal, Jr. and L'Esperance[38] prepared 3,7-bis(butyl(methylamino))- 1,5,2,4,6,8-dithiatetrazocine in order to study relative rates of amine rotation and ring inversion by ^{1}H NMR. They concluded that bent dithiatetrazocines show both *cis/trans* (amine rotation) and ring inversion isomerism on the NMR time scale but the activation energies of the two are too low to permit the isolation of stereoisomers at room temperature.

2.1.3.3 Molecular Orbital Studies

2.1.3.3.a A_8 Ring vs. A_4B_4 Ring

Many of the earlier studies involving the **II-4** systems focused on the molecular orbital energy levels[39,40,41] and, in particular, how they differ in the planar 10 π electron configuration and the bent 8 π electron conformation (two of the electrons having been used up to form the S-S transannular σ bond.) At the Hückel level, both the HOMO and the LUMO in a planar A_8 ring, with 10 π electrons, are doubly degenerate orbitals. For an A_4B_4 planar ring with alternating elements A and B, $S_4N_4^{2+}$ for example, the HOMO is no longer degenerate owing to a difference in electronegativities of the two elements. Which of the two orbitals is now the HOMO depends on the relative electronegativities of A and B. In considering our example $S_4N_4^{2+}$, we ought to be aware that there exists some degree of disagreement about which is, in general, the more electronegative, sulfur or nitrogen. For our purposes, we will employ the VOIPs[42] which indicate that the 2p orbital of nitrogen lies slightly below the 3p orbital for sulfur making nitrogen the more electronegative element. This gives reason to believe that, in $S_4N_4^{2+}$, the orbital with electron density on the sulfur atoms alone should be slightly higher in energy and therefore should be the HOMO. This is in agreement with the observed perturbative effects of ligands on the isolobal ring of $RC(NSN)_2CR$ type molecules **II-4**. If the opposite were true and the orbital with electron density on the four nitrogens was the HOMO, changing the ligand from R = Ph to R = NMe_2

would have no effect on the ring as, in this orbital, there are nodes at the ligand binding sites. There would be no overlap of ligand and ring orbitals implying that, to the first order, the two would not interact electronically. Since the orbital with electron density on the sulfur and carbon atoms is in fact the HOMO, the ring can be stabilized in the planar 10 π electron conformation by electron withdrawing ligands or folded into the butterfly conformation by electron donating ligands such that a transannular S-S σ bond is created as a result of "dumping" extra electron density on these atoms.

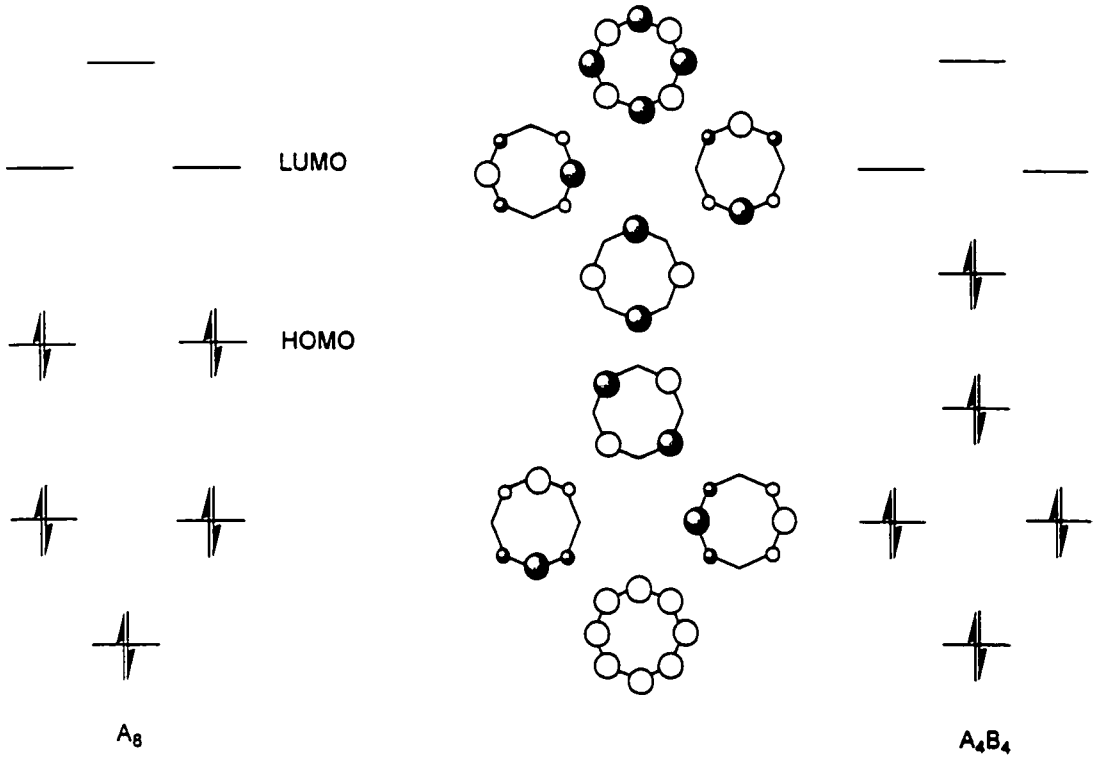

Figure 2.10 Hückel molecular orbital energy levels for the π system of A_8 and A_4B_4.

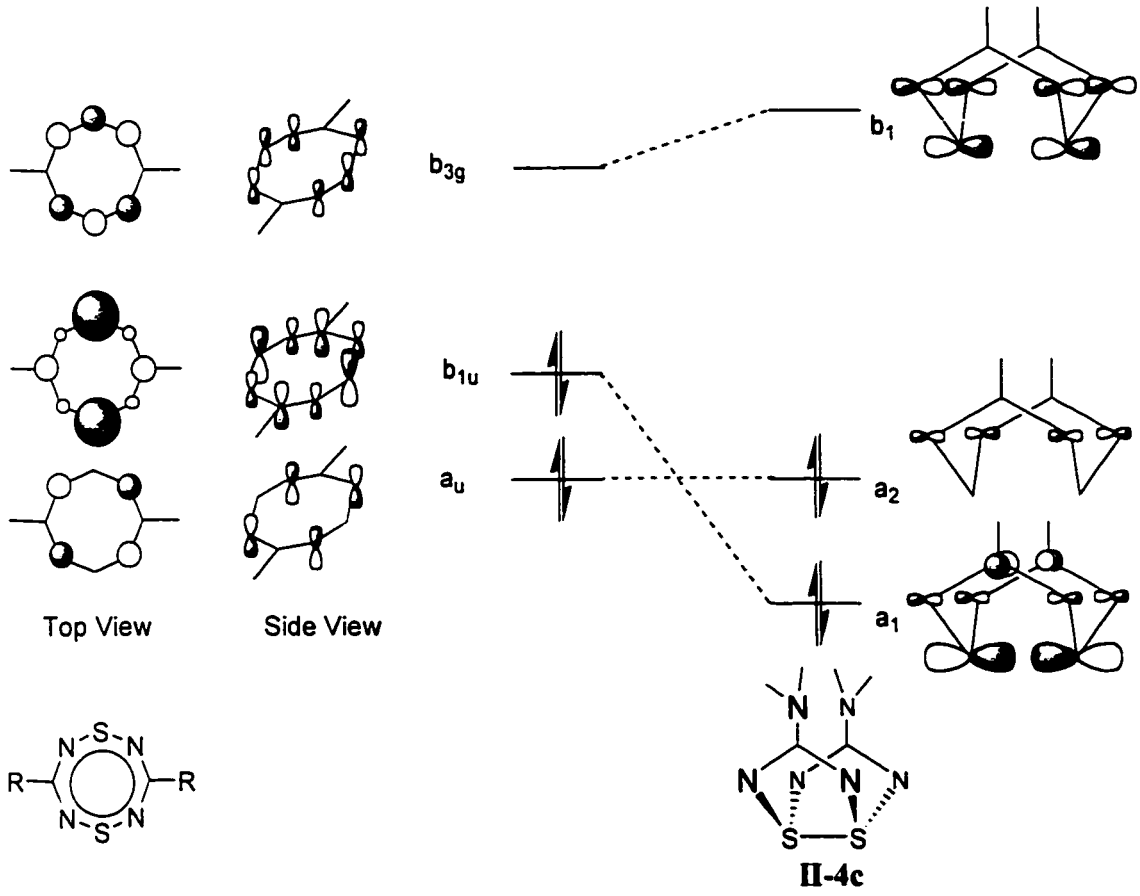

Figure 2.11 Frontier orbitals of the planar and bent dithiatetrazocines.

2.1.3.3.b E(NSN)$_2$E Ring

For the general E(NSN)$_2$E ring **II-17**, where E is some element, the Hückel π energy levels depend on three Coulomb parameters: α_E, α_S, α_N. It is the value of α_E that will vary according to the electronegativity of the element in the 3- and 7- positions. Examples that have been studied are E = phosphorus (*eg.* $Me_2P(NSN)_2PMe_2$), sulfur (*eg.* $S_4N_4^{2+}$), and carbon (*eg.* **II-4b** and **II-4c**). The S-S σ bond in the bent structure correlates with the π^* HOMO of the planar structure. According to VOIPs,[42] the sulfur 3p orbital lies below the carbon 2p orbital which in turn lies far below the phosphorus 3d orbital. The trend for the Coulomb parameters of E = C, P,

and S in this ring should then be $\alpha_S < \alpha_C < \alpha_P$.† Since the HOMO of the planar model is stabilized by more electronegative values of α_E, it is expected that it will be favoured most for E = S. Indeed, the $S_4N_4^{2+}$ cation is planar. The dependence of $RC(NSN)_2CR$ type molecules on the nature of the ligand R has already been discussed. Here, it suffices to say that these molecules can assume either the planar or the bent structure provided the ligand is either electron withdrawing or electron donating, respectively. Molecules of the type $R_2P(NSN)_2PR_2$ are generally bent.[39]

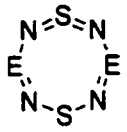

II-17

Figure 2.12 General $E(NSN)_2E$ ring.

2.1.3.3.c. Planar *vs.* Non-planar

In the HOMO of the planar structure, the electron density is concentrated on the sulfurs and carbons. When an electron donating ligand is present on the carbons, a sulfur-sulfur bond is formed and this orbital drops in energy. The orbital immediately beneath the HOMO in the planar structure, with electron density concentrated on the nitrogen atoms, is not, to the first order, affected by the change in conformation to the butterfly structure and it becomes the HOMO.

2.1.3.4. Reactivity Studies

For **II-4** in the planar conformation, the LUMO (b_{2g}) has a node at the carbon atoms. This implies that, to the first order, the LUMO would not be affected by changes made to the ligand. The reduction potential of the ring should remain relatively unchanged for all ligands. The HOMO,

† Recall that α is a negative number.

on the other hand, interacts electronically with the ligand orbitals. The oxidation potential of the ring is therefore sensitive to the nature of the ligand. The bent and planar structures of **II-4** would be expected to have different redox chemistry on the basis of their differing frontier orbitals. This, indeed, seems to be the case. The bent structure has proven to be subject to oxidation, whereas the planar structure is not easily oxidized. For example, a study published in 1987 by Oakley *et al.*[43] reported that while the S-S σ bond of the bent $Me_2NC(NSN)_2CNMe_2$ **II-4c** was oxidized by both an electrophilic oxidant (Cl_2 in CH_3CN) and a nucleophilic oxidant ($ON(CF_3)_2$), the planar $PhC(NSN)_2CPh$ **II-4b** was unreactive in the face of either. In both trial oxidations of **II-4c**, the oxidant added to the sulfurs rather than producing the radical cation or the dication and the resulting compounds were folded. It might, however, be expected that the radical cation $[Me_2NC(NSN)_2CNMe_2]^+$ should fall back into the planar (in this case 9 π electron) conformation, but as the cation has never been isolated, this expectation has never been verified.

Little work has been done on the chemical reactivity of the planar **II-4** owing to difficulties, only recently overcome,[36] in obtaining a sufficient synthetic yield of this material. However, electrochemical studies, in particular cyclic votammetry experiments, have been performed[36] in order to assess the redox behavior of this system and compare it to that of the folded system. It was found that both planar and folded compounds undergo a fully reversible one-electron reduction. The reduction potentials of the aryl planar systems tested (**II-4b(i-vi)**) exist within a narrow range (-0.90 to -1.02 V *vs.* SCE). The folded dimethylamino compound **II-4c**, in comparison, has a significantly lower reduction potential (-1.36V). Neither of the two types gave reversible oxidations at ambient temperatures and slow scan rates. It was found that oxidation of the planar structure was highly ligand-dependent, with oxidation potentials ranging from +1.54 V for **II-4b(iii)** to + 2.05 V for **II-4b(iv)**. For the bent structure, the oxidation potential was found to be lower (+1.28 V) implying that it is much more easily oxidized.

These results show that both the planar and the bent compounds have remarkably large thermodynamic stability "windows". The width of this window ranges form 2.49 to 2.96 V depending on substituents for the planar compounds and 2.63 V for the folded compound. The entire window for the folded structure is shifted toward negative potentials with respect to the planar structure indicating its relative ease of oxidation.

2.2 Attempts at Preparing Quinone/Hydroquinone Systems based on II-4

To date, only two conformations, the planar aromatic and the butterfly, are known for dithiatetrazocines. The question remains whether, like other aromatic rings, the planar conformation of **II-4** can be oxidized to a quinoid formulation. Our particular interest in this investigation is the possibility of developing a novel quinone/hydroquinone system with a potential application as the acceptor molecule in CT salts. In order for **II-4** to be feasibly considered in this role, a stable quinone must be accessible from the hydroquinone by a two-step oxidization via a semiquinone intermediate.

In our opinion, the most facile starting point for this inquiry was to prepare the hydroquinone **II-18** from which the quinone **II-19** is the expected oxidation product. As the planar 3,7-$(XC_6H_4)_2(CN_2S_2N_2C)$, X = 4-CH_3O, **II-4b(iii)**, has previously been characterized, it seems reasonable to think that the hydroquinone, X = 4-HO, **II-18** should be attainable. Furthermore, the successful oxidation of **II-18** would give enormous insight into the aromatic stability of **II-4** simply by analogy to similar known structures. The thiophene analogue **II-20**, for example, has recently been prepared and characterized,[27] while the triphenoquinone **II-9** is as yet unknown. The anthracene analogue **II-11** has been isolated,[28] however it appears to exist as a diradical rather than as a quinone, according to ESR data.

To our immediate disadvantage, however, is the high oxidation potential of known

aromatic **II-4** as studied by cyclic voltammetry. Granted, the methoxy analogue, **II-4b(iii)** has the lowest anodic potential of any of those measured, however it is still relatively high at +1.54 V *vs.* SCE. Furthermore, this oxidation is electrochemically irreversible, which although it does not rule out reversibility by chemical oxidation, neither does it support the possibility of a chemically reversible oxidative process.

In the course of this investigation, we isolated and characterized the hydroquinone **II-18**, and all the intermediates in the synthesis thereof. However, our many and varied attempts at oxidizing this material to the quinone **II-19** failed. Substitution of the peripheral phenol rings with *tert*-butyl groups in the 3- and 5- positions was briefly pursued in an attempt to block those sites from possible oxidative addition. This avenue was abandoned in favour of replacing the phenyl rings with a less aromatically stabilized heterocycle such as thiophene.

The thiophene substituted **II-4g** has been previously reported in low yield by Rees *et al.*[35] We developed a synthetic route to this material that affords a reasonable yield of a crystalline material suitable for structural analysis by X-ray diffraction. Furthermore, we prepared a series of substituted 3,7-$(XC_4H_2S)_2(CN_2S_2N_2C)$ compounds, including X = 5-CN, 5-Br, 4-Me, 4-*n*-Hex and 3,7-$(XYC_4HS)_2(CN_2S_2N_2C)$for which X = 5-Br and Y = 4-Me. These compounds and their precursors are characterized herein.

Although we did not attempt to prepare the hydroquinone of the thiophene substituted **II-4g**, we did pursue the synthesis of a quinoid structure of this compound by means of 5,5'-bis(dicyanoethylene) substitution. The anticipated product would then be structurally comparable to TCNQ. The outcome of this investigation, however, was that oxidative addition at the 4- and 5- positions of a terminal thiophene is favourable to an oxidative addition at the 5- and 5'-positions. Thus the generation of a quinoid structure is avoided. Not long after these results were

determined, this investigation was terminated in favour of the more promising research addressed in the remaining chapters.

2.2.1 A Dithiatetrazocine-Containing Hydroquinone

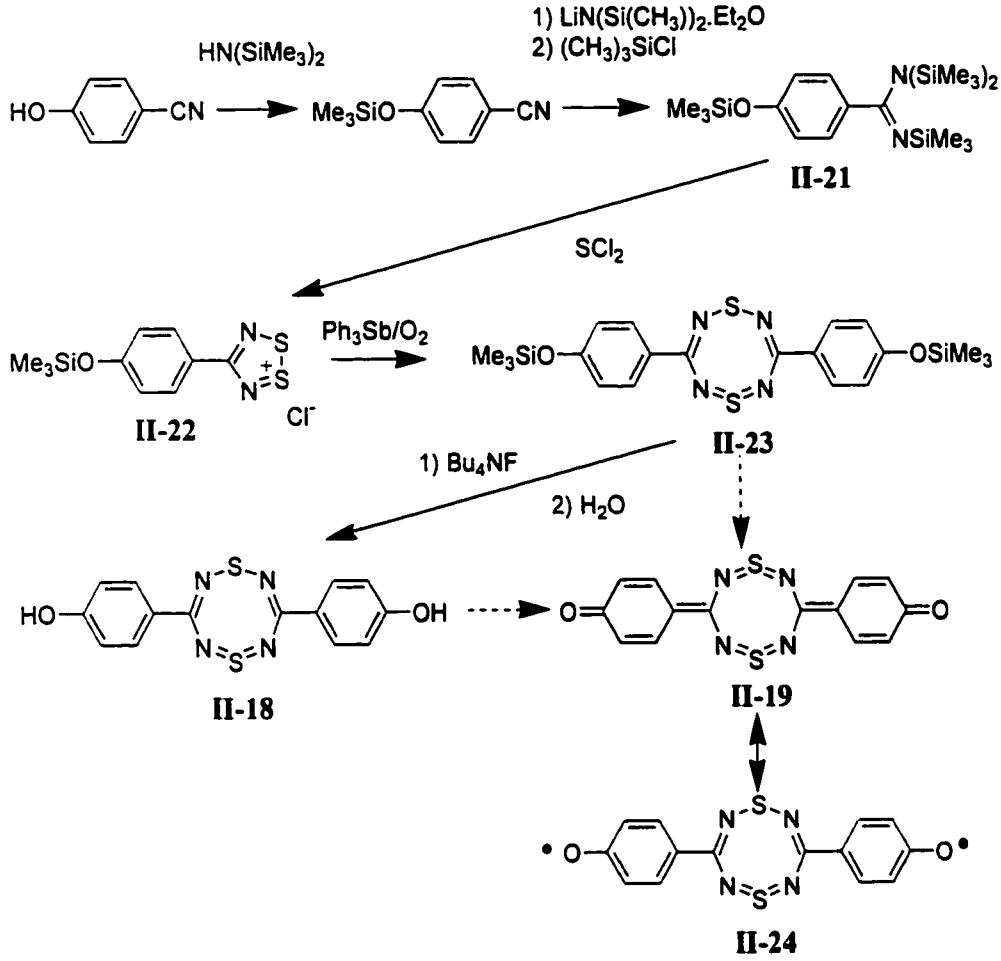

Figure 2.13 Preparation of the hydroquinone **II-18**.

Hydroquinone **II-18** is prepared in five steps from *p*-cyanophenol (**Figure 2.13**). The alcohol is first protected by conversion to a trimethylsiloxy group generating a colourless oily product that may be purified by distillation. Treatment of the resulting nitrile with

$LiN(Si(CH_3))_2 \cdot Et_2O$ followed by trimethylsilyl chloride yields an amidine (**II-21**), which again must be distilled for purification. The formation of a dithiadiazolylium salt (**II-22**) is effected by reacting **II-21** with two equivalents of sulfur dichloride. This is then reduced with triphenylantimony in the presence of oxygen to generate **II-23**. Finally, the trimethylsilyl protecting groups are removed by treatment with tetrabutylammonium fluoride followed by protonation with water resulting in the hydroquinone **II-18**.

While all the products leading up to and including the hydroquinone **II-18** have been isolated and characterized, oxidation to the quinone **II-19** was never accomplished despite attempts with many different oxidizing agents under various conditions. Two approaches were taken to effect this oxidation. First, the oxidation of the hydroquinone was attempted using PbO_2 in DMF, $K_3Fe(CN)_6$ in aqueous base, $PhI(OAc)_2$ in DMF, in CH_2Cl_2, and in CH_3CN, and $Pb(OAc)_4$ in CH_3CN. The failure of any of these oxidations to produce the desired quinone compelled us to explore a second route wherein **II-23** is first treated with tetrabutylammonium fluoride, removing the trimethylsilyl groups, followed by a two electron oxidation of the dianion and subsequent quenching with water. Several oxidizing agents were employed including $K_3Fe(CN)_6$ in CH_2Cl_2 and in CH_3CN, PbO_2 in DMF, $PhI(OAc)_2$ in CH_3CN, and $Pb(OAc)_4$ in CH_3CN. None of these oxidations successfully generated the quinone **II-19**.

In some instances, a reaction appeared to have taken place, however the desired quinone is not the resulting product. There is a possibility that the oxidations have formed a diradical **II-24** rather than a quinoid species. As previously mentioned, this phenomenon has been observed by Jorgensen and West in the anthracene-based compound **II-11**. Such a diradical would likely be extremely oxygen sensitive in solution, and as the oxidations were by and large performed in air, any diradical formed would have decomposed prior to our isolation of the product. In order to verify the generation of any such diradical species, stoichiometric oxidation under inert atmosphere

would be advisable, followed by an ESR study of the product.

Some insight may also be gained by assessing the relative stabilities of the quinoid structure and the triplet diradical state for this compound using computational methods. Preliminary results obtained for the proposed quinone **II-19** using MNDO indicate that the heat of formation of the diradical triplet state **II-24** is 31.3 kcal mol^{-1} lower in energy than that of the quinoid singlet. This is a significant energy difference. However, these results may greatly exaggerate the relative stability of the conformation **II-24** since MNDO not only has some difficulties in dealing with electron correlation but it also has problems dealing with high valent sulfur since it does not make use of d orbitals. The latter is apparent in the MNDO calculations on the dimethylamino substituted **II-4c** which imply that the ring should be more stable in the planar, aromatic 10 π form than in the observed non-planar non-aromatic conformation.

Another possible explanation for the aforementioned observations is that addition reactions may be occurring. The most common reaction undergone by quinones is a 1,4-reductive addition of the Michael type[44] where a nucleophile adds to the carbon next to the carbonyl group, at the same time reducing the carbon-oxygen double bond. In anticipation of such addition side-reactions, we briefly explored the possibility of sterically protecting the 3- and 5- positions of the peripheral phenyl rings with *t*-butyl groups. Although we were able to isolate and characterize the first three products up to and including the nitrile **II-25**[45,46] (**Figure 2.14**), difficulties in reproducibility and low yield made the pursuit of this material less appealing than that of the thiophene substituted compounds discussed in the next section.

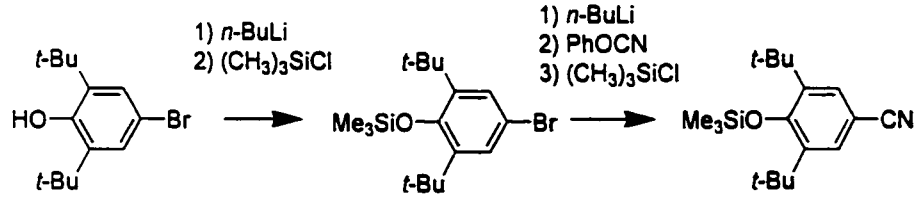

II-25

Figure 2.14 Synthetic route to precursors of *t*-butyl substituted quionoid.

2.2.2 3,7-Dithienyl-1,5,2,4,6,8-dithiatetrazocine

In light of our apparent inability to obtain the quinoid **II-19**, we turned to the pursuit of **II-4** with heterocyclic substituents in the place of phenyl groups. We chose thiophene as a good candidate for our purposes for a number of reasons. Primarily, although the theoretical compound triphenoquinone **II-9** is unknown, the thiophene analogues **II-10** and **II-20** have been isolated and characterized as species with quinoid character. Additionally, the thiophene substituted 3,7-dithienyl-1,5,2,4,6,8-dithiatetrazocine **II-4g** has been reported in low yield and has been ascribed to the planar, aromatic 10 π conformation for **II-4**.

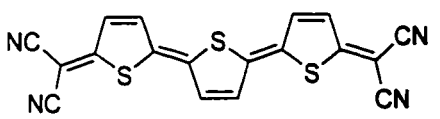

II-20

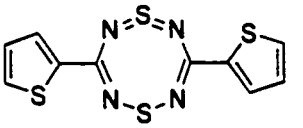

II-4g

Figure 2.15 Thiophene-based compounds.

Our first course of action was to improve the synthetic yield of **II-4g**. This we accomplished using the same techniques employed in the synthesis of the hydroquinone **II-18**. We prepared the amidine from the nitrile, followed by the dithiadiazolium salt, all of which are previously reported compounds. Finally, we applied the Boeré[36] reduction in the presence of oxygen technique to generate **II-4g**. We were able to obtain material of sufficient quality to determine the structure by single crystal X-ray diffraction.

In order to design a quinoid species based on **II-4g**, we pursued the substitution of the 5- and 5'- positions of the peripheral thiophenes with a dicyanoethylene group. The intent was to generate a quinoid analogous to TCNQ or **II-20**. The dibromo- substituted compound **II-27** was obtained both by bromination of **II-4g** and by synthesis from 2-bromo-5-cyanothiophene.

Following the Gronowitz reaction,[47] **II-26** was treated with tetracyanoethyleneoxide (TCNEO) in refluxing 1,2-dibromoethane. This afforded a blue compound which was recrystallized by vapour transfer of pentane into a methylene chloride solution. The structure, determined by single crystal X-ray diffraction, was not that of the anticipated quinoid species (**II-27**) but instead revealed oxidative addition across the 4- and 5- positions of one of the peripheral thiophenes, **II-28**.

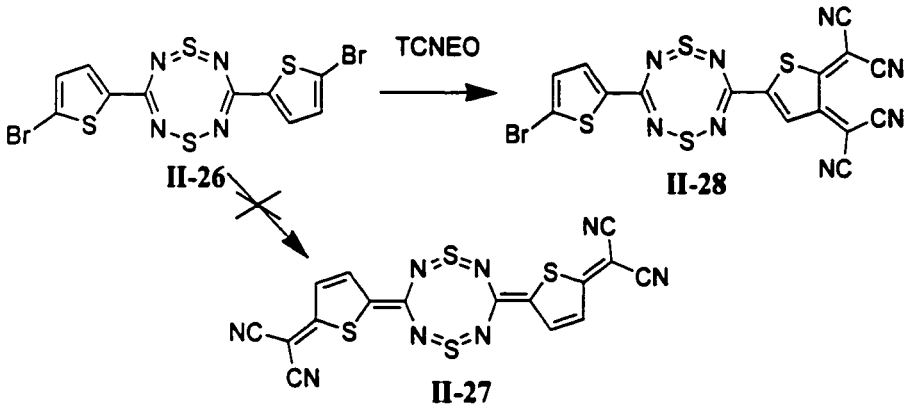

Figure 2.16 Attempt at preparing **II-27** yielded **II-28** instead.

In order to prevent substitution at the 4- and 4'- positions of the thienyl groups, we blocked these positions both with methyl groups and with *n*-hexyl groups. As the same synthetic route was applied to both, only the preparation of the methyl substituted species is described herein. Following a known procedure,[48] we prepared 4-methyl-2-thienaldehyde from 3-methylthiophene treated with butyllithium and DMF. This was then reacted with sodium acetate trihydrate and hydroxylamine hydrochloride affording 4-methyl-2-thienaldoxime.[49] From the latter, 4-methyl-2-cyanothiophene was prepared by dehydration with acetic anhydride. The dithiatetrazocine **II-29** was then generated via the series of reactions previously employed in the synthesis of **II-1g**. Finally this was brominated with NBS yielding **II-30**.

Attempts at oxidizing **II-30** to the desired quinoid via the Gronowitz reaction met with failure. A second approach was taken involving the reaction of **II-26** with sodium malononitrile, prepared *in situ* from sodium hydride and malononitrile, in the presence of tetrakis(triphenylphosphine) palladium (0). The product of this reaction, assumed to be the dianion **II-31**, was then oxidized by a variety of methods, but the anticipated quinoid **II-27** was never observed. Finally attempts at preparing **II-32**, either from **II-31** or by elaborating **II-33** with the dicyanomethyl group, were unsuccessful.

In anticipation of a successful preparation of a quinoid form of **II-4**, a goal that was never realized, we synthesized the 5,5'-dicyano substituted compound **II-34**. The objective of this particular project was the generation of a conjugated oligomer consisting of alternate **II-4** and thiophene rings. In the case that a quinoid form of **II-4** was achieved, this structure held interest as it was presumed to be comparable to hexathiophene oligomers and the derivatives thereof.

The synthesis of compound **II-34** was achieved in the same manner as those **II-4** derivatives already elaborated upon. The 2,5-dicyanothiophene starting material was prepared from commercially available 2,5-dibromothiophene treated with copper (I) cyanide in refluxing quinoline. The amidine, the dithiadiazole, and **II-34** were each prepared, without complications, following the preparative route for the thiophene substituted **II-4g**. Although this project was terminated with the isolation of **II-34**, the nitrile groups were intended to provide a means of building diaminodithiazole rings onto both ends of the structure. Condensation of this material would form the desired oligomer.

Our lack of success at establishing a quinoid formulation for any of the substituted **II-4** discussed herein prompted us to briefly explore the possibility of preparing the simple quinone **II-35**. Attempts were made at reacting both urea and 1,3-bis(trimethylsilyl)urea with thionyl chloride in the presence of pyridine. Neither method procured **II-35**.

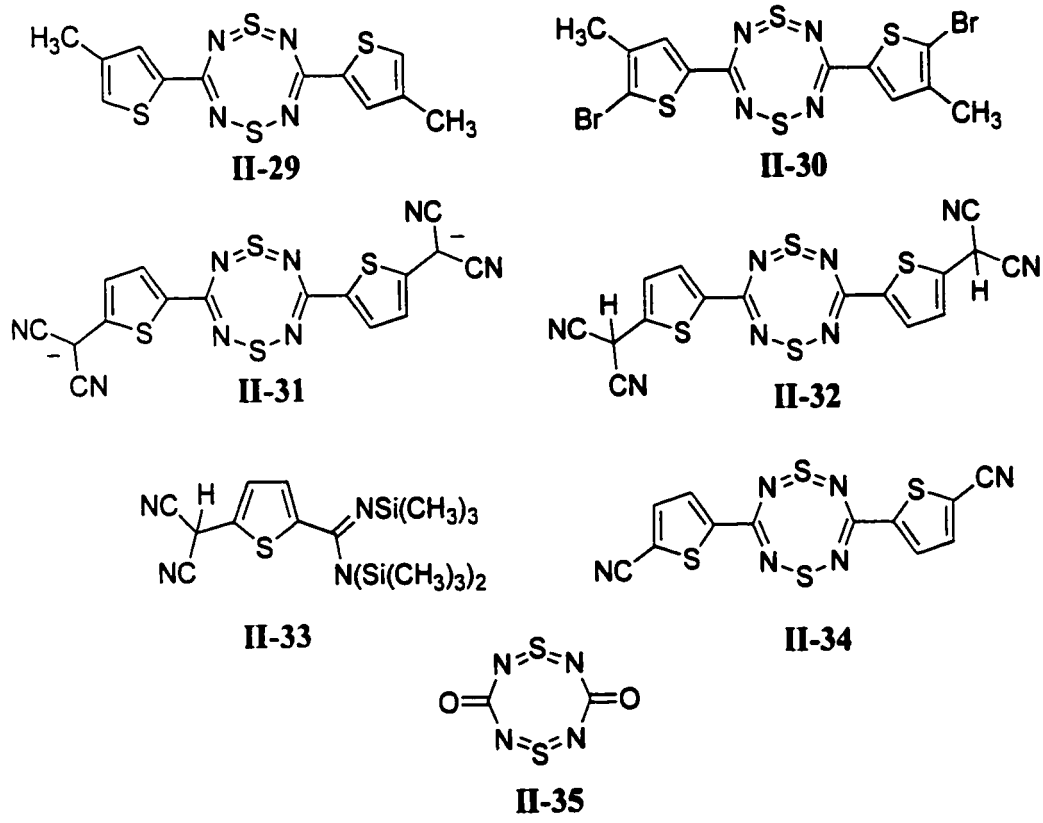

Figure 2.17 Further attempts at quinoid formation.

In summary, we have explored a variety of synthetic routes in an attempt to generate the quinoid formulation of the 1,5,2,4,6,8-dithiatetrazocine ring. We have come to the conclusion that this quinoid formulation, if it can be prepared at all, is not readily accessible. This does not augur well for its potential use as a CT salt electron acceptor nor for its role in a hexathiophene-type oligomer. In light of these findings, we have suspended our work in this area and concentrated our efforts on the research reported in the remaining chapters of this thesis.

2.3 Crystal Structures

2.3.1 3,7-Bis(2-thienyl)-1,5,2,4,6,8-dithiatetrazocine[50]

3,7-Bis(2-thienyl)-1,5,2,4,6,8-dithiatetrazocine (**II-4g**) crystallizes from chlorobenzene as yellow blocks in the monoclinic space group $P2_1/c$. The entire molecule is planar to within 0.069 (5) Å. Thus the planarity of the central ring is confirmed and the measured bond distances and angles are comparable with those reported for the phenyl, 4-methoxyphenyl and 4-trifluoromethylphenyl compounds (see **Table 2.1**) suggesting the existence of a delocalized 10 π electron system.

Table 2.1 Average[a] Bond Distances and Angles for Dithiatetrazocines.

	II-4g	**II-4b[b]**	**II-4b(iii)[b]**	**II-4b(v)[b]**
S-N (Å)	1.556(3)	1.5645(30)	1.5615(25)	1.562(2)
C-N (Å)	1.326(4)	1.323(4)	1.329(3)	1.3225(30)
N-S-N (deg.)	126.6(2)	127.0(2)	127.2(1)	126.8(1)
N-C-N (deg.)	130.0(3)	129.2(3)	128.5(2)	129.2(2)

[a] Values in parentheses are the larger of the uncertainty and the ESD. [b] Literature values.[36]

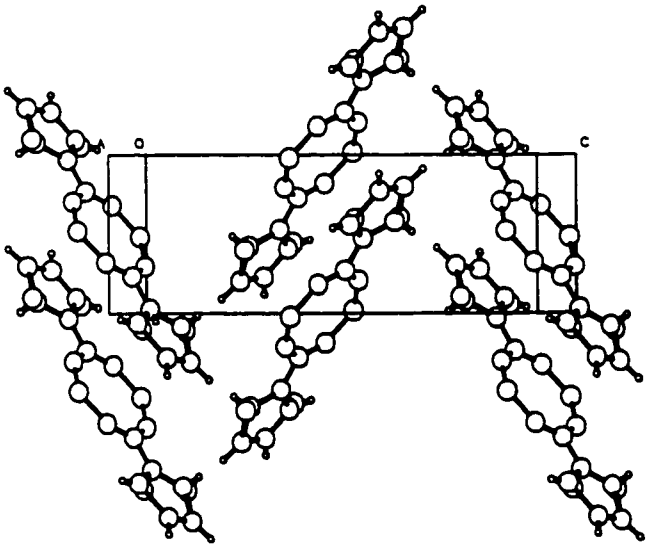

Figure 2.17 The packing of the molecules as viewed in the *bc* projection.

Disorder of the thienyl substituents is observed involving a 180° rotation about the C4-C5 bond such that only S2, C3 and H3 are affected. This is reminiscent of the disorder observed in a thienyl derivative of benzobis(1,2,5-dithiazole).[51,52] Herein, the disorder was modeled by applying a 0.80 to 0.20 occupancy to the affected atom positions. In so doing, the atoms at 20% occupancy were constrained to difference map positions with displacement parameters equal to their 80% counterparts. In constructing **Figure 2.17**, only the atoms at 0.80 occupancy were included.

2.3.2 3-(5-Bromo-2-thienyl)-7-(4,5-bis[dicyanomethylene]-2-thienyl)-1,5,2,4,6,8-dithiatetrazocine

The single crystal structure of the blue crystals of **II-28** was not fully refined. Once the molecular structure was revealed to be not that of the desired quinoid but of **II-28**, further refinement of the crystallographic data was discontinued. The *PLUTO* representation of this compound is shown in **Figure 2.18**.

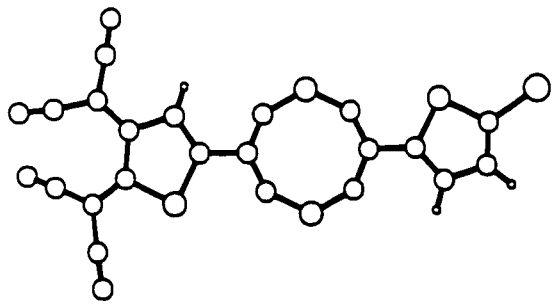

Figure 2.18 *PLUTO* representation of $C_{16}H_3BrN_8S_4$.

2.4 Syntheses

2.4.1 Synthesis of 4-cyano-1-trimethylsiloxybenzene: *p*-Cyanophenol (25.0 g, 0.210 mol) was dissolved in hexamethyldisilazane (75 mL) at 40°C and the reaction mixture was stirred at that

temperature for 0.5 h until the evolution of $NH_{3(g)}$ had ceased. The excess hexamethyldisilazane was removed *in vacuo* at room temperature. The colourless, oily product was distilled *in vacuo*; yield 39.7 g, (0.208 mol, 99%); bp 60°C at 10^{-1} Torr. IR (neat): 2968 (s), 2898 (m), 2221 (vs), 1602 (s), 1510 (s), 1415 (s), 1273 (s, br), 1170 (s), 1105 (s), 911 (s, br), 849 (s, br), 759 (s), 647 (m), 552 (s) cm^{-1}. ^1H NMR (δ, $CDCl_3$): 7.27 (d, J_{AB} = 8.7 Hz, 2 $H_{aromatic}$), 6.63 (d, J_{AB} = 8.7 Hz, 2 $H_{aromatic}$), 0.03 (s, $Si(CH_3)_3$). ^{13}C NMR ($CDCl_3$): 159.78, 134.46, 121.26, 119.52, 105.15, 0.23. Anal. Calcd. for $C_{10}H_{13}NOSi$: C, 62.78; H, 6.85; N, 7.32%. Found: C, 62.68; H, 6.69; N, 7.44%.

2.4.2 Synthesis of 4-trimethylsiloxybenzene-*N,N,N'*-tris(trimethylsilyl)carboximidamide (II-21): $LiNT_2 \cdot Et_2O$ (10.7 g, 44.3 mmol) was added to a solution of 4-cyano-1-trimethylsiloxybenzene (8.50 g, 44.4 mmol) in 100 mL of toluene, and the ensuing colourless solution was heated at 55°C for 2 h. Excess trimethylsilyl chloride (10 mL) was added and the reaction mixture was heated at 70°C overnight. The byproduct LiCl was filtered off as a white powder and the toluene was removed *in vacuo*. The resulting colourless oily product was distilled *in vacuo*; yield 13.99g (35.98 mmol, 81%); bp 138°C at 10^{-1} Torr. IR: 1631 (s, br), 1600 (s), 1504 (s), 1403 (w), 1252 (s, br), 1123 (m), 1097 (m), 1057 (w), 996 (m), 916 (s), 879 (m), 849 (s), 754 (m), 674 (m), 636 (w), 626 (w), 616 (w), 607 (w), 565 (w), 537 (w), 505 (w) cm^{-1}. Anal. Calcd. for $C_{16}H_{40}N_2OSi_4$: C, 49.42; H, 10.37; N, 7.20%. Found: C, 49.25; H, 10.60; N, 7.05%.

2.4.3 Synthesis of 4-(*p*-trimethylsiloxyphenyl)-1,2,3,5-dithiadiazolylium chloride (II-22): Sulfur monochloride (16.080 g, 156.16 mmol) in 30 mL of dry acetonitrile was added, dropwise, under inert atmosphere, to a solution of **II-21** (30.141 g, 77.513 mmol) in 150 mL of dry acetonitrile, on ice. The reaction mixture was warmed to room temperature and the red-orange powder product was filtered off, washed twice with 30 mL of dry acetonitrile, and dried *in vacuo*;

yield 15.031g (49.314 mmol, 64%). Recrystallization in hot CH_3CN yielded red crystals; dec. 132°C. IR: 1599 (s), 1515 (m), 1505 (w), 1402 (s), 1276 (s), 1174 (s), 926 (m), 909 (s), 849 (s), 757 (w), 742 (m), 723 (m), 693 (m), 656 (w), 650 (w), 641 (w), 545 (s), 524 (m) cm^{-1}. MS (*m/e*): 269 (M^+, 100%), 254 ($[M-CH_3]^+$, 12%), 223 ($[M-NS]^+$, 28%), 208 ($[M-NSCH_3]^+$, 8%), 191 ($[M-NS_2]^+$, 9%), 176 ($[M-NS_2CH_3]^+$, 57%), 78 (S_2N^+, 45%), 73 (Me_3Si^+, 48%) Anal. Calcd. for $C_{10}H_{13}ClN_2OS_2Si$: C, 39.40; H, 4.30; N, 9.19%. Found: C, 39.90; H, 3.98; N, 10.34%.

2.4.4 Synthesis of 3,7-bis(4-trimethylsiloxyphenyl)-1,5,2,4,6,8-dithiatetrazocine (II-23): Oxygen gas was bubbled through a slurry of 4-(*p*-trimethylsiloxyphenyl)-1,2,3,5-dithiadiazolylium chloride (1.2×10^1 g, 0.039 mol) in 50 mL dry acetonitrile for 1 m. Excess triphenylantimony (2.0×10^1 g, 0.057 mol) was then added and $O_{2(g)}$ was bubbled through the mixture for another 10 m. A bright yellow precipitate began to appear from an exothermic reaction. The slurry was heated until reaction completion, then cooled on ice, filtered, washed with acetonitrile, and dried in air. Yellow crystals were obtained from recrystallization in hot ethyl acetate (400 mL); yield 5.291 g (11.15 mmol, 56%); dec. 212°C. IR: 1597 (m), 1504 (s), 1265 (s), 1253 (m), 1155 (m), 955 (w), 928 (s), 848 (s), 751 (w), 658 (m), 646 (m), 524 (w), 508 (w) cm^{-1}. ^1H NMR (δ, $CDCl_3$): 8.38 (d, J_{AB} = 8.8 Hz, 4 $H_{aromatic}$), 6.98 (d, J_{AB} = 8.8 Hz, 4 $H_{aromatic}$), 0.30 (s, $Si(CH_3)_3$, 18 H). ^{13}C NMR ($CDCl_3$): 157.59, 140.62, 131.68, 130.12, 120.80, 0.41. MS (*m/e*): 474 (M^+, 46%), 269 ($[Me_3SiOC_6H_4CN_2S_2]^+$, 17%), 223 ($[Me_3SiOC_6H_4CNS]^+$, 84%), 176 ($[Me_2SiOC_6H_4CN]^+$, 100%). Anal. Calcd. for $C_{20}H_{26}N_4O_2S_2Si_2$: C, 50.60; H, 5.52; N, 11.80%. Found: C, 50.46; H, 5.62; N, 11.86%.

2.4.5 Synthesis of 3,7-bis(4-phenol)-1,5,2,4,6,8-dithiatetrazocine (II-18): 3,7-bis(4-trimethylsiloxyphenyl)-1,5,2,4,6,8-dithiatetrazocine (0.479 g, 1.01 mmol) was slurried in 15 mL

of acetonitrile. Excess 1.0 M tetrabutylammonium fluoride in THF (2 mL, 2 mmol) was added slowly, with stirring. The yellow slurry became a red solution with a red precipitate. Water (150 mL) was added slowly and a fine yellow precipitate formed. This was filtered, washed with 5 mL of acetonitrile, and dried in air; yield 0.344g (1.04 mmol, 103 %); dec. 209°C. IR: 3172 (m, br), 1597 (s), 1507 (s), 1236 (s), 1013 (w), 943 (w), 838 (m), 810 (m), 648 (s), 603 (s), 524 (w) cm^{-1}. ^1H NMR (δ, DMSO): 9.35 (s, O*H*), 7.28 (d, J_{AB} = 8.3 Hz, $H_{aromatic}$), 6.05 (d, J_{AB} = 8.3 Hz, $H_{aromatic}$). MS (*m/e*): 330 (M^+, 23%), 197 ($[HOC_6H_4CN_2S_2]^+$, 21%), 151 ($[HOC_6H_4CNS]^+$, 54%) 119 ($[HOC_6H_4CN]^+$, 100%) . Anal. Calcd. for $C_{14}H_{10}N_4O_2S_2$: C, 50.90; H, 3.05; N, 16.96%. Found: C, 51.06; H, 3.09; N, 16.86%.

2.4.6 Synthesis of 4-bromo-2,6-bis(*tert*-butyl)-1-trimethylsiloxybenzene:[45] A 1.6 M solution of *n*-butyllithium in hexanes (12 mL, 19 mmol) was added to a solution of 2,6-bis(*tert*-butyl)-4-bromophenol (5.090 g, 17.85 mmol) in dry THF (80 mL), under inert atmosphere, on ice. The reaction mixture was warmed to RT and an excess of chlorotrimethylsilane (8 mL, 0.06 mol) was added to get a lilac colour followed by a colour change to pale yellow. The solution was stirred for 3h after which time the byproduct lithium chloride was filtered off. The solvent was removed *in vacuo*. The resulting white solid was recrystallized from hot acetonitrile (150 mL) to give off-white crystals; yield 5.734 g (16.04 mmol, 90%). IR: 1566 (w), 1406 (s), 1386 (w), 1359 (m), 1266 (s), 1254 (s), 1227 (s), 1202 (m), 1148 (w), 1118 (s), 1027 (w), 1016 (w), 919 (s), 887 (m), 850 (s), 778 (m), 767 (s), 678 (m), 643 (m), 560 (m), 521 (m) cm^{-1}. ^1H NMR (δ, $CDCl_3$): 7.30 (s, 2 $H_{aromatic}$), 1.36 (s, *t*-Bu, 18 H), 0.39 (s, Me_3SiO, 9 H)

2.4.7 Synthesis of 4-cyano-2,6-bis(*tert*-butyl)-1-trimethylsiloxybenzene (II-25): A 1.6 M solution of *n*-butyllithium in hexanes (8.0 mL, 13 mmol) was added dropwise to a solution of 4-

bromo-2,6-bis(*tert*-butyl)-1-trimethylsiloxybenzene (3.837 g, 10.73 mmol) in 100 mL dry ether, under inert atmosphere, on ice. Subsequently, the reaction mixture was stirred at RT for 3h to get a fine white precipitate. The slurry was cooled to -70°C and a solution of phenylcyanate[46] (1.314 g, 11.02 mmol) in 20 mL dry ether was added over a period of 7m. The mixture was stirred at -70°C for a further 45m and then warmed to RT to yield an orange-brown solution. Excess chlorotrimethylsilane (10 mL, 0.08 mol) was added and a yellow powder precipitated from solution. This was stirred overnight. The byproduct lithium chloride was filtered off and the solvent was removed *in vacuo*. The remaining orange sludge was dissolved in 10 mL hot acetonitrile and cooled to -10°C to yield yellow crystals. These were recrystallized a second time in hot acetonitrile resulting in white crystals; yield 0.444g (1.46 mmol, 14%); mp 120-124°C. IR: 2229 (m), 1593 (w), 1417 (s), 1365 (m), 1269 (m), 1261 (m), 1238 (s), 1205 (m), 1125 (s), 945 (w), 922 (w), 889 (vs), 842 (s), 785 (m), 766 (m), 680 (w), 656 (m), 618 (m), 581 (w) cm^{-1}. ^1H NMR (δ, $CDCl_3$): 7.51 (s, 2 $H_{aromatic}$), 1.37 (s, *t*-Bu, 18 H), 0.41 (s, Me_3SiO, 9 H). ^{13}C NMR ($CDCl_3$): 157.92, 143.02, 130.61, 120.60, 104.52, 35.54, 31.12, 3.94. MS (*m/e*): 303 (M^+, 38%), 288, ($[M-CH_3]^+$, 94%), 233 ($[M-CN(CH_3)_3]^+$, 29%), 73 ($[SiMe_3]^+$, 100%).

2.4.8 Synthesis of thiophene-2-*N,N,N'*-tris(trimethylsilyl)carboximidamide: $LiNT_2 \cdot Et_2O$ (24.268 g, 100.51 mmol) was added to a solution of 2-cyanothiophene (10.906 g, 99.918 mmol) in 100 mL of dry toluene, and the initially colourless solution blackened almost immediately. This was stirred for 6 h at RT. Excess trimethylsilyl chloride (15 mL) was added and the reaction mixture was refluxed for 30 m. The byproduct LiCl was filtered off as a white powder and the toluene was removed *in vacuo*. The resulting colourless oily product was distilled *in vacuo*; yield 20.981g (61.219 mmol, 61 %); bp 81°C at 10^{-1} Torr.

2.4.9 Synthesis of 4-thienyl-1,2,3,5-dithiadiazolylium chloride: Sulfur monochloride (4.13 g, 40.1 mmol) in 20 mL of dry acetonitrile was added, dropwise, under inert atmosphere, to a solution of thiophene-2-*N,N,N'*-tris(trimethylsilyl)carboximidamide (6.85 g, 20.0 mmol) in 100 mL of dry acetonitrile, on ice. The reaction mixture was warmed to room temperature and the red-orange powder product was filtered, washed with acetonitrile and dried *in vacuo*. The product was converted directly to **II-4g**.

2.4.10 Synthesis of 3,7-bis(thienyl)-1,5,2,4,6,8-dithiatetrazocine (II-4g): Oxygen gas was bubbled through a slurry of 4-thiophene-1,2,3,5-dithiadiazolylium chloride (from **2.4.9**) in 60 mL dry acetonitrile. Triphenylantimony (3.5 g, 10 mmol) was then added and $O_{2\,(g)}$ was bubbled through the mixture for another 0.5 h with heating resulting in a bright orange slurry. The reaction mixture was cooled on ice, filtered, washed with acetonitrile, and dried in air. Yellow crystals were obtained from recrystallization in hot chlorobenzene (80 mL); yield 1.64 g (5.29 mmol, 53% based on amidine). IR: 1522 (vw), 1427 (w), 1340 (w), 1247 (w), 1221 (w), 1189 (vw), 1074 (w), 1029 (m), 908 (vw), 890 (w), 852 (w), 840 (s), 818 (s), 742 (w), 699 (vs), 660 (s), 647 (s), 616 (s), 571 (w), 523 (m) cm^{-1}. ^1H NMR (δ, $CDCl_3$): 7.95 (d, 2 H), 7.45 (d, 2 H), 7.15 (t, 2 H).

2.4.11 Synthesis of 2-bromothiophene-5-*N,N,N'*-tris(trimethylsilyl)carboximidamide: 2-Bromo-5-cyanothiophene (18.8 g, 100 mmol) was added to a slurry of $LiNT_2{\cdot}Et_2O$ (24.1 g, 100 mmol) in 100 mL of dry toluene, and a dark red solution was produced. This was warmed gently for 1 h. Excess trimethylsilyl chloride (15 mL) was added and the reaction mixture was refluxed for 90 m. The byproduct LiCl was filtered off as a white powder and the toluene was removed *in vacuo*. The resulting dark oily product was distilled *in vacuo* affording a yellow oil; yield 25.32g (61 mmol, 61 %); bp 128°C at 10^{-1} Torr.

2.4.12 Synthesis of 4-(2-bromothiophene)-1,2,3,5-dithiadiazolylium chloride: Sulfur monochloride (4.14 g, 40.1 mmol) in 15 mL of dry acetonitrile was added, dropwise, under inert atmosphere, to a solution of 2-bromothiophene-5-*N,N,N'*-tris(trimethylsilyl)carboximidamide (8.43 g, 20.0 mmol) in 100 mL of dry acetonitrile, on ice. The reaction mixture was warmed to room temperature and the yellow-orange solid product was filtered, washed with acetonitrile and dried *in vacuo*. The dry product was then converted directly into **II-26**.

2.4.13 Synthesis of 3,7-bis(2-bromothiophene)-1,5,2,4,6,8-dithiatetrazocine (II-26): Oxygen gas was bubbled through a slurry of 4-(2-bromothiophene)-1,2,3,5-dithiadiazolylium chloride (product used directly from **2.4.12**) in 60 mL dry acetonitrile. Triphenylantimony (3.5 g, 10 mmol) was then added and $O_{2(g)}$ was bubbled through the mixture for another 0.5 h with heating resulting in a dark solution with bright orange precipitate. The reaction mixture was cooled on ice, filtered, washed with acetonitrile, and dried in air. Orange crystals were obtained from recrystallization in hot chlorobenzene (120 mL); yield 2.10 g (4.47 mmol, 45 % based on 20.0 mmol amidine). IR: 1651 (w), 1601 (w), 1532 (w), 1420 (s), 1233 (m), 1209 (m), 976 (m), 878 (w), 820 (w), 797 (vs), 717 (m), 657 (vs), 637 (w), 521 (s), 468 (m) cm^{-1}. ^1H NMR (δ, $CDCl_3$): 7.69 (d, 2 H), 7.10 (d, 2 H).

2.4.14 Alternate synthesis of 3,7-bis(2-bromothiophene)-1,5,2,4,6,8-dithiatetrazocine (II-26): 3,7-bis(thiophene)-1,5,2,4,6,8-dithiatetrazocine (**II-4g**) (3.587 g, 11.56 mmol) was dissolved in dimethylformamide (550 mL) at 110°C. The solution was cooled to 95°C and *N*-bromosuccinimide (5.173 g, 2.906 mmol) was added. Yield 4.584 g (9.748 mmol, 84 %). ^1H NMR (δ, $CDCl_3$): 7.68 (d, J_{AB} = 4.0 Hz, 2 H), 7.10 (d, J_{AB} = 4.0 Hz, 2 H).

2.4.15 Synthesis of 3-(2-bromothiophene)-7-(2,3-bis(dicyanomethylene)thiophene)-1,5,2,4,6,8-dithiatetrazocine (II-28): 3,7-bis(2-bromothiophene)-1,5,2,4,6,8-dithiatetrazocine (0.100 g, 0.213 mmol) and tetracyanoethyleneoxide (0.113 g, 0.784 mmol) were stirred in refluxing 1,2-dibromoethane (20 mL) under inert atmosphere for 20 h. The solvent was removed *in vacuo* and the remaining solid was dissolved in a minimum amount of methylene chloride. A purple fraction of this solution was isolated on a silica gel column. Blue crystals were grown by slow solvent replacement using pentane; mp > 150°C. ^{1}H NMR (δ, $CDCl_3$): 7.93 (s, 1 H), 7.80 (d, J_{AB} = 4.0 Hz, 1 H), 7.15 (d, J_{AB} = 4.0 Hz, 1 H). MS (*m/e*): 361 (2.5%), 313 (M^+-[$Br(C_4H_2S)CN_2$], 7.4%), 269 (13%), 170 (34%). Anal. Calcd. for $C_{16}H_3BrN_8S_4$: C, 37.29; H, 0.59; N, 21.74%. Found: C, 37.72; H, 0.9; N, 20.86%.

2.4.16 Synthesis of 2-cyanothiophene-5-*N,N,N'*-tris(trimethylsilyl)carboximidamide: $LiNT_2{\cdot}Et_2O$ (19.520 g, 80.840 mmol) was added to a solution of 2,5-dicyanothiophene (10.826 g, 80.695 mmol) in 150 mL of dry toluene and was stirred for 4 h at RT. Excess trimethylsilyl chloride (15 mL) was added to the dark brown solution and the reaction mixture was warmed for 16h. The byproduct LiCl was filtered off as a white powder and the toluene was removed *in vacuo*. The resulting colourless oily product was distilled *in vacuo*; yield 15.58 g (42.36 mmol, 53 %); bp 135°C at 10^{-1} Torr.

2.4.17 Synthesis of 4-(2-cyanothiophene)-1,2,3,5-dithiadiazolylium chloride: Sulfur dichloride (8.8 g, 85 mmol) in 40 mL of dry acetonitrile was added, dropwise, under inert atmosphere, to a solution of 2-cyanothiophene-5-*N,N,N'*-tris(trimethylsilyl)carboximidamide (15.0 g, 40.8 mmol) in 100 mL of dry acetonitrile, on ice. The reaction mixture was warmed to room temperature and the red-orange powder product was filtered, washed with acetonitrile and dried *in vacuo*; yield 9.41g (38.3 mmol, 94 %). IR: 2217 (s), 1673 (w), 1529 (s), 1324 (w), 1239 (m), 1135 (m), 866

(m), 838 (s), 774 (w), 704 (s), 548 (w), 539 (m) cm^{-1}.

2.4.18 Synthesis of 3,7-bis(2-cyanothiophene)-1,5,2,4,6,8-dithiatetrazocine (II-34): Oxygen gas was bubbled through a slurry of 4-(2-cyanothiophene)-1,2,3,5-dithiadiazolylium chloride (11 g, 44 mmol) in 70 mL dry acetonitrile. Triphenylantimony (8.5 g, 24 mmol) was then added in 2 g aliquots and the solution was stirred overnight resulting in a dark solution with green-yellow precipitate. The reaction mixture was filtered, washed with water and then with acetone, and dried. Orange crystals were obtained by sublimation; IR: 2206(s), 1330 (w), 1252 (m), 1223 (m), 1156 (w), 1042 (w), 821 (s), 742 (w), 667 (s), 641 (s), 568 (m), 527 (s), 504 (w) cm^{-1}.

2.4.19 Synthesis of 4-methyl-2-thienaldehyde:[48] To a solution of butyllithium (130 mL of 1.6M, 208 mmol) in 200 mL dry ether, 3-methylthiophene (20.18 g, 205.6 mmol) was added in a slow stream at RT, under inert atmosphere. This solution was stirred for 2 h and then added, dropwise, to an ice-cold solution of DMF (14.654 g, 200.47 mmol) in 100 mL of dry ether over a period of 45 m. This solution was stirred for 16 h at RT, then poured onto ice, washed with 200 mL diluted $HCl_{(aq)}$, followed by 200 mL $Na_2CO_{3(aq)}$, and 200 mL water. The solution was dried with sodium sulfate and the ether was removed *in vacuo*. The colourless liquid product was distilled; yield 18.586g (147.30 mmol, 71 %). bp 51°C at 10^{-1} Torr. ^1H NMR (δ, $CDCl_3$): 9.85 (s, aldehyde), 7.56 (s, thiophene), 7.34 (s, thiophene), 2.30 (s, CH_3).

2.4.20 Synthesis of 4-methyl-2-thienaldoxime : In 100 mL of 1:4 ethanol:water, 4-methyl-2-thienaldehyde (17.601 g, 139.5 mmol), sodium acetate trihydrate (19.047 g, 139.97 mmol) and hydroxylamine hydrochloride (9.725 g, 140.0 mmol) were stirred for 3 h producing a yellow precipitate. The reaction mixture was cooled on ice to further precipitation of the product. The yellow solid was collected by filtration and recrystallized in ethanol to give yellow crystals; yield

10.542 g (74.665 mmol, 54 %).^{1}H NMR (δ, $CDCl_3$): 9.03 (s, NO*H*), 7.64 (s, C(NOH)*H*), 7.19 (d, J_{AB} = 1.4 Hz, 1 $H_{heterocyclic}$), 7.15 (d, J_{AB} = 1.4 Hz, 1 $H_{heterocyclic}$), 2.27 (s, CH_3, 3 H).

2.4.21 Synthesis of 4-methyl-2-cyanothiophene: Excess acetic anhydride (20 mL) was added to a slurry of 4-methyl-2-thienaldoxime in 200 mL of dichloroethane immediately producing a dark yellow solution which gradually faded in colour over a 15 m period. The reaction mixture was refluxed for 22 h, then poured, hot, onto ice and neutralized with sodium bicarbonate. The organic phase was separated from the aqueous phase and any remaining product in the aqueous phase was extracted with methylene chloride. The organic phases were combined, the solvent was removed *in vacuo*, and the colourless liquid product was distilled *in vacuo*; yield 6.380 g (57.79 mmol, 69 %). bp 35°C at 10^{-1} Torr. ^{1}H NMR (δ, $CDCl_3$): 7.40 (s, 1 $H_{heterocyclic}$), 7.16 (s, 1 $H_{heterocyclic}$), 2.27 (s, CH_3, 3 H).

2.4.22 Synthesis of 4-methylthiophene-2-*N,N,N'*-tris(trimethylsilyl)carboximidamide: 4-methyl-2-cyanothiophene (12.436 g, 100.96 mmol) was added to a slurry of $LiNT_2{\cdot}Et_2O$ (24.372 g, 100.94 mmol) in 100 mL of dry toluene resulting in a dark brown solution. This was stirred for 5 h. Excess trimethylsilyl chloride (15 mL) was added and the reaction mixture was warmed for 16 h. The byproduct LiCl was filtered off as a white powder and the toluene was removed *in vacuo*. The resulting dark oily product was distilled *in vacuo* affording a yellow oil; yield 22.04 g (63.39 mmol, 63 %); bp 95-102°C at 10^{-2} Torr.

2.4.23 Synthesis of 4-(3-methylthiophene)-1,2,3,5-dithiadiazolylium chloride: Sulfur dichloride (13.195 g, 127.48 mmol) in 20 mL of dry acetonitrile was added, dropwise, under inert atmosphere, to a solution of 4-methylthiophene-2-*N,N,N'*-tris(trimethylsilyl)carboximidamide (22.04 g, 63.39 mmol) in 150 mL of dry acetonitrile, on ice. The reaction mixture was warmed

to room temperature and the orange powder product was filtered, washed with acetonitrile and dried *in vacuo*; yield 13.0 g (54.9 mmol, 86.7 %).

2.4.24 Synthesis of 3,7-bis(3-methylthiophene)-1,5,2,4,6,8-dithiatetrazocine (II-29): Oxygen gas was bubbled through a slurry of 4-(3-methylthiophene)-1,2,3,5-dithiadiazolylium chloride (13.0 g, 54.9 mmol) in dry acetonitrile. Triphenylantimony (15 g, 42 mmol) was then added resulting in a dark solution with yellow precipitate. The reaction mixture was filtered and and the product was dried. Orange crystals were obtained by recrystallization in chlorobenzene; yield 3.7 g (11 mmol, 40 %). ^{1}H NMR (δ, $CDCl_3$): 7.75 (s, 2 $H_{heterocyclic}$), 7.02 (s, 2 $H_{heterocyclic}$), 2.31 (s, 6 H, CH_3).

2.4.25 Synthesis of 3,7-bis(2-bromo-3-methylthiophene)-1,5,2,4,6,8-dithiatetrazocine (II-30): 3,7-bis(3-methylthiophene)-1,5,2,4,6,8-dithiatetrazocine (680 mg, 2.01mmol) and *N*-bromosuccinimide (800 mg, 4.49 mmol) were heated to 90°C in DMF under inert atmosphere. An bright orange precipitate was filtered, washed, and dried *in vacuo*; yield 880 mg (1.77 mmol, 88 %). IR:1252 (m), 1207 (w), 1160 (w), 1030 (m), 846 (s), 826 (w), 743 (m), 661 (vs), 637 (vs), 590 (m), 529 (s) cm^{-1}. MS (*m/e*): 496 (M^+, 27.6%), 418 ($C_{12}H_9BrN_4S_4^+$, 27.1%), 416 ([M-Br] , 22.8%), 338 ($C_{12}H_{10}N_4S_4^+$, 3.8%).

2.4.26 Synthesis of 4-hexyl-2-thienaldehyde: To a solution of butyllithium (37 mL of 1.6M, 59 mmol) in 100 mL dry ether at 0°C, 3-hexylthiophene (10 g, 59 mmol) was added in a slow stream, under inert atmosphere. This solution was stirred for 18 h, and then added, dropwise, to an ice-cold solution of DMF (4.354 g, 59.56 mmol) in 100 mL of dry ether over a period of 45 m. This solution was stirred for 24 h at RT, then quenched on ice, washed with 200 mL diluted $HCl_{(aq)}$, followed by 200 mL $Na_2CO_{3(aq)}$, and 200 mL water. The solution was dried with sodium sulfate

and the ether was removed *in vacuo*. The colourless liquid product was distilled; yield 9.751g (49.67 mmol, 84 %). bp 66-105°C at 10^{-2} Torr. ^{1}H NMR (δ, $CDCl_3$): 9.86 (s, aldehyde, 1 H), 7.59 (s, 1 $H_{heterocyclic}$), 7.35 (s, 1 $H_{heterocyclic}$), 2.62 (t, J = 7.5 Hz, hexyl, 2 H), 1.61 (m, hexyl, 2 H), 1.28 (m, hexyl, 6 H), 0.86 (t, J = 6.4 Hz, 3 H, hexyl).

2.4.27 Synthesis of 4-hexyl-2-thienaldoxime: In 150 mL of 1:4 ethanol:water, 4-hexyl-2-thienaldehyde (32.681 g, 166.48 mmol), sodium acetate trihydrate (22.672 g, 166.61 mmol) and hydroxylamine hydrochloride (11.588 g, 166.76 mmol) were warmed for 2 h and then stirred at RT for 72 h producing a white precipitate. The reaction mixture was cooled on ice to further precipitation of the product. The white solid was collected by filtration and recrystallized in hexanes to give white crystals; yield 20.399 g (96.531 mmol, 58 %). ^{1}H NMR (δ, $CDCl_3$): 8.21 (s, NO*H*, 1 H), 7.64 (s, C(NOH)*H*, 1 H), 7.21 (s, 1 $H_{heterocyclic}$), 7.16 (s, 1 $H_{heterocyclic}$), 2.59 (t, J = 7.7 Hz, hexyl, 2 H), 1.59 (m, hexyl, 2 H), 1.27 (m, hexyl, 6 H), 0.86 (t, J = 6.6 Hz, hexyl, 3 H).

2.4.28 Synthesis of 4-hexyl-2-cyanothiophene: Excess acetic anhydride (40 mL) was added to a slurry of 4-hexyl-2-thienaldoxime in 200 mL of dichloroethane immediately producing a bright yellow solution which gradually faded in colour. The reaction mixture was refluxed for 22 h, then poured, hot, onto ice and neutralized with sodium bicarbonate. The organic phase was separated from the aqueous phase and the solvent was removed *in vacuo*. The colourless liquid product was distilled *in vacuo*; yield 23.34 g (120.7 mmol, 86 %). bp 83-95°C at 10^{-1} Torr. ^{1}H NMR (δ, $CDCl_3$): 7.42 (d, J_{AB} = 1.0 Hz, 1 $H_{heterocyclic}$), 7.16 (d, J_{AB} = 1.0 Hz, 1 $H_{heterocyclic}$), 2.59 (t, J = 7.6 Hz, hexyl, 2 H), 1.58 (m, hexyl, 2 H), 1.27 (m, hexyl, 6 H), 0.86 (t, J = 6.6 Hz, hexyl, 3 H).

2.4.29 Synthesis of 4-hexylthiophene-2-*N,N,N'*-tris(trimethylsilyl)carboximidamide: 4-hexyl-2-cyanothiophene (22.37 g, 115.7 mmol) was added to a slurry of $LiNT_2{\cdot}Et_2O$ (27.95 g, 115.7

mmol) in 150 mL of dry toluene resulting in a orange-brown solution. This was stirred for 5 h. Excess trimethylsilyl chloride (20 mL) was added and the reaction mixture was warmed for 18 h. The byproduct LiCl was filtered off as a white powder and the toluene was removed *in vacuo*. The resulting dark oily product was distilled *in vacuo* affording a yellow oil; yield 34.02 g (79.70 mmol, 69 %); bp 103°C at 10^{-2} Torr. ^{1}H NMR (δ, $CDCl_3$): 7.19 (s, 1 $H_{heterocyclic}$), 6.98 (s, 1 $H_{heterocyclic}$), 2.57 (t, J = 7.5 Hz, hexyl, 2 H), 1.59 (m, hexyl, 2 H), 1.27 (m, hexyl, 6 H), 0.86 (t, J = 6.4 Hz, hexyl, 3 H), 0.12 (m, trimethylsilyl, 9 H), 0.04 (m, trimethylsilyl, 18 H).

2.4.30 Synthesis of 4-(3-hexylthiophene)-1,2,3,5-dithiadiazolylium chloride: Sulfur dichloride (5.022 g, 48.51 mmol) was added, dropwise, under inert atmosphere, to a solution of 4-hexylthiophene-2-*N,N,N'*-tris(trimethylsilyl)carboximidamide (9.686 g, 22.69 mmol) in 100 mL of dry acetonitrile, on ice. The reaction mixture was warmed to room temperature and the orange powder product was filtered, washed with acetonitrile and dried *in vacuo*; yield 4.11 g (13.4 mmol, 59 %). IR: 1669 (s), 1549 (s), 1238 (w), 1154 (m), 1115 (s), 960 (w), 895 (m), 858 (m), 834 (m), 764 (w), 709 (m), 644 (w), 623 (w), 586 (w), 542 (m) cm^{-1}. MS (*m/e*): 271 (M^+, 100.0%), 225 ([M-NS]$^+$, 6.2%), 201 ([M-C_5H_{10},]$^+$, 41.6%).

2.4.31 Synthesis of 3,7-bis(3-hexylthiophene)-1,5,2,4,6,8-dithiatetrazocine: Oxygen gas was bubbled through a slurry of 4-(3-hexylthiophene)-1,2,3,5-dithiadiazolylium chloride (4 g, 13 mmol) in dry acetonitrile. Triphenylantimony (5 g, 14 mmol) was then added resulting in a dark solution with yellow precipitate. The reaction mixture was filtered and and the product was dried. Yellow crystals were obtained by recrystallization in ethyl acetate; yield 0.59 g (1.2 mmol, 19 %). IR: 1276 (m), 1249 (m), 1221 (m), 1188 (m), 1131 (w), 1111 (m), 867 (s), 852 (s), 825 (m), 793 (w), 752 (s), 732 (s), 662 (vs), 637 (vs), 610 (m), 590 (s), 529 (s), 482 (w) cm^{-1}. ^{1}H NMR (δ, $CDCl_3$): 7.78 (d, J_{AB} = 1.5 Hz, 2 $H_{heterocyclic}$), 7.03 (d, J_{AB} = 1.5 Hz, 2 $H_{heterocyclic}$), 2.63 (t, J = 7.5 Hz,

hexyl, 4 H), 1.66 (m, hexyl, 4 H), 1.30 (m, hexyl, 12 H), 0.89 (m, hexyl, 6 H).

References for Chapter 2

1. Ferraris, J.; Cowan, D. O.; Walatka, Jr., V.; Perlstein, J. H.; *J. Am. Chem. Soc.*, **1973**, *95*, 948.
2. Engler, W.; Patel, V. W.; *J. Am. Chem. Soc.*, **1974**, *96*, 7877.
3. Phillips, T. E.; Kistenmacher, T. J.; Ferraris, J. P.; Cowan, D. O.; *J. C. S. Chem. Commun.*, **1973**, 471.
4. Torrance, J. B.; Mayerle, J. J.; Lee, V. Y.; Bechgaard, K.; *J. Am. Chem. Soc.*, **1979**, *101*, 4747.
5. Hünig, S.; Erk. P.; *Adv. Mater.*, **1991**, *3*, 225.
6. (a) Grossel, M. C.; Weston, S. C.; *Cont. Org. Synth.*, **1994**, *1*, 317. (b) Ogura, F.; Otsubo, T.; Yasuso, Y.; Yui, Koji; **Jpn. Kokai Tokkyo Koho JP 02 67,279 [90 67,279]**, 07 Mar **1990**; *Chem. Abs. 113*:P78375x.
7. Boeré, R. T.; *Coord. Chem.*, in press, **2000**.
8. Torrance, J. B.; Pedersen, H. J.; Bechgaard, K.; *Phys. Rev. Lett.*, **1982**, *49*, 881.
9. Bechgaard, K.; Jacobsen, C. S.; Mortensen, K.; Pedersen, H. J.; Thorup, N.; *Solid State Comm.*, **1980**, *33*, 1119.
10. Takahashi, K.; Tarutani, S.; *Chem. Commun.*, **1998**, 1233.
11. (a) Yamashita, Y.; Saito, K.; Suzuki, T.; Kabuto, C.; Mukai, T.; Miyashi, T.; *Angew. Chem. Int. Ed. Engl.*, **1988**, *27*, 434. (b) Mukai, T.; Yamashita, T.; **Jpn. Kokai Tokkyo Koho JP 01 68,380 [89 68,380]**, 14 Mar **1989**; *Chem. Abs. 111*:P174129z.
12. Haddon, R. C.; Hebard, A. F.; Rosseinsky, M. J.; Murphy, D. W.; Duclos, S. J.; Lyons, K. B.; Miller, B.; Rosamilia, J. M.; Fleming, R. M.; Kortan, A. R.; Glarum, S. H.; Makhija, A. V.; Muller, A. J.; Eick, R. H.; Zahurak, S. M.; Tycko, R.; Dabbagh, G.; Thiel, F. A.;

Nature, **1991**, *350*, 320.

13. Ege, S.; *Organic Chemistry, Second Edition*, D. C. Heath and Company, Lexington, Massachussetts, **1989**, 847.

14. Patai, S.; *The Chemistry of the Quinonoid Compounds, Vol. 1, Part 2*, John Wiley & Sons, London, **1974**.

15. a) Deuchert, K.; Hünig, S.; *Angew. Chem. Int. Ed. Engl.*, **1978**, *17*, 875. b) Fabian, J.; Hartman, H.; *Light Absorption of Organic Colorants, Ch. 9*, Springer-Verlag, Berlin, **1980**. c) Matsuoka, M.; Kishimoto, M.; Kitao, T.; *J. Soc. Dyes Colorists*, **1978**, *94*, 435. d) Kago, Y.; Kikuchi, H.; Matsuoko, M.; Kitao, T.; *J. Soc. Dyes Colorists*, **1980**, *96*, 526.

16. Workman, P.; *Oncol. Res.*, **1994**, *6*, 461.

17. Patai, S.; *The Chemistry of the Quinonoid Compounds, Vol. 1, Part 1*, John Wiley & Sons, London, **1974**.

18. Osman, M. A.; Pietronero, L.; Sheffer, T. J.; Zeller, H. R.; *J. Chem. Phys.*, **1981**, *74*, 5377.

19. Misran, M.; Matthews, D.; Valente, P.; Hope, A.; *Aust. J. Chem.*, **1994**, *47*, 209.

20. Fox, M. A.; Channon, M., Ed. *Photoinduced Electron Transfer, Part D.*, Elsevier, Amsterdam, **1988**.

21. Mann, C. K.; Barnes, K. K. *Electrochemical Reactions in Non-aqueous Systems, Ch. 6*, Marcel Dekker, New York, **1970**.

22. Collins, P. M.; Christophorou, L. G.; Chaney, E. L.; Carter, J. G.; *Chem. Phys. Lett*, **1970**, *4*, 646.

23. Heinis, T.; Chowdhury, S.; Scott, S. L.; Kebarle, P.; *J. Am. Chem. Soc.*, **1988**, *110*, 400.

24. (a) Casalone, G.; Mariani, C.; Mugnoli, A.; Simonetta, M.; *Acta Cryst.*, **1969**, *B 25*, 1741. (b) Hargreaves, A.; Rizvi, S. H.; *Acta Cryst.*; **1962**, *15*, 365. (c) Michelsen, H.; Klæboe,

P.; Hagen, G.; Stroyer-Hansen, T.; *Acta Chem. Scand.*, **1972**, *26*, 1576. (d) Coulson, C. A.; *Faraday Soc. Trans*, **1946**, *42*, 106.

25. Patai, S.; Rappoport, Z. *The Chemistry of the Quinonoid Compounds, Vol. 2, Part 1*, John Wiley & Sons, London, **1988**.

26. Ege, S.; *Organic Chemistry: Structure and Reactivity, Third Ed.*, D. C. Heath and Company, Lexington, Massachusetts, **1994**, 1061.

27. Takahashi, K.; Suzuki, T.; Akiyama, K.; Ikegami, Y.; Fukazawa, Y.; *J. Am. Chem. Soc.* **1991**, *113*, 4576.

28. Jorgensen, J. Ph.D. Thesis, University of Wisconsin-Madison, **1981**. (As cited in Wellman, D. E.; Lassila, K. R.; West, R.; *J. Org. Chem.* **1984**, *49*, 965.)

29. (a) Cohen, M. J.; Garito, A. F.; Heeger, A. J.; MacDiarmid, A. G.; Mikulski, C. M.; Saran, M. S.; Kleppinger, J.; *J. Am. Chem. Soc.*, **1976**, *98*, 3844. (b) Burt, F. P.; *J. Chem. Soc.*, **1910**, *97*, 1171.

30. Ernest, I.; Holick, W.; Rihs, G.; Schomburg, D.; Shoham, G.; Wenkert, D.; Woodward, R. B.; *J. Am. Chem. Soc.*, **1981**, *103*, 1540.

31. Lide, D. R., Ed.-in-chief; *CRC Handbook of Chemistry and Physics, 80^{h} Ed.*, **1999**, CRC Press, Boca Raton, Florida.

32. Bondi, A.; *J. Phys. Chem.*, **1964**, *68*, 441.

33. Gleiter, R.; Bartetzko, R.; Cremer, D.; *J. Am. Chem. Soc.*, **1984**, *106*, 3437.

34. Klein, H.; Oakley, R. T.; Michl, J.; *Inorg. Chem.*, **1986**, *25*, 3194.

35. Amin, M.; Rees, C. W.; *J. Chem. Soc. Chem. Commun.*, **1989**, 1137.

36. Boeré, R. T.; Moock, K. H.; Derrick, S.; Hoogerdijk, W.; Preuss, K.; Yip, J.; *Can. J. Chem.*, **1993**, *71*, 473.

37. Pascal, R. A. Jr.; *Pure & Appl. Chem.*, **1993**, *65*, 105.

38. Pascal, R. A. Jr.; L'Esperance, R. P.; *J. Am. Chem. Soc.*, **1994**, *116*, 5167.

39. Burford, N.; Chivers, T.; Codding, P. W.; Oakley, R. T.; *Inorg. Chem.*, **1982**, *21*, 982.

40. Oakley, R. T.; *Can. J. Chem.*, **1984**, *62*, 2763.

41. Boutique, J. P.; Riga, J.; Verbist, J. J.; Delhalle, J.; Fripiat, J. G.; Haddon, R. C.; Kaplan, M. L.; *J. Am. Chem. Soc.*, **1984**, *106*, 312.

42. Basch, H.; Viste, A.; Gray, H. B.; *Theor. Chim. Acta*, **1965**, *3*, 458.

43. Boeré, R. T.; Cordes, A. W.; Craig, S. L.; Oakley, R. T.; Reed, R. W.; *J. Am. Chem. Soc.*, **1987**, *109*, 868.

44. Gross, H.; Bischoff, Ch.; Höft, E.; Gründemann, E., *Preparative Organic Chemistry*, Hilgetag, G.; Martini, A., Eds., John Wiley & Sons, Inc., N. Y., **1972**.

45. (a) Wendling, L. A.; Koster, S. K.; Murray, J. E.; West, R.; *J. Org. Chem.*, **1977**, *42*, 1126. (b) Gierke, W.; Harrer, W.; Kurreck, H.; Reusch, J.; *Tetrahedron Lett.*, **1973**, 3681.

46. Zweifel, G.; Murray, R. E.; *Synthesis*, **1980**, 150.

47. Gronowitz, S.; Uppström, B.; *Acta Chem. Scand. B.*, **1974**, *28*, 981.

48. Sicé, J.; *J. Org. Chem.*, **1954**, *19*, 70.

49. Dean, J. A.; *Handbook of Organic Chemistry*, McGraw-Hill Book Company, N. Y., **1987**.

50. Barclay, T. M.; Cordes, A. W.; Oakley, R. T.; Preuss, K. E.; *Acta Cryst. C*, **1996**, *52*, 3250.

51. Kitamura, C.; Tanaka, S.; Yamashita, Y.; *J. Am. Chem. Soc.*, **1995**, *117*, 6791.

52. Kitamura, C.; Tanaka, S.; Yamashita, Y.; *Chem. Mater.*, **1996**, *6*, 570.

Chapter 3 Closed-Shell Bis-1,2,3-Dithiazoles and Their Charge-Transfer Salts.

3.1 Introduction

The idea of designing molecular conductors based on 1,2,3-dithiazole (DTA) rings (**III-2**) evolved from our continuing work with sulfur-nitrogen heterocycles. Among other issues, lowering the Coulombic barrier to conduction ($U \approx \Delta H_{disp}$ = IP - EA for a neutral radical), introduced in Chapter 1, is a primary goal in the design of conducting molecular materials. The incorporation of 1,2,3-dithiazole rings (**III-2**) represents a step in the right direction. The gas phase disproportionation enthalpy (ΔH_{disp}) for compounds based on **III-2** is calculated to be smaller than that of analogous 1,3,2-dithiazoles (**III-1**) that previously had been our focus. Consequently, the Coulombic barrier, U, is expected to be smaller as well. This is due, in great part, to the difference in spin density distribution. Unlike 1,3,2-dithiazole (**III-1**), the 1,2,3-dithiazole (**III-2**) has spin density on one of the two carbon atoms. This allows for the delocalization of spin density onto a substituent thereby spreading the spin density over a greater molecular area. Accordingly, we believe that, in principle at least, the 1,2,3-dithiazole (**III-2**) ring system has superior properties in terms of its use as a building block for designer solid state molecular conductors.

As discussed in Chapter 1, a decrease in the calculated value of ΔH_{disp} suggests a lower barrier to conduction in a solid state material. Whether conduction in the crystalline state is actualized is also dependent on the degree of intermolecular electronic interaction and therefore on the orientation and proximity of the molecules. In the case of 1,2,3-dithiazole-based ring systems, π-stacking is desirable such that intermolecular interactions of the π SOMOs are maximized.

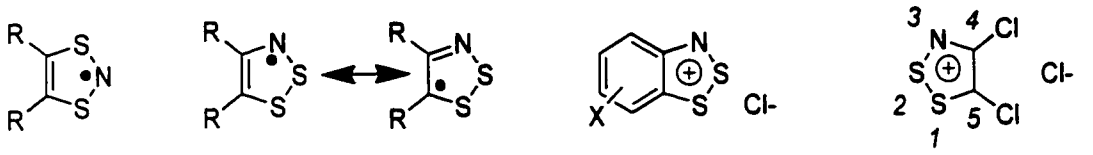

III-1
a) R = H

III-2
a) R = H
b) R = Cl

III-3

[III-2b][Cl]

Figure 3.1 Simple dithiazoles.

From a synthetic standpoint, building compounds that incorporate the 1,2,3-dithiazole heterocycle (**III-2**) is more challenging than the synthesis of systems based on the sister 1,3,2-dithiazole (**III-1**). Nevertheless examples of both as salts of their cations have been known for many decades. Substituted 1,2,3-benzodithiazolium chlorides (Herz compounds, **III-3**) were first reported in the 1920s.[1] These cation salts are the product of the Herz reaction,[2] the treatment of aromatic amines with sulfur monochloride. A second well-known simple 1,2,3-dithiazole compound is 4,5-dichloro-1,2,3-dithiazolium chloride, otherwise known as Appel's salt[3] [**III-2b**][Cl]. It is the product of the treatment of acetonitrile, chloroacetonitrile, or dichloroacetonitrile with sulfur monochloride. Both the Appel's synthesis and the Herz reaction are discussed in greater detail in Chapter 4.

In the present chapter, the reactivity of Appel's salt [**III-2b**][Cl] and its products will be highlighted. The chlorine at the 5-position of [**III-2b**][Cl] has been shown to react readily with a number of nucleophiles.[3,4] It was our intention to use this reactivity to build bis(1,2,3-DTA) systems that have stable radical cation oxidation states. In this manner, new charge transfer molecular semiconductors might be designed. Several bridged bis(1,2,3-DTA)s arising from this work are discussed herein.

3.2 The Logistics of Linking Two 1,2,3-Dithiazole Rings

Let us consider the three ways in which two 1,2,3-DTA rings (**III-2**) might be connected *via* the carbon sites. In theory, bridging is possible from the carbon C5 of one ring to C5' of the second ring, from C4 to C4', and from C4 to C5'. The nature of the electronic interaction between dithiazole rings is greatly influenced by the manner in which they are linked. A variety of possible interactions are presented qualitatively in the following scheme (**Figure 3.2**).

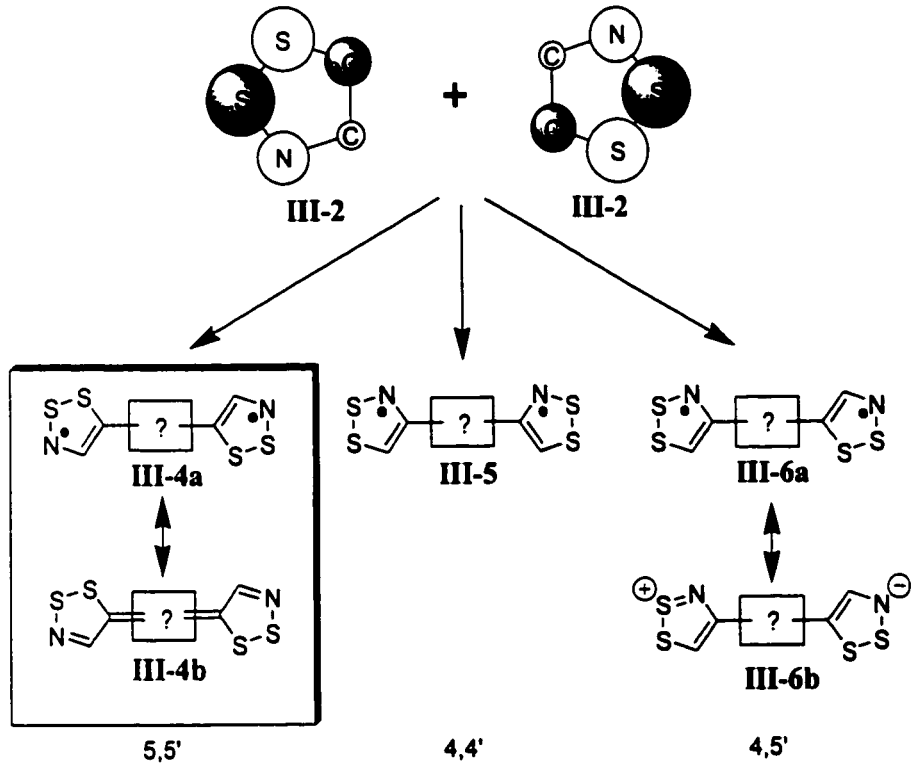

Figure 3.2 Logistics of linking two 1,2,3-DTA rings.

The location of the spin density of the one unpaired electron in a simple 1,2,3-dithiazolyl ring (**III-2**) is an important factor in predicting the electronic interactions that arise from the different possible ring connectivities. *Ab initio* calculations performed on 4,5-diprotio-1,2,3-dithiazolyl (**III-2a**) predict a large spin density on sulfur, nitrogen and the carbon C5 but a small,

almost nodal, spin density on carbon C4. This is shown qualitatively in **Figure 3.2** as the top view of p-type orbitals of the SOMO located at each ring atom. The amplitude of the circles reflects the orbital coefficients and the shading of the circles represents the phase of the orbital. As shown, the SOMO for this radical is antibonding over the S-N and S-S linkages. The quantitative results of the calculations are given below in **Table 3.1**.

Table 3.1 Calculated Spin Density Distribution[a] for Three Comparable Heterocycles.

	III-1a		**III-2a**		**III-8**
S1	0.200	S1	0.194	S1	0.256
S3	0.200	S2	0.192	S2	0.256
N2	0.586	N3	0.385	N3	0.316
C4	0.009	C4	-0.160	C4	-0.150
C5	0.009	C5	0.404	N5	0.316

[a] Spin densities reported as results from the Gaussian *G98W* package using B3LYP/6-31G**.

Determining the ground state of a bis(1,2,3-DTA) harkens back to the discussion in Chapter 1 on the possible states arising from two electrons in two orbitals. There are four possible states (six microstates) available to such a system. In the case of linkage *via* the 5,5' carbons, two possible ground state configurations are considered. The first is the diradical triplet configuration (**III-4a**) in which there is very little interaction between the two rings. The second is the lower of the two possible closed-shell singlets, characterized by double bonding at the carbon 5 position giving rise to a quinoid species (**III-4b**). The open shell singlet configuration is not considered here since the triplet is generally assumed to be the lower of the two open shell configurations, in accord with Hund's rules. It should be noted, however, that there do exist rare exceptions to this edict.[5] The higher closed shell singlet is disregarded as it is apparent that it does not represent the

ground state.

Which of the two configurations under consideration dominates as the ground state depends on the nature of the bridge linking the rings. One can imagine that a system in which conjugation is possible will favour the closed shell configuration. The open shell configuration might be favoured when conjugation is impossible or requires that a large energy barrier due to steric interactions or aromatic stabilization be overcome.

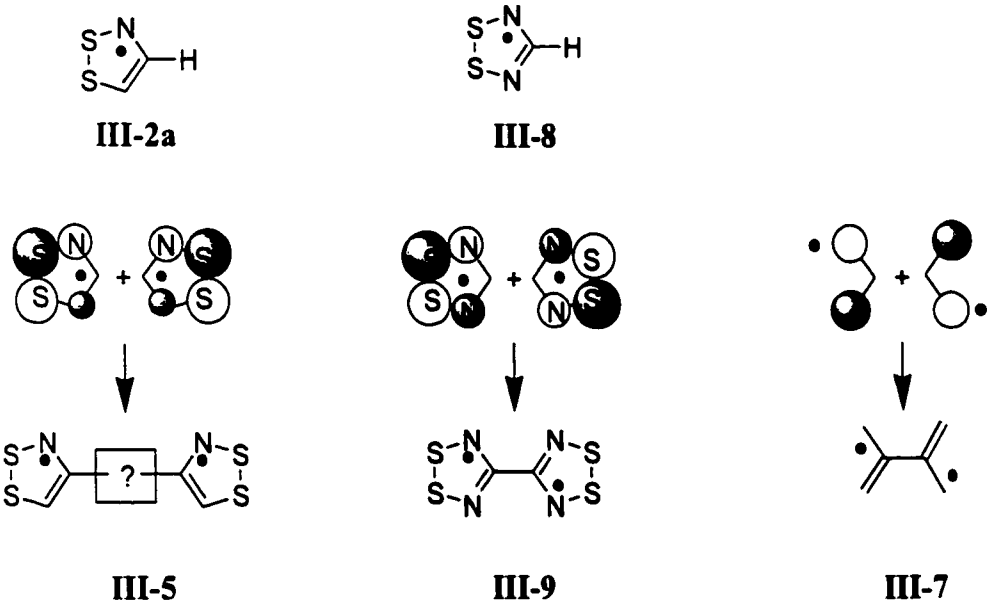

Figure 3.3 Figurative comparison of the spin distribution in known bis(1,2,3,5-dithiadiazolyl), theoretical 4,4'-bis(1,2,3-DTA)s, and tetramethylenethane.

The almost nodal character of the C4 site in the SOMO greatly decreases the possibility of ground state electronic interactions between dithiazole ring π systems in any species based solely on a 4,4' linkage. The prediction that a theoretical 4,4'-bis(1,2,3-DTA) has a diradical ground state (**III-5**) is supported by the examination (Borden and Davidson, 1977)[6] of analogous conjugated hydrocarbon diradicals. Tetramethylenethane (**III-7**), for example, can be regarded as the union of two allyl radicals at the central (nodal) carbon giving rise to a disjoint diradical (a

molecule possessing two non-bonding molecular orbitals occupied by two electrons). In this same vein, a parallel can be drawn between a theoretical **III-5** and the known bis(1,2,3,5-dithiadiazolyl)[7], **III-9**. The SOMO of the parent 1,2,3,5-dithiadiazolyl (**III-8**) has a node at the bridgehead carbon, thus dimerization at this site gives rise to a molecule that is perfectly disjoint. By analogy, **III-5** can be expected to exist as a disjoint species.

The third possible carbon-carbon linkage is the 4,5' type. In this case, one of the bridgehead carbons, C4, is almost nodal while a relatively large spin density resides on the C5' carbon. As with the 4,4' and the 5,5' linkages, a diradical triplet (**III-6a**) is expected to be one possible ground state.[8] In this case, however, a closed shell configuration based on charge separation (**III-6b**) is also a viable ground state configuration. Species based on a 4,5' linkage are intermediate between the 5,5' case in which a close shell quinoid is expected unless the bridging system prevents it and the 4,4' connectivity which theoretically gives rise to an open shell triplet. Some degree of electronic interaction between the rings may be expected in a 4,5' linkage, but a quinoid structure is not possible in this case. The only ground state closed shell species that may be possible is a zwitterionic structure.

3.3 Proposed Bridging Groups for the 5,5' Closed Shell Linkage

Since the discovery of charge transfer salts based on a 1,1',3,3'-tetrathiafulvalene (TTF, **III-10**) donor accompanied by an appropriate acceptor, many new donor designs based on the TTF skeleton have been devised. One year after TTF-TCNQ was first prepared,[9] the selenium analogue 1,1',3,3'-tetraselenafulvalene (TSF, **III-11**)-TCNQ was reported.[10] Variations of TTF by substitution at the 4, 4', 5, and 5' positions are ubiquitous.[11] Donor compounds of this ilk include BEDT-TTF (**III-12**) and MDT-TTF (**III-13**).[12] The isomeric 1,1',2,2'-tetrathiafulvalene (**III-14**) is also reported to have electronic properties similar to TTF.[13] With these thoughts in

mind, a closer inspection of the closed shell 5,5' linked bis(1,2,3-DTA) system, **III-4b**, reveals a remarkable physical and electronic resemblance to previously known TTF-based donor molecules. We have investigated a variety of closed shell 5,5' linked bis(1,2,3-DTA) designs with the intention of synthesizing compounds that may act as charge transfer donors in a manner similar to TTF.

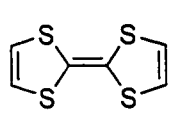

III-10

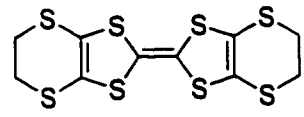

III-12

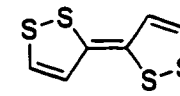

III-14

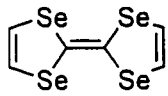

III-11

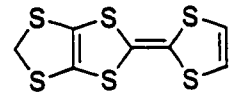

III-13

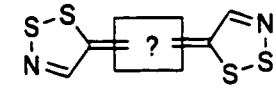

III-4b

Figure 3.4 A variety of TTF-like CT donors.

In order for a neutral compound to act as a one-electron charge transfer donor, a stable radical cation oxidation state must be accessible. In practical terms, with regard to bis(1,2,3-DTA) systems, this means that the individual dithiazole rings must be able to interact electronically with one another through the bridging structure. A one-electron oxidation of one ring affects the oxidation potential of the other. In molecular orbital (MO) terms, the degenerate SOMOs of each dithiazole must mix with the π system of the bridging structure such that they generate two molecular orbitals of different energies. Double occupancy of the lower energy MO gives rise to a closed shell ground state. In the case that the dithiazole SOMOs do not mix with the bridging structure MOs, a set of singly occupied degenerate MOs is the result. The oxidation potential of the two unpaired electrons is identical, and a radical cation is not attainable.

This chapter focuses on bis(1,2,3-DTA) systems that are bridged exclusively through C5 to C5' in a manner that results in a closed shell quinoid ground state, **III-4b**. The important issue

in this investigation is developing a type of bridge that favours a closed shell ground state and enables intramolecular electronic interaction between the peripheral dithiazole rings. In other words, we are probing the necessary structural conditions for the design of a group of bridged bis(1,2,3-DTA)s in which there is an observable trend toward greater electronic interaction between DTA rings.

Our choice of linkage structures for the design of a series of such molecules was based on three criteria. First, it was necessary that conjugation through the bridge be possible so that the dithiazole rings should interact electronically, enabling the viability of a radical cation species. Second, the various linkage structures were chosen in order to form a coherent series of bridged compounds in which the influence of the linkage design on the electronic structure of the molecule was apparent. Finally, for synthetic ease and consistency, the bridged compounds presented herein were available from a reaction of Appel's salt **[III-2b]**[Cl].

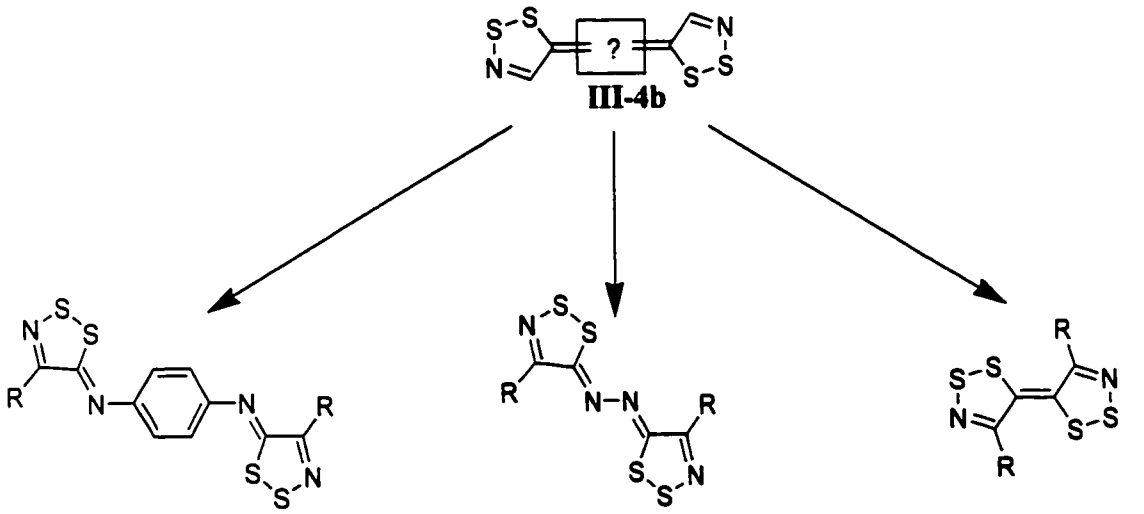

Figure 3.5 Series of 5,5'- linked bis(1,2,3-DTA)s.

The three 5,5'-linked bis(1,2,3-DTA)s that we have successfully isolated and characterized are **III-15b**, **III-16b**, and **III-17b**. These compounds and the theoretical prototypal **III-15a**, **III-16a**, and **III-17a** are discussed herein. Additionally, failed attempts at the synthesis of other 5,5'-linked bis(1,2,3-DTA)s are summarized. As Appel's salt **[III-2b]**[Cl] is the starting material for all these compounds, a section outlining the reactivity of **[III-2b]**[Cl] is appropriate.

3.4 Reactivity of Appel's Salt

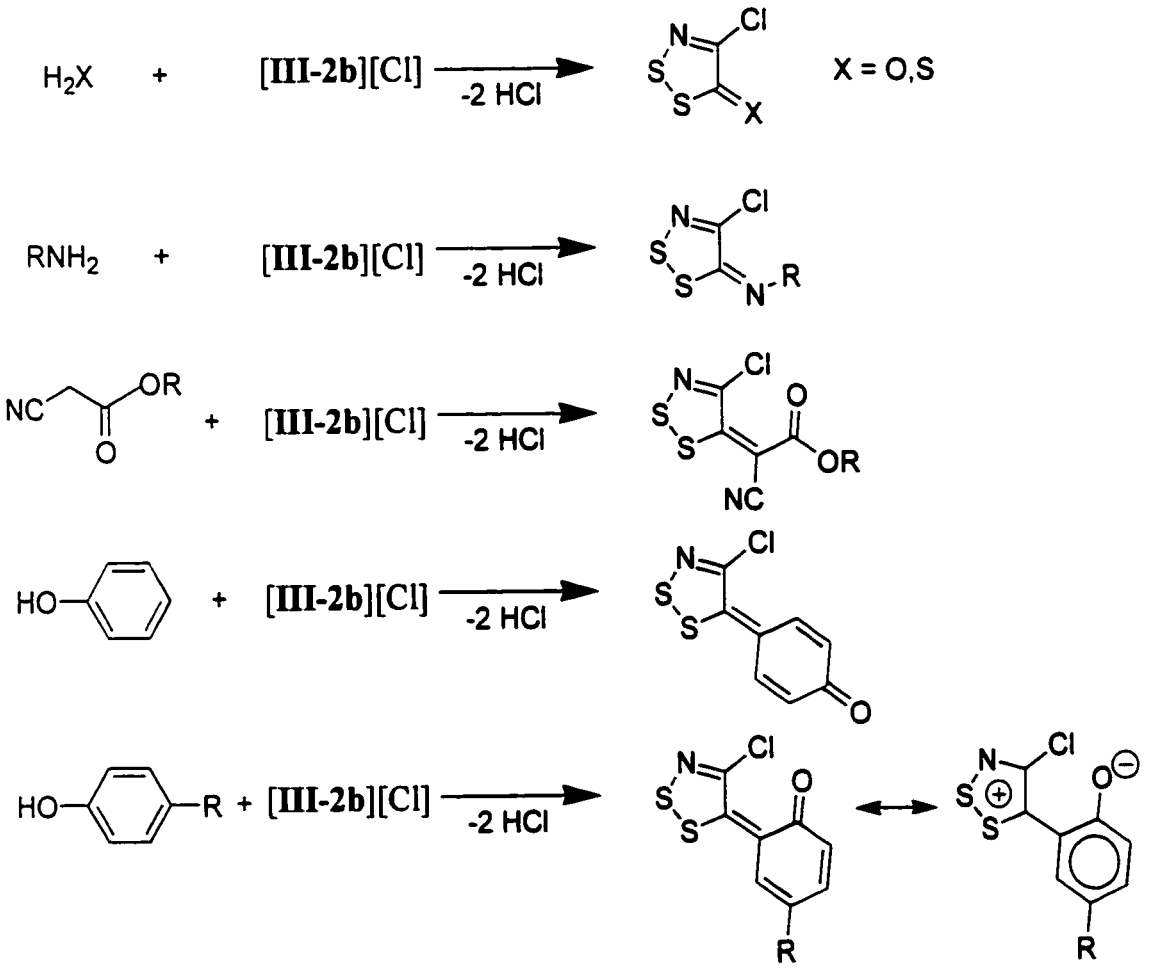

Figure 3.6 Reaction of various nucleophiles with Appel's salt, **[III-2b]**[Cl].

4,5-Dichloro-1,2,3-dithiazolium chloride **[III-2b]**[Cl], otherwise known as Appel's salt, is produced by treating acetonitrile with sulfur monochloride (see Chapter 4). The chlorine at the 5-position of this salt has been shown to readily undergo substitution with a number of nucleophiles.[3] Much of the current investigation into the reactivity of **[III-2b]**[Cl] deals with its usefulness as a synthetic precursor to other important heterocycles and chemical moieties.[14] It is worth noting that 5-arylimino-4-chloro-5*H*-1,2,3-dithiazoles, the product of the treatment of primary aryl amines with **[III-2b]**[Cl], are discussed at length in a recent review[15] where it is suggested that these compounds may be useful fungicides, ovicides, insecticides and herbicides. **Figure 3.6** shown below lists a variety of nucleophiles and the resulting known products upon reaction with **[III-2b]**[Cl].

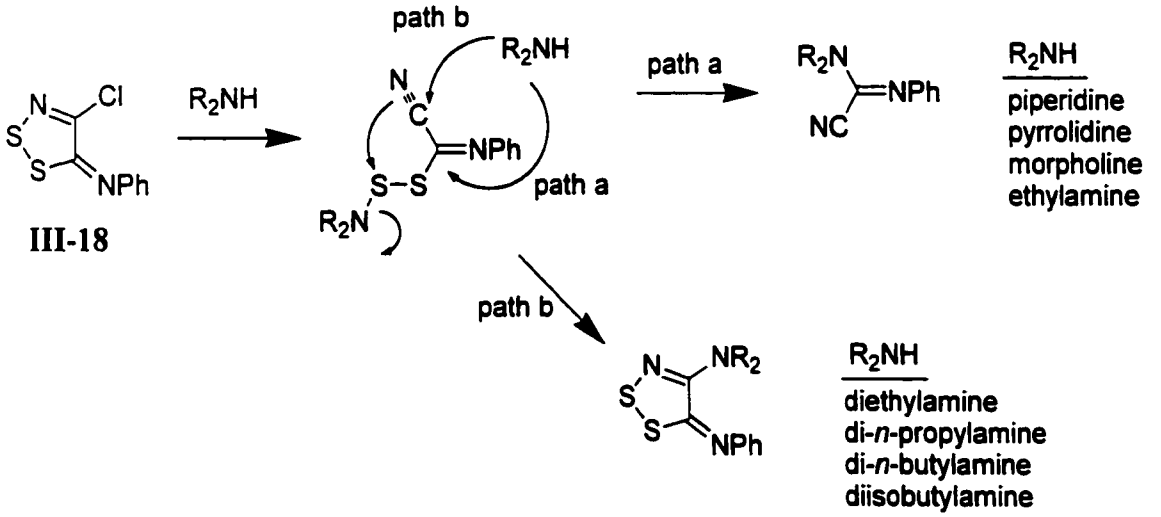

Figure 3.7 Proposed reaction pathway for **III-18**.

While the chlorine at the 5-position of **[III-2b]**[Cl] is easily substituted, the chlorine at the 4-position appears to be relatively inert. Substitution at this position was first reported by Rees[16], however no characterization data was published to validate the claim. Kim *et al.*[17] report the

replacement of the chlorine of 5-phenylimino-4-chloro-5*H*-1,2,3-dithiazole (**III-18**) with a -NR_2 group (where R = ethyl, *n*-propyl, *n*-butyl, isobutyl) by reaction with the appropriate secondary amine (crystal structure has been reported[17]). No reaction was observed with primary amines, nor was this reaction observed with *all* secondary amines. It was suggested that the reaction was not strictly a substitution, but proceeded *via* a ring opening followed by a ring closure. This was deduced on the basis of the isolation of a ring-opened intermediate. Two mechanistic pathways were suggested in order to explain the observed outcome.

A method to obtain a 4-substituted equivalent of [**III-2b**][Cl] has been reported by Rees *et al.*[18] The reaction of acetophenone oxime with an excess of sulfur monochloride produces a solid which, when subsequently treated with water, yields 4-phenyl-1,2,3-dithiazol-5-one or, when treated with aniline, yields 4-phenyl-5-phenylimino-1,2,3-dithiazole (**III-20**, crystal structure published *ibid.*). The reasonable assumption is that the solid intermediate product is 4-phenyl-5-chloro-1,2,3-dithiazolium chloride, **III-19**.

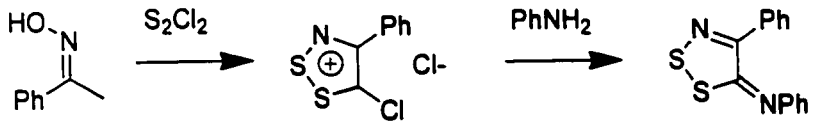

III-19 **III-20**

Figure 3.8 Suggested synthetic route to 4-phenyl-5-chloro-1,2,3-dithiazolium chloride.

We have chosen Appel's salt [**III-2b**][Cl] as a synthetic precursor to bis(1,2,3-DTA) charge transfer donors for two reasons. First, the ease of reactivity of the 5-position without the destruction of the 1,2,3-dithiazole ring makes it an obvious candidate. Second, *ab initio* calculations of the parent 1,2,3-dithiazolyl (**III-2**) show that the spin density on carbon C5, the

carbon at which substitution takes place, is sufficient with respect to the other ring atoms to expect the unpaired electron to delocalize to some extent off the DTA ring and onto a substituent, particularly an electron withdrawing substituent.

In order to effect the synthesis of the bis(1,2,3-DTA)s, we performed the reaction of **[III-2b]**[Cl] with two different diamine binucleophiles: 1,4-phenylenediamine and anhydrous hydrazine. It is worth noting that these are the first reported bis[5-imino-4-chloro-5*H*-1,2,3-dithiazoles]. In addition, we attempted to react **[III-2b]**[Cl] with a variety of other bi-nucleophiles including thiophene, bithiophene, and 2,5-dichloro-3,6-diaminopyrazine. In these latter reactions, we met with little success. Finally, we synthesized **III-17** by the reduction of **[III-2b]**[Cl].

3.5 General Discussion of Closed Shell 5,5'-bis(1,2,3-DTA) Syntheses

3.5.1 The Reaction of Appel's Salt [III-2b][Cl] with 1,4-phenylenediamine

The reaction of Appel's salt **[III-2b]**[Cl] with 1,4-phenylenediamine yields 1,4-diimino-1*H*,4*H*-bis[4-chloro-5*H*-1,2,3-dithiazole]benzene (**III-15b**). The product of this reaction under strictly dry conditions is the yellow dichloride salt **[III-15b]**$[Cl]_2$. This is easily reduced to the neutral material by washing the solid product with ethanol. The resulting dark orange compound **III-15b** is air-stable and easily recrystallized from toluene or chlorobenzene. The literature reactions of **[III-2b]**[Cl] with primary amines suggest that the addition of a base or an excess of the amine is required in order to neutralize the hydrochloric acid biproduct. We found that neither an alkaline medium nor an excess of amine is necessary. On the contrary, excess amine does not yield the expected product whereas an excess of **[III-2b]**[Cl] seems to produce the best results.

The 1,4-phenylenediimino- bridge was considered for a number of reasons. In theory, conjugation through the continuous π system of this bridge is possible allowing the dithiazole rings double bonded to the nitrogens to undergo electronic interactions. Should such interactions

be permissible, a radical cation species might be accessible. In addition, it is unlikely that such a structure would have a triplet ground state as that would require overcoming the aromatic stabilization energy of the phenyl ring. Thus, the ground state is expected to be closed shell.

Although it would seem that **III-15** meets all the necessary criteria for the design of a charge transfer donor compound, in practice, a radical cation oxidation state is not accessible. The same aromatic stabilization energy barrier that prevents a triplet ground state also inhibits conjugation through the bridge to any great extent. This is borne out in the solid state structure in which the dithiazole rings of **III-15b** are not coplanar with the phenyl linkage. This effectively prevents the formation of a radical cation and therefore excludes this species as a possible charge transfer donor.

Attempts to synthesize the *ortho* isomer of **III-15b** met with limited success. Steric hindrance may be a limiting factor. Alternatively, it is possible that the dithiazole ring of the mono- substituted intermediate undergoes a reaction with the *ortho* amino group leading to some sort of ring closure. Similar reactions have been reported of *ortho* substituted 5-arylimino-4-chloro-5*H*-1,2,3-dithiazoles.[3]

[**III-2b**][Cl] does not react with 1,3-phenylenediamine nor with melamine to give a bis- or tris- substituted product. This observation suggests that although the conjugation in the **III-15b** is not great enough to allow the formation of a radical cation, it may be necessary in order to allow bis- substitution to take place.

3.5.2 The Reaction of Appel's Salt [III-2b][Cl] with Hydrazine

If the phenyl ring is removed from the bridging structure of **III-15**, then the aforementioned barrier to conjugation is no longer problematic. The dinitrogen-bridged compound, 1,2-bis[4-chloro-5*H*-1,2,3-dithiazole]dinitrogen (**III-16b**) is obtained as a neutral

species from the reaction of anhydrous hydrazine with **[III-2b]**[Cl]. Red, air-stable crystals with a green opalescence are produced by recrystallization from chlorobenzene or toluene. Crystals suitable for cyclic voltammetry and single crystal X-ray diffraction were grown by sublimation *in vacuo* at 130°C (10^{-2} Torr) as beautiful blocks. In this simple diazine- bridged compound, **III-16b**, a closed shell ground state can be expected, and indeed is observed.

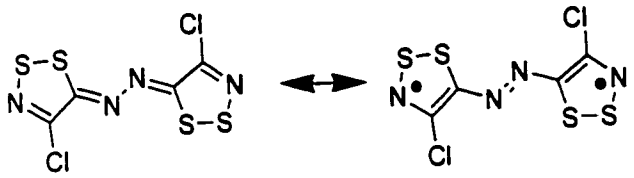

III-16b

Figure 3.9 Possible ground state configurations of **III-16b**.

The structure of **III-16b** is planar in the crystal state. Interestingly, only the C_{2h} symmetry is observed for this compound. There is no spectroscopic evidence for rotation about the diazine bond to give a C_{2v} compound (**III-16ib**). Neither is there evidence of the other possible isomer (**III-16iib**) that may form in the initial synthesis or by rotation about the bond between a bridge nitrogen and a dithiazole carbon C5.

A comparison of the closed shell ground state energies for these three isomers is presented in **Table 3.2**. As shown, the energies of the geometry optimized rotational structures are 29.0 and 10.2 kcal higher (for **III-16ib** and **III-16iib** respectively) than the crystallographically observed conformation. The extent to which this may be due to steric interactions involving chlorine, or conversely stabilization effects involving chlorine, can be determined by comparison of the protio-structures of the each of these rotomers.

Table 3.2 Energy Differences[a] Between Several III-16 Conformations and Configurations.

compound	total E (hartrees)	rel. E (eV)	rel. E (kcal)
III-16a (singlet)	-1965.31615210	0	0
III-16a (triplet)	-1965.26746400	1.32	30.5
III-16ia (singlet)	-1965.27327600	1.17	26.9
III-16iia (singlet)	-1965.30779590	0.23	5.2
III-16b (singlet)	-2884.49184570	0	0
III-16b (triplet)	-2884.40827540	2.27	52.4
III-16ib (singlet)	-2884.44563370	1.26	29.0
III-16iib (singlet)	-2884.47552230	0.44	10.2

[a] Values obtained from B3LYP/6-31G** with geometries restricted to planarity.

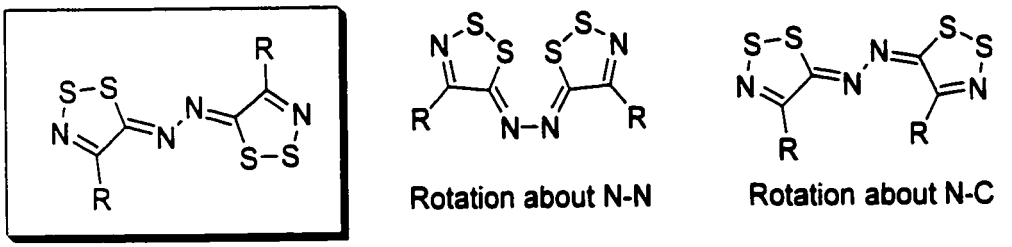

III-16
a) R = H
b) R = Cl

III-16i
a) R = H
b) R = Cl

III-16ii
a) R = H
b) R = Cl

Figure 3.10 Possible rotamers of **III-16**.

In theory, a low lying triplet structure for this compound indicates that there is conjugation *via* the diazine- bridge that enables the dithiazole rings to interact electronically. Thus, it is not unreasonable to propose the synthesis of cation salts based on this compound. Satisfyingly, we have been able to isolate the radical cation **[III-16b]**$^{+}$ in the crystal state.

3.5.3 The Reduction of Appel's Salt

The simplest structure in this study is **III-17**, in which the dithiazole rings are directly bonded to one another through C5 to C5'. The lack of any bridge effectively enables a strong inter-dithiazole electronic interaction. Thus we have a benchmark against which the effectiveness of any bridging structure can be judged.

The synthesis of **III-17b** was, in fact, the result of an attempt to explore the possibility of isolating, or simply observing, a simple 4,5-dichloro-1,2,3-dithiazolyl, **III-2b**. We performed the reduction of [**III-2b**][Cl] with both triphenylantimony and zinc in a variety of solvents. While organic solvents seem to be generally ineffective, the reduction of [**III-2b**][Cl] with triphenylantimony in liquid sulfur dioxide produces a black solid that is easily isolated. This reaction does not afford the expected 4,5-dichloro-1,2,3-dithiazolyl radical **III-2b**. Instead, a dimerization at the C5 carbon occurs yielding the novel *trans*-4,4'-dichloro-1,1',2,2',3,3'-tetrathiadiazafulvalene[19] (**III-17b**) when two equivalents of triphenylantimony are used.

As with the bis(1,2,3-DTA) systems previously discussed, both a closed-shell singlet structure and a diradical triplet structure can be envisioned as representative of neutral **III-17b**. While **III-17b** is diamagnetic, solutions in organic media appear dark purple with an absorption maximum near 565 nm, indicating a small HOMO - LUMO gap. The single crystal X-ray structure of **III-17b** is consistent with the closed-shell fulvalene rather than the diradical formulation. *Ab initio* calculations (B3LYP/6-31G**) performed on the prototypal *trans*-4,4'-diprotio-1,1',2,2',3,3'-tetrathiadiazafulvalene **III-17a** confirm that the fulvalene-like ^1A_g state is lower in energy than the ^3B_u state by 21.8 kcal mol^{-1}.

The radical cation oxidation state [**III-17b**]$^+$ is readily accessible as expected. If only one equivalent of triphenylantimony is used in the reduction of [**III-2b**][Cl], the resulting black solid is the radical cation chloride of the dimerization product ([**III-17b**][Cl]), as can be deduced from

its infrared and ESR spectra. A variety of charge transfer salts have been prepared for this compound. A more detailed discussion of the nature and physical properties of these materials is presented later in this chapter.

As a consequence of the use of **[III-2b]**[Cl] as a precursor to this compound and the aforementioned materials, the C4 of the dithiazole rings is chlorinated, **III-17b**. In order to be able to use **III-17b** as a true standard for comparison for this series, it is appropriate to determine the extent to which chlorination at the C4 dithiazole sites affects the energetics of this species. The outcome of comparative *ab inito* calculations for the **III-17a** versus **III-17b** indicates that the chlorines have very little effect on the energetics (see **Table 3.3**). This is to be expected given the almost nodal character of the C4 carbon. In addition, the chlorines do not interfere sterically with the planarity of the compound.

Table 3.3 Calculated Energy Difference[a] Between the Singlet and Triplet Configurations of Compound III-17.

	E(triplet-singlet) hartrees	eV	kcal
III-17a	0.03466830	0.94	21.7
III-17b	0.03502190	0.95	22.0

[a] Values obtained from B3LYP/6-31G**.

It has been previously noted herein that *ab initio* calculations performed on the simple 1,2,3-dithiazolyl radical **III-2a** indicate a large spin density on the C5 carbon. It is therefore not surprising that reduction of a simple DTA system such as **[III-2b]**[Cl] yields a C5-C5' dimer product. This is reminiscent of previous work on the reduction of 3-chlorodithiolylium salts.[13] In Chapter 4, steric protection of the C5 position in order to prevent dimerization is discussed.

Only the *trans*- isomer of **III-17b** has been isolated. There is no evidence suggesting the existence of the *cis*- isomer. Steric repulsion between the two chlorines in the latter configuration

is most likely the major factor in this preference.

3.5.4 Unsuccessful Reactions of Appel's Salt with Binucleophiles

The reaction of [**III-2b**][Cl] was attempted with 2,5-dichloro-3,6-diaminopyrazine **III-21** as well as several non-amine nucleophiles including bithiophene and thiophene. Of these nucleophiles, only the reactions with **III-21** and with bithiophene yielded promising products.

The reaction of [**III-2b**][Cl] with **III-21** yields air-stable, dark orange crystals of 2,5-dichloro-3,6-diimino-3*H*,6*H*-*bis*[4-chloro-5*H*-1,2,3-dithiazole]pyrazine (**III-22**). These are easily recrystallized from hot dichloroethane. However, crystals of **III-22** grown by sublimation *in vacuo* at 150°C (10^{-2} Torr) were never of suitable quality for X-ray structural analysis or cyclic voltammetry. This compound was investigated as an extension of **III-15** and **III-16** in order to probe the issues involved in decreasing the barriers to conjugation through a bridge by decreasing the aromatic stabilization energy and increasing the electron withdrawing capacity of the bridge. The chloro- substituted pyrazine ring was chosen as a replacement for the phenyl ring since it offers the possibility of sulfur - nitrogen inter-ring stabilizations that may favour a planar structure. While we were able to synthesize **III-22** reliably and reproducibly according to mass spectrometry and IR spectra, we were unable to obtain crystals suitable for X-ray analysis. Furthermore, this compound did not provide a CV of sufficient quality to be interpreted in terms of the donor abilities of **III-22**.

Reaction of Appel's salt [**III-2b**][Cl] with bithiophene yields a material that is metallic green in appearance and gives a bright blue solution in methylene chloride, despite its sparing solubility. Extraction of this solid over a period of days into methylene chloride yields the purified material as a precipitate in the extraction liquor. Characterization by elemental analysis militates against the proposed bis(1,2,3-DTA) substituted structure (**III-23**) and does not seem to support

any simple dithiazole substituted bithiophene structures adequately. The mass spectrum of this compound, however, shows a mono- substituted bithiophene plus one proton, possibly the imide of the dithiazole ring, as the parent ion. The poor solubility of this compound prevented the generation of crystals suitable for X-ray analysis. We were unable to identify this material conclusively as **III-23**.

Although the combined aromatic stabilization energy of two thiophene rings is greater than that of a single benzene ring, direct bonding of the dithiazole rings to the 2 and 5' positions of bithiophene, thereby bypassing the need for amino groups, may decrease the barrier to conjugation. This was one of the reasons bithiophene was investigated as a possible bridging ligand. A closed shell quinoid configuration (**III-23**) and a diradical triplet configuration (**III-23i**) are the two competing possible ground states for the theoretical bithiophene linked system. In this case, however, should the ground state be quinoid, the molecule is forced to be planar and the dithiazole rings must interact electronically. As with the aforementioned systems, if the ground state is a triplet, the dithiazole rings will most likely not interact to any appreciable extent.

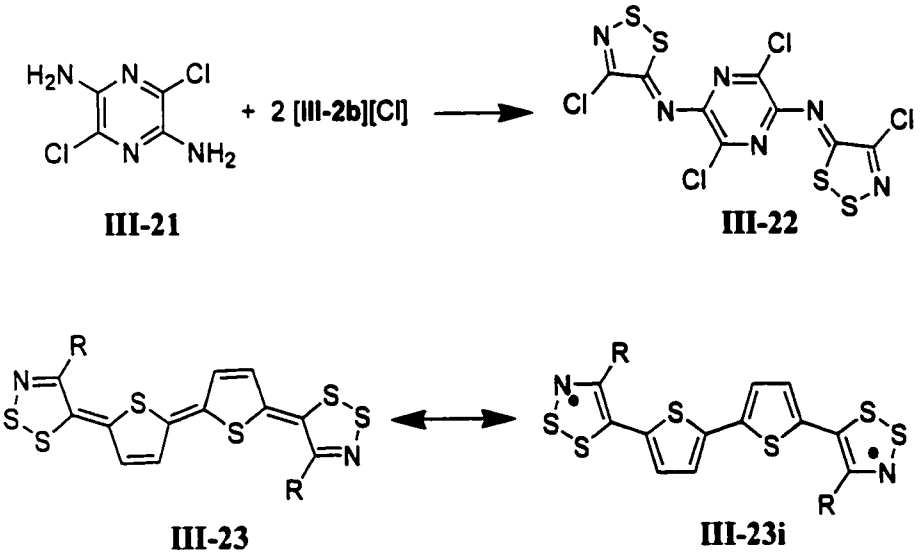

III-21 **III-22**

III-23 **III-23i**

Figure 3.11 Pyrazine-linked and bithiophene-linked bis(1,2,3-DTA)s.

3.6 "Enabling the Interaction": Comparing III-15, III-16, and III-17

A brief comparison of **III-15b**, **III-16b**, and **III-17b** is valuable in order to understand this concept of progressively increasing the degree to which the dithiazole rings interact electronically by decreasing the barrier to conjugation. All three compounds are fully characterized and thus lend credence to the calculated results discussed herein.

As previously stated, the barrier to conjugation in **III-15** is great enough that dithiazole interaction is not observed. **III-16** can be described as **III-15** with the central phenyl ring removed. The conjugation now enables some degree of interaction. Accordingly, **III-16b** is planar in the solid state. The chemical or electrochemical oxidation of one electron from the system is possible such that a stable radical cation species can be isolated. By discarding the linkage structure altogether, the barrier to conjugation is minimized and the resulting compound, **III-17**, provides a benchmark in which the interaction between dithiazole rings is fully enabled.

In the introductory chapter, a justification was presented for approximating the barrier to charge transfer for a neutral compound by the gas phase disproportionation enthalpy, the difference between the ionization potential and the electron affinity ($U \approx \Delta H_{disp} = IP - EA$). For a radical cation conductor, the relevant disproportionation enthalpy is the difference between the first and second ionization potentials ($U \approx \Delta H_{disp} = IP_2 - IP_1$).

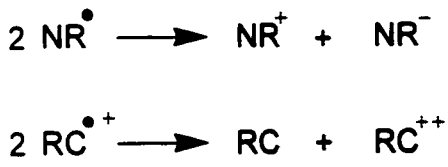

Figure 3.12 Relevant disproportionation reactions for a neutral radical (NR) and a radical cation (RC).

In designing effective molecular conductors, a small U is desirable. A theoretical value for a radical cation conductor can be obtained by comparing the energy difference between the geometry optimized neutral species and the radical cation to the energy difference between the radical cation and the dication. The results obtained from *ab initio* calculations for **III-16** and **III-17** are presented in **Table 3.4**. Calculations for **III-15** have not been included in the above table since the radical cation is experimentally inaccessible.

In practice, ΔH_{disp} can be approximated for a species by E_{cell}, obtained from solution cyclic voltammetry (*e.g.*, $E_{cell} = E_{0/+} - E_{-/0}$ for a neutral radical, where $E_{x/y}$ is the half-wave potential corresponding to the redox reaction relating two oxidation states, x and y). It is important to recognize, however, that there are solvation energies and dielectric constants influencing the measured redox potentials,[20] hence they are only an approximation to the gas phase. Furthermore, the CV experiment is a measure of ΔG, not ΔH. Nevertheless, the trends in observed E_{cell} are generally accepted as a good indication of the trends in the gas phase disproportionation enthalpies.[21] Results from the CV experiments are presented later in this chapter.

Table 3.4 Comparison of Electronics[a] of III-16 and III-17.

	E(cation-neutral) eV	E(dication-cation) eV	E(diff) $IP_2 - IP_1$, eV
III-16a	7.28	11.67	4.39
III-16b	7.51	11.74	4.23
III-17a	6.90	11.75	4.85
III-17b	7.01	11.69	4.95

[a] Values obtained from B3LYP/6-31G**.

The calculated $IP_2 - IP_1$ values are listed in the above table for the theoretical **III-17a** and **III-16a** and for both chloro-substituted compounds that we have isolated and characterized, **III-17b** and **III-16b**. As expected, there is little difference in the $IP_2 - IP_1$ trends for

these species. This lends validity to the assumption that the chlorinated species which we have prepared are representative of the unknown simple diprotio- species.

Two important differences between **III-17** and **III-16** can be identified from these calculations. The first is the increase in the first ionization potential with the insertion of a diazine-linkage. **III-16** is more electronegative than **III-17**, hence the oxidation potential of the neutral species is greater. This militates against the oxidation of **III-16b** experimentally. It also indicates that, once isolated, the **III-16b** radical cation may be very oxidizing and hence more difficult to manipulate than the radical cation of **III-17b**. In other words, while a charge transfer salt of **III-17b** may be relatively air-stable for short periods of time, such a salt based on **III-16b** may decompose much more readily in air.

The second important difference is the smaller $IP_2 - IP_1$ for **III-16**. For these compounds, a small disproportionation enthalpy may be attributed to one of two scenarios. The first, and the more desirable in terms of materials design, is a high degree of conjugation providing a HOMO that is spread over a large molecular area. Conversely, a small disproportionation enthalpy may arise when the first and second electrons removed from the system originate from two non-interacting molecular orbitals. In the extreme case, where the two orbitals do not interact at all, the redox potentials tend to merge and one two-electron redox peak is observed in the CV. A stable radical cation is not accessible by chemical or electrochemical oxidation and the difference between IP_2 and IP_1 is attributed to through space Coulombic interactions. For **III-16**, the smaller $IP_2 - IP_1$ is due to the second scenario. The diazine bridge provides a barrier to conjugation that decreases the electronic interaction between the dithiazole rings. This is borne out by the ESR spectrum and by calculated spin densities presented later in this chapter.

Charge transfer salts of both **III-16b** and **III-17b** have been isolated and characterized. The syntheses and physical measurements are reported herein.

3.7 Crystal Structures of Closed Shell 5,5'-bis(1,2,3-DTA)s

Single crystal X-ray diffraction of **III-15b** reveals a monoclinic $P2_1/n$ space group. The molecules are stacked forming columns in the *x*-direction. In the solid state, the molecule is not planar as the dithiazole rings lie out of plane with the phenyl ring. Neutral **III-15b** is a singlet species wherein the phenyl ring maintains its aromatic character, demonstrated as roughly equivalent C-C bond distances around the ring. The dithiazole rings show a short bond distance between carbon C4 and the ring nitrogen, implying a nominally double bond. Thus the structure of **III-15b** in the solid state is in agreement with the prediction of a singlet ground state. The crystal data is shown in **Table 3.5**.

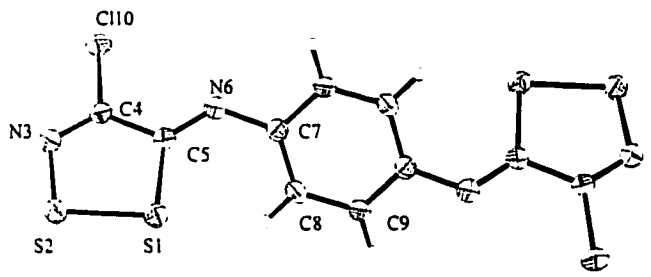

Table 3.5 Bond Lengths in III-15b.

Bond	Length[a] (Å)
C7 - C8	1.389(3)
C7 - N6	1.4047(23)
N6 - C5	1.2691(25)
C5 - C4	1.4778(24)
C4 - N3	1.2708(24)
S1 - S2	2.0780(7)

[a] ESDs are in parentheses.

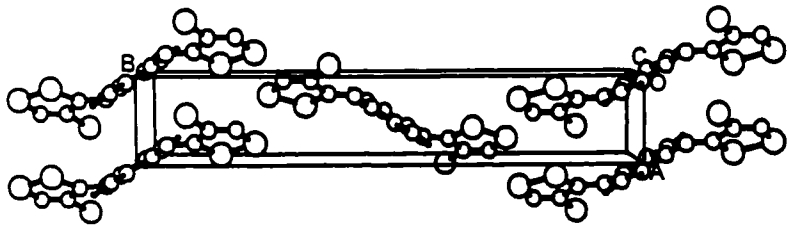

Figure 3.13 Crystal structure of **III-15b**. Space group $P2_1/n$, a = 3.9477(6), b = 23.790(3), c = 7.3769(9) Å, β = 90.793(12) °.

III-16b crystallizes in the space group *Pbca*. The crystal structure of this compound reveals only one conformation in the solid state (**Figure 3.14**). Comparison of the infrared spectrum of these crystals with that of the crude product shows no evidence of any other conformers in the solid state.

That the **III-16b** molecule is planar in the solid state lends weight to the prediction that the π-systems of the DTA rings are capable of interaction *via* conjugation. The bond lengths between carbon C4 and the ring nitrogen and between carbons C4 and C5 are 1.2690 Å and 1.4581 Å respectively. The dinitrogen bond length is 1.381 Å and the bondlength between carbon C5 and the bridging nitrogen is 1.2994 Å. This pattern of alternating long and short bond lengths is in agreement with a closed shell azine species rather than a diradical triplet.

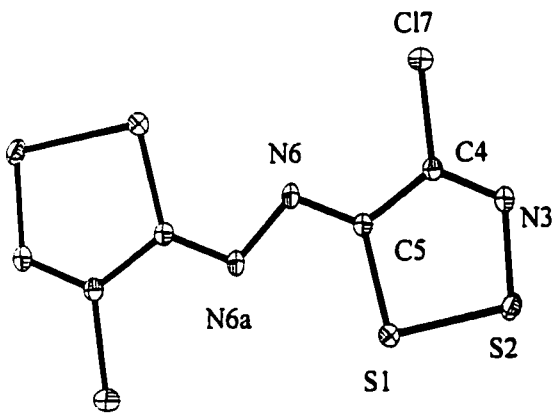

Table 3.6 Bond Lengths of III-16b.

Bond	Length[a] (Å)
N6 - N6a	1.381(3)
C5 - N6	1.2994(20)
C5 - C4	1.4581(22)
C4 - N3	1.2690(21)
S1 - S2	2.0865(7)

[a] ESDs are in parentheses.

Figure 3.14 *ORTEP* of **III-16b**. Space group *Pbca*, a = 5.1469(15), b = 13.343(2), c = 14.203(17) Å.

III-17b crystallizes in a monoclinic $P2_1/c$ arrangement. Slipped stacks of the **III-17b** molecules run along the x-direction. The bond lengths of the C-N and the C-C bonds are consistent with the predicted double bonds of the closed shell configuration.

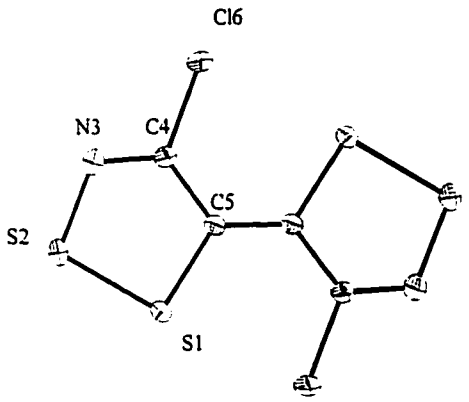

Table 3.7 Bond Lengths in III-17b.

Bond	Length[a] (Å)
C5 - C5'	1.383(7)
C4 - C5	1.458(5)
N3 - C4	1.276(6)

[a] ESDs are in parentheses.

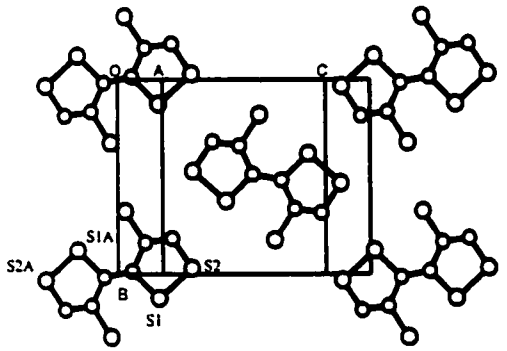

Figure 3.15 Crystal structure of **III-17b**. Space group $P2_1/c$, a = 3.9795(10), b = 8.9447(14), c = 11.973(2) Å, β = 92.537(17) °.

3.8 Cyclic Voltammetry of Closed Shell 5,5'-bis(1,2,3-DTA)s

The nature of the redox manifolds of **III-15b**, **III-16b** and **III-17b** was investigated using cyclic voltammetry. **III-15b** in 0.1 M tetrabutylammonium hexafluorophosphate in dry, degassed acetonitrile, shows only one reversible oxidation peak at 1.27 V *vs.* SCE using ferrocene as an internal reference. This indicates that oxidation of the two DTA rings of the compound occurs simultaneously to give the dication species confirming that the rings are electronically isolated. The oxidation potentials of the two DTA rings are identical and the radical cation species is not accessible.

In contrast to **III-15b**, cyclic voltammetry of **III-17b** performed in approximately 0.1 M tetrabutylammonium hexafluorophosphate in acetonitrile reveals *two* reversible oxidations. The

half-wave potential of the first oxidation corresponding to the formation of the radical cation is at 0.80 V *vs* SCE and the second corresponding to the dication is at 1.25 V *vs* SCE. These results augur well for the possible chemical or electrochemical synthesis of charge transfer salts based on a **III-17b** donor. Indeed, we have prepared a series of these salts, discussed in detail in the following section. What is more, although the half-cell potential for oxidation of **III-17b** is more anodic than that of TTF (**III-10**) due to the inclusion of a nitrogen in the framework, the overall cell potential ΔE ($\Delta E = E_{(+/2+)} - E_{(0/+)}$) for disproportionation of the radical cation **[III-17b]**$^{+}$ is comparable to that of **[III-10]**$^{+}$ (0.3 V).[22]

III-15b and **III-17b** are good examples of two possible redox scenarios for bridged bis(1,2,3-DTA)s. In **III-15b**, the dithiazole rings are oxidized at the same potential, rendering a stable radical cation state unattainable. By contrast, the electronic interaction between the dithiazole rings in **III-17b** permits the formation of a stable radical cation. In the case of **III-16b**, however, the cyclic voltammetry results are surprising as they reveal a richer redox manifold than either of the two scenarios exemplified by **III-15b** and **III-17b**.

Cyclic voltammetry of **III-16b** in 0.1 M tetrabutylammonium hexafluorophophate in dry dichloroethane reveals *three* reversible oxidation peaks at half-cell potentials of 1.41 V, 1.68 V and 1.86 V *vs*. SCE. The first two oxidations presumably correspond to the formation of the radical cation species followed by oxidation to the dication. This being so, the IP_2 - IP_1 window for the radical cation of **III-16b** is relatively small in comparison with most other species discussed within this thesis. Although a small IP_2 - IP_1 may indicate a small energy barrier to conduction for a material, it is important to appreciate that this correlation is based on the assumtion that the frontier molecular orbital from which the electrons are ionized is spread over a large molecular area. In the case of **III-16b**, the small IP_2 - IP_1 undoubtably arises from the near electronic isolation of the terminal rings. In the extreme case, the IP_2 and IP_1 are the same, as observed for

III-15b, and high conductivity in the solid state is not likely. Furthermore, the high oxidation potentials involved in these electrochemical reactions are a major obstacle to the synthesis of radical cation salts. In spite of these difficulties, we have isolated a radical cation salt of **III-16b**.

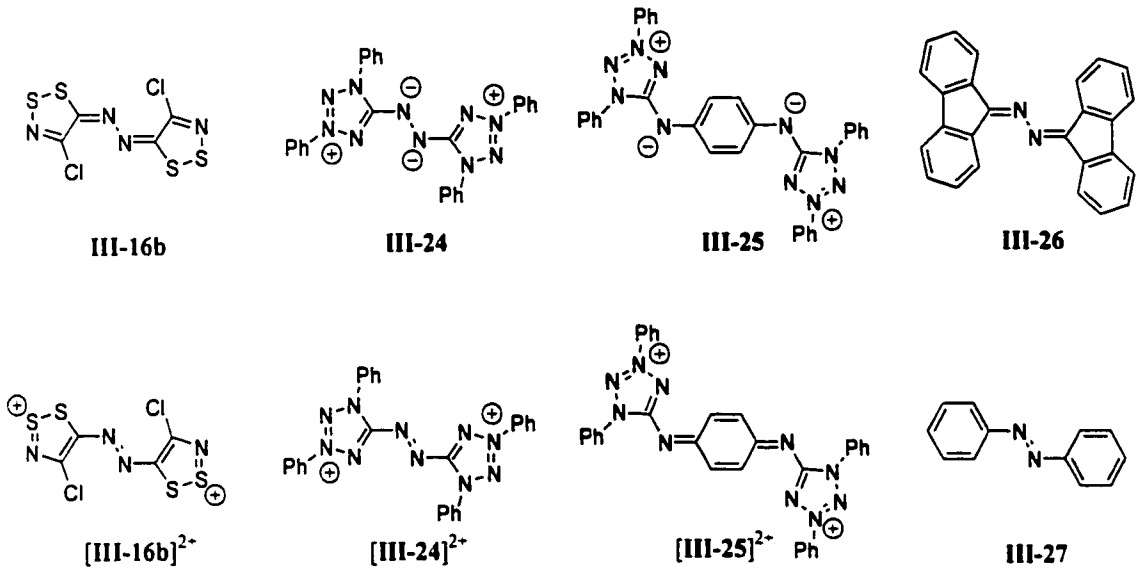

Figure 3.16 A series of azine compounds for which electrochemical studies have been reported.

The cyclic voltammetry results for **III-16b** can be compared to the findings of electrochemical studies on other similar azine compounds. A recent report[23] of the redox manifold of mesoionic **III-24**, as investigated by cyclic voltammetry, reveals two reversible one-electron oxidations, to a radical cation (-0.136 V *vs.* $Ag/AgClO_4$ in dichloromethane) and a dication species (+0.610 V *vs.* $Ag/AgClO_4$ in dichloromethane). Isolation of salts of both oxidation states by chemical oxidation of neutral **III-24** is also described. Differential pulse voltammetry and ESR studies involving selective ^{15}N labeling indicate that the electrons removed in these two oxidation steps originate from the two bridging nitrogens. Our ESR studies and calculated spin densities for **III-16b**, discussed in detail in a later section of this chapter, are in agreement with these findings.

In addition to the two reversible oxidations, there are two reversible reduction peaks in the

cyclic voltammetry **III-24** corresponding to the radical anion (-1.856 V *vs.* $Ag/AgClO_4$ in dichloromethane) and the dianion (-2.006 V *vs.* $Ag/AgClO_4$ in dichloromethane). The observation of reversible reduction peaks in the cyclic voltammetry of azine compounds does not appear to be unusual. **III-26**, for example, is also reported[24] to have two reversible one-electron reduction peaks corresponding to a radical anion (-0.45 V *vs.* SCE in DMSO) and a dianion (-0.82 V *vs.* SCE in DMSO). In the case of **III-26**, however, reversible oxidation peaks are not observed. By contrast, the cyclic voltammetry of **III-16b** does not indicate the presence of reversible reduction processes. The observed irreversible reduction at -0.97 V *vs.* SCE is reminiscent of the majority of 1,2,3-dithiazole-based materials (**III-15b**, irreversible reduction at -1.24 V *vs.* SCE; **III-17b**, irreversible reduction at -1.11 V *vs.* SCE).

Although the redox manifold of **III-24** is comprised of four reversible processes, oxidation beyond the dication is not observed. However, the compound **III-25**, which bears a resemblance to **III-15b**, is reported[23] to have four quasi-reversible oxidation peaks when performed in pyridine (0.03 V, 0.227 V, 0.598 V, and 0.870 V *vs.* $Ag/AgClO_4$). It is tempting to assign these four peaks to a radical cation, a dication, a radical trication, and a tetracation species. The questionable reversibility of the these peaks, together with the absence of any peaks beyond the second oxidation when performed in dichloromethane, suggests that the third and fourth peak may arise from the formation and oxidation of some sort of pyridine adduct in solution. Nevertheless, it is worth noting that there are at least two reversible one-electron oxidations for **III-25**, whereas **III-15b** shows only one reversible two-electron oxidation. This suggests that, in the absence of steric hindrance to planarity, the bridging moiety common to these two compounds is capable of permitting electronic interaction through the phenyl ring.

Of the azine materials discussed thus far, only **III-16b** has a third oxidation peak. We have concluded that the origin of this peak is most likely a trication species. It is worth noting, however,

that the structures of the dications $[\mathbf{III\text{-}16b}]^{2+}$ and $[\mathbf{III\text{-}24}]^{2+}$ are closely related to the structure of many known azo- compounds, azobenzene (**III-27**) for example. The presence of a one-electron oxidation peak in the cyclic voltammetry of **III-27** (1.856 V *vs.* SCE in acetonitrile)[25] can be attributed to the loss of an electron from a bridging nitrogen. This is a good indication that it is plausible to assign the third oxidation peak in the CV of **III-16b** (1.86 V *vs.* SCE in acetonitrile) to a $[\mathbf{III\text{-}16b}]^{3+}$ radical trication.

3.9 Isolation of Radical Cations and Synthesis of Charge Transfer Salts

Chemical oxidation of **III-16b** to the radical cation was a difficult task. The relatively high oxidation potential of this material makes it crucial that the solvents used be dry and that the reaction conditions be strictly air-free. In addition, a very powerful oxidizing agent must be employed. The cyclic voltammetry of this species provides evidence of a narrow IP_2 - IP_1 window implying that the dication is not much higher in oxidation potential than the radical cation. Therefore, too powerful an oxidizing agent may overshoot the desired radical cation state. Reactions of the neutral material with nitrosonium salts in acetonitrile or sulfur dioxide were generally unsuccessful in attaining a stable radical cation salt. The materials recovered from these reactions showed promising infrared spectra (*i.e.*, the peak shifts were consistent with those expected for the oxidized species) but were not easily purified and had a tendency to "fall" back down to the neutral oxidation state in solution. Oxidation with chlorine gas, neat sulfuryl chloride, or neat bromine were likewise unsuccessful, either for a lack of reaction or due to an oxidative decomposition of the starting material. Successful oxidation to a stable radical cation, however, was eventually achieved by 1:1 reaction of neutral **III-16b** with iodine trichloride in sulfur dioxide.

The iodine trichloride oxidation of **III-16b** yields an insoluble black powder. Although the synthesis provides a relatively clean material, according to the infrared spectrum, it is difficult to

purify and hence properly characterize. While oxidations using iodine trichloride generally yield a chloride salt, we have come to conclude that the black product generated in this case is, in fact [**III-16b**][ICl_2]; the observed yield of what appears to be clean material is significantly greater than the theoretical yield were the product a chloride salt. Furthermore, the oxidation does not proceed if a stoichiometric amount of ICl_3 (*i.e.*, $^1/_3$ equivalent) is used nor if a slight excess is employed (*i.e.* ½ equivalent).

The inability to purify the [**III-16b**][ICl_2] has prevented a definitive characterization of this compound. To this end, metathesis of the salt to a more soluble material was attempted. Reaction of [**III-16b**][ICl_2] with gallium trichloride in sulfur dioxide yields a golden microcrystalline gallate salt, however attempts at recrystallization of this material were unsuccessful due mainly to its insolubility. The nitrosonium salts of hexafluoroantimonate and tetrafluoroborate also fail to provide stable **III-16b** salts when reacted 1:1 with the [**III-16b**][ICl_2] in SO_2. The most successful preparative route to a crystalline **III-16b** salt is by treating the black [**III-16b**][ICl_2] powder with silver tetrafluoroborate or silver hexafluorophosphate in sulfur dioxide. The former yields small gold-black crystalline blocks. The latter generates two morphologies, gold needles and black trapezoidal blocks, both of which are extremely air sensitive. X-ray analysis of the blocks has been accomplished and is presented herein.

We attempted to obtain crystals of [**III-16b**][Cl] by subliming the [**III-16b**][ICl_2] *in vacuo* in a sealed tube. The crude ICl_2^- salt was loaded into the end of a heavy pyrex tube which was sealed under vacuum. This was heated in a gradient furnace with the compound-containing end of the tube at 150°C and the other end at 80°C. The intention was that the salt, when heated, would revert to the neutral material releasing chlorine gas and ICl. Thus the neutral material would sublime in a chlorine gas atmosphere, possibly recrystallizing as the chloride salt in the cool end of the tube. A small number of black needles were generated under these conditions, however we

were unable to retrieve them due to their great instability in air.

Electrocrystallization of the **III-16b** was attempted in 1,2-dichloroethane with tetrabutylammonium tetrachlorogallate, tetrafluoroborate, hexafluorophosphate, and perchlorate. While a dark green solution was produced at the anode, no crystals were grown in any case.

As previously discussed, computational results, cyclic voltammetry, and ESR results from the reduction of [**III-2b**][Cl] with a half molar equivalent of triphenylantimony support the possibility of [**III-17b**]$^{+}$ radical cation salts. **III-17b** is not oxidized by iodine, nor were we able to prepare charge transfer salts of **III-17b** with TCNE, TCNQ, or chloranil. This, however, is to be expected due to the higher oxidation potential of this material compared with TTF (**III-10**). To address this issue, bromine was chosen as a stronger oxidizing agent and indeed oxidation of **III-17b** can be carried out with bromine to yield a 1:1 bromide salt. We were not able to recrystallize this material for more detailed study.

However, we have successfully prepared CT salts by electrochemical oxidation of **III-17b**. We explored a variety of octahedral and tetrahedral inorganic counterions. While the octahedral counterions failed to yield any crystalline material, we had relative success with the tetrahedral salts. We performed a methodical test employing several solvents and a range of current densities for a series of simple tetrahedral inorganic counterions introduced as tetra-*n*-butylammonium salts. We found the most effective solvent - current density combination to be pure 1,2-dichloroethane at currents of 1-5 μA. While no deposition at the anode was observed using the larger tetrahedral anions ($FeCl_4^-$, $GaCl_4^-$), the smaller anions FSO_3^-, ClO_4^-, and BF_4^- afforded well-formed crystals after a period of days. The same 1:1 morphology was observed for all three CT salts. Structures of these complexes were solved from single crystal X-ray diffraction and the results are discussed in the following section.

Table 3.8 Thermochemical Radii of Tetrahedral Inorganic Anions.

Anion	Radius (Å)	Anion	Radius (Å)
$FeCl_4^-$	3.44[a]	FSO_3^-	2.68[b], 2.29[c]
$GaCl_4^-$	2.75[a]	ClO_4^-	2.26[a]
		BF_4^-	2.18[a]

[a] These are thermochemical radii derived by the Yatsimirskii method[26] to determine the radius that is consistent with the Born-Haber lattice energy.[27] [b] Effective ionic radius.[28] [c] Experimental result.[28]

3.10 Crystal Structures of the Charge Transfer Salts

The crystal structure of **[III-16b][PF_6]** belongs to the monoclinic space group *C*2/*c*. The **[III-16b]**$^+$ radical cations and the PF_6^- counterions are arranged in a simple ionic lattice. The lack of short contacts between **[III-16b]**$^+$ cations suggests that this material is not a good candidate for high conductivity. Accordingly, pressed pellet conductivity measurements reveal $\sigma < 10^{-6}$ S cm^{-1}.

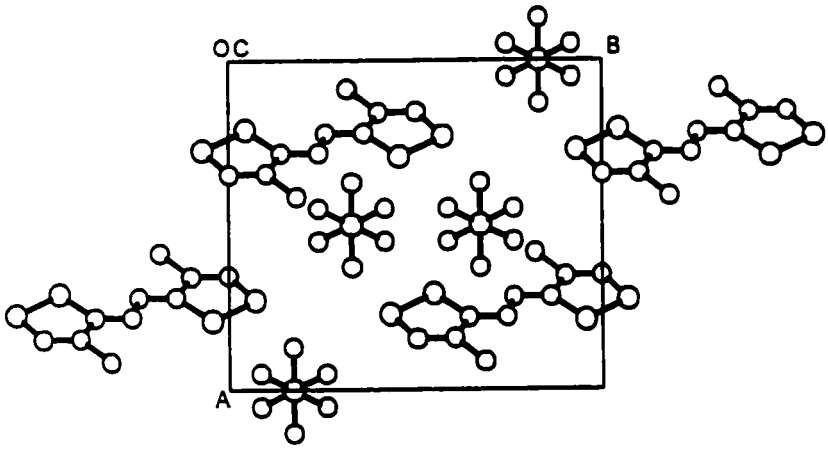

Figure 3.17 Crystal structue of **[III-16b][PF_6]**. Space group *C*2/*c*; a = 11.699(4), b = 12.753(5), c = 10.461(4) Å; β = 112.170(10) °.

The molecular structure of **[III-16b]**$^{+}$ is planar, as is the neutral species. Furthermore, there is no evidence of rotation about any of the bridging bonds to form other isomers. Bond length changes upon oxidation of **III-16b** are summarized in **Table 3.9**. There is a general contraction, upon oxidation, of all the bond lengths with the exception of the C - N bonds (both (C)C - N(N) and (S)N - C(C)). Notably, there is a significant shortening in the length of the diazine bond, which may be interpreted as a shift away from the nominally single bond observed in neutral **III-16b** to a more doubly bonded character in **[III-16b]**$^{+}$.

Table 3.9 Measured and Calculated Internal Bond Lengths[a] for Oxidation States of 3-16b.

	Crystal Data		Computational Results[b]	
Bonds	**3-16b**	**[3-16b]**$^{+}$	**3-16b**	**[3-16b]**$^{+}$
N - N	1.381(3)	1.332(7)	1.3694	1.3215
(C)C - N(N)	1.2994(20)	1.324(5)	1.2928	1.3267
C - C	1.4581(22)	1.423(6)	1.4669	1.4518
(S)N - C(C)	1.2690(21)	1.302(6)	1.2843	1.3020
N - S	1.6467(16)	1.618(4)	1.6670	1.6338
S - S	2.0865(7)	2.0405(17)	2.1377	2.1017
S - C	1.7402(16)	1.713(4)	1.7789	1.7500

[a] All bond lengths in Å; ESDs are in parentheses. [b] B3LYP/6-31G** geometry optimization in C_{2h} symmetry.

The three **[III-17b]**[X] (X = FSO_3^-, ClO_4^-, BF_4^-) CT salts are isomorphous, belonging to the space group $P2_1/n$. Subtle changes in bond lengths are observed within the **[III-17b]**$^{+}$ skeleton in comparison to the neutral **III-17b** species. The central C-C bond lengthens upon oxidation, accompanied by a shortening of the S-S, S-N, and S-C bonds. These changes are in accord with the *ab initio* calculated geometries for the two oxidation states.

Table 3.10 Measured and Calculated Internal Bond Lengths[a] for Oxidation States of III-17b.

	Crystal Data[b]		Computational Results[c]	
Bonds	**III-17b**	**[III-17b]$^{+}$**	**III-17b**	**[III-17b]$^{+}$**
(C)C - C(C)	1.383(7)	1.410(5)	1.3729	1.4131
(C)C - C(N)	1.458(5)	1.438(8)	1.4518	1.4387
C - N	1.276(6)	1.286(14)	1.2899	1.3017
S - S	2.076(15)	2.050(5)	2.1570	2.1200
S - N	1.657(4)	1.622(5)	1.6705	1.6314
S - C	1.768(4)	1.726(4)	1.7889	1.7459

[a] All bond lengths in Å; the number in parentheses is the greater of the ESD or range. [b] Radical cation bond lengths are given for the BF_4 salt. [c] Geometry optimization in C_{2h} symmetry using B3LYP/6-31G**.

An interesting feature of all three **[III-17b][X]** (X = FSO_3^-, ClO_4^-, BF_4^-) CT salts is the arrangement of **III-17b** radical cations in the crystal structure. When viewed down the y-axis, layers of **[III-17b]$^{+}$** interspersed by X^- counterions are apparent. Intermolecular S2- - -S3' contacts close to the van der Waals radii for two sulfurs link each cation to a cation in an adjacent layer both above and below. In addition S1- - -S3' and S2- - -S4' contacts near the van der Waals limit connect molecules in the same layer. In **Figures 3.17** and **3.18**, the resulting ladder-like array of **[III-17b]$^{+}$** is easily recognized by rotating the cell and removing the anions for clarity.

Table 3.11 Intermolecular Contacts (Å) in [III-17b][X] (X^- = BF_4^-, ClO_4^-, FSO_3^-).[a]

	BF_4^-	ClO_4^-	FSO_3^-
S1 - - - S3'	3.605(2)	3.641(2)	3.688(2)
S2 - - - S3'	3.535(2)	3.563(2)	3.524(2)
S2 - - - S4'	3.636(2)	3.670(2)	3.659(2)

[a] ESDs are in parentheses.

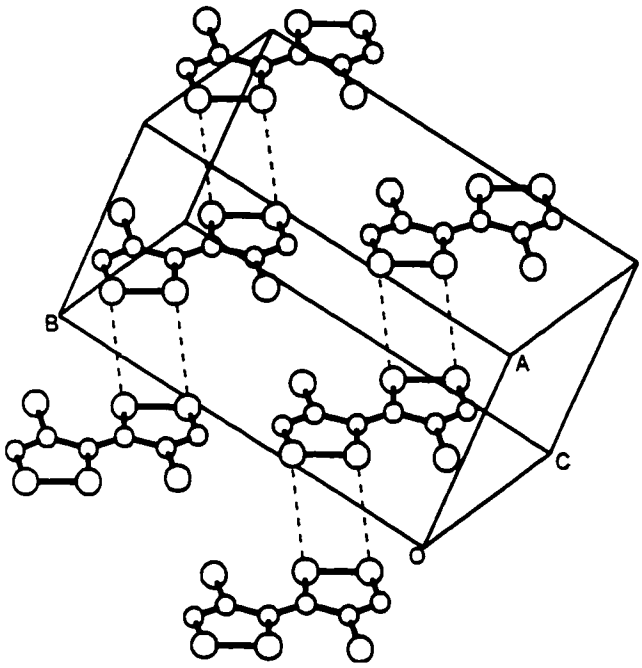

Figure 3.18 Ladder-like arrays of radical cations in **[III-17b]**[BF_4] (anions omitted for clarity).

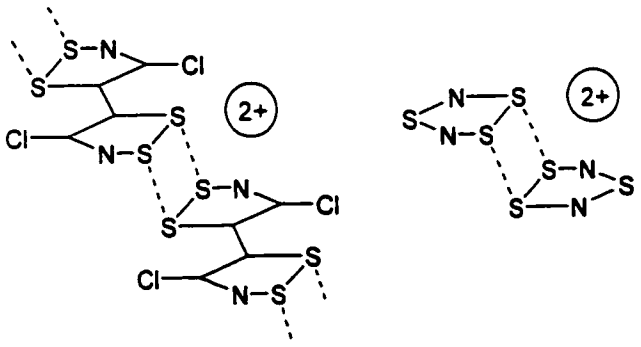

Figure 3.19 Figurative representation of the ladder-like arrangement of **[III-17b]**$^+$ in a 1:1 salt compared to the well-known $[S_3N_2]^+$ radical cation dimers.

3.11 ESR Data of Charge Transfer Salts

Chemical oxidation of **III-16b** with nitrosonium hexafluoroantimonate in sulfur dioxide yields a dark orange solution from which a dark red solid can be isolated. When this solid is redissolved in sulfur dioxide along with **III-16b**, a turquoise solution is produced from which an

ESR spectrum has been obtained. A subsequent ESR of **[III-16b]**[$GaCl_4$] in sulfur dioxide yielded an identical spectrum, although the originally blue solution had become red by the time the data was collected.

The ESR spectrum of the **[III-16b]**$^+$ radical cation is a 1:2:3:2:1 pentet indicative of hyperfine coupling to two nitrogens. Coupling to the other two nitrogens and to the chlorines is not observed. This is in keeping with the calculated Mulliken spin density distribution and hyperfine coupling for **[III-16b]**$^+$. The calculated spin density resides mainly on the bridging nitrogens, as shown in **Table 3.11**. Simulation of the experimental ESR shows a_N of 2.365 for two equivalent nitrogens, which is in accord with the calculated value.

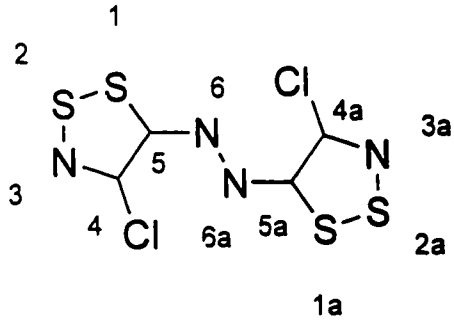

Figure 3.20 Labelling Scheme of **III-16b** skeleton.

Table 3.12 [III-16b]$^+$ *Ab Initio* Calculations[a]

Atom	Mulliken Spin Density	Isotropic Fermi Contact Couplings (gauss)
N3	0.027	0.63
N6	0.146	2.39
Cl	0.002	-0.01 (^{35}Cl)
S1	0.155	
S2	0.185	

[a] B3LYP/6-31G**.

In an attempt to observe the expected 4,5-dichloro-1,2,3-dithiazolyl radical as an intermediate to the dimerization that produces **III-17b**, the reduction of **[III-2b]**[Cl] was performed in an ESR cell and monitored as the SO_2 melted. An ESR spectrum was recorded, however it was not the three-line pattern expected for coupling of an unpaired electron with one

nitrogen. Observed was a 1:2:3:2:1 pentet indicative of coupling to two equivalent nitrogens. This spectrum is, in fact, that of the radical cation of the dimerization product. The above dimerization reaction appears to be very rapid, reaching completion by the time the solvent SO_2 has melted, at ca. -70°C.

A solution of **[III-17b]**[ClO_4] in sulfur dioxide yields an identical ESR spectrum to that observed for the above *in situ* reduction confirming the identification of the ESR active species as the **[III-17b]**$^{+}$ radical cation. Hyperfine coupling to the nitrogens (a_N = 0.096 mT) is smaller than in other bis(1,2,3-DTA) systems discussed in Chapter 5 (for which values are generally closer to a_N = 0.2 mT) indicating significant spin density on the sulfur atoms. This observation is reinforced by a *g*-value (2.0117) slightly closer to that of a free electron compared to those same systems. These results are in accord with the computational values. Furthermore, hyperfine coupling to chlorine is not observed. This, too, is predicted by calculation which places a low spin density on the carbon C4 positions.

Table 3.13 [III-17b]$^{+}$ *Ab Initio* Calculations.[a]

Atom	Mulliken Spin Density	Isotropic Fermi Contact Couplings (gauss)
N3	0.061	1.29
C5	0.078	
C4	-0.031	
Cl	0.011	-0.14 (^{35}Cl)
S2	0.193	
S1	0.198	

[a] B3LYP/6-31G**.

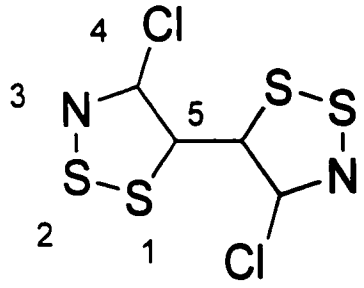

Figure 3.21 Labelling scheme for **III-17b** skeleton.

3.12 Conductivity and Magnetic Measurements of Charge Transfer Salts

Although the **[III-17b]**$^{+}$ molecules are not dimerized in the solid state, the S- - -S contacts are surprisingly short, nearing the van der Waals limit at which appreciable intermolecular overlap might be expected to occur. Described in the context of a simple band model, the electronic structures of the 1:1 **[III-17b]**[X] salts produce an exactly half-filled energy band. The bandwidth arising from the intermolecular S- - -S contacts must be sufficiently large to offset the Coulombic barrier to charge transfer. For these salts, that band width is not quite enough. In other words, the 1:1 **[III-17b]**[X] salts are Mott insulators.

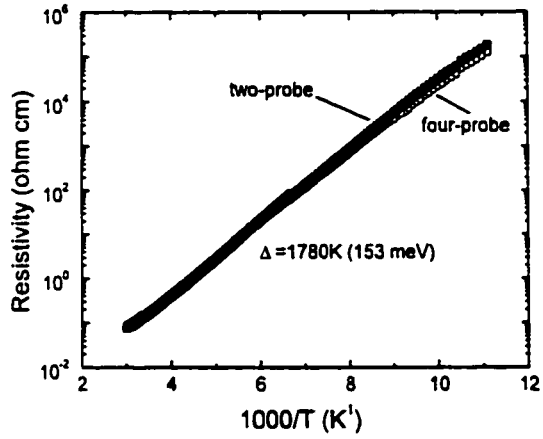

Figure 3.22 Variable-temperature single crystal conductivity measurements for **[III-17b]**[ClO_4].

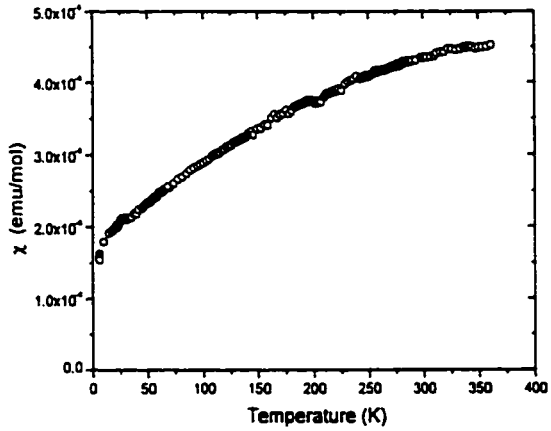

Figure 3.23 Variable-temperature magnetic susceptibility measurements for **[III-17b]**[ClO_4].

Conductivity and magnetic susceptibility measurements were performed in order to assess the bulk properties of these salts. Pressed pellet measurements of all three salts **[III-17b]**[X] ($X^- = FSO_3^-, ClO_4^-, BF_4^-$) show room temperature conductivities in the 10^{-1} to 10^{-3} S cm^{-1} range. This is consistent with semiconductive Mott insulator behavior. Further variable-temperature single-crystal conductivity measurements were carried out on **[III-17b]**[ClO_4]. The results of these measurements are plotted in terms of resistivity in **Figure 3.22**. Both two-probe and four-probe measurements indicate that the room-temperature conductivity of this salt is higher than the pressed pellet measurements had indicated, at close to 10^1 S cm^{-1}. In addition, the temperature dependence of the conductivity confirms that the material is a semiconductor with a band gap E_g ($E_g = 2\Delta$) of 0.30 eV. The variable-temperature magnetic susceptibility measurements are plotted in **Figure 3.23** in terms of the effective fraction of Curie spins. These measurements confirm thermal generation of free spins, as would be expected from a semiconductive Mott insulator.

To summarize Chapter 3, three novel closed shell bis(1,2,3-DTA)s were prepared by the reaction of Appel's salt **[III-2b]**[Cl] with 1,4-phenylenediamine, with hydrazine, and by the reduction of Appel's salt **[III-2b]**[Cl]. These three compounds, **III-15b**, **III-16b**, and **III-17b**, were isolated and characterized by X-ray crystallography. Cyclic voltammetry ruled out the possibility of obtaining a stable radical cation salt of **III-15b**, however, a stable radical cation oxidation state was attained for both **III-16b** and **III-17b**. Salts of both these compounds were isolated and characterized by X-ray crystallography. Both the crystal structure and the calculated spin density distribution of **[III-16b]**[PF_6] militated against its being a useful CT donor. The salts of **III-17b**, however, showed intermolecular sulfur contacts in the crystal structure that correlate with the high single-crystal conductivity of **[III-17b]**[ClO_4] ($\sigma = 10^1$ S cm^{-1}).

3.13 Syntheses

3.13.1 Synthesis of 4,5-dichloro-1,2,3-dithiazolylium chloride,[16] [III-2b][Cl]: Chloroacetonitrile (11 mL, 0.17 mol) and sulfur monochloride (66 mL, 0.83 mol) were stirred in 90 mL of dry methylene chloride, under inert atmosphere, with 1.5 mL of Adogen®464. After 2 h, a yellow precipitate appeared. The reaction mixture was left stirring for another 18 h, then the solid was collected by filtration, washed 4 x 50 mL dry methylene chloride, and dried *in vacuo*; yield 21.97 g (0.1054 mol, 62 %). IR: 1708 (w), 1278 (s), 1251 (m), 1080 (s), 913 (m), 827 (s), 626 (w), 605 (s), 524 (m), 441 (s) cm^{-1}.

3.13.2 Synthesis of *n*-tetrabutylammonium tetrachlorogallate[29]: A solution of *n*-tetrabutylammonium chloride (15 g, 50 mmol) in deionized water was added to a solution of gallium trichloride (5.0 g, 28 mmol) in 30 mL of 15 % aqueous HCl to generate a white precipitate. The solid was collected by filtration and dried in air. The product was recrystallized twice as large white crystals from 60 mL of 2:1 ethylacetate and ether, and dried in air; yield 10.991 g (24.209 mmol, 86 %).

3.13.3 Synthesis of *n*-tetrabutylammonium tetrachloroferrate[30] : A solution of *n*-tetrabutylammonium chloride (4.052 g, 14.60 mmol) in 50 mL conc. HCl was added to a solution of ferric chloride (2.09 g, 12.8 mmol) in 200 mL conc. HCl to generate a yellow precipitate. The solid was collected by filtration and washed with conc. HCl followed by 10 mL of ethanol. The product was then recrystallized from 70 mL of ethanol, collected by filtration, and washed with 10 mL of ethanol followed by 20 mL of ether. The white crystals were dried *in vacuo*, warm, for 18 h; yield 3.0 g(6.8 mmol, 53 %).

3.13.4 Synthesis of tetrachloropyrazine: A bomb reactor was loaded with 2-chloropyrazine (15 g, 0.13 mol) and phosphorus pentachloride (100 g, 0.43 mol). The reactor was heated to 280 °C for 18 h. Once the reactor had cooled to RT, it was cooled further on $CO_{2(s)}$ and the $HCl_{(g)}$ side product was vented into a container of ice for 30 m. Once the venting had ceased, the product was washed from the reactor with ice water, and extracted with 4 x 250 mL of ether. The ether extraction was dried with sodium sulfate and the solvent was removed *in vacuo*. The solid tetrachloropyrazine was recrystallized as yellow crystals from 150 mL of ethanol; yield 22 g (0.10 mol, 77 %).

3.13.5 Synthesis of 2,5-diamino-1,4-dichloropyrazine, III-21: Tetrachloropyrazine (2.065 g, 9.470 mmol) and potassium phthalimide (3.536 g, 19.09 mmol) were stirred together in 50 mL of dry DMF, warmed to 40 °C under inert atmosphere, for 18 h. The white precipitate was collected by filtration and washed with water. The solid was then slurried with 50 mL of water to which excess hydrazine (5 mL of 35 % in water by weight) was added dropwise. The reaction mixture was stirred for a further 2 h. The bright yellow precipitate was collected by filtration, washed with water, and dried in air. The product was recrystallized from 150 mL of ethanol; yield 1.014 g (5.665 g, 60 %). IR: 3448 (s), 3288 (s), 3175 (s), 1604 (s), 1225 (m), 1152 (s), 1052 (w), 853 (w), 566 (m), 467 (m) cm^{-1}.

3.13.6 Synthesis of 1,4-diimino-1*H*,4*H*-bis[4-chloro-5*H*-1,2,3-dithiazol]benzene, III-15b: A slurry of 1,4-phenylenediamine (519 mg, 4.80 mmol) and **[III-2b]**[Cl] (2.57g, 12.3 mmol) in 30 mL of dichloroethane was stirred at 35°C for 18h under inert atmosphere. The reaction mixture was cooled to room temperature and the dichloride salt **[III-15b]**$[Cl]_2$ was collected by filtration as a yellow powder and washed with methylene chloride. IR: 2670 (b), 1601 (w), 1536 (vs), 1231

(m), 1195 (m), 1014 (w), 914 (m), 865 (w), 835 (w), 816 (w), 782 (m), 700 (m), 641 (w), 618 (w), 536 (w), 515 (m), 481 (w) cm^{-1}. The solid product was washed with ethanol yielding an orange powder of **III-15b**. Recrystallization from hot toluene (15 mL per 100 mg) yielded red needle-like crystals; yield 1.6 g, (4.22 mmol, 88 %); mp > 200 °C. IR:1584 (s), 1543 (w), 1483 (m), 1412 (w), 1286 (w), 1234 (m), 1220 (m), 1141 (s), 1106 (s), 1009 (w), 955 (w), 860 (s), 835 (m), 823 (m), 774 (w), 763 (s), 640 (m), 629 (s), 551 (m), 525 (s), 438 (m) cm^{-1}. UV / Vis ($CHCl_3$): λ_{max} (log ϵ) = 421 (4.1) nm. MS (*m/e*): 378 (M^+, 21 %) Anal. Calcd. for $C_{10}H_4N_4S_4Cl_2$: C, 31.67; H, 1.06; N, 14.77 %. Found: C, 31.80; H, 0.91; N, 14.64 %.

3.13.7 Synthesis of 2,5-dichloro-3,6-diimino-3*H*,6*H*-bis[4-chloro-5*H*-1,2,3-dithiazole]pyrazine, III-22: 2,5-dichloro-3,6-diaminopyrazine, **III-21** (455 mg, 2.54 mmol) and [**III-2b**][Cl] (1.036 g, 4.97 mmol) were stirred in 70 mL dry dichloroethane under inert atmosphere for 18h yielding orange fibrous crystals. These were recovered by filtration, washed with dichloroethane, dried *in vacuo*, and recrystallized in 100 mL of toluene; yield 720 mg (1.60 mmol, 64 %); mp > 200 °C. Vacuum sublimation at 150°C (10^{-2} Torr) yielded orange crystalline blocks and red fibrous crystals. Orange crystals have been characterized as 2,5-dichloro-3-amino-6-imino-6*H*[4-chloro-5*H*-1,2,3-dithiazole]pyrazine. IR: 3458 (m), 3291 (m), 3190 (w), 3153 (w), 1621 (s), 1556 (s), 1541 (w), 1495 (w), 1360 (s), 1337 (m), 1215 (m), 1168 (m), 1143 (s), 903 (s), 866 (w), 789 (s), 723 (m), 625 (s), 520 (s), 465 (w) cm^{-1}. The red crystals have been identified as the desired disubstituted product, **III-22**. IR: 1519 (s), 1338 (m), 1204 (s), 1134 (m), 916 (m), 868 (w), 785 (m), 670 (m), 549 (w), 534 (w), 516 (w), 477 (w), 463 (w) cm^{-1}. MS (DCI, $+NH_3$, *m/e*): 314 ([$M^+ + NH_3 - C_2N_2S_2Cl$], 100 %). Anal. Calcd. for $C_8N_6S_4Cl_4$: C, 21.34; H, 0.0; N, 18.67 %; Found: C, 23.07; H, trace; N, 18.51 %.

3.13.8 Attempted synthesis of 2,5'-bis[4-chloro-5*H*-1,2,3-dithiazole]bithiophene, III-23: Bithiophene (0.210 g, 1.27 mmol) was added to a slurry of **[III-2b]**[Cl] (0.517 g, 2.43 mmol) in 40 mL dry dichloroethane under inert atmosphere. A gradual darken of the slurry and a blue solution was observed. This was stirred for 18h. A dark green precipitate with a gold sheen was filtered from the bright blue solution. The precipitate was extracted with methylene chloride over a period of 4 days yielding a bright green-gold precipitate. IR: 3068 (w), 1524 (w), 1486 (m), 1435 (s), 1246 (w), 1230 (w), 1187 (m), 1162 (s), 1094 (m), 1075 (w), 1046 (w), 922 (w), 908 (w), 895 (w), 857 (w), 849 (w), 814 (s), 798 (s), 744 (w), 690 (s), 655 (s), 552 (w), 523 (m), 584 (w), 474 (m) cm^{-1}. MS (*m/e*): 302 ($C_{10}H_5NS_4Cl$, 51 %), 235 ($C_{10}H_5NS_3$, 22 %), 209 ($C_8H_3NS_3$, 100 %). Anal. Calcd. for $C_{12}H_4N_2S_6Cl_4$: C, 28.24; H, 0.79; N, 5.49 %. Calcd. for $C_{10}H_5NS_4Cl_2$: C, 35.50; H, 1.49; N, 4.14 %. Found: C, 28.17; H, 1.20; N, 3.62 %.

3.13.9 Synthesis of 1,2-bis[4-chloro-5*H*-1,2,3-dithiazole]dinitrogen, III-16b: To a slurry of **[III-2b]**[Cl] (3.125 g, 14.987 mmol) in 50 mL dry dichloroethane, on ice, in inert atmosphere, a solution of anhydrous hydrazine (0.25 mL, 8.0 mmol) in 15 mL dry dichlororethane was added dropwise. The red slurry was stirred at room temperature for 18 h, then refluxed for 4 h. Upon cooling to room temperature, red crystals were collected by filtration. These were recrystalized in chlorobenzene; yield 0.752 g (2.48 mmol, 33 %); mp 249 °C. Crystals suitable for single crystal X-ray diffraction were obtained by vacuum sublimation at 130°C (10^{-2} Torr). IR: 1562 (w), 1536 (s), 1505 (w), 1176 (s), 890 (s), 879 (s), 733 (w), 693 (s), 525 (m), 441 (m), 424 (m) cm^{-1}. UV / Vis ($CHCl_3$): λ_{max} (log ϵ) = 505 (4.9), 472 (5.0), 455.5 (4.8) nm. MS (*m/e*): 302 (M^+, 47 %) . Anal. Calcd. for $C_4N_4S_4Cl_2$: C, 15.84; H, 0.0; N, 18.48 %. Found: C, 16.08; H, trace; N, 18.36 %.

3.13.10 Synthesis of 1,2-bis[4-chloro-5*H*-1,2,3-dithiazole]dinitrogen iododichloride, [III-16b][ICl_2]: Under inert atmosphere, **III-16b** (0.561 g, 1.85 mmol) and iodine trichloride (0.460 g, 1.97 mmol) were loaded into an h-cell and sulfur dioxide (10 mL) was condensed into the reaction vessel. This was stirred at RT for 18 h yielding a black precipitate. The solid was collected by filtration and washed with sulfur dioxide (7 x 5 mL) then dried in vacuo; yield: 0.835 g (1.67 mmol, 90 %). IR (NaCl plates, nujol): 1564 (w), 1530 (m), 1504 (w), 1423 (s), 1444 (s), 1205 (s), 906 (s), 828 (s), 798 (w), 711 (s) cm^{-1}.

3.13.11 Synthesis of 1,2-bis[4-chloro-5*H*-1,2,3-dithiazole]dinitrogen hexafluorophosphate, [III-16b][PF_6]: Silver hexafluorophosphate (0.200 g, 0.791 mmol) and **[III-16b]**[ICl_2] (0.359 g, 0.716 mmol) were loaded into an h-cell and sulfur dioxide (10 mL) was condensed onto the solid reagents. After 15 m stirring at RT, a deep blue solution formed with white AgCl precipitate visible. This was filtered and the SO_2 was removed slowly yielding gold oblong blocks. IR: 1536 (w), 1442 (s), 1426 (s), 1328 (m), 1250 (w), 1194 (s), 1145 (w), 1007 (w), 907 (s), 844 (vs), 742 (w), 710 (m) cm^{-1}. Black blocks were grown from an identical reaction procedure on a later date.

3.13.12 Synthesis of *trans*-4,4'-dichloro-1,1',2,2',3,3'-tetrathiadiazafulvalene, III-17b: Sulfur dioxide (50 mL) was condensed into an evacuated h-cell containing **[III-2b]**[Cl] (2.08 g, 10.0 mmol) and triphenylantimony (3.88 g, 11.0 mmol) and the mixture was stirred and allowed to warm slowly (2 h) from -70°C to RT. The black powder product was collected by filtration, washed twice with sulfur dioxide, removed from the reactor and washed sequentially with acetonitrile (50 mL), aqueous ethanol (50 mL), and methylene chloride (50 mL). The remaining solid was then extracted with hot carbon disulfide (4 x 80 mL) and the crude product was obtained by removal of the solvent from the combined deep purple extracts. Recrystallization from hot

toluene produced black/purple needles; yield: 0.42 g (1.5 mmol, 30 %); mp 120-121°C; γ_{max} (CH_2Cl_2) 565 nm (ϵ = 1.3 x 10^4 L mol^{-1} cm^{-1}). IR: 1487 (m), 1123 (vs), 877 (m), 791 (s), 767 (vs) 604 (w), 498 (w), 473 (s) cm^{-1}. MS (*m/e*): 274 (M^+, 100 %), 210 ($[M-S_2]^+$, 30 %). Anal. Calcd for $C_4N_2S_4Cl_2$: C, 17.46; N, 10.18. Found: C, 17.57; N, 9.97 %.

3.13.13 Electrocrystallization of *trans*-4,4'-dichloro-1,1', 2,2',3,3'-tetrathiadiazafulvalene tetrafluoroborate, fluorosulfate, and perchlorate, [III-17b][X], X = BF_4^-, FSO_3^-, ClO_4^-: A sample of **III-17b** (8 mg) dissolved under nitrogen in dry dichloroethane (20 mL) containing 0.02 - 0.05 M [*n*-Bu_4N][X] (X^- = BF_4^-, FSO_3^-, and ClO_4^-) was oxidized with a current density of 1 to 5 μA for 7 - 10 days. Air-stable crystals of all three CT salts were grown at the anode. [**III-17b**][ClO_4^-]: dec. > 100 °C. (**WARNING: this material detonates upon heating to temperatures above 100°C.**) IR: 1167 (s), 1117 (s), 1104 (s), 1091 (s), 1059 (s), 843 (m), 796 (s), 624 (m), 617 (m), 507 (m), 488 (w) cm^{-1}. Anal. Calcd for $C_4N_2O_4S_4Cl_3$: C, 12.82; N, 7.48. Found: C, 13.03; N, 7.32 %. [**III-17b**][FSO_3]: dec. > 220 °C. IR: 1290 (s), 1253 (s), 1165 (s), 1065 (s), 842 (m), 789 (s), 724 (m), 625 (vw), 581 (w), 574 (w), 557 (vw), 510 (vw), 488 (vw) cm^{-1}. Anal. Calcd for $C_4N_2O_3S_5Cl_2F$: C, 12.84; N, 7.48. Found: C, 13.06; N, 7.49 %. [**III-17b**][BF_4]: dec > 220 °C. IR: 1168 (s), 1125 (m), 1084 (s), 1050 (s), 1038 (m), 1010 (s), 844 (m), 797 (vs), 627 (w), 523 (vw), 517 (vw), 507 (w), 496 (w) cm^{-1}. Anal. Calcd for $C_4N_2S_4Cl_2BF_4$: C, 13.27; N, 7.74. Found: C, 13.40; N, 7.58 %.

References for Chapter 3

1. Herz, R.; *Chem. Zentr*, **1922**, *4*, 948.
2. Warburton, W. K.; *Chem. Rev.*, **1957**, 1011.
3. (a) Appel, R.; Janssen, H.; Siray, M.; Knoch, F.; *Chem. Ber.*, **1985**, *118*, 1632. (b) Besson, T.; Dozias, M.-J.; Guillard, J.; Rees, C. W.; *J. Chem. Soc., Perkin Trans. 1*, **1998**, 3925.
4. Kim, K.; *Phosphorus, Sulfur, and Silicon*, **1997**, *120-1*, 229.
5. Matsuda, K.; Iwamura, H.; *J. Am. Chem. Soc.*, **1997**, *119*, 7412.
6. (a) Borden, W. T.; Davidson, E. R.; *J. Am. Chem. Soc.*, **1977**, *99*, 4587. (b) Pranata, J.; *J. Am. Chem. Soc.*, **1992**, *114*, 10537.
7. Bryan, C. D.; Cordes, A. W.; Haddon, R. C.; Hicks, R. G.; Oakley, R. T.; Palstra, T. T. M.; Perel, A. J.; *J. Chem. Soc., Chem. Commun.*, **1994**, 1447.
8. Genin, H.; Hoffmann, R.; *Macromolecules*, **1998**, *31*, 444.
9. Ferraris, J.; Cowan, D. O.; Walatka, V., Jr.; Perlstein, J. H.; *J. Am. Chem. Soc.*, **1973**, *95*, 948. (b) Phillips, T. E.; Kistenmacher, T. J.; Ferraris, J. P.; Cowan, D. O.; *J. Chem. Soc., Chem. Commun.*, **1973**, 471.
10. Engler, E. M.; Patel, V. V.; *J. Am. Chem. Soc.*, **1974**, *96*, 7376.
11. Engler, E. M.; *Chemtech*, **1976**, 274.
12. Bryce, M. R.; *Chem. Soc. Rev.*, **1991**, *20*, 355.
13. (a) Behringer, H.; Meinetsberger, E.; *Tetrahedron Letters*, **1975**, *40*, 3476. (b) Behringer, H.; Meinetsberger, E.; *Liebigs Ann. Chem.*, **1981**, 1928.
14. (a) O'Mahony, M. J.; Rees, C. W.; Saville-Stones, E. A.; White, A. J. P.; Williams, D. J.; *Chem. Commun.*, **1998**, 1459. (b) Besson, T.; Emaya, K.; Rees, C. W.; *J. Chem. Soc. Perkin Trans. 1*, **1995**, 2097. (c) Choi, S. H.; Kim, K.; *Tetrahedron*, **1996**, *52*, 8413. (d)

Rakitin, O. A.; Rees, C. W.; Vasova, O. G.; *Chem. Commun.*, **1996**, 1273. (e) L'Abbé, G.; D'hooge, B.; Dehaen, W.; *J. Chem. Soc. Perkin Trans. 1*, **1995**, 2379.

15. Kim, K.; *Sulfur Rep.*, **1998**, *21*, 147.

16. Rees, C.; *J. Heterocycl. Chem.*, **1992**, *29*, 639.

17. Lee, H.; Kim, K.; Whang, D.; Kim, K.; *J. Org. Chem.*, **1994**, *59*, 6179.

18. (a) Gray, M. A.; Rees, C. W.; Williams, D. J.; *Heterocycles*, **1994**, *37*, 1827. (b) Emayan, K.; Rees, C. W.; *Bull. Soc. Chim. Belg.*, **1997**, *106*, 605.

19. (a) Barclay, T. M.; Beer, L.; Cordes, A. W.; Haddon, R. C.; Itkis, M. I.; Oakley, R. T.; Preuss, K. E.; Reed, R. W.; *J. Am. Chem. Soc.*, **1999**, *121*, 6657. (b) Barclay, T. M.; Cordes, A. W.; Oakley, R. T.; Preuss, K. E.; Reed, R. W.; *Chem. Commun.*, **1998**, 1039.

20. Roncali, J.; *Chem. Rev.*, **1997**, *97*, 173.

21. Boeré, R. T.; Moock, K. H.; *J. Am. Chem. Soc.*, **1995**, *117*, 4755.

22. Sandman, D. J.; Zoski, G. D.; Burke, W. A.; Hamill, G. P.; Ceasar, G. P.; Baker, A. D.; *J. Chem. Soc., Chem. Commun.*, **1981**, 829.

23. Araki, S.; Yamamoto, K.; Inoue, T.; Fujimoto, K.; Yamamura, H.; Kawai, M.; Butsugan, Y.; Zhou, J.; Eichhorn, E.; Rieker, A.; Huber, M.; *J. Chem. Soc., Perkin Trans. 2*, **1999**, 985.

24. Bethell, D.; Kang, D.-H.; Zerbi, G.; *J. Chem. Soc., Perkin Trans. 2*, **1996**, 1081.

25. Dabrowiak, J. C.; Fisher, D. P.; McElroy, F. C.; Macero, D. J.; *Inorg. Chem.*, **1979**, *18*, 2304.

26. Yatsimirskii, K. B.; *Izv. Akad. Nauk SSSR, Otdel, Khim. Nauk*, **1947**, 453.

27. Huheey, J. E.; Keiter, E. A.; Keiter, R. L.; *Inorgic Chemistry*, HarperCollins College, Publishers, N.Y., **1993**, 117.

28. Ferraro, J. R.; Williams, M. W.; *Introduction to Synthetic Electronic Conductors*,

Academic Press, Inc., Harcourt Brace Jovanovich, San Diego, **1987**, 32.

29. Taylor, M. J.; Tuck, D. G.; *Inorg. Synth., Vol. 22*, Holt, S. L. Ed.-in-chief, John Wiley & Sons, N.Y., **1983**, 135.

30. Ryan, J. L.; *Inorganic Syntheses, Vol. XV*, Parshall, G. W. Ed.-in-chief, McGraw-Hill Book Co., N.Y., **1974**, 231.

Chapter 4 A Mono- and a Bis- (1,2,3-Dithiazole) Neutral Radical.

4.1 Introduction

The stable radical cation salts discussed in Chapters 3 and 5 emerged from attempts to design new charge transfer salts. They belong to the radical ion conductor (RIC) class of molecular conducting materials. In this class of conductors, oxidation of a neutral closed shell donor molecule, or reduction of a neutral closed shell acceptor, generates a salt with conduction properties arising from the partially filled solid state band structure.

As detailed in Chapter 1, there is a second possible model for the design of molecular conductors. Neutral radical conductors (NRCs) are based on stable neutral radical building blocks in which a π - type SOMO is distributed over a large area of the molecule. Intermolecular overlap of the SOMOs must be such that a half-filled band is created in the solid state. Therefore, the proximity and orientation of the individual radicals relative to one another must allow intermolecular electronic interaction without permitting spin pairing through dimerization.

Since the NRC model was first devised[1] our research group has investigated a variety of stable neutral radical species in an effort to determine the molecular features necessary to design neutral radical conducting materials. Our labours have not been in vain, as one of my co-workers[2] has recently reported the first ever NRC (in the strictest sense), a fused 1,2,3-dithiazolyl system. The discussion herein addresses the design elements required in order to stabilize a 1,2,3-dithiazolyl radical heterocycle.

There are two carbon positions, C4 and C5, in a 1,2,3-dithiazole at which substituent groups may be added. In practice, the synthesis of a C5 substituted 1,2,3-dithiazole or a fused ring system involving both C4 and C5 is more easily accomplished than is the synthesis of a C4 only substituted 1,2,3-dithiazole (see discussion of C4 substitution of Appel's salt,[3] **IV-1**, Chapter 3).

Our investigation of stabilized 1,2,3-dithiazolyl radicals is focused, therefore, on C5 substituted rings and fused ring systems.

Two 1,2,3-dithiazolium salts, the Herz compound[4] ([**IV-3**][Cl]) and Appel's salt (**IV-1**), were introduced in Chapter 3. These are representative of the simplest ring-fused and non-fused 1,2,3-dithiazoles respectively. The attempted one-electron reduction of these cations to neutral radicals is a good starting point for the discussion of 1,2,3-dithiazolyl stabilization issues. These reductions do not yield a stable mono-1,2,3-dithiazolyl radical that can be isolated in the solid state. In the case of the Herz compound, reduction to the neutral radical gives a persistent ESR signal in solution and the product can be isolated as a black powder. However, all attempts at obtaining the radical species in the crystalline state have failed thus far.

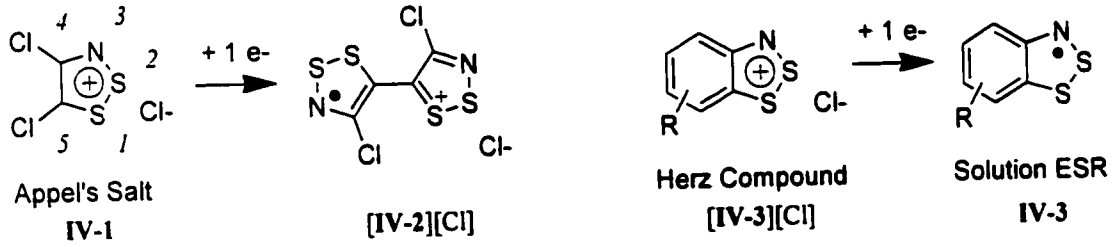

Figure 4.1 The reduction of Appel's salt yields **IV-2**. The Herz compound is reduced to a neutral radical observed in solution by ESR.

As discussed in detail in Chapter 3, the one electron reduction of Appel's salt (**IV-1**) yields the radical cation [**IV-2**]$^{+}$, a product of dimerization through the carbon C5, with no observation of a 4,5-dichloro-1,2,3-dithiazolyl radical intermediate.[5] This can be attributed to the large spin density that resides on the carbon C5 of a simple 1,2,3-dithiazolyl radical, as determined from *ab initio* geometry optimization of the 4,5-diprotio-1,2,3-dithiazolyl. Thus, a reasonable approach to the design of a stable radical is to block the C5 site from dimerization sterically with a bulky group, electronically by substitution of a very electron withdrawing group, or by a combination

of both. We now can refer back to the qualitative drawings of Chapter 3 (summarized in **Figure 4.2**) and ask what kind of bridge between two dithiazoles will prevent electronic interaction such that a triplet state is stabilized. Since the nature of such a bridging group is to isolate the dithiazole rings, it could also be employed as a substituent on a single 1,2,3-dithiazole to bring about a stable mono-substituted neutral radical.

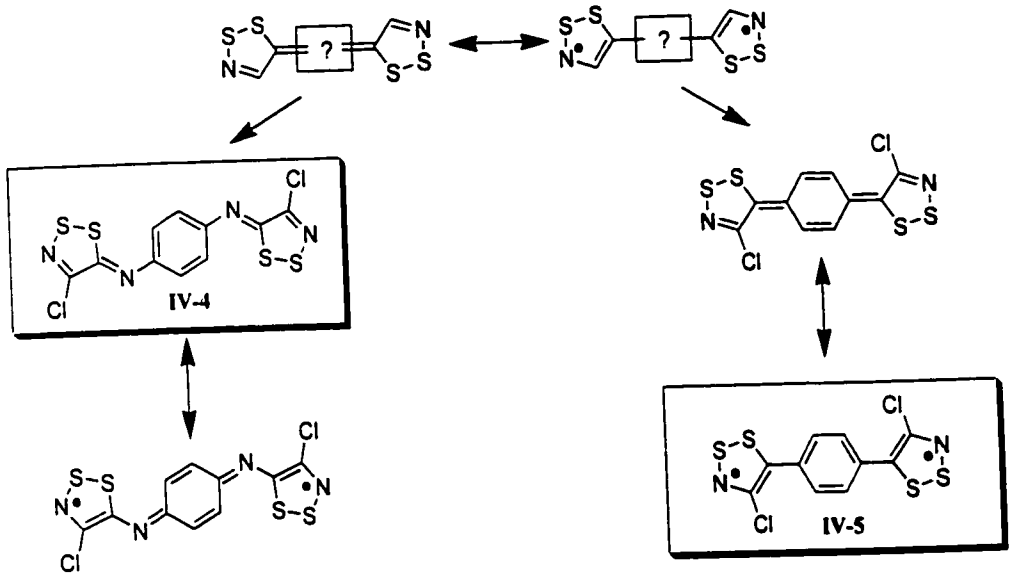

Figure 4.2 Comparison of **IV-4**, a closed shell singlet, and **IV-5**, a triplet diradical.

In the bis-1,2,3-dithiazole compound **IV-4**, the dithiazole rings are bridged at C5 and C5' by a 1,4-phenylenediamine linkage. Although the dithiazole rings are prevented from interacting electronically with one another, presumably due to the large aromatic stabilization energy of the bridging phenyl ring, they are closed shell as a result of bonding to the intervening nitrogens. What, then, would be the ground state of a species in which the dithiazole rings are directly bonded to the phenyl ring? The two possibilities considered herein† are a closed shell compound

† There are six microstate arising from four states possible for two electrons in two orbitals. This is covered in Chapter 1.

in which the phenyl ring assumes a quinoid structure and a triplet diradical compound in which the aromaticity of the phenyl ring is maintained. We have isolated this phenyl bridged bis-(1,2,3-dithiazole), **IV-5**, and it has a diradical ground state, as might be expected due to the aromatic stabilization of the phenyl ring. Furthermore, the bulkiness of the phenyl group prevents dimerization at the carbon C5.

In a similar fashion, we have stabilized a mono-1,2,3-dithiazolyl radical **IV-6a** by substitution with a perfluorophenyl group at the C5 position. The isostructural phenyl substituted dithiazolium cation [**IV-6b**][Cl] has also been characterized, however isolation of the neutral radical **IV-6b** has yet to be attempted.

Finally, 1,2,3-dithiazolyl radicals can be stabilized by building the heterocycle onto a fused ring system with a certain amount of electron withdrawing capacity. The extent to which this fused structure must be able to withdraw electrons from the heterocycle in order to stabilize the neutral radical species is investigated in the research of my co-workers, Mr. H. Zhang[2] and Mr. J. R. Mingie. The fused 1,2,3-dithiazolyl NRC **IV-7** isolated by my fellow group members is briefly discussed herein.

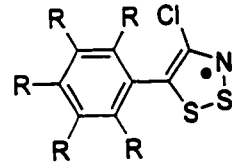

IV-6
a) R = F
b) R = H

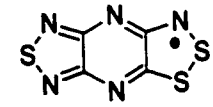

IV-7

Figure 4.3 A simple and a ring-fused mono-1,2,3-dithiazolyl neutral radical.

4.2 The Herz Reaction and Attempted Reduction of Herz Compounds

Substituted benzo-1,2,3-dithiazolylium chlorides (Herz compounds [**IV-3**][Cl]) were first reported in the 1920s.[6] They are the products of the reaction of sulfur monochloride with aromatic

amines. Since their discovery, there has been much interest in the mechanism of the Herz reaction and several papers have been published on this subject.[7] It was observed that the Herz reaction always produces a species ([**IV-3a**][Cl]) that is chlorinated on the phenyl ring in the *para*- position with respect to the dithiazole nitrogen. This prompted investigations into the substitution of the phenyl ring[8] including an alternate synthesis of Herz compounds involving the reaction of substituted 2-aminobenzethiol hydrochloride with thionyl chloride.[7,9] In this manner, the parent unchlorinated Herz compound ([**IV-3b**][Cl]) was finally prepared.

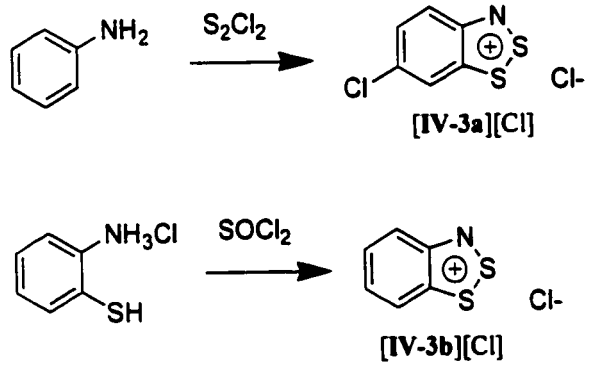

Figure 4.4 The Herz reaction chlorinates the phenyl ring. A more recent synthetic route avoids this chlorination.

The Herz reaction produces 1,2,3-dithiazolium chloride salts which are notoriously insoluble and thus difficult to purify. One approach to improving the solubility of these compounds is to exchange the chloride with some other counterion by metathesis. Syntheses of Herz salts [**IV-3**][Cl] with counterions other than chloride have been reported.[9, 10] These salts are much more easily purified and can be obtained as crystals. Substitution of the benzene ring of **IV-3** can also improve the solubility of these salts. Hence, it has been possible to determine the single crystal structure of a di(*tert*-butyl) substituted Herz salt.[11]

More recently, interest in stable free radicals has prompted investigations into the reduction of [**IV-3**]$^{+}$ with a view to isolating the corresponding 1,2,3-dithiazolyl neutral radical species **IV-3**.

The solution ESR spectra of several Herz radicals, as well as some selenium analogues, have been reported.[12] In fact, the radical has been observed as an intermediate in the Herz reaction, which eventually yields the chloride salt. However the characterization of these species in the solid state has not been achieved. It was the dearth of structural information which drove us to attempt the isolation of the Herz radical in the crystalline state as the first step in our investigation of 1,2,3-dithiazolyl compounds.

The original Herz reaction, the treatment of aniline with sulfur monochloride, yields 5-chlorobenzo[1,2-*d*]-(1,2,3-dithiazolium) chloride ([**IV-3a**][Cl]). In order to avoid chlorination of the benzene ring, we chose to treat 2-aminobenzenethiol with sulfur dichloride producing the parent 1,2,3-benzodithiazolium chloride ([**IV-3b**][Cl]) in a manner similar to that suggested by Huestis *et al.*[9] The insolubility of this compound makes it difficult to purify, therefore we explored the substitution of the chloride counterion for a variety of other anions. Metathesis of the chloride salt to the hexafluoroantimonate, the hexafluorophosphate, and the tetrafluoroborate was achieved by reaction with the corresponding nitrosonium salt in acetonitrile. These were all readily recrystallized in mixtures of approximately 1:5 acetonitrile in chlorobenzene.

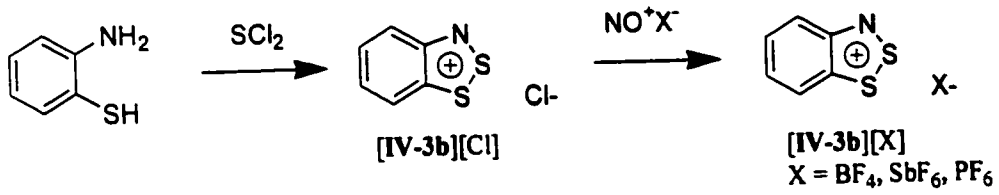

[**IV-3b**][Cl]

[**IV-3b**][X]
X = BF_4, SbF_6, PF_6

Figure 4.5 The synthesis of 1,2,3-benzodithiazolium salts.

From the purified hexafluoroantimonate salt, we were able to synthesize pure samples of halide salts. Although the reaction of [**IV-3b**][Cl] with potassium iodide fails to produce the iodide salt cleanly, the slow mixing of a solution of [**IV-3b**][SbF_6] in acetonitrile with a solution of

tetrabutylammonium iodide in acetonitrile across a glass frit yields black crystals of **[IV-3b][I]**. The reaction of **[IV-3b]**[SbF_6] with bis(triphenylphosphine)iminium chloride in acetonitrile yields a clean sample of the chloride salt, **[IV-3b]**[Cl].

In order to ascertain the electrochemical properties of benzo-1,2,3-dithiazole *in solvo*, cyclic voltammetric measurements of the **[IV-3b]**[SbF_6] in dry acetonitrile containing 0.1 M tetrabutulammonium hexafluorophosphate were recorded. These reveal a reversible oxidation-reduction peak centered at 0.18 V *vs.* SCE corresponding to the reversible redox process between the Herz cation **[IV-3b]**$^+$ and the neutral Herz radical **IV-3b**. There is also an irreversible reduction at -1.0 V.

Attempts at chemically reducing **[IV-3b]**[Cl] with a half equivalent of tin(II)chloride or with one equivalent of silver metal in acetonitrile failed to yield a retrievable solid. However, from careful reduction with a half equivalent of triphenylantimony in acetonitrile we were able to isolate a purple-black powder. Many attempts to sublime this material in a gradient furnace were made. The material, however, seemed to be thermally unstable with decomposition occurring at temperatures as low as 60°C. Thus we failed to obtain crystals or otherwise pure samples.

4.3 A Stable Ring-Fused 1,2,3-Dithiazolyl Radical: The First NRC

Recently, members of our research group published[2] the synthesis, characterization, and solid state properties of 1,2,5-thiadiazolo[3,4-b]-1,2,3-dithiazolo[3,4-b]pyrazin-2-yl, **IV-7**. This extended fused-ring 1,2,3-dithiazolyl is a development on the simple Herz compound **IV-3**. In this case, however, the neutral radical species can be isolated in the solid state due in great part to stabilization by the heavily electron withdrawing heterocycle.

A variety of important features in the design of this molecule lead to a thermally and chemically stable crystal state with semiconducting properties. Not only does the extended

heterocyclic system provide electronic stabilization of the radical, it affords a π SOMO that is delocalized over the entire molecule. Furthermore, the lack of peripheral groups, such as protons, facilitates potential intermolecular SOMO overlap in all three packing directions in the solid state.

IV-7 is the first crystalline 1,2,3-dithiazolyl reported and has the highest room temperature conductivity of any single-component sulfur based material to date ($\sigma = 1 \times 10^{-4}$ S cm^{-1}). The crystal structure is an arrangement of slipped-stack weakly associated dimers. At low temperatures, the spins are quenched and the material is essentially diamagnetic (5 - 200 K, residual spin concentration is 0.2 %). Above 200 K, paramagnetic behaviour becomes apparent and at 380 K approximately 2% of the molecules carry free Curie spins. The most important feature of this material is that bulk conductivity increases dramatically with the increase free Curie spins at higher temperatures. In other words, although only a small percentage of the electrons is free at higher temperatures, those free electrons contribute to the conductivity of the material. This is the first neutral radical compound in which the unpaired electrons are not trapped on the individual molecules but are able to move between molecular sites in the solid state giving rise to bulk conduction.

From the analysis of the conductivity data, it has been determined that conduction in this material follows a one-dimensional variable range electron hopping model (*i.e.*, the logarithm of conductivity is proportional to $T^{-1/2}$). Furthermore, it appears from the extended Hückel band calculations that the largest conductivity may occur through sulfur contacts *between* the slipped stacks rather than in the stacking direction.

4.4 Appel's Salt Synthesis and Reduction Revisited

4,5-Dichloro-1,2,3-dithiazolium chloride, otherwise known as Appel's salt (**IV-1**), is the product of a reaction between acetonitrile and sulfur monochloride. Since the first step in this

synthesis is chlorination of the acetonitrile, it is common practice to use chloroacetonitrile as the starting material. Furthermore, this synthesis, performed in dry methylene chloride, can take upwards of a week to initiate. The addition of a phase transfer catalyst such as Adogen®464 ensures that the reaction proceeds in a matter of hours.

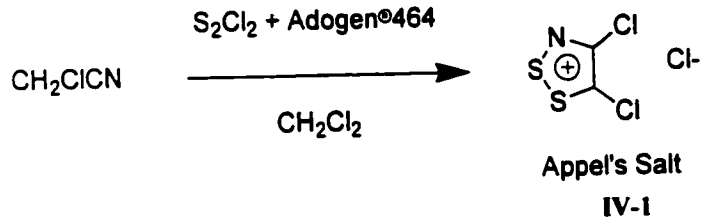

Appel's Salt
IV-1

Figure 4.6 Synthesis of Appel's salt.

The reduction of **IV-1** is discussed in detail in Chapter 3. The closed-shell dimer product, **IV-2** is recovered from a two-electron reduction. When Appel's salt is reduced with only a half equivalent of triphenylantimony (*i.e.*, a one-electron reduction) the radical cation **[IV-2]**$^{+\cdot}$ is produced. Attempts at observing by ESR the neutral radical species of **IV-1** as an intermediate to the dimerization product have been unsuccessful.

4.5 The First Stable Simple 1,2,3-Dithiazolyl Radical

Ab initio calculations on the unknown 4,5-diprotio-1,2,3-dithiazolyl radical predict that the spin density resides heavily on the carbon C5. The dimerization at this carbon observed upon reduction of **IV-1** is a foreseeable consequence of this distribution of the SOMO. Dimerization can be blocked by substituting a perfluorophenyl group at the C5 position. The resulting neutral radical material **IV-6a** is the first non-fused 1,2,3-dithiazolyl reported in the crystal state.

Reaction of 2,3,4,5,6-pentafluorophenylacetonitrile with sulfur monochloride in methylene

chloride closes the 1,2,3-dithiazole ring such that it is substituted at the C5 position by the perfluorophenyl ring and at the C4 position by chlorine. A catalytic amount of Adogen®464 or tetrabutylammonium chloride is added in order to increase the rate of reaction. The product of this reaction is a chloride salt ([**IV-6a**][Cl]) that, when treated with either zinc or triphenylantimony in sulfur dioxide, can be reduced to a black solid. Lustrous green-black blocks of the 4-chloro-5-pentafluorophenyl-1,2,3-dithiazolyl neutral radical (**IV-6a**) are obtained by sublimation at 45 °C/10^{-2} Torr.

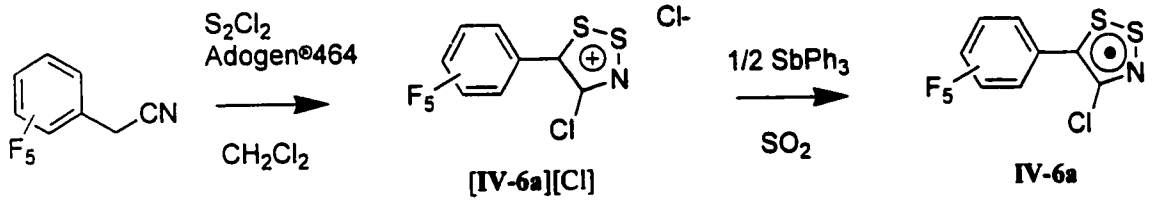

Figure 4.7 Preparation of the first stable simple 1,2,3-dithiazolyl radical.

The bulky perfluorophenyl group serves its intended purpose of preventing dimerization at the C5 carbons. However, this group might also be expected to inhibit intermolecular πoverlap between the dithiazolyl rings preventing conduction in the solid state material. If such is the case, it may also prevent dimer formation through sulfur, possibly generating a material with interesting bulk magnetic properties. This is not the case. The dithiazolyl radicals do indeed dimerize through sulfur in the crystal state. The dimers are oriented such that inter-dimer contacts do not permit the formation of a band structure. It is worth noting, however, that the interannular S ··· S dimer contacts are exceptionally long at 3.2987(13) Å. This is longer than any such contacts previously observed for the sister 1,3,2-dithiazolyl radicals.

A second interesting observation regarding this dimerization is that it occurs through S1 ··· S1' resulting in hypervalent sulfurs with a nominal sulfur-carbon double bond. This arrangement

is the least energetically favoured of the four possible cofacial dimer orientations that might occur for a generic 1,2,3-dithiazolyl. Dimerization through sulfur at the 2-position would generate a hypervalent sulfur with a sulfur nitrogen double bond and the two possible four-center modes would be favoured by increased delocalization. For steric reasons, however, the observed dimer orientation is the most energetically favorable for the perfluorophenyl substituted species, **IV-6a**.

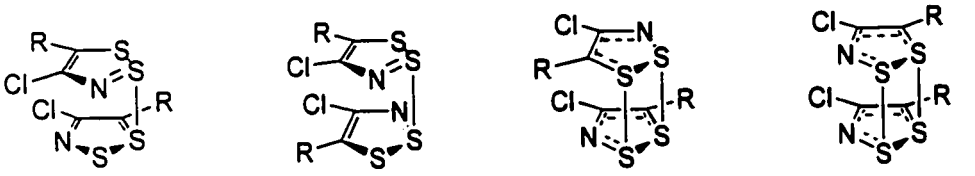

Figure 4.8 The four possible co-facial modes of dimerization for a generic 1,2,3-dithiazole.

4.6 A Bridged Bis-1,2,3-Dithiazolyl Biradical

The **IV-6a** radical does not undergo an irreversible C ··· C dimerization due in great part to steric factors. The bulkiness of the perfluorophenyl group simply will not allow the proximity necessary for such an interaction. An inductive argument can also be made in order to account for the lack of observed C ··· C dimers since the perfluorophenyl group is a particularly electron withdrawing substituent. In the spirit of further determining what is necessary in order to stabilize 1,2,3-dithiazolyl radicals against C ··· C dimerization, we have synthesized both the isostructural phenyl-substituted 1,2,3-dithiazolium salt [**IV-6b**][Cl] and a 1,4-phenyl-bridged bis-1,2,3-dithiazolium salt [**IV-5**][Cl]$_2$. Single electron reduction of the 4-chloro-5-phenyl-1,2,3-dithiazolium chloride [**IV-6b**][Cl] has yet to be attempted. The two-electron reduction of [**IV-5**][Cl]$_2$, however, yields a stable biradical species.

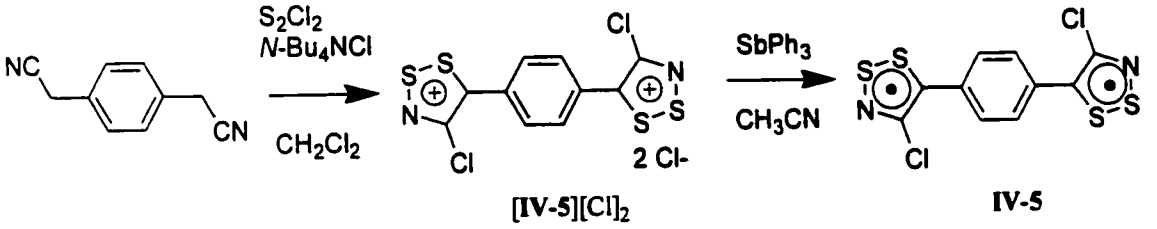

Figure 4.9 Preparation of a 1,4-phenyl-bridged bis-1,2,3-dithiazolyl.

The reaction of benzyl cyanide with sulfur monochloride in CH_2Cl_2 using Adogen®464 yields bright yellow crystals of **[IV-6b]**[Cl]. Similarly, 1,4-phenylenediacetonitrile and sulfur monochloride in CH_2Cl_2 with *N*-Bu_4NCl produces orange crystals of **[IV-5]**$[Cl]_2$. Reduction of this salt with triphenylantimony in dry acetonitrile yields a black powder which has been characterized as the neutral biradical **IV-5**. Attempts at obtaining crystals of this material either by sublimation or *in solvo* recrystallization have failed due to the insolubility and thermal instability of the compound.

4.7 Crystal Structures

The solid state structures of both **[IV-6a]**[Cl] and **IV-6a** have been determined by X-ray diffraction. The **[IV-6a]**[Cl] salt crystallizes in the monoclinic space group $P2_1/n$. Each chloride anion is paired with a **[IV-6a]**$^+$ such that it bridges the internal S-S bond, with S ··· Cl contacts of 2.8947(16) and 2.9617(18) Å. The mean plane of the dithiazole ring makes a dihedral angle of 68.6° with the plane of the perfluorophenyl group.

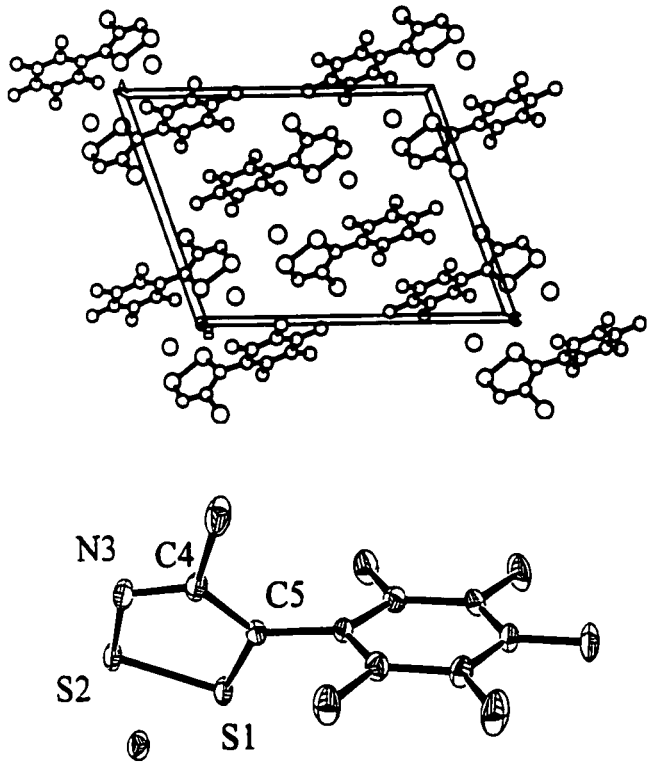

Figure 4.10 PLUTO and ORTEX drawings of the chloride salt [**IV-6a**][Cl]. Bond distances within the heterocyclic ring are: *d*(S-S) 2.0284(4), *d*(S-N) 1.605(4), *d*(S-C) 1.673(4), *d*(N-C) 1.309(5), *d*(C-C) 1.393(2) Å.

The neutral **IV-6a** crystallizes in the tetragonal space group $I\bar{4}2d$. The crystal structure is composed of dimer pairs in which the individual **IV-6a** units are related by a two-fold axis, and are linked by a single interannular S ··· S′ contact of 3.2987(13) Å. The perfluorophenyl ring is twisted by 58.3° away from the plane of the dithiazole ring. This provides the steric hindrance necessary to prevent irreversible C-C dimer formation. The bulkiness of the perfluorophenyl group also prevents π-stacking of the dimer units. Thus, the solid state packing is based on dimer units arranged about a $\bar{4}$ symmetry site. The dimers are linked to one another by S ··· S′ contacts of 3.7286(9) Å.

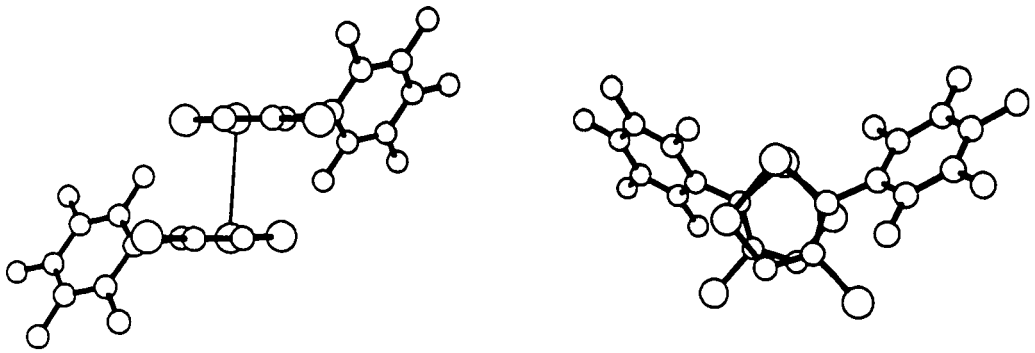

Figure 4.11 PLUTO drawings of the radical **IV-6a**. The orientation of the overlap of the heterocyclic rings is shown, as is the interannular S ··· S′ contact. Bond distances within the heterocyclic ring are: *d*(S-S) 2.0717(8), *d*(S-N) 1.639(2), *d*(S-C) 1.724(2), *d*(N-C) 1.317(3), *d*(C-C) 1.390(3) Å.

4.8 Cyclic Voltammetry

Cyclic voltammetry was performed on solutions of **IV-6a** in CH_3CN using 0.1 M *n*-Bu_4NPF_6 as a supporting electrolyte and ferrocene as an internal reference. A reversible oxidation wave at $E_{½}(ox)$ = 0.38 V (*vs.* SCE) and an irreversible reduction wave at $E_{pc}(red)$ = -1.1 V (*vs.* SCE) were recorded. The features of this cyclic voltammogram are similar to those of the Herz salt discussed herein ($E_{½}(ox)$ = 0.18 V, $E_{pc}(red)$ = -1.0 V). The oxidation potential, corresponding to the reversible redox process between the cation and the neutral radical, is more anodic for **IV-6a** than for the Herz salt, **[IV-3b][SbF$_6$]**. This is due in part to the electronegative perfluorophenyl group of **IV-6a**. Furthermore, benzodithiazolyls such as the Herz radical (**IV-3b**) tend to have less anodic first oxidation potentials as a result of a more delocalized electron distribution.

Cyclic voltammetry of **[IV-5][GaCl$_4$]$_2$** was undertaken with 0.1 M *n*-Bu_4NPF_6 in acetonitrile as the supporting electrolyte. In this case, ferrocene could not be used as an internal reference owing to its capacity as a reducing agent. Instead, the internal reference employed was 1,4-diimino-1*H*,4*H*-bis[4-chloro-5*H*-1,2,3-dithiazole]benzene (see Chapter 3 for the referenced

CV of this compound). One reversible reduction peak was measured at 0.349 V *vs.* SCE. This peak corresponds to a two-electron redox reaction, effectively between the dication and the neutral oxidation states. A more accurate description is that the formation of an unstable radical cation at the working electrode is followed by a disproportionation reaction more rapid than the cyclic rate of the experiment. A stable radical cation is not observed in the electrochemical redox process.

4.9 Electron Paramagnetic Resonance

The simple 1,2,3-dithiazole heterocycle possesses only one EPR spin-active nucleus, the nitrogen atom with a spin of 1. It is expected, therefore, that any radical species in which the unpaired electron is essentially localized on this heterocycle will yield an EPR signal based on a three-line pattern (hyperfine coupling to this nitrogen). The further the EPR signal deviates from this fundamental three-line pattern, the more spin density resides on the substituent groups, assuming that they possess spin-active nuclei.

In the case of both **IV-6a** and **IV-5**, solution EPR reveals a three line pattern with a secondary fine structure indicating that the majority of the spin density is trapped on the heterocycle. Thus, the case of **IV-5**, the phenyl bridge has provided an effective barrier to intermolecular electronic interactions between the dithiazole rings. This biradical does not demonstrate quinoid closed-shell character to any perceivable degree.

Bright yellow solutions of **IV-6a** in CH_2Cl_2 exhibit a strong and persistent EPR signal at room temperature (g = 2.0089). The hyperfine coupling constants have been derived by simulation using Brüker Simfonia. A rich secondary structure arising from coupling to the 4-chlorine (a_{Cl} = 1.050 (^{37}Cl), 0.875 (^{35}Cl) Gauss) and all five fluorines on the perfluorophenyl group (a_F = 1.75 (2F), 0.38 (1F), 0.31 (2F) Gauss) overlies the dominant triplet arising from hyperfine coupling

to nitrogen (a_N = 6.10 Gauss).

IV-5 dissolved in CH_2Cl_2 yields a blue solution with a strong and persistent EPR signal similar to that of **IV-6a**. The spectrum is dominated by the three line pattern arising from coupling to *one* nitrogen (a_N = 5.533 Gauss). The implication being that the radicals are trapped to a large extent on the individual dithiazole rings such that coupling is only observed to the nitrogen of that heterocycle. The strength and persistence of the EPR signal generated by **IV-5** at room temperature in the absence of direct light is indicative of an open shell ground state. For a signal of such great intensity to be generated by population of a low lying excited triplet state, the energy difference between the closed shell ground state and the triplet would have to be very small indeed (k_B x (300 K) x N_A x 0.24 cal/J = 0.6 kcal/mol, therefore for the population of the excited state to be as large as 1% at room temperature, the energy gap would have to be as small as 2.8 kcal/mol according to the Boltzmann expression). As with **IV-6a**, a secondary hyperfine coupling pattern (a_{small} = 0.592 Gauss), presumably to the protons on the phenyl ring, is observed in the EPR. The g-value is 2.00841 which is slightly less than that of **IV-5**. Finally, at 20 Gauss, the spectral width of the **IV-5** EPR signal is approximately the same as that for **IV-6a**, as might be expected from systems with isolated dithiazolyl rings.

To summarize Chapter 4, the reactions of pentafluorophenylacetonitrile and of 1,4-phenylenediacetonitrile with sulfur monochloride, followed by reduction, yielded the first simple 1,2,3-dithiazolyl radicals stable in the solid state. The crystal structure of **IV-6a** is discouraging in terms of the possibility of neutral radical conduction, revealing dimerization of the neutral radicals and no apparent close inter-dimer contacts. Crystals of **IV-5** of sufficient size and quality for X-ray diffraction were never prepared. The cyclic voltammetry of **[IV-5]**$[GaCl_4]_2$ gave no evidence of a stable radical cation oxidation state. This finding was supported by the ESR of **IV-5**, which showed coupling to only one of the two nitrogens in the molecule, indicating that the spins

were isolated on the peripheral dithiazole rings.

4.10 Syntheses

4.10.1 Synthesis of 1,2,3-benzodithiazolium chloride, [IV-3b][Cl]: Sulfur dichloride (24.65 g, 239.4 mmol) in dry acetonitrile (70 mL) was added over a 20 m period to a solution of 2-aminothiophenol (9.984 g, 79.75 mmol) in acetonitrile (200 mL) at 0 °C. The mixture was stirred at RT for 1 h to yield an orange precipitate. This was recovered by filtration and washed in hot toluene (30 mL) to remove any biproduct sulfur; yield 10.08 g (53.14 mmol, 67 %). IR:1582 (m), 1517 (s), 1428 (w), 1338 (s), 1307 (m), 1131 (m), 1062 (w), 942 (m), 821 (s), 773 (s), 729 (m), 695 (w), 614 (w), 526 (w), 488 (w), 459 (w) cm^{-1}.

4.10.1.1 Synthesis of 1,2,3-benzodithiazolium chloride [IV-3b][Cl], by metathesis: 1,2,3-benzodithiazolium hexafluorophosphate **[IV-3b][SbF_6]** (0.502 g, 1.29 mmol) and bis(triphenyl-phospine) iminium chloride (0.743 g, 1.29 mmol) were stirred in 50 mL of dry acetonitrile for 90 m. The resulting yellow solid was collected by filtration, washed with 15 mL dry acetonitrile, and dried *in vacuo*. IR: 1585 (m), 1519 (m), 1438 (w), 1426 (w), 1339 (m), 1309 (w), 1133 (w), 1065 (w), 956 (w), 942 (m), 820 (s), 774 (s), 730 (s), 696 (w), 615 (m), 525 (w), 490 (w), 460 (w) cm^{-1}.

4.10.2 Synthesis of [1,2,3-benzodithiazolium][X], [IV-3b][X], X = BF_4, PF_6, SbF_6: 1,2,3-benzodithiazolium chloride **[IV-3b][Cl]** (1.0 g, 5.3 mmol) and nitrosonium tetrafluoroborate (0.63 g, 5.4 mmol) were stirred in acetonitrile (25 mL) at RT, under inert atmosphere, for 2 h. The solvent was removed from the dark solution *in vacuo*. The remaining solid was recrystallized as brown crystals from a 4:1 mixture of chlorobenzene and acetonitrile (50 mL); yield 0.75 g (3.1

mmol, 59 %); IR [**IV-3b**][BF_4]: 1591 (s), 1522 (m), 1430 (m), 1346 (s), 1325 (m), 1287 (w), 1185 (w), 1141 (s), 1062 (vs, b), 948 (w), 818 (s), 776 (s), 729 (m), 701 (m), 621 (m), 525 (m), 458 (w). IR [**IV-3b**][PF_6]: 1585 (s), 1517 (s), 1430 (m), 1343 (s), 1324 (m), 1246 (w), 1177 (w), 1138 (m), 1062 (b), 981 (w), 960 (s), 876 (w), 842 (vs, b), 776 (s), 743 (w), 724 (m), 697 (w), 615 (m), 557 (s), 534 (w), 518 (w), 493 (w), 478 (w), 450 (m). IR [**IV-3b**][SbF_6]: 1586 (s), 1521 (m), 1427 (s), 1342 (s), 1318 (m), 1246 (w), 1175 (w), 1137 (w), 955 (m), 867 (w), 817 (s), 771 (s), 725 (m), 697 (m), 660 (vs, b), 614 (m), 565 (w), 520 (w), 454 (m).

4.10.3 Synthesis of 4,5-dichloro-1,2,3-dithiazolium chloride, IV-1[13]: Cloroacetonitrile (11 mL, 0.17 mol) and sulfur monochloride (66 mL, 83 mol) were stirred in 90 mL dry methylene chloride with 1.5 mL Adogen®464. After 2 h, a yellow precipitate started to form. The reaction mixture was stirred for a further 24 h. The yellow solid was collected by filtration, washed 4 x 20 mL dry methylene chloride, and dried *in vacuo*; yield 21.97 g (0.105.4 mol, 62 %). IR: 1706 (vw), 1284 (s), 1252 (m), 1085 (s), 918 (m), 827 (s), 629 (w), 606 (s), 558 (vw), 524 (m), 441 (s) cm^{-1}.

4.10.4 Synthesis of 4-chloro-5-(2,3,4,5,6-pentfluorophenyl)-1,2,3-dithiazolium chloride [IV-6a][Cl]: A mixture of 2,3,4,5,6-pentafluorophenylacetonitrile (2.60 g, 12.6 mmol) and excess sulfur monochloride (approx. 5 mL) in methylene chloride (8 mL) with 2 drops of Adogen®464 was left undisturbed under inert atmosphere for 14 days. Bright yellow square-needle shaped crystals grew in solution. Chlorobenzene (20 mL) was added and the crystals were collected by filtration. These were washed with chlorobenzene (3 x 20 mL) and dried *in vacuo*; yield 2.70 g, (7.94 mmol,63 %); mp 211-213 °C. IR:1584 (s), 1543 (w), 1483 (m), 1412 (w), 1286 (w), 1234 (m), 1220 (m), 1141 (s), 1106 (s), 1009 (w), 955 (w), 860 (s), 835 (m), 823 (m), 774 (w), 763 (s), 640 (m), 629 (s), 551 (m), 525 (s), 438 (m) cm^{-1}. MS (*m/e*): 378 (M^+, 21 %). Anal. Calcd. for

$C_8F_5NS_2Cl_2$: C, 28.25; H, 0.0; N, 4.12 %. Found: C, 28.40; H, 0.0; N, 4.06 %.

4.10.5 Synthesis of 4-chloro-5-(2,3,4,5,6-pentfluorophenyl)-1,2,3-dithiazolyl, IV-6a: 4-Chloro-5-(2,3,4,5,6-pentfluorophenyl)-1,2,3-dithiazolium chloride **[IV-6a]**[Cl] (0.68 g, 2.0 mmol) was reduced in liquid sulfur dioxide (5 mL) at -70 °C with triphenylantimony (0.38 g, 1.06 mmol). After 5 m, the solvent was removed *in vacuo* from the still cold mixture leaving a black matrix, from which **IV-6a** was sublimed as lustrous green-black blocks (45 °C/10^{-2} Torr); yield 0.17 g, (0.54 mmol, 27 %); mp > 52 °C (decomp.). IR:1584 (s), 1543 (w), 1483 (m), 1412 (w), 1286 (w), 1234 (m), 1220 (m), 1141 (s), 1106 (s), 1009 (w), 955 (w), 860 (s), 835 (m), 823 (m), 774 (w), 763 (s), 640 (m), 629 (s), 551 (m), 525 (s), 438 (m) cm^{-1}.

4.10.6 Synthesis of 4-chloro-5-phenyl-1,2,3-dithiazolium chloride [IV-6b][Cl]: Benzyl cyanide (2.0 g, 17 mmol) and sulfur monochloride (7 mL) were stirred in chlorobenzene (10 mL) with a drop of Adogen®464 under inert atmosphere for 10 days. Two yellow liquid layers formed upon sitting for 0.5 h. Vigourous shaking followed by cooling to -10 °C yielded a yellow precipitate which was collected by filtration and dried *in vacuo*; yield 3.2 g (13 mmol, 76%). IR: 1677 (w), 1590 (m), 1344 (s), 1200 (s), 914 (w), 843 (s), 767 (s), 693 (s), 683 (s), 549 (w), 510 (m), 450 (w), 423 (s) cm^{-1}.

4.10.7 Synthesis of [IV-5][Cl]$_2$: A solution of 1,4-phenylenediacetonitrile (0.507 g, 3.25 mmol) and sulfur monochloride (5 mL) in methylene chloride (10 mL) with *n*-tetrabutylammonium chloride (0.100 g, 0.360 mmol) was left undisturbed under inert atmosphere for 7 days. The resulting orange crystals were collected by filtration, washed with a small amount of cold methylene chloride, and dried *in vacuo*; yield 0.890 g (2.10 mmol, 42 %). IR: 1682 (vw), 1595

(w), 1410 (w), 1335 (s), 1285 (w), 1200 (s), 1017 (w), 987 (s), 915 (m), 845 (s), 822 (s), 760 (vw), 657 (w), 595 (m), 548 (s), 535 (w), 437 (s), 425 (w) cm^{-1}.

4.10.8 Synthesis of IV-5: [**IV-5**][Cl]$_2$ (0.250 g, 0.541 mmol) and triphenylantimony (0.299 g, 0.847 mmol) were slurried at 50 °C under inert atmosphere, for 2 h. The resulting black microcrystalline precipitate was collected by filtration and dried *in vacuo*; yield 0.165 g (0.470 mmol, 87 %). IR: 1675 (w), 1602 (w), 1571 (w), 1417 (w), 1310 (m), 1256 (w), 1183 (s), 1133 (s), 1016 (w), 993 (w), 948 (s), 851 (s), 798 (s), 785 (s), 729 (m), 684 (m), 613 (w), 577 (s), 512 (w), 494 (m), 453 (w) cm^{-1}.

References for Chapter 4

1. (a) Haddon, R. C.; *Nature*, **1975**, *256*, 394. (b) Haddon, R. C.; *Aust. J. Chem.*, **1975**, *28*, 2343.
2. Barclay, T. M.; Cordes, A. W.; Haddon, R. C.; Itkis, M. E.; Oakley, R. T.; Reed, R. W.; Zhang, H.; *J. Am. Chem. Soc.*, **1999**, *121*, 969.
3. Appel, R.; Janssen, H.; Siray, M.; Knoch, F.; *Chem. Ber.*, **1985**, *118*, 1632.
4. Warburton, W. K.; *Chem. Rev.*, **1957**, 1011.
5. (a) Barclay, T. M.; Beer, L.; Cordes, A. W.; Haddon, R. C.; Itkis, M. I.; Oakley, R. T.; Preuss, K. E.; Reed, R. W.; *J. Am. Chem. Soc.*, **1999**, *121*, 6657. (b) Barclay, T. M.; Cordes, A. W.; Oakley, R. T.; Preuss, K. E.; Reed, R. W.; *Chem. Commun.*, **1998**, 1039.
6. Herz, R.; *Chem. Zentr.*, **1922**, *4*, 948.
7. Huestis, L. D.; Walsh, M. L.; Hahn, N.; *J. Org. Chem.*, **1965**, *30*, 2763.
8. (a) Mayer, R.; Domschke, G.; Bleisch, S.; Fabian, J.; Bartl, A.; Staško, A.; *Collection Czechoslovak Chem. Commun.*, **1984**, *49*, 684. (b) Mayer, R.; Domschke, G.; Bleisch, S.; Bartl, A.; *Z. Chem.*, **1981**, *21*, 324.
9. Huestis, L.; Emery, I.; Steffensen, E.; *J. Heterocycl. Chem.*, **1966**, *3*, 518.
10. (a) Huestis, L.; Brownell, M.; *J. Heterocycl. Chem.*, **1968**, *5*, 427. (b) Zibarev, A. V.; Gatilov, Y. V.; Bagrayanskaya, I. Y.; Maksimov, A. M.; Miller, A. O.; *J. Chem. Soc. Chem. Commun.*, **1993**, 2993.
11. Bats, J. W.; Fuess, H.; Weber, K. L.; Roesky, H. W.; *Chem. Ber.*, **1983**, *116*, 1751.
12. (a) Harrison, S. R.; Pilkington, R. S.; Sutcliffe, L. H.; *J. Chem. Soc., Faraday Trans. 1*, **1984**, *80*, 669. (b) Preston, K. F.; Sutcliffe, L. H.; *Magn. Res. Chem.*, **1990**, *28*, 189. (c) Mayer, R.; *Phosphorus and Sulfur*, **1985**, *23*, 277. (d) Tsveniashvili, V. Sh.; Malashkhiya,

M. V.; *Elektrokhimiya*, **1984**, *20*, 381.

13. Rees, C. W.; *J. Heterocycl. Chem.* **1992**, *29*, 639.

Chapter 5 Closed Shell Ring-Fused Bis-1,2,3-DTAs and Their CT Salts.

5.1 Introduction

In the last quarter century, advances in polymer technology have greatly influenced the nature and variety of consumer products. The generation of inexpensive, durable plastics, non-stick surfaces, and impact resistant materials has become commonplace. With the intent of expanding the scope of polymer applications, much research is currently being directed at developing polymers with new properties such as ferromagnetism, metallic conduction, and semiconduction. In a recent publication, Genin and Hoffmann[1] explored the possibilities of creating polymers based on SN heterocyclic units with odd electron counts in order to design conducting materials. Among the heterocycles featured in this computational study was the simple 1,2,3-dithiazolyl radical (**V-1**). It is with respect to the possible 1,2,3-DTA polymeric structures that the ring-fused bis-1,2,3-DTA molecules presented herein will be introduced.

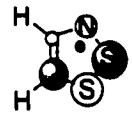

V-1

Figure 5.1 Experimentally unknown 4,5-diprotio-1,2,3-dithiazolyl.

As a first approximation to the properties of SN heterocyclic polymers, Genin and Hoffmann compared the electronic energies of closed shell and open shell SN heterocyclic dimers at the extended Hückel level. There are, in fact, three connectivities possible for a 1,2,3-DTA dimerized at a carbon site. The two 1,2,3-DTA rings can be connected via the carbons 5 and 5' (**V-2**), carbons 4 and 4' (**V-3**), or carbons 4 and 5' (**V-4**). Genin and Hoffmann chose the 4,5'-dimer (**V-4**) as the most likely to yield an open shell ground state structure upon polymerization.

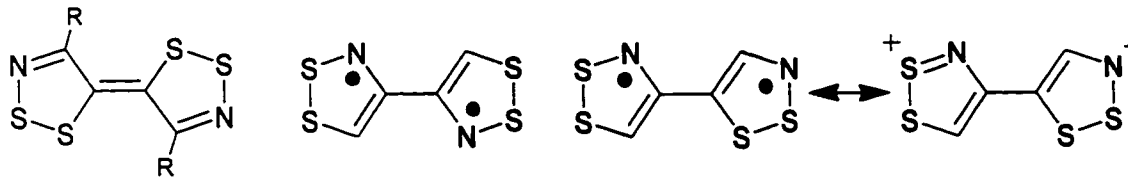

V-2, R=H
V-2a, R=Cl

V-3

V-4a

V-4b

Figure 5.2 Three possible connectivities for a 1,2,3-DTA dimerized at a carbon site.

In Chapter 3, the electronic configurations of the three theoretical bis-1,2,3-DTA dimers are discussed. *Ab initio* calculations predict that **V-3** exists as a ground state diradical whereas the ground state of **V-2** is a closed shell species. This can be understood from the large spin density calculated at C5 compared with the almost nodal lack of spin density at C4 of the experimentally unknown 4,5-diprotio-1,2,3-dithiazolyl **V-1**. Furthermore, the isolation and characterized of *trans*-4,4'-dichloro-1,1',2,2'3,3'-tetrathiadiazafulvalene **V-2a** presented in Chapter 3 confirms the theoretical prediction that a **V-2** will be a closed shell species in the ground state.

In order to design a polymer based on the diradical **V-3**, each dimer unit must be bonded to the adjacent units via the carbons C5 and C5' (*i.e.* ...4,4',5',5",4",4'"...). Given that **V-3** is an open shell diradical due to the lack of electronic interaction between DTA rings, and that **V-2** is closed shell, a polymer constructed in this manner (**V-5**) would necessarily be closed shell. It would, in fact, be a series of **V-2** units with little or no electronic interaction between them. In order to generate a ground state open shell polymer from this configuration, oxidation of a fraction of the DTA rings would be necessary. In effect, this would be a charge transfer polymer.

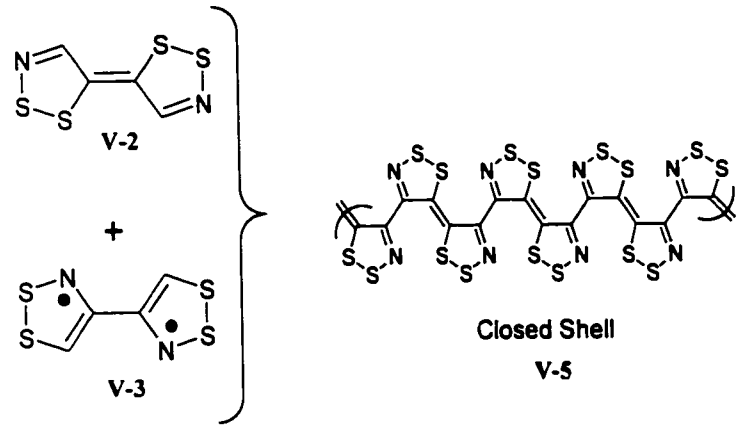

Figure 5.3 Theoretical polymer based on **V-2** and **V-3**.

Genin and Hoffmann report extended Hückel calculations that predict an open shell ground state configuration **V-4a** for a C4 to C5' linked dimer. *Ab initio* computational methods lend weight to this prediction, calculating the triplet diradical to be 18.95 kcal lower than the closed shell singlet (B3LYP/6-31G**). Theory predicts that although there is substantial spin density on the carbon C5', the lack of significant spin density on carbon C4 minimizes the intramolecular electronic interactions between the two rings.

In order for the C4 to C5' dimer to adopt a closed shell ground state configuration **V-4b**, charge separation must occur. The closed shell species must be zwitterionic. Thus, the two competing electronic configurations for a polymer based on **V-4** units are an extended open shell multiradical polymer (**V-6a**) and a charge separated zwitterionic polymer (**V-6b**). In the case that the theoretical polymer were open shell, Genin and Hoffmann suggest that it may possess interesting conductive and magnetic properties. Since an open shell ground state configuration implies that there is little interaction between adjacent dithiazole rings in the ground state, it is unlikely that conduction should occur along the backbone of such a polymer. Only in the event that a low lying closed shell excited state is easily accessible would through-polymer conduction

be possible. Should such an excited state not be accessible, the bulk polymeric material would only display conductive properties due to interactions *between* polymeric chains.

Since the zwitterionic configuration of a **V-6** polymer would be closed shell (**V-6b**), it would require that a fraction of the DTA rings be oxidized in order to create an open shell charge transfer system. It is possible that the zwitterionic ground state configuration of this polymer may show conductivity in the backbone direction. For example, if one electron were removed from the terminal DTA ring of a polymer of finite length, electronic interactions between adjacent DTA rings may allow the hole then created to move along the chain. Such a polymer might be employed as a nanowire.

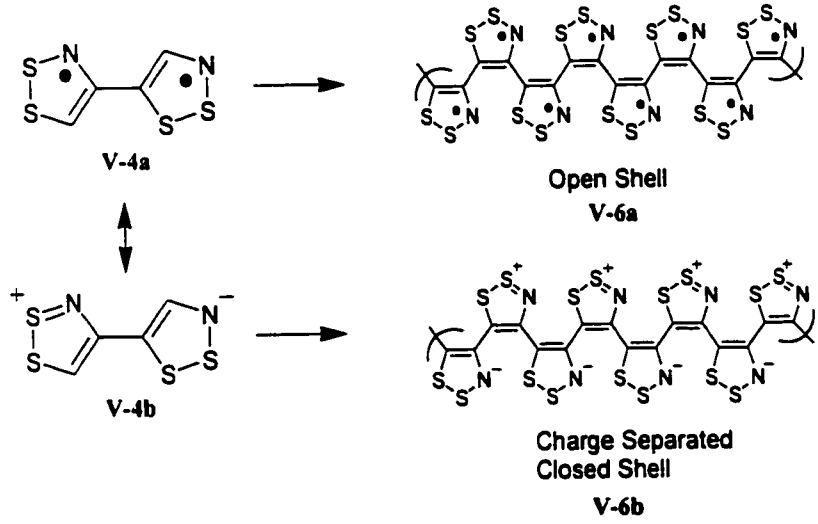

Figure 5.4 Theoretical polymer based on **V-4**; both open-shell and zwitterionic configurations are shown.

In the present chapter, benzo-bridged bis-1,2,3-DTA systems that are comparable to the **V-5** polymer are discussed. A variety of charge transfer salts derived by oxidation of these materials is also presented herein. Discussion of a similar benzo-bridged system representative of the **V-6** polymer is discussed in the following chapter.

5.2 V-7, V-15, and Their Selenium Analogs

In Chapters 3 and 4, the discussion focuses on bis-1,2,3-DTAs that are linked through carbons C5 and C5' via a variety of bridging groups. Both closed shell and open shell ground state structures are presented, including the simple C5 to C5' dimer, *trans*-4,4'-dichloro-1,1',2,2'3,3'-tetrathiadiazafulvalene **V-2a**. Currently, however, the analogous C4 to C4' linked systems (**V-3**) remain unknown as the synthesis of such compounds is greatly more challenging. Thus a potential problem is presented to the synthetic study of a 4,4',5',5"- linkage DTA oligomer. This barrier is circumvented by fusing two DTAs to a central aromatic ring such that the carbons that could be regarded as C4 and C4' are related to one another by conjugation, as are the C5 and C5' carbons.

The synthesis and characterization of **V-7** provides an analog to the theoretical 4,4',5',5"-DTA oligomer. In the ground state, this compound is a closed shell quinoid with a triplet excited state lying 0.85 eV (19.5 kcal/mol) higher in energy, according to *ab initio* calculations (B3LYP/6-31G**). This is in accord with the predicted electronic distribution given the theoretical insights into the location of spin density distribution of **V-1** previously discussed.

A further insightful comparison can be made between the experimentally unknown unchlorinated **V-7a** and the previously studied[2,3] benzo-bridged 1,3,2-DTA compound **V-8**. The spin density in a 1,3,2-DTA **V-9** is predicted to reside primarily on the SNS unit, thus the unpaired electrons tend to be "trapped" at either end of the neutral **V-8** giving rise to a diradical ground state. In molecular orbital (MO) terms, the energy difference between the two frontier orbitals (FMOs) is less than the electron pairing energy. A simple molecular orbital picture of the FMO manifold, derived from mixing of the singly occupied molecular orbitals (SOMOs) of two **V-9** radicals with the π-system of the central benzene ring, generates the b_{1u} symmetry MO and the b_{3g} symmetry MO shown qualitatively in **Figure 5.4**. These two molecular orbitals are not degenerate and thus the **V-8** system is not formally disjoint. However, the two frontier orbitals are

sufficiently close in energy that the diradical ground state is preferred. From *ab initio* calculations (B3LYP/dcep-31G*), the energy of the triplet and open shell singlet states are within 1 kcal/mol.[4]

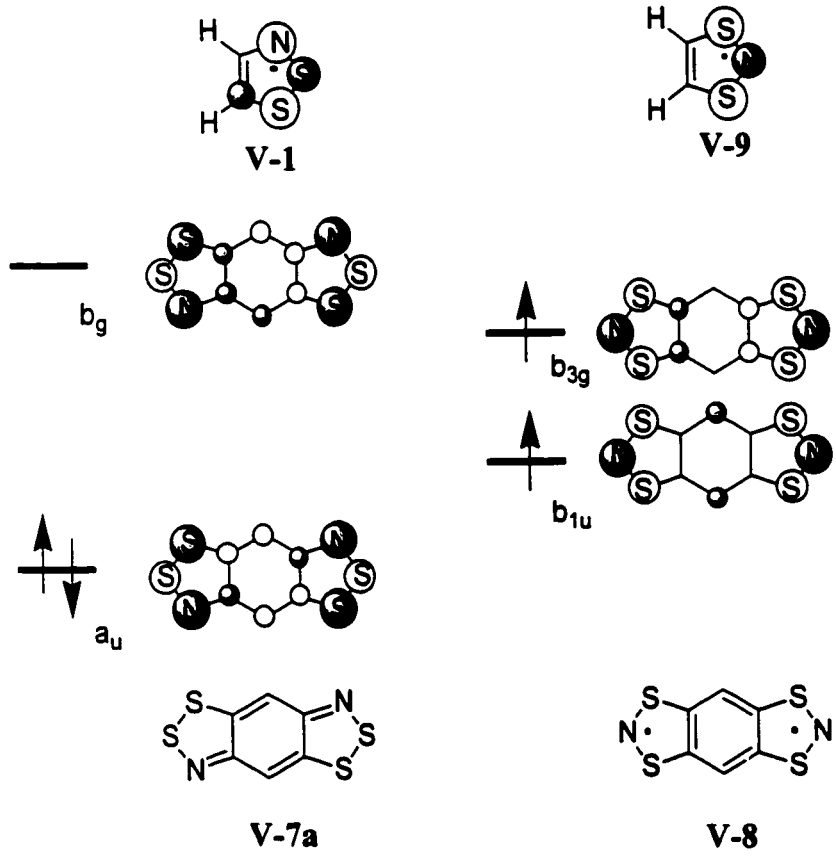

Figure 5.5 Qualitative FMO comparison of **V-8** and unchlorinated **V-7a**.

In comparison, two **V-1** radical SOMOs undergo strong mixing with the π-system of a central benzene ring giving rise to a HOMO, with a_u symmetry, much lower in energy than the b_g LUMO for **V-7a**. As a result of this larger splitting, the 16 π electron system has a closed shell ground state.

Ab initio calculations predict that the triplet $^3B_{2u}$ lies 0.48 eV below the closed shell singlet $^1A_{1g}$ for **V-8** whereas the triplet ^3B_u lies 0.72 eV *above* the ^1A_g singlet for **V-7a**. Furthermore, the

excited triplet state of **V-7a** lies 1.04 eV *below* the ground state triplet of **V-8** indicating that the bis-1,2,3- variant is the more stable of the two isomeric structures.

Further computational results indicate that the IP of **V-7a** is larger than that of **V-8** (6.92 and 6.58 eV respectively). The second ionization potential to a dication is again larger for **V-7a** (18.50 eV) than for the bis-1,3,2- isomer (17.77 eV) making the "window" between the radical cation and the dication for **V-7a** 11.58 eV. The EA for neutral **V-7a** is calculated to be 0.63 eV compared to 1.43 eV for **V-8**.

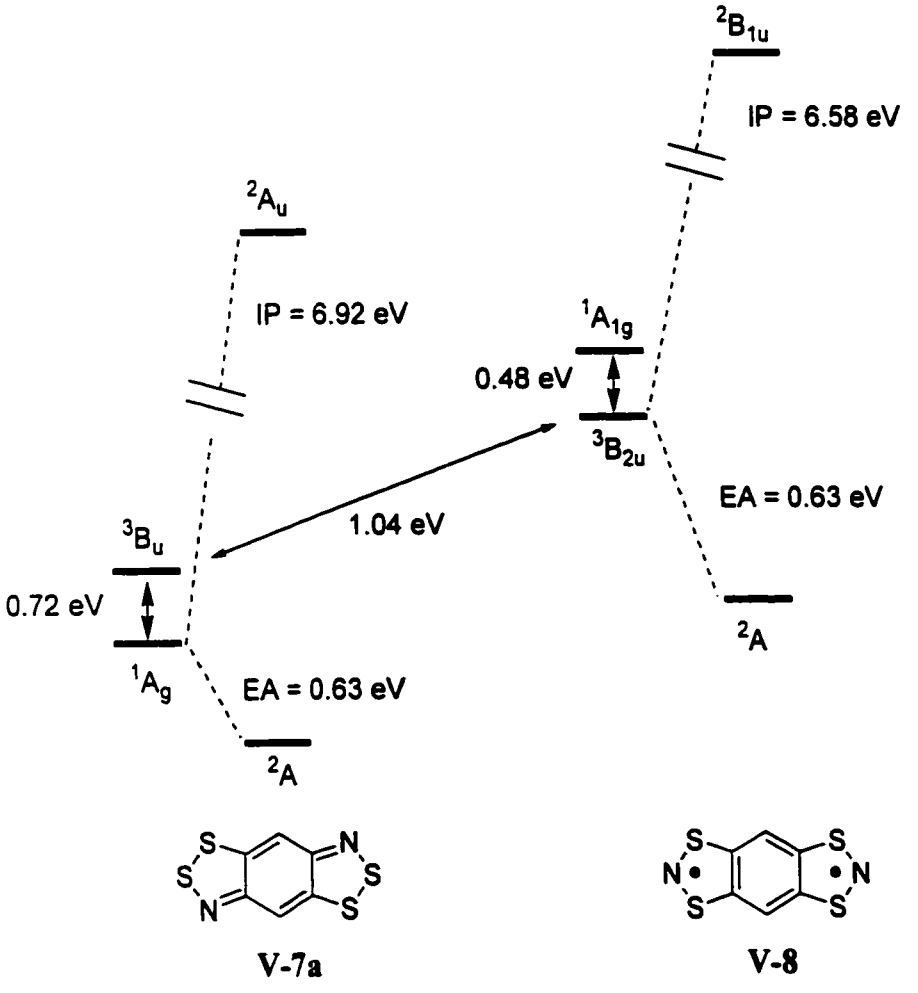

Figure 5.6 Relative energies (eV) of **V-7a** and **V-8**, their anions and cations.

The electronic and chemical properties of these two isomeric compounds can be compared. Characterization of the redox manifold by cyclic voltammetry reveals that a radical cation oxidation state is accessible for **V-8**. This is confirmed by the successful preparation of [**V-8**][$FeCl_4$].[5] Although the energy difference between the two FMOs is smaller than the electron pairing energy, giving rise to a diradical ground state, it is nevertheless possible to electrochemically oxidize one electron from the system to generate a stable radical cation. The redox manifold of **V-7** is equally rich with both a stable radical cation and dication oxidation state readily accessible. Thus, **V-7** enters into the realm of CT salt donors alongside the well-known TTF[6] and the analogous **V-2a**.

V-7 thus provides a novel structural skeleton for a CT salt donor. Furthermore, we have pursued a number of possible avenues for "fine tuning" the solid state properties of this type of donor compound. By incorporating selenium into the 2-position of the DTA rings (**V-10**) the intermolecular interactions in the solid state may be increased. In the course of the synthesis of **V-7** chlorination at both "open" sites on the central phenyl ring appears to be unavoidable. Although attempts have thus far been unsuccessful, it may yet be possible to perform a chemical substitution at these sites. A fluoro group, for instance, would be less bulky than the existing chlorine and would thus facilitate intermolecular overlap interactions in the solid state, thereby possibly improving conductive properties.

The synthetic route to **V-7** involves a multi-step preparation and isolation of 1,4-diaminobenzene-2,5-dithiol dihydrochloride **V-14** followed by closing of the DTA rings with either a sulfur or a selenium in the 2-position.[7] The reaction of 1,4-phenylenediamine with ammonium thiocyanate in an aqueous acidic medium generates **V-11**. Treatment of this compound with bromine produces the ring-closed compound **V-12**. Aqueous base cleaves the heterocyclic rings

open to yield the potassium salt, **V-13**, which is subsequently treated with aqueous hydrochloric acid generating the 1,4-diaminobenzene-2,5-dithiol dihydrochloride **V-14**.

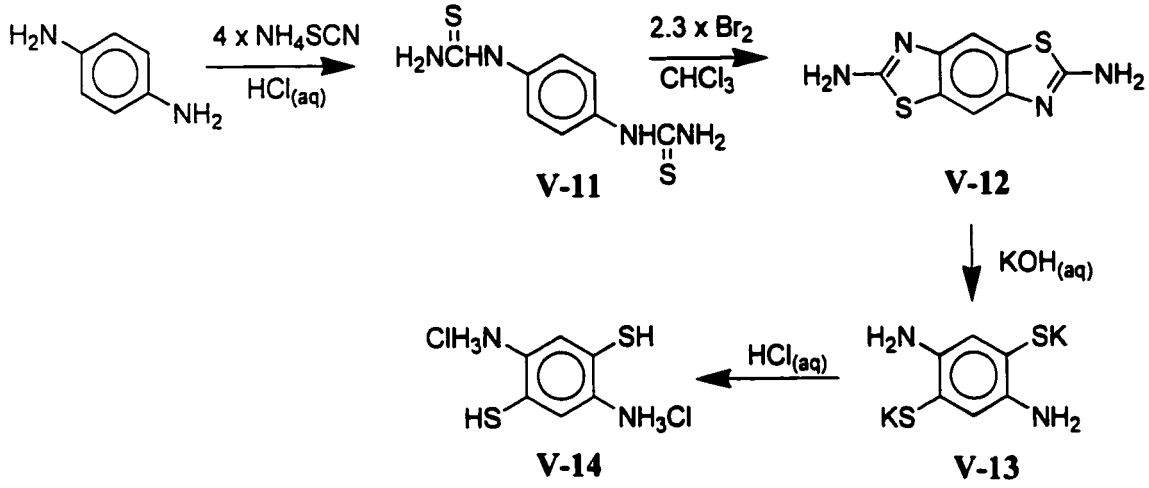

Figure 5.7 Synthetic route to **V-14** starting material.

The *cis*- variant **V-15** can be prepared from 1,4-diaminobenzene-2,3-dithiol dihydrochloride[8,9] **V-16** as the starting material (**Figure 5.8**). Furthermore, chlorination of the "open" sites on the central phenyl ring does not occur in the case of this isomer. The diprotio- (**V-15a**), monochloro- (**V-15b**) and dichloro- (**V-15c**) species have all been identified and are reported herein.[10]

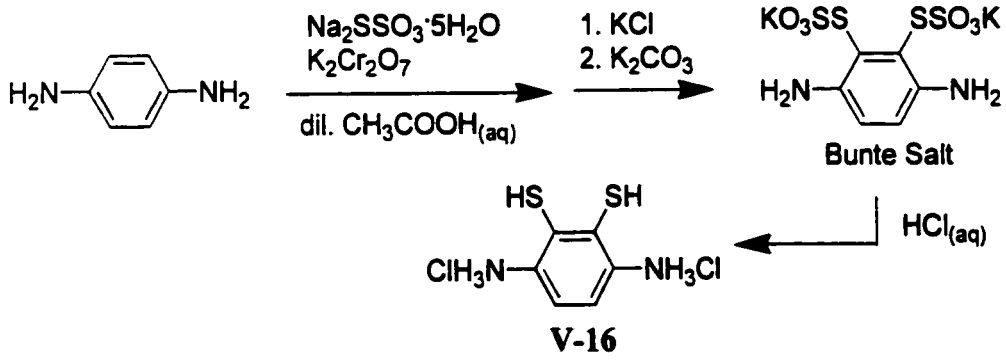

Figure 5.8 Preparation of starting material **V-16** follows literature procedures.[8,9]

In the wake of **V-7** and **V-15**, other members of the Oakley group have shown that the central ring need not be restricted to a phenyl ring. The naphthalene-based **V-17** compound has been isolated and characterized. It, too, acts as a CT salt donor with a BF_4^- counterion.

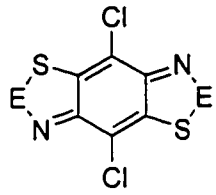

V-7, E = S
V-10, E = Se

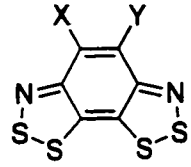

V-15
a, X = H, Y = H
b, X = H, Y = Cl
c, X = Cl Y = Cl

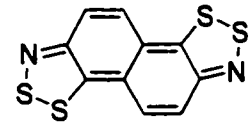

V-17

Figure 5.9 Bridged bis(1,2,3-dithiazoles) **V-7**, **V-10**, **V-15**, and **V-17**.

5.3 Charge Transfer Salts of V-7, V-15, and V-17

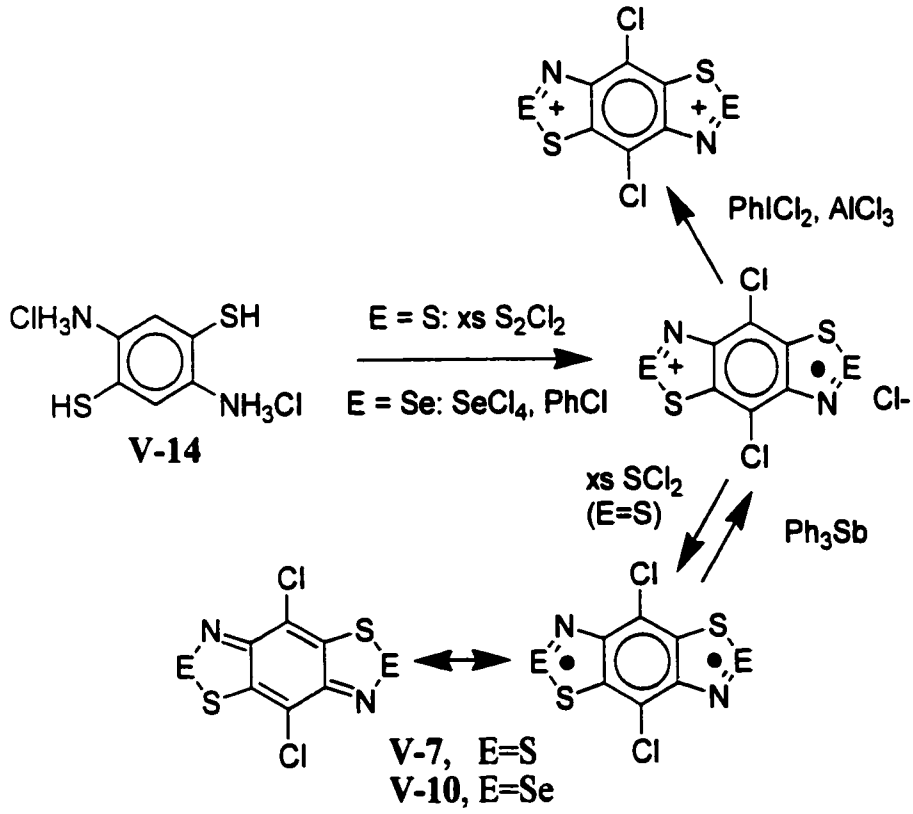

Figure 5.10 Synthesis of **V-7** and **V-10**.

The **V-7** framework is prepared under oxidizing conditions, in the presence of an excess of sulfur monochloride. As a result, the product is obtained in the stable radical cation oxidation state as the chloride salt **[V-7][Cl]**. The preparatory conditions do not yield the dication oxidation state $[\mathbf{V\text{-}7}]^{2+}$. This was somewhat surprising to us in light of previous work with the bis-1,3,2-isomer which is obtained as $[\mathbf{V\text{-}8}]^{2+}$ under mildly oxidizing conditions. In our experience, the $[\mathbf{V\text{-}7}]^{2+}$ salt must be prepared by further oxidation of **[V-7][Cl]** with $PhICl_2$ or SO_2Cl_2 and two equivalents of $AlCl_3$ in SO_2 yielding the closed shell dicationic $[\mathbf{V\text{-}7}][AlCl_4]_2$. The neutral closed shell species **V-7** can be obtained easily as lustrous black crystals by reduction of the radical cation with excess triphenylantimony followed by sublimation.

In comparison to other well-known organic CT donors (*e.g.*, TTF), **V-7** is a relatively weak donor. However, that the radical cation oxidation state is isolated in the initial preparation of **V-7** is significant in terms of the large stability of $[\mathbf{V\text{-}7}]^{+}$ with respect to disproportionation. Furthermore, although a dication salt of $[\mathbf{V\text{-}7}]^{2+}$ has been prepared by chemical oxidation, the cyclic voltammetry of the neutral compound reveals an *irreversible* oxidation process corresponding to the radical cation/dication pair. We theorize that this is as a result of rapid comproportionation between the dication produced at the electrode and the excess neutral material in solution. This is not an uncommon phenomenon[11] and we expect that cyclic voltammetry of a solution of the cation salt would reveal a fully reversible redox peak for the cation/dication pair. Again, this is indicative of the stability of the radical cation oxidation state. This augurs well for the use of this **V-7** in the design of new molecular CT conductors.

A variety of $[\mathbf{V\text{-}7}]^{+}$ salts were prepared both by metathesis from the radical cation chloride and by electro-oxidation of the neutral species in solution. Numerous difficulties including solubility, crystal size, and inherent disorder in the solid state prevented the proper characterization of most of those CT salts prepared.

Black crystalline blocks of [V-7][$AlCl_4$] were obtained from the reaction of [V-7][Cl] with $AlCl_3$ in SO_2 followed by the slow evaporation of the solvent. These were of sufficient quality to obtain a clean infrared spectrum, a good elemental analysis, and the expected 1:2:3:2:1 EPR pattern indicative of coupling to two nitrogens (discussed in greater detail in the following sections). Unfortunately, however, the crystal structure could not be refined beyond a 20% solution. The relative sizes of radical cation and the aluminum tetrachloride counterion are such that the ionic lattice allows two possible orientations of the pseudo-symmetric cations without much difference in energy. Hence, there is an inherent disorder in the ionic lattice. Faced with this dilemma, we explored a variety of other possible counteranions.

Both [V-7][$SbCl_6$] and [V-7][$GaCl_4$] were prepared in a manner similar to the preparation of the tetrachloroaluminate salt. The reaction of [V-7][Cl] with antimony (V) chloride in thionyl chloride yields a floccullent dark green precipitate that, upon isolation, and after several washings, gives a clean infrared spectrum that compares well with the tetrachloroaluminate. Since this method, albeit successful, does not yield crystalline material and requires the initial preparation of antimony (V) chloride, we abandoned it in favour of an initially more promising and less arduous synthetic route. The reaction of [V-7][Cl] with gallium (III) chloride in either thionyl chloride or SO_2 yields green microcrystals of [V-7][$GaCl_4$]. Once again, the infrared analysis of this material compares favourably with that of the previously characterized tetrachloroaluminate. However, the low solubility of either of these products prevents the regrowth of larger crystals suitable for X-ray analysis.

Once we were able to prepare and purify the neutral V-7, a second approach to the synthesis of radical cation salts, involving the reaction of V-7 with nitrosonium salts in SO_2, became available to us; [V-7][X] (X = SbF_6, PF_6, and BF_4) were prepared accordingly as dark, powder-like materials. While the infrared spectrum of each recovered solid compared nicely to that

of the tetrachloroaluminate salt, the products all appeared to be very insoluble and we were unable to obtain crystals of any kind by this method. In the case of [**V-7**][BF_4], we pursued an alternate, and ultimately cleaner, synthetic route from [**V-7**][Cl] and $AgBF_4$ in SO_2. Attempts at recrystallization of this material led only to an irretrievably small amount of microcrystalline material.

The advent of our ability to isolate and purify neutral **V-7** led to a second synthetic option for the production of crystalline radical cation salts. Crystalline CT salts can be grown by electro-oxidation of a saturated solution of **V-7** in the presence of inorganic counterions. The latter are introduced as 0.1 M solutions of their tetra-*n*-butylammonium salts. A variety of solvents and solvent mixtures and a wide range of current densities were explored for several counterions. A summary of the various combinations of solvent system, current density, and anion type is given in **Table 5.1**.

The most promising combinations were *n*-Bu_4NFeCl_4 and *n*-Bu_4NGaCl_4 in 50/50 dichloroethane and carbon disulfide at a current density of 0.5 μA over a period of 25 days. These consistently yielded highly conductive, but very fine, square needles of up to 0.8 cm in length. From elemental analysis, it was determined that this material is a salt with a 3:2 stoichiometry, *i.e.*, [**V-7**]$_3$[$FeCl_4$]$_2$. Our initial interest in the tetrachloroferrate counterion was derived from the suggestion that the interaction between the unpaired π electrons of [**V-7**]$^+$ and the *d* electrons of high-spin iron (III) might lead to interesting ferromagnetic or antiferromagnetic properties.[12] Our inability to grow crystals of sufficient dimensions for X-ray analysis prompted us to focus on the tetrachlorogallate counterion as an alternative. Many of these needles showed good extinction under a polarized light microscope indicating that they were indeed single crystals. A unit cell was obtained by single crystal X-ray diffraction using a CCD detector, however the crystals proved to be too small for sufficient data to be collected in order to solve the crystal structure. Attempts at

obtaining a diffraction pattern by synchrotron radiation were equally fruitless.

While the $[V\text{-}7]_3[GaCl_4]_2$ needles could be grown consistently under the aforementioned conditions, it sometimes occurred that a microcrystalline block phase also appeared to grow on the anode. On one such occasion, a block large enough for single crystal X-ray diffraction was recovered. The solved structure revealed that the crystalline blocks are a 2:1 stoichiometric phase, *i.e.*, $[V\text{-}7]_2[GaCl_4]$. These are significantly less conducting than the 3:2 phase needles.

It is worth mentioning that many of the attempted electrocrystallizations of various salts yielded a microcrystalline material. In the case of *n*-Bu_4NFeCl_4, fine, hair-like needles accompanied by a small number of microcrystalline blocks grew consistently on the anode. While we made several attempts to obtain crystallographic data of these materials, we were unsuccessful for the same reasons as with the tetrachlorogallate salts. Again, we confirmed by elemental analysis that the highly conductive needles are a 3:2 phase and we predict that the blocks are the 2:1 phase.

Table 5.1 Summary[a] of Electrocrystallization of Potential CT Salts based on V-7.

Counteranion	Solvent	Current Density (μA)	Days	Outcome
NO_3^-	$Cl_2CHCHCl_2$	4	4	no growth
ClO_4^-	$Cl_2CHCHCl_2$	3 - 4	3	no growth
BF_4^-	$Cl_2CHCHCl_2$	4	4	no growth
[13] $CoCl_4^-$	$Cl_2CHCHCl_2$	3 - 4	5	microcrystals
ReO_4^-	$Cl_2CHCHCl_2$	3 - 4	5	microcrystals
PF_6^-	$Cl_2CHCHCl_2$	3 - 4	3	microcrystals
$FeCl_4^-$	$Cl_2CHCHCl_2$	4	4	$[t\text{-}BT]_3[FeCl_4]_2$ needle $[t\text{-}BT]_2[FeCl_4]$ block
[14] $GaCl_4^-$	50 / 50 CS_2, $ClCH_2CH_2Cl$	0.500	25	$[t\text{-}BT]_3[GaCl_4]_2$ needle $[t\text{-}BT]_2[GaCl_4]$ block

[a] Only the most promising conditions are tabulated for each counterion.

The selenium-based derivative, [**V-10**][Cl], is generated from the condensation of **V-14** and selenium tetrachloride in refluxing chlorobenzene. As in the case of the sulfur variant, the stable radical cation species is the only oxidation state isolated from this reaction. The dication salt can be prepared from a mixture of the crude [**V-10**][Cl] with excess $AlCl_3$ and $PhICl_2$ heated at gentle reflux in thionyl chloride to give a high yield of [**V-10**][$AlCl_4$]$_2$. The neutral species, **V-10**, is easily obtained by reduction of [**V-10**][Cl] with a half equivalent of triphenylantimony. Furthermore, as in the case of the sulfur-based material, chlorination of the benzene ring on [**V-10**][Cl] occurs upon synthesis and appears to be unavoidable. For both these *trans-* materials, when a deficit of either S_2Cl_2 or $SeCl_4$ is employed, a mixture of the chlorinated material, along with unreacted starting material is recovered.

The larger atomic radius of selenium compared to sulfur may facilitate intermolecular overlap in π-stacked [**V-10**]$^+$ salts in comparison with [**V-7**]$^+$ salts. This may result in better CT conducting properties of these materials, hence our interest in the selenium variants.

In our investigation of CT salts based on the [**V-10**]$^+$ radical cation, we were limited by the insolubility of the neutral **V-10** to metathesis from the radical cation chloride or chemical oxidation of the neutral closed shell species. Electro-oxidation is not a viable option for an insoluble starting material. We prepared [**V-10**][$AlCl_4$] from the radical cation chloride and $AlCl_3$ in CH_2Cl_2 but were unable to purify the solid product. Similarly, we effected a metathesis of the chloride salt with silver tetrafluoroborate in an attempt to generate the [**V-10**][BF_4] salt, but were once again unsuccessful. Our attempts at preparing [**V-10**][SbF_6] from the neutral **V-10** with one equivalent of $NOSbF_6$ in either SO_2 or degassed CH_3CN proved promising according to the infrared spectrum of the green powder-like product. The insolubility of this solid, however, prevented the isolation of any crystalline material.

The preparation of both **V-7** and **V-10** involves the condensation of **V-14** with either S_2Cl_2

or $SeCl_4$, and as previously outlined, the benzene ring is fully chlorinated in the process. By contrast, the reaction of **V-16** with S_2Cl_2 generates almost exclusively the *unchlorinated* [**V-15a**][Cl] with only trace amounts of the monochlorinated and dichlorinated species ([**V-15b**][Cl] and [**V-15c**] respectively). This black solid can be reduced with triphenylantimony to the neutral **V-15a**, which can be recrystallized from toluene as lustrous purple/black needles. **V-15b** and **V-15c** can be obtained in small amount by heating **V-15a** in refluxing S_2Cl_2 for 72 h.

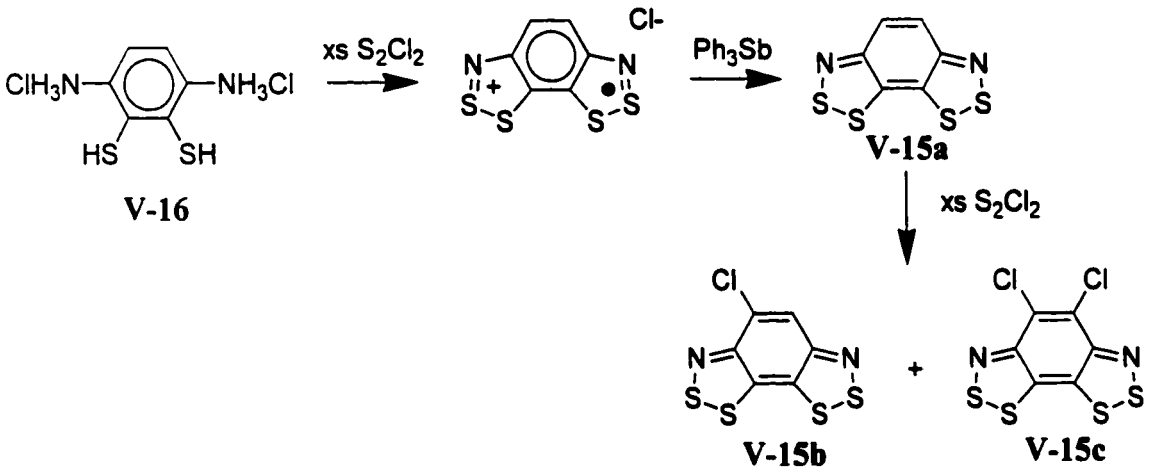

Figure 5.11 Preparative route for **V-15(a-c)**.

It is worth mentioning that, while all the aforementioned benzene-bridged bis(1,2,3-dithiazole) and bis(1,2,3-thiaselenazole) variants are prepared efficiently and relatively cleanly from condensation of a diaminobenzenedithiol with a chalcogen halide, there is a second preparative route to **V-15**. The reaction of *p*-phenylenediamine with excess of S_2Cl_2 followed by the addition of excess pyridine effects a Herz-type ring closure, the product of which is a mixture of **V-15a**, **V-15b**, and **V-15c**. Although this synthetic route is comparatively inefficient and yields a highly contaminated crude material, these three products can be isolated in small amounts by chromatography.

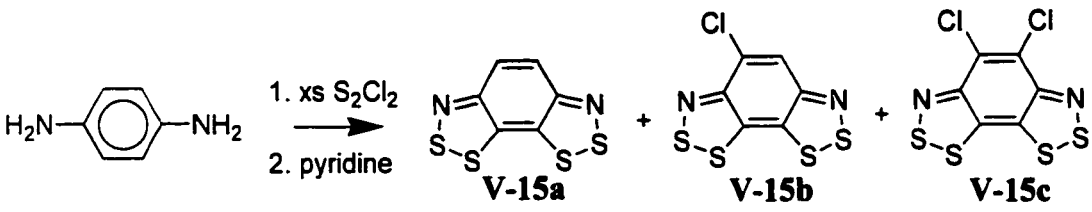

Figure 5.12 Herz-type ring closure leading to the formation of **V-15(a-c)**.

In order to prepare CT salts of **V-15a**, we again performed a comprehensive and systematic study of the electro-oxidation of solutions of **V-15a** in the presence of soluble tetra-*n*-butylammonium salts over a range of current densities and in a variety of solvent systems. To date, the most effective combination is pure 1,2-dichloroethane with currents of 1-5 μA. Both large ($FeCl_4^-$, $GaCl_4^-$) and small (BF_4^-) counteranions fail to deposit any crystalline materials under these conditions. However, electro-oxidation of *cis*-BT in the presence of anions of an intermediate size (ClO_4^-, FSO_3^-) affords well-formed crystals at the anode. Only one morphology (3:2) of the fluorosulfonate salt is observed, i.e., **[V-15a]**$_3$[FSO_3]$_2$. In the case of the perchlorate, however, both a 1:1 and a 3:2 stoichiometry are generated at the anode, *i.e.*, **[V-15a]**[ClO_4] and **[V-15a]**$_3$[ClO_4]$_2$. Under higher current density conditions, these two morphologies often co-crystallize making it impossible to isolate either one. Fortuitously, at lower current density (1-2 μA) it often happens that only one or the other morphology nucleates and grows, thus rendering their individual isolation and characterization possible.

Another member of the fused-ring bis-1,2,3-DTA series of CT salts has been prepared by members of the Oakley group. Electro-oxidation of **V-17** in the presence of *n*-Bu_4NBF_4 affords well-formed crystals of **[V-17]**$_3$[BF_4]$_2$.

5.4 Crystal Structures

5.4.1 Neutral Closed Shell Materials and Closed Shell Dication Salts

The solid state structures of **V-7**, **V-10**, and **V-15a** have been determined by single crystal X-ray diffraction. Suitable crystals of each of these compounds were grown by fractional sublimation *in vacuo*.

V-7 crystallizes in the monoclinic space group $P2_1/c$ while the selenium variant **V-10** belongs to the monoclinic space group $P2_1/n$. This seemingly small change in molecular structure has a significant effect on the packing orientation of the molecules in the solid state. Both molecules lie on a crystallographic center of inversion and both are essentially planar to within 0.02 and 0.06 Å respectively. In both cases the packing pattern can be described as slipped π-stacks of the planar molecules with cell repeats along the stacking axis of 3.8496(10) and 3.9733(17) Å respectively. The orientation of these slipped stacks is quite different in these two structures. In **V-7**, adjacent molecules approach one another in a side-on manner such that there is an alternation in the orientation of the long axes of the molecules in adjacent rows. In **V-10**, the adjacent molecules are packed in a more or less head-on fashion such that the long axes of all the molecules are oriented in the same direction.

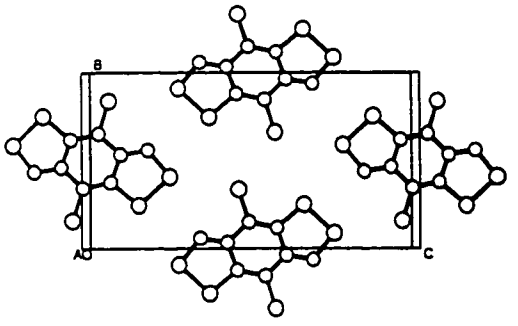

Figure 5.13 Crystal structure of **V-7**.

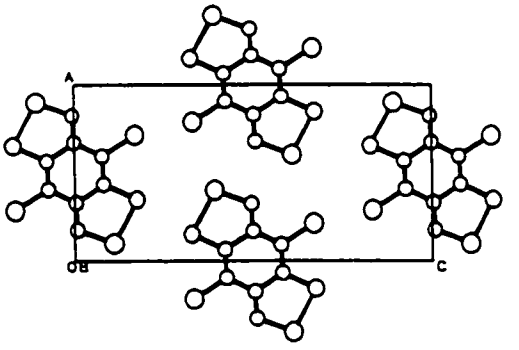

Figure 5.14 Crystal structure of **V-10**.

In accord with **V-7** and **V-10**, **V-15a** crystallizes in the monoclinic space group $P2_1/c$. The molecules are packed in a slipped π-stack arrangement with a cell repeat in the stacking direction of 3.9033(8) Å.

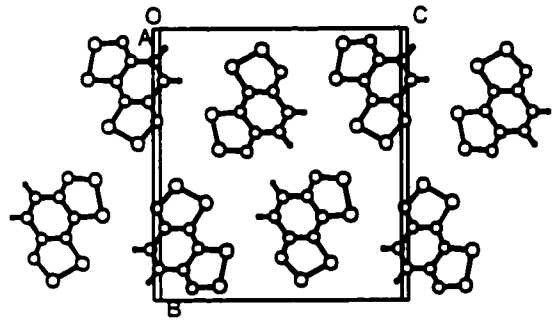

Figure 5.15 Crystal structure of **V-15a**.

According to *ab initio* calculations presented herein, the ground states of **V-7**, **V-10**, and **V-15** are all closed shell with some quinoid character. In addition, solutions of these compounds are all ESR silent. In agreement with these facts, the solid state intramolecular distances for all three are consistent with a closed shell quinoid formulation. These compounds, however, are all expected to have low lying triplet excited states in which the central benzene can be described as having more aromatic character than quinoid. Thus, it is not surprising that the C-C bond variation observed in the solid state is not as pronounced as it is in, for example, *p*-benzoquinone-*N,N'*-bis(methylsulfonyldiimine) (**V-18**). In fact the pattern is very similar to that observed for 1,4-phenylene bridged bis(1,3,2,4-dithiadiazolyl) (**V-19**) which is reported to exist in the solid state as an associated diradical.

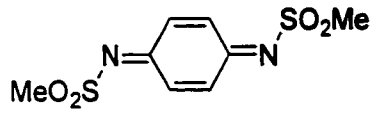

V-18

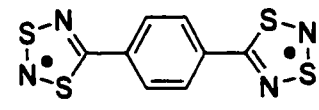

V-19

Figure 5.16 *p*-Benzoquinone-*N,N'*-bis(methylsulfouldiimine) **V-18** and **V-19**.

The solid state structures for the dicationic [**V-7**][$AlCl_4$]$_2$ and [**V-10**][$AlCl_4$]$_2$ have been determined by single crystal X-ray diffraction. Suitable crystals of these compounds were grown as dark red/green plates and lustrous black blocks respectively from the addition of an SO_2 solution of excess $AlCl_3$ and crude dication tetrachloroaluminate salt to neat $SOCl_2$.

The sulfur variant, [**V-7**][$AlCl_4$]$_2$, crystallizes in the triclinic space group $P\bar{1}$ while [**V-10**][$AlCl_4$]$_2$ adopts the monoclinic space group $P2_1/c$. The bond lengths of the central benzene ring and the heterocycles for both dications are considerably different from those of the respective neutral species. The bonds (N)C-C(Cl) and (S)C-C(Cl) are more or less equivalent and are therefore no longer in accord with a quinoid formulation. Furthermore, the N-C bond distance lengthens considerably upon oxidation to the dication (from 1.306(3) to 1.349(6) Å for the [**V-7**][$AlCl_4$]$_2$) confirming the loss of quinoid character. A comparison of the S-S, S-N, and N-C bond distances in [**V-7**][$AlCl_4$]$_2$ to those observed in the solid state for a simple benzo-1,2,3-dithiazolylium salt shows them to be very similar.[15]

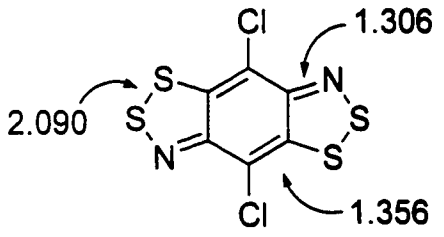

V-7

Figure 5.17 Bond lengths (Å) of [**V-7**] as determined from the crystal structure.

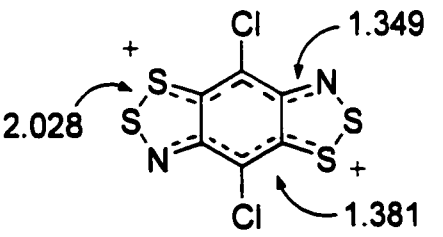

[V-7]$^{2+}$

Figure 5.18 Bond lengths (Å) of [**V-7**][$AlCl_4$]$_2$ as determined from the crystal structure.

5.4.2 CT Salts

There are three observed morphologies in this series of fused-ring bis(1,2,3-dithiazole) CT salts. The initial synthesis of each of the species covered in this chapter produces a radical cation chloride salt with a 1:1 stoichiometry. Metathesis from this chloride salt to other salts does not alter the cation/anion ratio. Furthermore, chemical oxidation from the neutral species in all cases yields the same 1:1 morphology. None of these chemically prepared salts have been characterized crystallographically. However, electro-oxidation of **V-15a** in the presence of the perchlorate anion produces a salt with a 1:1 stoichiometry, *i.e.*, [**V-15a**][ClO_4], as crystals suitable for analysis by single crystal X-ray diffraction. In addition, this same electro-oxidation produces crystals of the 3:2 salt, *i.e.*, [**V-15a**]$_3$[ClO_4]$_2$. This morphology is also observed for [**V-15a**]$_3$[FSO_3]$_2$, [**V-7**]$_3$[$GaCl_4$]$_2$, and [**V-17**]$_3$[BF_4]$_2$. Finally, a 2:1 morphology reminiscent of those seen in Beechgard and ET salts is observed for [**V-7**]$_2$[$GaCl_4$].

The 1:1 morphology is characterized by a simple ionic packing arrangement involving alternating cations and anions and affording few intermolecular cation/cation contacts. The metallic green blocks of [**V-15a**][ClO_4] belong to the orthorhombic space group *Pcab* and consist of layer of tilted [**V-15a**] radical cations interspersed by layers of perchlorate anions. This arrangement cannot be expected to display high conductivity in the bulk crystalline material given that the shortest intermolecular S···S distance is 3.740 Å, well outside the van der Waals distance (3.6 Å) for two sulfurs. Comparing the bond lengths for neutral **V-15a** with the radical cation, it is observed that the S-S, S-N, and S-C bonds are shortened, and the N-C bonds are lengthened by the one electron oxidation. As expected, the degree to which the bond distances change is approximately half as much as that observed for the two-electron oxidation of **V-7** to [**V-7**][$AlCl_4$]$_2$.

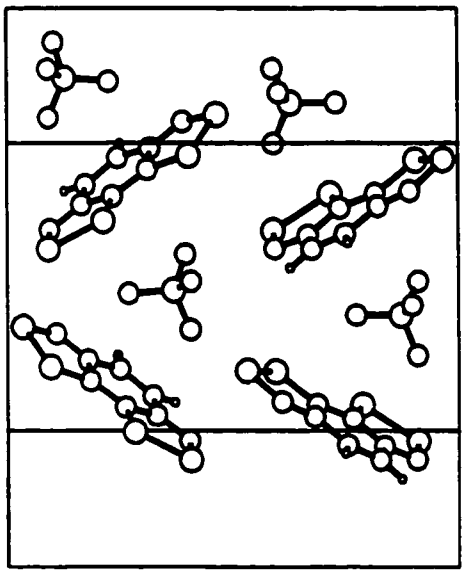

Figure 5.19 Crystal structure of [**V-15a**][ClO_4].

In the 1:1 morphology, a full unit of positive charge resides on each [**V-15a**]$^{+}$ molecule. Likewise, a formal approach to the 3:2 stoichiometry would suggest the presence of $^{2}/_{3}$+ charge per heterocyclic ring. However, comparing the intramolecular distances in [**V-15a**]$_3$[ClO_4]$_2$ and [**V-15a**]$_3$[FSO_3]$_2$ with those found in **V-15a** and [**V-15a**][ClO_4], we are led to draw a different conclusion. It appears that within the triple-decker slipped π-stack [**V-15a**]$_3^{2+}$ unit, of which these 3:2 morphologies are both comprised, there are two molecules that are nominally oxidized to the radical cation level with one full unit of charge and one molecule that is formally chargeless. The two radical cations associate into a dimeric unit with the shortest interannular S···S contacts at 3.272(4) Å in [**V-15a**][ClO_4] and 3.208(3) Å in [**V-15a**]$_3$[FSO_3]$_2$.

Although these 3:2 salts share a common building block at a molecular level, their crystal morphologies are quite different signaling considerable differences in their solid state structures. Lustrous purple plates are observed for the 3:2 perchlorate salt, which belongs to the monoclinic space group $P2_1/c$. The asymmetric unit consists of the three approximately coplanar **V-15a**

molecules that comprise the $[\mathbf{V\text{-}15a}]_3^{2+}$ triple-decker unit, and two ClO_4^- anions, one of which is disordered. By contrast, the 3:2 fluorosulfate salt forms purple needles and belongs to the monoclinic space group *C*2/*c*. Thus the asymmetric unit of the fluorosulfate salt is comprised of only half the triple-decker chemical building block. It contains one of the radical cations and half of the neutral **V-15a**, which sits on a crystallographic 2-fold rotation axis. Accordingly, there is only one disordered FSO_3^- ion per asymmetric unit.

In both of these 3:2 salts, the triple-decker units are arranged into ribbons with the ClO_4^- or FSO_3^- anions interspersed between them. When viewed side-on, these ribbons reveal a slipped π-stack molecular ordering. Essentially, it is the degree of slippage between adjacent levels in these ribbons that determines the crystallographic differences between the two structures. In $[\mathbf{V\text{-}15a}]_3[FSO_3]_2$, the slippage between the neutral layer and the radical cation dimer layers within each trimer is identical to the translation of successive layers, defined by the 2-fold axis through the neutral **V-15a**. The slippage observed in $[\mathbf{V\text{-}15a}]_3[ClO_4]_2$ is more pronounced such that the trimers are almost completely out of register.

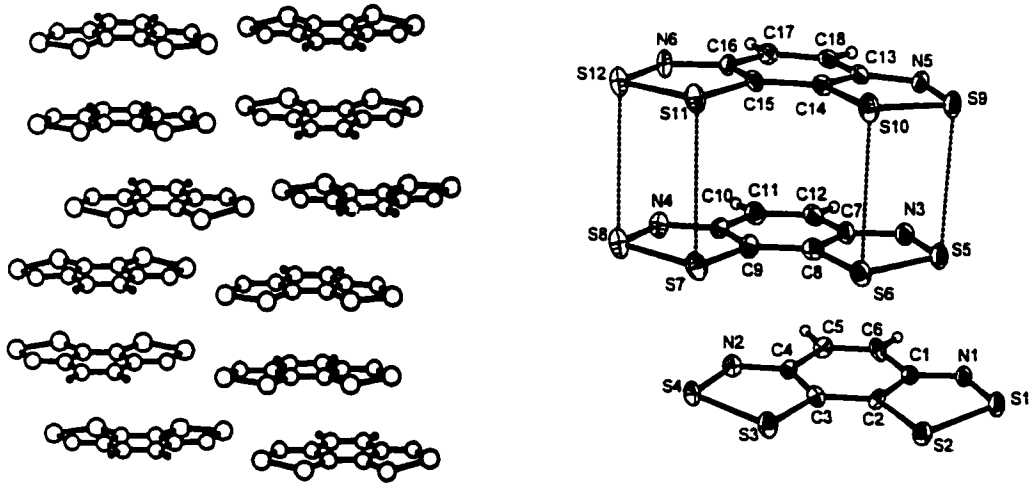

Figure 5.20 Crystal structure of $[\mathbf{V\text{-}15a}]_3[ClO_4]_2$, anions not shown.

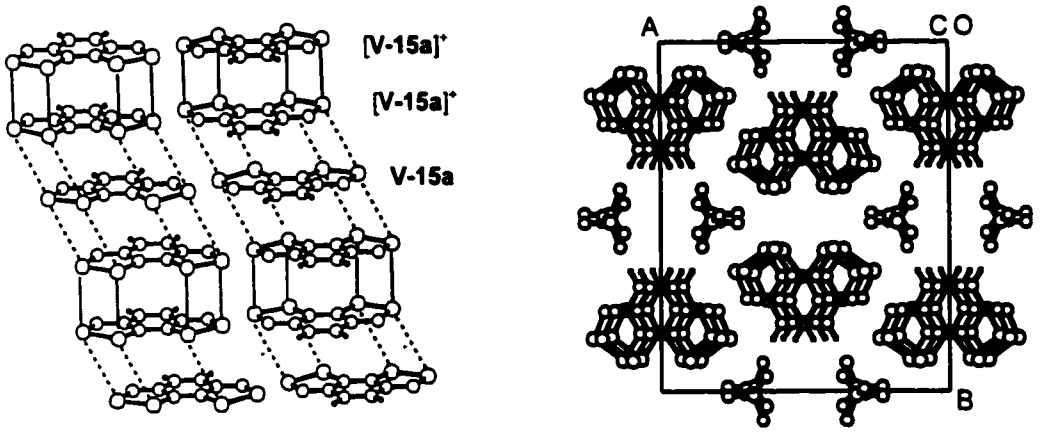

Figure 5.21 Crystal structure of $[\mathbf{V\text{-}15a}]_3[FSO_3]_2$, anions not shown in lateral view.

The triple-decker chemical building blocks observed in these two salts is not unique to **V-15a**. Similar units have been identified in the solid state for $[\mathbf{V\text{-}17}]_3[BF_4]_2$ as well as other thiazyl radical ion dimers and mixed valence trimers.[16] As the crystal structure of $[\mathbf{V\text{-}7}]_3[GaCl_4]_2$ has not been determined, it is not known whether it, too, is defined by such trimer units. The fine hair-like structure of the crystals and the notably high conductivity of this material suggest that there may be less lateral translation between the presumably π-stacked molecules than is observed in any of the previous 3:2 salts. This predicts a less rigidly defined trimer unit. The high conductivity arises from a more even intermolecular spacing such that there are no longer distinct radical cation dimers and neutral molecules observable, *i.e.*, each molecule may take on some degree of charge and open-shell-edness.

A third morphology, 2:1, is observed for the block-like crystals of $[\mathbf{V\text{-}7}]_2[GaCl_4]$ belonging to the monoclinic space group *C*2/*c*. While this stoichiometry is often observed in Bechgaard salts, it is unprecedented in binary or heterocyclic sulfur nitrogen chemistry. The crystal structure consists of $[\mathbf{V\text{-}7}]_2^{+\cdot}$ units, *i.e.*, ***open-shell dimeric cations***, in a slipped π-stack arrangement

interspersed by the $GaCl_4^-$ anions located on a 2-fold rotation axis of the lattice. Within the dimeric radical cation unit, the S-S and S-N bond distances are comparatively shorter than those of the parent molecule **V-7**. However, these bond lengths are still greater than those observed in the isolated or dimerized radical cation **[V-15a]**$^+$. In addition, the C-C bond alternation attributed to a quinoid formulation is observed in $[\mathbf{V\text{-}7}]_2^{+\cdot}$ whereas it is entirely lost in the **[V-15a]**$^+$, $[\mathbf{V\text{-}15a}^+]_2$, and $[\mathbf{V\text{-}17}^+]_2$ units.

Each molecule in the dimer $[\mathbf{V\text{-}7}]_2^{+\cdot}$ unit is essentially planar to within 0.03 Å. The two planes are separated by 3.421 Å and there are intradimer S···S contacts (3.616(2) and 3.570(3) Å) that are close to the van der Waals separation. Slight slippage of the two halves of the dimer is observed, presumably to relieve interannular Cl···Cl contacts (3.554(2) Å).

The slipped stacks are arranged such that the molecular planes in one stack are nearly perpendicular to those of neighboring stacks. Within the stacks, each dimer interacts with a single neighbor on either side through an S···N′ contact of 3.148(4) Å. The distance between dimer units within a stack is 3.468 Å, which is not far off that of the interplanar separation within the dimer units themselves. The relatively low conductivity of this material can be explained by the slippage between consecutive layers within a stack. Thus there are no close interlayer S···S or S···N contacts resulting in weak electronic communication along the π-stack.

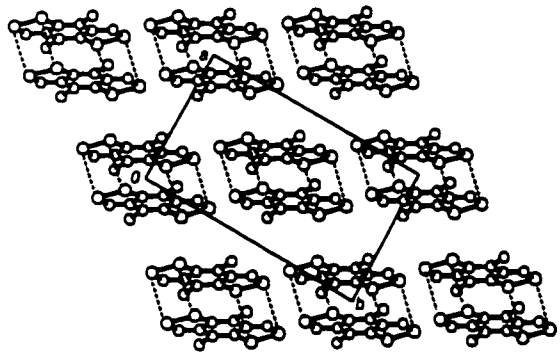

Figure 5.22 Crystal structure of $[\mathbf{V\text{-}7}]_2[GaCl_4]$, anions not shown.

5.5 Cyclic Voltammetry

Cyclic voltammetry measurements on a solution of **V-7** in CH_3CN (with Pt electrodes and 0.1 M *n*-Bu_4NPF_6 as supporting electrolyte, ref. SCE) reveal a reversible oxidation process at $E_{1/2}(ox) = 0.93$ V. This corresponds to the **V-7**/[**V-7**]$^+$ pair. A second irreversible anodic wave at $E_{pa} = 1.5$ V for the [**V-7**]$^+$/[**V-7**]$^{2+}$ couple is also observed along with a broad and strongly irreversible wave with a cathodic peak potential $E_{pc} = -0.95$ V. As previously outlined, it is suspected that the irreversibility of the second anodic wave is primarily due to rapid comproportionation between excess **V-7** present in solution and [**V-7**]$^{2+}$ produced at the anode. Variations in the voltage sweep rate and the substrate concentration failed to suppress the irreversibility of this peak. It is likely that cyclic voltammetry of a solution of the [**V-7**]$^+$ radical cation would reveal a reversible anodic wave for the [**V-7**]$^+$/[**V-7**]$^{2+}$ couple. This would require the generation of a radical cation salt of higher solubility than we have seen to date.

Both **V-15a** and **V-15c** yield the expected cyclic voltammograms. Acetonitrile solutions of either compound (Pt electrodes and 0.1 M *n*-Bu_4NPF_6 as a supporting electrolyte, ref. SCE) reveal two reversible oxidation waves, corresponding to the 0/+ and the +/++ pairs respectively, and a single irreversible reduction wave. The first and second oxidation half-cell potentials are for both **V-15a** ($E_{1/2} = 0.61$ and 1.10 V) and **V-15c** ($E_{1/2} = 0.81$ and 1.37 V) are less anodic than those of **V-7**. **Table 5.2** shows a comparative summary the redox potentials of **V-15a**, **V-15c**, **V-7**, **V-17** and **V-2a**. There is a noticeable trend toward more anodic oxidation potentials upon chlorination and with a decrease in the overall size, and therefore the extent of delocalization within the heterocyclic molecule. Also included in **Table 5.2** are visible absorption maxima (λ_{max} values) of the various compounds. Although the trends are a little less obvious here, increasing the amount of delocalization by adding another aromatic ring (as in **V-17**) lowers the excitation energy as can be expected.

Table 5.2 Redox Potentials[a] and Visible Absorption Maxima[b] for Bis(1,2,3-DTA)s.

Compound	V-17	V-15a	V-2a	V-15c	V-7
$E_{1/2}^{(0/+)}$	0.41	0.61	0.80	0.81	0.93
$E_{1/2}^{(+/++)}$	0.66	1.10	1.25	1.37	1.5 [c]
ΔE	0.25	0.49	0.45	0.56	0.57
$E_{pc}^{(0/-)}$	-1.06	-0.98	-1.11	-0.96	-0.95
λ_{max}	622	572	565	600	525

[a] Volts vs SCE, in CH_3CN. [b] Nanometers, in CH_2Cl_2 or $C_2H_4Cl_2$. [c] The anodic peak potential E_{pa} is cited for this irreversible reduction.

5.6 Electron Paramagnetic Resonance

Solutions of **V-7**, **V-10**, **V-15a** and **V-15c** are EPR inactive. This is in agreement with the predicted closed-shell quinoid formulation for the ground state. The radical cations of all four compounds have been characterized by EPR spectroscopy. In all cases, the EPR spectrum consists of a strong 1:2:3:2:1 pentet characteristic of hyperfine coupling to two equivalent nitrogens. This indicates that the unpaired electron is fully delocalized over both terminal heterocyclic rings.

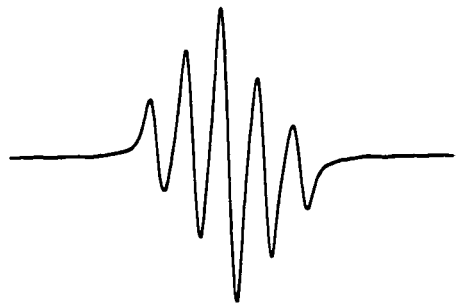

Figure 5.23 EPR spectrum of [**V-7**][$AlCl_4$]. An example of the 1:2:3:2:1 pentet universally observed for fused-ring bis(1,2,3-DTA)s.

The hyperfine coupling constants at nitrogen (a_N) and the *g*-values for these four compounds and for [**V-2a**]$^+$ and [**V-17**]$^+$ are listed in **Table 5.3**. Some general trends can be discerned from this data. The a_N constants for the dithiazole compounds, on the whole, are

approximately one-half the values of those observed in simple monofunctional 1,2,3-DTAs.[17] This can be understood by considering that the spin delocalization covers two DTA rings rather than one. Meanwhile, there is a significant increase in the a_N value for the selenium isomer. This can be attributed to the previously observed tendency of selenium (relative to sulfur) to partition spin density more heavily onto a neighboring nitrogen.[18]

Further trends concerning the *g*-values can be deduced. There is a consistent shift toward larger *g*-values in the bis(1,2,3-DTA)s compared to the simple monofunctional benzo-1,2,3-dithiazolyl ($g = 2.008$)[4], for example. This can be attributed to the larger cumulative effect of spin-orbit coupling to four sulfur atoms as opposed to two in the simple 1,2,3-DTAs. This increase in *g*-value is larger still for the selenium-based **[V-10]**$^+$ as can be expected from the inclusion of a heavier chalcogen.

Table 5.3 ESR Data for Bis(1,2,3-DTA)s.

Compound	**[V-2a]**$^+$	**[V-15a]**$^+$	**[V-15c]**$^+$	**[V-7]**$^+$	**[V-17]**$^+$	**[V-10]**$^+$
a_N [a]	0.096	0.161	0.143	0.201	0.235	0.44
g-value	2.0117	2.0117	2.0117	2.0114	2.0106	2.0211

[a] In millitesla, for radical cation.

5.7 Conductivity Measurements

Room temperature pressed pellet conductivity measurements for the 1:1 salt **[V-15a]**$[ClO_4]$ are in the order of 10^{-5} S cm^{-1}. This low conductivity is consistent with the ionic packing in which close intermolecular interactions between neighboring cations is noticeably absent. The result is a narrow bandwidth for the associated, formally half-filled energy band and the material behaves as a Mott insulator.

In the case of the two 3:2 salts for which X-ray structural analysis has been achieved, **[V-**

15a]$_3$[ClO_4]$_2$ and [**V-15a**]$_3$[FSO_3]$_2$, it is observed that the building blocks in the solid state consist of a closed shell dimer of radical cations and a neutral closed-shell molecule. This being so, these materials are expected to behave as small band gap semiconductors.[19] In accordance with this prediction, both [**V-15a**]$_3$[ClO_4]$_2$ and [**V-15a**]$_3$[FSO_3]$_2$ have pressed pellet conductivity measurements in the order of 10^{-2} S cm^{-1} at room temperature. A similar value is exhibited by the analogous [**V-17**]$_3$[BF_4]$_2$ salt.

Conductivities of [**V-7**]$_3$[X]$_2$ (X = $FeCl_4^-$, $GaCl_4^-$) and [**V-7**]$_2$[$GaCl_4$] have been measured. Of these, only the latter has been structurally determined in the crystal state. The lack of close contacts between consecutive layers within the stacks of radical cation dimers forecasts low conductivity measurements for this solid state material. Indeed, the pressed pellet conductivity of [**V-7**]$_2$[$GaCl_4$] is on the order of 10^{-4} S cm^{-1} at room temperature. By contrast, the 3:2 phases, for which the crystal structures have not been determined, show a remarkably high conductivity at room temperature (pressed pellet $\sigma_{RT} > 10$ S cm^{-1}).

To summarize Chapter 5, a series of ring-fused benzo-bis(1,2,3-DTA)s with closed shell quinoid-like ground states were prepared and isolated from the reaction of a diaminodithiolbenzene with sulfur monochloride, followed by the reduction of the product radical cation chloride with triphenylantimony. Compounds **V-7** and **V-15a**, as well as the selenium analog **V-10**, were characterized by X-ray crystallography. A variety of salts based on the stable radical cation oxidation states of these compounds have been grown by electrocrystallization. Ionic ratios of 1:1, 2:1, and 3:2 have been observed in the crystal structures of the various salts, and pressed pellet conductivities from 10^{-5} S cm^{-1} to greater than 10^{1} S cm^{-1} have been observed.

5.8 Syntheses

Selenium tetrachloride,[20] iodobenzene dichloride,[21] 1,4-diaminobenzene-2,5-dithiol dihydrochloride,[22] and 1,4-diamino-2,3-dithiol dihydrochloride[8,9] were prepared according to literature procedures.

5.8.1 Synthesis of 1,4-phenylene-bis(thiourea), V-11: 1,4-Phenylenediamine (35.42 g, 327.5 mmol) was purified with 2.3 g activated charcoal in 365 mL of 2 M $HCl_{(aq)}$ at 50 °C. The charcoal was removed by filtration and ammonium thiocyanate (100 g, 1.31 mol) was added to the remaining solution. This mixture was refluxed, under inert atmosphere, for 20 h. Upon cooling to RT, the off-white, powdery product was collected by filtration and washed with methanol. It was then dried, *in vacuo*, warmed in an oil bath at 90 °C, for 18 h; yield 64.3 g (284 mmol, 87 %)

5.8.2 Synthesis of V-12: Under an inert atmosphere, bromine (108.9 g, 679.6 mmol) in 50 mL of dry $CHCl_3$ was added, dropwise, to a slurry of **V-11** (64.3 g, 284 mmol) in 250 mL of dry $CHCl_3$, on ice. The resulting orange slurry was stirred mechanically until the solid product formed a large ball. The reaction mixture was allowed to stand for 2 h, until the solid product become porous enough to be broken up into a powder. This slurry was stirred for another 48 h at RT and then refluxed gently for 10 h. The orange powder was collected by filtration, washed with 125 mL of chloroform, and dried in air. It was then stirred with $NaHSO_3$ (42.9 g, 412 mmol) in 325 mL of H_2O. The resulting yellow powder was collected by filtration, washed with 100 mL of conc. $NH_4OH_{(aq)}$ followed by 200 mL of H_2O. The product was recrystallized twice from hot glacial acetic acid (2500 mL followed by 1000 mL), then dried *in vacuo*, at 85 °C, for 18 h; yield 11.74 g (52.81 mmol, 19 %).

5.8.3 Synthesis of 1,4-diaminobenzene-2,5-dithiol dihydrochloride,[22] V-14: **V-12** (11.74 g, 52.81 mmol) was added to KOH (41.01 g, 730.9 mmol) in 50 mL of degassed H_2O, under inert atmosphere. The reaction mixture was refluxed for 5 h. The green solution was cooled to 5 °C for 3 h. The resulting pale yellow potassium salt (**V-13**) was collected by filtration and re-dissolved in 50 mL of degassed H_2O. To this solution, 180 mL of degassed 6 M HCl was added. The solid, yellow product precipitated from this solution upon stirring for 18 h. This was collected by filtration; crude yield 9.85 g (36.5 mmol, 69 %). The product was recrystallized three times by stirring 5 g with 200 mL of H_2O and 8 mL of HCl until it had dissolved completely, then adding 70 mL conc. HCl and letting the mixture sit for 18 h, yielding small yellow crystals. IR: 2566 (m), 2452 (m), 1570 (s), 1526 (s), 1292 (m), 1132 (w), 1115 (w), 1106 (w), 960 (m), 885 (s), 773 (w), 720 (m), 597 (w), 535 (m), 433 (s) cm^{-1}. Anal. Calcd. for $C_6H_{10}Cl_2N_2S_2$: C, 29.39; H, 4.11; N, 11.43; Cl, 28.92 %. Found: C, 29.58; H, 4.36; N, 11.38; Cl, 29.26 %.

5.8.4 Synthesis of 3,6-dichlorobenzo[1,2-*d*:4,5-*d'*]bis(1,2,3dithiazolylium) chloride, [V-7][Cl]: A mixture of **V-14** (3.006 g, 12.26 mmol) and neat sulfur monochloride (approx. 50 mL) was heated slowly up to reflux for 14 h. Upon cooling to RT, the black precipitate of crude [V-7][Cl] was collected by filtration, washed 3 x 20 mL chlorobenzene, and dried *in vacuo*; yield 3.78 g, (11.3 mmol, 92 %); IR: 1614 (w), 1517 (w), 1434 (s), 1405 (s), 1336 (w), 1314 (w), 1290 (w), 1163 (s), 1041 (m), 840 (m), 809 (s), 708 (s), 658 (m), 545 (m), 492 (s) cm^{-1}.

5.8.5 Synthesis of 3,6-dichlorobenzo[1,2-*d*:4,5-*d'*]bis(1,2,3dithiazole), V-7: The crude [V-7][Cl] (2.5 g, 7.5 mmol) was heated to reflux in 150 mL of dry acetonitrile with excess triphenylantimony (5.4 g, 15 mmol), for 18 h. A black solid was filtered off and crystallized from 200 mL chlorobenzene to give purple/black microcrystals of **V-7**; yield 1.3 g, (4.5 mmol, 59 %);

further purification by gradient sublimation over the temperature range 150-80 °C/10^{-3} Torr afforded lustrous black needles, dec > 290 °C. IR: 1495 (s), 1287 (w), 1152 (s), 959 (w), 785 (w), 777 (vs), 706 (s), 646 (m), 541 (w), 476 (w) cm^{-1}. UV/Vis ($CHCl_3$): λ_{max} (ϵ) = 522 (4 x 10^4) nm; MS (*m/e*): 298 (M^+, 100 %), 263 ([M-Cl]$^+$, 9 %), 228 ([M-2Cl]$^+$, 4 %). Anal. Calcd. for $C_6Cl_2N_2S_4$: C, 24.08; H, 0.0; N, 9.36 %. Found: C, 23.99; H, 0.0; N, 9.16 %.

5.8.6 Synthesis of 3,6-dichlorobenzo[1,2-*d*:4,5-*d'*]bis(1,2,3dithiazolylium) tetrachloroaluminate, [V-7][$AlCl_4$]: SO_2(l) was condensed onto crude [V-7][Cl] (1.41 g, 3.42 mmol) and $AlCl_3$ (0.603 g, 4.45 mmol) and the brown mixture was stirred in one arm of a sealed H-cell for 30 m. The resulting black precipitate was isolated by filtration and back-washed with 3 x 5 mL SO_2(l). The crude product was retrieved (1.16 g) and extracted with SO_2(l) using a sealed Soxhlet extractor;[23] yield 0.39 g, (0.80 mmol, 23 % based on crude [V-7][Cl]); a small amount of black block-shaped crystalline material was obtained by slow evaporation of a saturated solution in SO_2(l). IR: 1435 (s), 1405 (s), 1318 (w), 1299 (w), 1170 (s), 817 (s), 737 (m), 661 (m), 553 (w), 491 (br, vs) cm^{-1}. Anal. Calcd. for $C_6Cl_6AlN_2S_4$: C, 15.40; H, 0.0; N, 5.99 %. Found: C, 15.60; H, 0.0; N, 5.78 %.

5.8.7 Electrosynthesis of [3,6-dichlorobenzo[1,2-*d*:4,5-*d'*]bis(1,2,3dithiazolylium)]$_2$ tetrachlorogallate, [V-7]$_2$[$GaCl_4$], and [3,6-dichlorobenzo[1,2-*d*:4,5-*d'*]bis(1,2,3dithiazolylium)]$_3$ [tetrachlorogallate]$_2$, [V-7]$_3$[$GaCl_4$]$_2$: A saturated solution of **V-7** in dichloroethane was oxidized at a Pt wire anode with a current in the range of 0.2 to 2 μA in the presence of 0.1 M *n*-Bu_4NGaCl_4. A mass of long, fine hair-like gold crystals of [V-7]$_3$[$GaCl_4$]$_2$ grew outward from the shaft of the anode; pressed pellet σ_{RT} > 10 S cm^{-1}. A small number of crystalline black blocks of [V-7]$_2$[$GaCl_4$] also grew on the tip of the electrode; pressed pellet σ_{RT} = 10^{-4} S cm^{-1}. Fine, hair-like

crystals of $[V\text{-}7]_3[FeCl_4]_2$ were grown in the same manner using Bu_4NFeCl_4 as the electrolyte; Anal. Cald. for $C_{18}Cl_{14}Fe_2N_6S_{12}$: C, 16.72; H, 0.0; N, 6.50 %. Found: C, 17.12; H, 0.0; N, 6.88%.

5.8.8 Synthesis of 3,6-dichlorobenzo[1,2-*d*:4,5-*d'*]bis(1,2,3dithiazolium) di(tetrachloro-aluminate), [V-7][$AlCl_4$]$_2$: Crude [V-7][Cl] (0.334 g, 1.00 mmol), excess $AlCl_3$ (0.533 g, 4.00 mmol), and $PhICl_2$ (0.277 g, 1.00 mmol) were slurried together and heated to gentle reflux under N_2 in 20 mL of $SOCl_2$ for 16 h. Upon cooling to RT, the crude [V-7][$AlCl_4$] was isolated by filtration as a green precipitate. This material was washed with $SOCl_2$ and dried *in vacuo*; yield 0.52 g (0.82 mmol, 82 % based on crude [V-7][Cl]). Crystals suitable for structural determination by X-ray diffraction were obtained by adding $AlCl_3$ to a slurry of crude [V-7][$AlCl_4$] in SO_2(l) in one arm of an H-cell. The resulting green solution was filtered to the other arm, which contained neat $SOCl_2$. Dark red/green plates grew on standing; dec > 300 °C. IR: 1340 (w), 1293 (s), 1194 (m), 858 (m), 842 (m), 751 (w), 669 (w), 562 (w), 521 (w), 500 (vs), 467 (s) cm^{-1}. Anal. Calcd. for $C_6Cl_{10}Al_2N_2S_4$: C, 11.32; N, 4.40 %. Found: C, 11.22; N, 3.92 %.

5.8.9 Synthesis of 3,6-dichlorobenzo[1,2-*d*:4,5-*d'*]bis(1,2,3-thiaselenazole), V-10: V-14 (1.00 g, 4.08 mmol) and selenium tetrachloride (2.20 g, 9.96 mmol) were heated together in refluxing chlorobenzene (40 mL) for 18 h. Upon cooling to RT, the crude [V-10][Cl] was collected by filtration, washed with 3 x 20 mL chlorobenzene and dried *in vacuo*. This material was reduced with excess triphenylantimony (1.00 g, 2.80 mmol) in acetonitrile at reflux for 30 m. The resulting black solid was filtered off and extracted with 3 x 500 mL of hot benzonitrile. The combined extracts were concentrated and cooled to afford golden green microcrystals; yield 0.75 g (1.9 mmol, 49 %). Crystals suitable for X-ray analysis were grown as green gold blocks by gradient sublimation over the temperature range 190 - 100 °C/10^{-3} Torr; mp 289 °C. IR: 1486 (m), 1280

(w), 933 (w), 792 (w), 763 (m), 700 (w), 650 (w), 623 (vs), 499 (w) cm^{-1}. UV/Vis ($CHCl_3$): λ_{max} (ϵ) = 536 (4 x 10^4) nm. MS (*m/e*): 394 (M^+, 100 %), 346 ([M-CCl]$^+$, 90 %), 298 ([M-SeN]$^+$, 26 %) Anal. Calcd. for $C_6Cl_2N_2S_2Se_2$: C, 18.34; N, 7.13 %. Found: C, 18.54; N, 7.39 %.

5.8.10 Synthesis of 3,6-dichlorobenzo[1,2-*d*:4,5-*d'*]bis(1,2,3-thiaselenazolium) di(tetrachloroaluminate), [V-10][$AlCl_4$]$_2$: Crude [V-10][Cl] (0.312 g, 0.729 mmol) was refluxed in 20 mL $SOCl_2$ in the presence of excess $AlCl_3$ (0.508g, 3.82 mmol) for 18 h. Crude [V-10][$AlCl_4$]$_2$ was recovered by filtration as a black solid and dried *in vacuo*; yield 0.306 g (0.419 mmol, 58 % based of crude [V-10][Cl]). Crystals suitable for analytical and X-ray analysis were grown by adding $AlCl_3$ to a slurry of crude [V-10][$AlCl_4$]$_2$ in SO_2(l) in one arm of an H-cell. The resulting green solution was then transferred to the other arm, which contained neat $SOCl_2$. Lustrous black blocks grew upon standing; dec > 300 °C. IR: 1325(w), 1297 (s), 1187 (m), 792 (s), 667 (w), 493 (br, vs), 426 (w) cm^{-1}. Anal. Calcd. for $C_6Cl_{10}Al_2N_2S_2Se_2$: C, 9.86; N, 3.83 %. Found: C, 9.73; N, 3.56 %.

5.8.11 Reaction of *p*-phenylenediamine with S_2Cl_2: A mixture of *p*-phenylenediamine (2.06 g, 19.0 mmol) and excess S_2Cl_2 (12 mL) in 100 mL of CH_2Cl_2 was stirred at RT for 18 h. Excess pyridine (20 mL) was then added and the mixture was again stirred at RT for 24 h. The resulting dark brown precipitate was collected by filtration, washed with 2 x 100 mL of CH_2Cl_2, then 2 x 100 mL CH_3CN, and dried *in vacuo*. The solid was extracted three times with 200 mL of 10 % ethanol in CH_2Cl_2. The solvent was removed from the combined extracts affording a dark semisolid that was then dissolved in 100 mL of CH_2Cl_2 and filtered through a small (50 mL) plug of silica. Analysis of the purple filtrate by TLC (SiO_2, CH_2Cl_2) revealed a purple (R_f = 0.65) and two almost coincident blue components (R_f = 0.69 and 0.70). Column chromatography (SiO_2, 3:1

hexane:$CHCl_3$) successfully isolated the purple material (75 mg) which was characterized as **V-15a** (see below for full characterization). The two blue materials (combined weight 40 mg) could not be completely separated by chromatography, however fractions enriched in one or the other component were evaporated and analyzed by mass spectrometry which indicated the presence of both **V-15b** (R_f = 0.70) and **V-15c** (R_f = 0.69). Pure **V-15c** was obtained by fractional sublimation at 120 - 90 °C/10^{-2} Torr followed by recrystallization from hot toluene as bronze blocks; mp 248 - 251 °C. IR: 1500(w), 1410 (w), 1151 (s), 1029 (m), 783 (vs), 738 (m), 663 (vs), 635 (m), 583 (w), 509 (s) cm^{-1}. UV/Vis ($C_2H_4Cl_2$): λ_{max} (log ϵ) = 600 (4.1), 346 (4.4) nm. MS (*m/e*): 298 (M^+, 100 %) Anal. Calcd. for $C_6Cl_2N_2S_4$: C, 24.08 N, 9.36 %. Found: C, 24.41; N, 9.28 %.

5.8.12 Synthesis of benzo[2,1-*c*:3,4-*c'*]bis(1,2,3-dithiazole), V-15a: A slurry of 1,4-diaminobenzene-2,3-dithiol dihydrochloride (1.00 g, 4.05 mmol) and excess S_2Cl_2 (5 mL) was heated to reflux in chlorobenzene for 3 h. Upon cooling to RT, the resulting black precipitate of crude [**V-15a**][Cl] was recovered by filtration, washed 2 x 10 mL chlorobenzene, and dried *in vacuo*. This material was reduced with excess triphenylantimony (1.43, 4.05 mmol) in refluxing acetonitrile (40 mL). The crude **V-15a** was filtered off and extracted into toluene (4 x 50 mL). The solvent was removed from the combined extracts affording pure **V-15a** which was crystallized from hot toluene as lustrous purple-black needles; yield 0.55 g (2.4 mmol, 59 %); mp 187 - 189 °C. Material for electrocrystallization work was further purified by fractional sublimation at 100 - 60 °C/10^{-2} Torr. IR: 1391 (w), 1317 (w), 1298 (m), 1122 (w), 1071 (m), 806 (s), 790 (vs), 767 (m), 707 (vs), 592 (m), 525 (m), 471 (m) cm^{-1}. UV/Vis (CH_2Cl_2): λ_{max} (log ϵ) = 572 (4.2), 329 (4.0) nm. MS (*m/e*): 230 (M^+, 70 %), 133 (24 %), 88 (40 %), 76 (100 %). Anal. Calcd. for $C_6H_2N_2S_4$: C, 31.29; H, 0.88; N, 12.16 %. Found: C, 31.53; H, <0.05; N, 12.08 %.

5.8.13 Synthesis of 5,6-dichlorobenzo[2,1-*c*:3,4-*c'*]bis(1,2,3-dithiazole), V-15c: A slurry of **V-15a** (0.35 g, 1.52 mmol) was heated in refluxing neat sulfur monochloride (10 mL) for 72 h. The resulting black precipitate was recovered by filtration, washed with 3 x 20 mL of dichloroethane, and dried *in vacuo*. This material was then reduced with triphenylantimony (0.54 g, 1.52 mmol) in refluxing acetonitrile (40 mL). Filtration of this mixture afforded a black solid which, according to TLC analysis, was ca. 20 % **V-15b** and 80 % **V-15c**. The **V-15c** (50 mg) was isolated by fractional sublimation at 110 - 80 °C/10^{-2} Torr, followed by crystallization from toluene.

References for Chapter 5

1. Genin, H.; Hoffman, R.; *Macromolecules,* **1998**, *31*, 444.
2. Dormann, E.; Nowak, M. J.; Williams, K. A.; Angus, R. O. Jr.; Wudl, F.; *J. Am. Chem. Soc.*, **1987**, *109*, 2594.
3. Barclay, T. M.; Cordes, A. W.; de Laat, R. H.; Goddard, J. D.; Haddon, R. C.; Jetter, D. Y.; Mawhinney, R. C.; Oakley, R. T.; Palstra, T. T. M.; Patenaude, G. W.; Reed, R. W.; Westwood, N. P. C.; *J. Am. Chem. Soc.*, **1997**, *119*, 2633.
4. Barcaly, T. M.; Cordes, A. W.; Goddard, J. D.; Mawhinney, R. C.; Oakley, R. T.; Preuss, K. E.; Reed, R. W.; *J. Am. Chem. Soc.*, **1997**, *119*, 12136.
5. Oakley, R. T.; Patenaude, G. W.; unpublished results.
6. (a) Phillips, T. E.; Kistenmacher, T. J.; Ferraris, J. P.; Cowan, D. O.; *J.C.S. Chem. Comm.*, **1973**, 471. (b) Ferraris, J.; Cowan, D. O.; Walatka, V. Jr.; Perlstein, J. H.; *J. Am. Chem. Soc.*, **1973**, *95*, 948. (c) Engler, E. M.; *Chemtech*, **1976**, 274.
7. Huestis, L. D.; Walsh, M. L.; Hahn, N.; *J. Org. Chem.*, **1965**, *30*, 2763.
8. Green, A. G.; Perkin, A. G. *J. Chem. Soc.*, **1903**, *83*, 1201.
9. Lakshmikantham, M. V.; Raasch, M. S.; Cava, M. P.; Bott, S. G.; Atwood, J. L. *J. Org. Chem.*, **1987**, *52*, 1874.
10. Barclay, T. M.; Cordes, A. W.; Oakley, R. T.; Preuss, K. E.; Reed, R. W.; *Chem. Mater.*, **1999**, *11*, 164.
11. Boeré, R. T.; *Coord. Chem.*, in press, **2000**.
12. Kobayashi, H.; Sato, A.; Arai, E.; Akutsu, H.; *J. Am. Chem. Soc.*, **1997**, *119*, 12392.
13. Gill, N. S.; Taylor, F. B.; *Inorg. Synth., Vol IX*, Tyree, S. Y., Ed.-in-Chief, McGraw-Hill Book Company, N.Y., **1967**,139.

14. Taylor, M. J.; Tuck, D. G.; Jaselskis, B. J.; *Inorg. Synth. 22*, Holt, S. L. Ed.-in-Chief, John Wiley & Sons, N.Y., **1983**, 135.

15. Rabe, S.; Müller, U.; *Z. Kristallogr. New Cryst. Struct.*, **1999**, *214* 68.

16. (a) Wolmershäuser, G.; Wortmann, G.; Schnauber, M.; *J. Chem. Res. (S)*, **1988**, 358. (b) Bryan, C. D.; Cordes, A. W.; Haddon, R. C.; Hicks, R. G.; Oakley, R. T.; Palstra, T. T. M.; Perel, A. S.; Scott, S. R.; *Chem. Mater.*, **1994**, *6*, 508.

17. Mayer, R.; *Phosphorus Silicon*, **1985**, *23*, 277.

18. (a) Bestari, K.; Cordes, A. W.; Oakley, R. T.; Young, K. M.; *J. Am. Chem. Soc.*, **1990**, *112*, 2249. (b) Oakley, R. T.; Reed, R. W.; Cordes, A. W.; Craig, S. L.; Graham, S. B.; *J. Am. Chem. Soc.*, **1987**, *109*, 7745.

19. Torrance, J. B.; in *Molecular Metals*, Hatfield, W. E., Ed., Plenum Press, NY, **1979**, 7.

20. Brauer, G.; *Handbook of Preparative Inorganic Chemistry*, Academic Press, New York, **1963**, *1*, 423.

21. Lucas, H. J.; Kennedy, E. R.; *Org. Synth. Coll. Vol. 3*, **1955**, 482.

22. Wolfe, J. F.; Loo, B. L.; Arnold, F. E.; *Macromolecules*, **1981**, *14*, 915.

23. Small, R.W. H.; Banister, A. J.; Hauptman, Z. V.; *J. Chem. Soc., Dalton Trans.*, **1984**, 1377.

Chapter 6 A Non-Quinoid Ring-Fused Bis-1,2,3-DTA and a Potential Neutral Radical Conductor.

6.1 Introduction

The ring-fused bis(1,2,3-DTA)s discussed in Chapter 5 belong to a class of neutral closed shell molecules with a quinoid formulation in the ground state. These compounds can be regarded as systems analogous to the theoretical 4,4',5',5"- multi-(1,2,3-DTA) oligomer **VI-1** formed by successively linking simple DTA rings to one another via the carbon C4 to C4' and C5' to C5" and so on. The applicability of several compounds, including **VI-3**, as electron donors in CT salts is covered in Chapter 5.

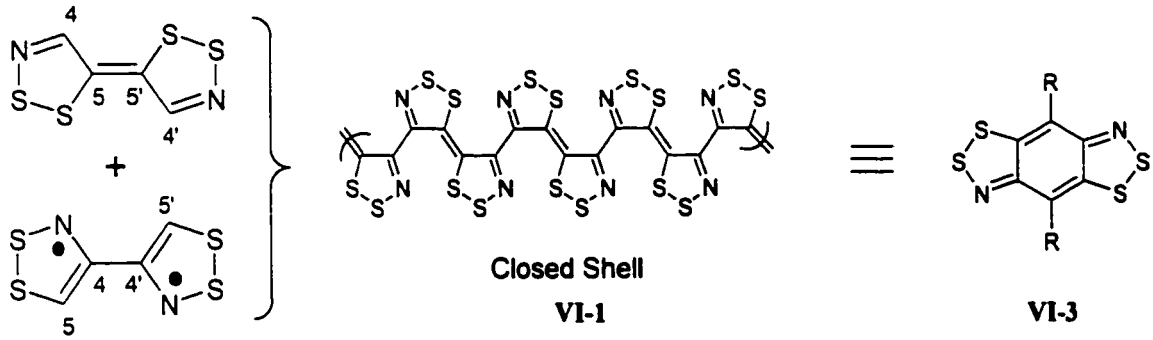

Figure 6.1 Theoretical polymer based on 4,4',5',5"- multi-(1,2,3-DTA) linkage.

There is a second possible theoretical multi-(1,2,3-DTA) oligomer, this one arising from linking the C4 to the C5' of the adjacent DTA rings (see **Figure 6.2**). The resulting oligomer, or polymer, cannot adopt a closed shell quinoid ground state structure in this arrangement. Instead, it must adopt one of two possible formulations left available, *i.e.*, an open shell uncharged multiradical **VI-2a** or a closed shell zwitterion **VI-2b**. Once again, this theoretical system can be

represented by a fused-ring compound (*e.g.*, **VI-4**) wherein the carbons that can be regarded as C4 and C5' of two DTA rings are related to one another by conjugation.

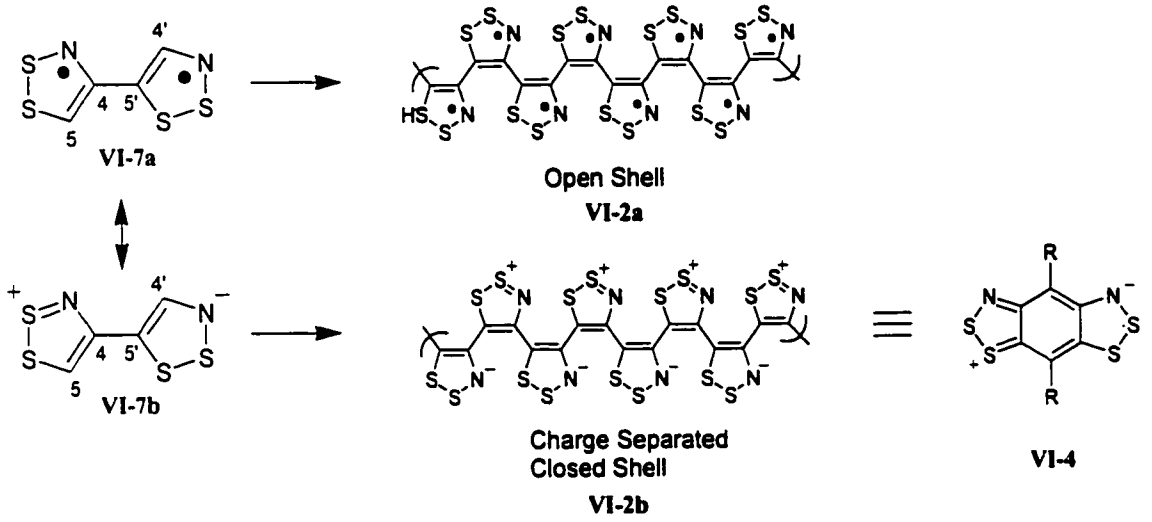

Figure 6.2 Theoretical polymer based on 4,5',4',5''- multi-(1,2,3-DTA) linkage.

Discussed within this chapter are two ring-fused compounds based on the 4,5'-linkage shown in **Figure 6.2**. The first of these two compounds, **VI-4**, is unknown in the neutral oxidation state. It may be either a closed shell zwitterion or a neutral diradical. There is, however, a stable radical cation oxidation state available, and we have isolated a salt of this species. Consequently, this compound, like **VI-3**, potentially belongs to the class of radical ion conductor (RIC) donors presented in Chapter 5.

The second compound discussed herein is a radical in the neutral oxidation state, **VI-6**. Although it originates from the protonation of **VI-5**, a compound that is isolobal with **VI-4**, it is no longer a candidate for a radical ion conductor donor design. It is more aptly classified as a possible molecular neutral radical conductor (NRC).

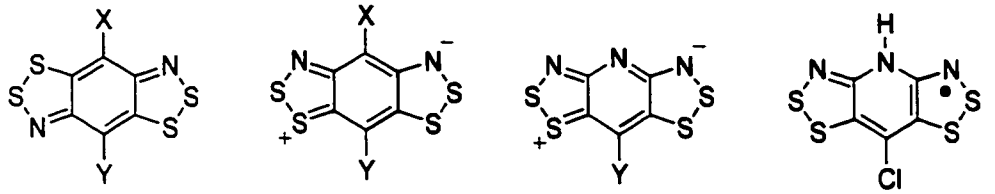

VI-3
a) X=Y=H
b) X=Cl, Y=H
c) X=Y=Cl

VI-4
a) X=Y=H
b) X=Cl, Y=H
c) X=Y=Cl

VI-5
a) Y=H
b) Y=Cl

VI-6

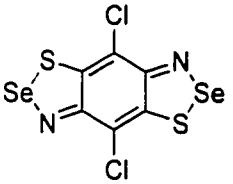

VI-10

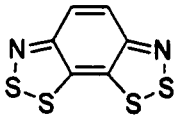

VI-11

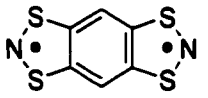

VI-13

Figure 6.3 Ring-bridged bis(DTA) systems discussed herein.

While **VI-4** and **VI-6** are based on a similar structural design, and are therefore presented together in this chapter, they are quite different electronically. It is for this reason that the chapter is divided into two sections. Part A is devoted to the discussion of **VI-4**. Part B deals with the issues surrounding **VI-6** and the current results in its on-going study.

The results presented within this chapter are the first steps taken in a research project that will undoubtably continue to be pursued by the Oakley group. It is, therefore, appropriate that the last section of this chapter encompasses current advances in this study.

6.2 Part A: Discussion of VI-4.

This section deals with **VI-4**, the benzo-bridged bis(1,2,3-DTA) system that is representative of the theoretical 4,5'- linked poly-DTA **VI-2**. As is evident from **Figure 6.3**, **VI-4** is structurally closely related to **VI-3**, a bis(1,2,3-DTA) presented in Chapter 5 as a system analogous to the 4,4',5',5''- linked poly-DTA **VI-1**. The most notable difference between these two

compounds is observed in the electronic configuration of their (overall) neutral oxidation ground states. The two-electrons-in-two-molecular-orbitals model introduced in Chapter 1 illustrates the four possible states (six microstates) available to either of these two systems. It has been established (Chapter 5) that the ground state of **VI-3** is a closed shell quinoid singlet. In order for **VI-4** to adopt a similar closed shell ground state, charge separation must occur generating a zwitterionic, rather than a quinoid, formulation. There is another electronic configuration that can be considered as a reasonable option for the ground state of **VI-4**, and that is a diradical (only the triplet is considered herein, although it should be noted that a singlet diradical is also an option).[†]

In spite of the differences between the ground state configurations of **VI-3** and **VI-4**, their respective electronic structures bear certain similarities. A radical cation oxidation state is available to both systems, and thus both are candidates for electron donors in CT salts.

The pyridine variant, **VI-5**, is also introduced herein. This compound is isolobal with **VI-4** and therefore is faced with the same issues surrounding the electronic configuration of the ground state. More important, however, is its high proton affinity. This property presents a major obstacle to the isolation and characterization of **VI-5**, however it has led to the preparation of salts of the [**VI-6**]$^{+}$ closed shell cation. In the neutral oxidation state, **VI-6** is a stable radical. It and its cationic salts are discussed separately in Part B.

6.2.1 Some Theoretical Considerations

To summarize a prior discussion (see Section 5.1), our series of semi-empirical and *ab initio* calculations are in agreement with extended Hückel level calculations performed by Genin and Hoffman[1] in predicting that the ground state of the theoretical 4,5'-linked 1,2,3-DTA dimer

---

[†] The fourth state not considered herein as viable ground state is a singlet in which the two electrons are paired in the higher of the two orbitals.

is a triplet, **VI-7a**, rather than a charge separated closed shell species, **VI-7b** (see **Figure 6.2**). Furthermore, there is no apparent trend toward a narrowing of the energy gap between the triplet and the closed shell zwitterion upon improvement of the computational level or enlargement of the basis set. This indicates that the calculated preference for the open shell configuration is not simply a result of a computational inadequacy in handling electron correlation in a closed shell species.

From these results, it is tempting to draw the conclusion that **VI-4**, since it seems to be an electronically analogous system, will exist in the neutral oxidation state as a triplet. We have studied the theoretical compounds **VI-4a**, **VI-4b**, and **VI-4c** by our usual series of semi-empirical and *ab initio* computational methods in order to assess this prediction. The geometry optimized energies of the triplet and the closed shell quinoid formulations for these molecules, constrained to planarity, are compared.

To begin with, our results indicate that chlorination of the internal phenyl ring has little effect on the relative geometry optimized energies. Therefore, although the numerical results for all three compounds are found in **Table 6.1**, only the **VI-4c** will be discussed since it is the compound that we have attempted to prepare.

Table 6.1 Geometry Optimized Energy Differences (Triplet - Closed Shell Zwitterion)[a] for VI-4a, VI-4b, and VI-4c.

	VI-4a	VI-4b	VI-4c
MNDO	-50.82 [b]	-48.74	-49.43
B3LYP/STO-3G	-14.39	-12.79	-13.61
B3LYP/3-21G	-10.04	-8.65	-10.10
B3LYP/6-31G**	-5.06	-4.41	-5.33

[a] All energies reported in kcal / mol. [b] Since the geometry optimized energies have negative values, a negative value for $E_{diff} = E_{triplet} - E_{singlet}$ indicates that the triplet is lower in energy.

The ground state of **VI-4** is predicted to be a triplet, according to our series of calculations. This is in agreement with the computational results for the analogous **VI-7**. However, in the case of **VI-4**, as the computational level is improved and the basis set is increased in size, a trend toward a narrowing of the energy gap between the geometry optimized energies of the triplet and the closed shell singlet is apparent. This observation has a number of implications.

The most pronounced decrease in E_{diff} appears between the semi-empirical MNDO and the *ab initio* B3LYP/STO-3G computational levels. MNDO, like all other semi-empirical methods, employs empirical data in order to simplify the solution to the Schrödinger equation. Such methods are most meaningful when employed on the ground state molecular systems for which they are designed. By and large, this implies small organic molecules with an uncharged, closed-shell ground state. That MNDO might have difficulty dealing adequately with a ground state triplet or a zwitterionic species is not surprising. The significant decrease in E_{diff} observed when B3LYP is employed is due, in large part, to the superior handling of electron correlation in closed shell systems by density functional theory (DFT).[2] Semi-empirical methods tend to favour a triplet configuration over a closed shell singlet, all else being equal, as they are unable to adequately deal with defining two electrons of opposite spins by the same molecular orbital function.[†]

That this trend persists upon enlargement of the basis set at a B3LYP level is significant. This demonstrates that as the theory becomes more closely able to mimic reality, the stability of the triplet state as compared to the closed shell singlet state decreases. This energy difference calculated at B3LYP/6-31G** is *ca.* -5 kcal/mol (see **Table 6.2** for details). In our experience, this value is on the edge of being too small to be meaningful. In other words, although the triplet state is predicted to be lower in energy for this series of calculations, we cannot definitively say

---

[†] B3LYP is actually a hybrid DFT. It employs mixtures of HF and DFT exchange terms along with DFT correlation terms. DFT correlation terms rely on the use of functionals (functions of functions).

that this will be so in reality.

Furthermore, the same series of calculations performed on the pyridine variant, **VI-5**, again displays this trend with one significant difference. At the B3LYP/6-31G** level, the calculated E_{diff} is *ca.* +3 kcal/mol. The closed shell singlet, at the highest computational level employed, is *lower* in energy than the diradical conformation, albeit by an admittedly small amount.

The prediction that a zwitterionic singlet dominates as the ground state in **VI-5** is reinforced, to some extent, by the recent discovery that a tetraphenylhexaazaanthracene, **VI-8**, for which a diradical configuration can be drawn, also exists as a charge-separated species. The remarkable feature of the ground state in this case is that by adopting the zwitterionic conformation over the diradical conformation, the aromatic character of the central benzene ring is sacrificed in favour of two independent cyanine subunits with a total of 16 π electrons. Photoexcitation TREPR, computational, and solid state structural evidence has been cited.[3,4]

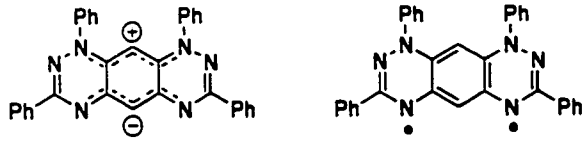

VI-8

Figure 6.4 The dominant zwitterionic and the unobserved diradical conformations of **VI-8**.

Table 6.2 Geometry Optimized Energy Differences (Triplet - Closed Shell Zwitterion)[a] for VI-5a and VI-5b.

Compound	**VI-5a**	**VI-5b**
MNDO	-40.23 [b]	-40.59
B3LYP/STO-3G	-9.18	-9.64
B3LYP/3-21G	-0.69	-1.70
B3LYP/6-31G**	+3.04	+2.43

[a] All energies reported in kcal / mol. [b] Since the geometry optimized energies have negative values, a negative value for $E_{(triplet - singlet)}$ indicates that the triplet is lower in energy.

The geometry optimized triplet and closed shell, charge-separated singlet are calculated to be very close in energy for all the chlorinated, partially chlorinated, and unchlorinated variations of **VI-4** and **VI-5**, so much so that it is not possible to predict with any certainty the actual ground state configuration of these compounds. We have not yet been able to prepare any of the above materials in the neutral oxidation state. We expect, however, that the spin states of these compounds (*i.e.*, zwitterionic singlet *vs.* open shell triplet) may be dependent upon their chemical environment. For example, in a solvent with a high dielectric constant, they will more than likely exist as a closed shell zwitterion, whereas a less polar solvent is expected to stabilize the diradical state.

In addition, it is not unlikely that dimerization through sulfur may occur in a non-polar environment. This scenario is reminiscent of the observed behaviour of 1,3,2,4,6-dithiatetrazines (**VI-9**). *Ab initio* calculations[5] for the prototypal compound **VI-9a** predict a distorted (C_s symmetry) closed shell singlet ground state. Isolation of the phenyl derivative **VI-9b** reveals a stable, insoluble, cofacial dimer. This observed dimerization has been attributed to the coupling of triplet ground states to achieve a closed shell ground state.[6]

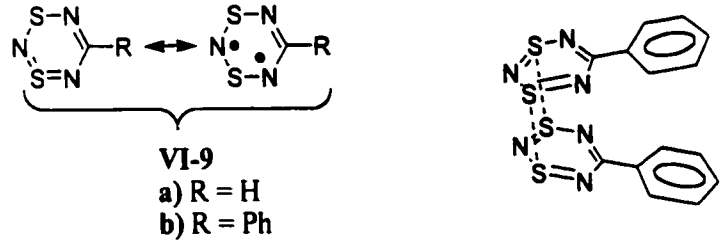

VI-9
a) R = H
b) R = Ph

Figure 6.5 1,3,2,4,6-Dithiatriazines dimerize in a cofacial manner.

In the case of the pyridine based compound, **VI-5**, there is a second factor which may prevent the isolation of any of these compounds in the neutral oxidation state, and that is its chemical reactivity, or more precisely, the high proton affinity of the charge-separated species. The

proton affinity of **VI-5** is such that, in practical terms, protonation is unavoidable in the course of synthesis. This is further discussed in Part B of this chapter.

6.2.2 Radical Cation of VI-4

VI-3c,[7] **VI-10**,[6] and **VI-11**[8] are all prepared by condensation of the appropriate diaminodithiolbenzene dihydrochloride salt with a chalcogen halide.[9] The resulting oxidation state in each case is the singly charged radical cation which must be reduced in order to obtain the neutral material. Similarly, the treatment of 1,3-diaminobenzene-4,6-dithiol, **VI-12**, with excess sulfur dichloride affords [**VI-4c**][Cl]. However, to date, we have been unable to reduce this compound to a neutral oxidation state.

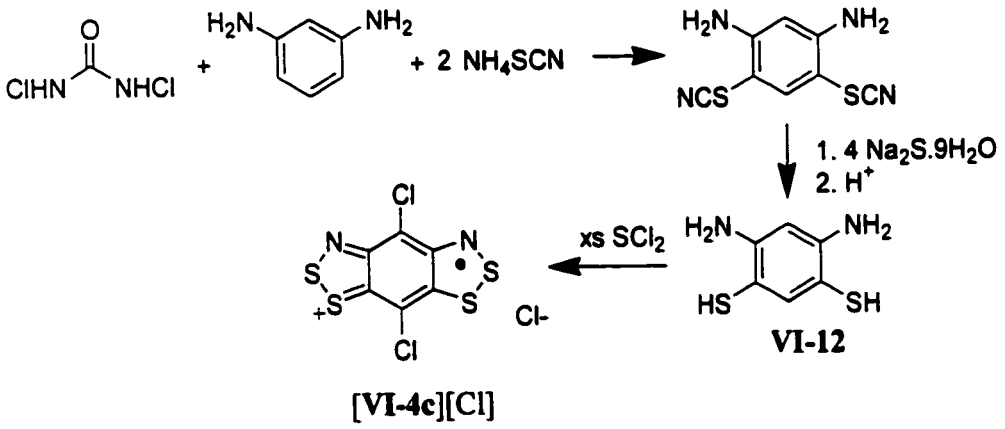

Figure 6.6 Preparative route to [**VI-4c**][Cl].

Although we were ultimately able to isolate and characterize the dicationic oxidation states $[\mathbf{VI\text{-}3c}]^{2+}$ and $[\mathbf{VI\text{-}10}]^{2+}$ in the form of tetrachloroaluminate salts, it was no easy task. We have had even greater trouble attempting to isolate $[\mathbf{VI\text{-}4c}]^{2+}$. Reactions of [**VI-4c**][Cl] with two equivalents of nitrosonium hexafluoroantimonate in sulfur dioxide afford a red, semicrystalline material with

a promising infrared spectrum (meaning that the peak pattern is similar to that observed for the starting material with peak shifts indicative of an oxidized species). However, the oxidation of the radical cation by $PhICl_2$ in the presence of excess $AlCl_3$ fails to produce any retrievable material.

Our efforts to isolate the radical cation oxidation state, however, have been more successful. Treatment of the crude **[VI-4c]**[Cl] with $AlCl_3$ in sulfur dioxide affords bronze crystals of **[VI-4c]**$[AlCl_4]$ which become green upon drying. For these, we have obtained a clean infrared spectrum and an EPR spectrum (*vide infra*) dominated by the familiar 1:2:3:2:1 pentet consistent with coupling to two equivalent nitrogens. This project is still in progress and we expect that the radical cation will be properly characterized in the fullness of time.

6.2.3 Electron Paramagnetic Resonance

The bronze crystals of **[VI-4c]**$[AlCl_4]$ dissolve in SO_2 to afford a purple solution with an EPR signature dominated by the expected 1:2:3:2:1 pentet arising from hyperfine coupling to two equivalent nitrogens (a_N = 4.3 gauss[†]). This confirms the delocalization of spin over both DTA rings. The pentet is further split by hyperfine coupling to only one of the two chlorines (a_{35Cl} = 0.9, a_{37Cl} = 0.7 gauss[†]). Accordingly, the calculated spin density in the SOMO predicts there to be spin density only on one of the two central carbons, that located on the nitrogen-containing side of the molecule.

Comparing the hyperfine coupling to nitrogen of **[VI-4c]**$^{\cdot+}$ to that of the isomeric **[VI-3c]**$^{\cdot+}$ (a_N = 2.01 gauss), we find that the spin density in the **VI-4c** system is more highly concentrated on the nitrogens. Consistently, there is a decrease in the g-value for **[VI-4c]**$^{\cdot+}$ (g = 2.0073), indicative of a lesser degree of spin-orbit coupling effects (at sulfur), in comparison to **[VI-3c]**$^{\cdot+}$ (g = 2.0114). These observations imply a less extensive delocalization of the spin density in **[VI-**

[†] Coupling constants calculated by simulation with WINEPR Simfonia.

4c]$^{+}$ relative to [**VI-3c**]$^{+}$. However, while both isomers are chlorinated at the central benzene, hyperfine coupling to chlorine is observed in the [**VI-4c**]$^{+}$ system but no such coupling to chlorine is apparent in the EPR of [**VI-3c**]$^{+}$.

Although the spin density in [**VI-4c**]$^{+}$ is not as delocalized as that in [**VI-3c**]$^{+}$, it is not yet as localized as that of the isomeric, albeit unchlorinated, [**VI-13**]$^{+}$ radical cation.[10] Comparison of the EPR spectra of the two reveals a smaller g-value and a larger hyperfine coupling to nitrogen for [**VI-13**]$^{+}$ (g = 2.0068, a_N = 6.24 gauss).

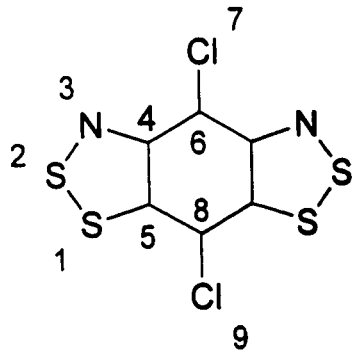

Figure 6.7 Qualitative representation of [**VI-4c**]$^{+}$ radical cation.

Table 6.3 Calculated† Hyperfine Coupling, and Spin Density for [VI-4c][AlCl$_4$].

Atom	Mulliken Spin Density	Isotropic Fermi Contact Couplings (gauss)
N3	0.265324	5.09
S1	-0.018928	
S2	0.164963	
C6	0.381141	
Cl7	0.058679	1.53(^{35}Cl)
C8	-0.018239	
Cl9	-0.002502	-0.20(^{35}Cl)

† B3LYP/6-31G**.

6.3 Part B: Protonation of VI-5b Leads to a Neutral Radical Precursor

Replacement of one or both of the C-Cl groups in **VI-4c** with a nitrogen generates an isolobal compound. With this in mind, we pursued the synthesis of **VI-5b**. Once again we followed a preparative route based upon the condensation of an aromatic diaminodithiol with a sulfur halide. In this case, however, the desired 2,6-diaminopyridine-3,5-dithiol **VI-15** is not a previously known

compound. We successfully prepared this compound by a route analogous to that for the known 1,3-diamino-4,6-dithiolbenzene **VI-12**. The substitution of 2,6-diaminopyridine with two thiocyano- groups is accomplished by treatment with ammonium thiocyanate and *N,N'*-dichlorourea, freshly prepared by bubbling chlorine gas through an aqueous solution of urea, to generate 2,6-diamino-3,5-bis(thiocyano)pyridine **VI-14**. This product is then treated with sodium sulfide nonahydrate and the resulting **VI-15** is precipitated by the addition of acetic acid. While this material can be used directly in the condensation reaction with sulfur monochloride, treatment with 4 M HCl generates a hydrochloride salt that proves to be more easily purified by recrystallization.

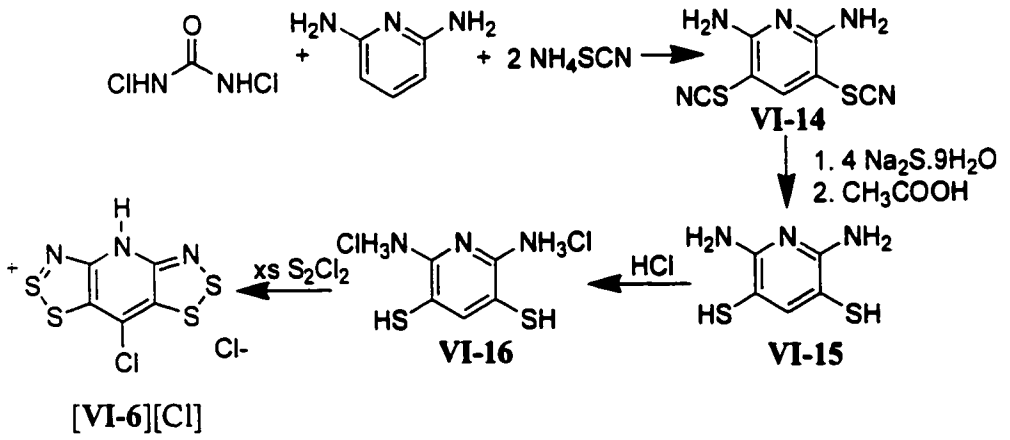

Figure 6.8 Preparation of **[VI-6][Cl]**.

The condensation of **VI-16** with sulfur monochloride successfully generates the pyridine-bridged bis(1,2,3-DTA) framework, however the black powder product is *not* the radical cation **[VI-5b][Cl]**, but in fact the protonated *closed shell* cation **[VI-6][Cl]**. Evidently, **VI-5b** has an unusually high proton affinity for a SN heterocycle. This is confirmed by *ab initio* calculated results (*vide infra*). This property dictates that the protonated cation, $[\mathbf{VI\text{-}6}]^+$, is lower in energy

than the zwitterionic **VI-5b** in a proton-rich environment. While protonation has produced a cation [**VI-6**]$^{+}$ that is no longer a radical, and therefore not useful as a RIC, the reduction of this compound in theory generates a neutral radical species that may have applicability as a NRC. Thus, we were catapulted out of the chemistry of CT salt donors and into the realm of neutral radical conduction.

The high proton affinity of **VI-5** was somewhat surprising to us in light of the remarkably low proton affinities generally displayed by SN heterocycles. The 1,5,2,4,6,8-dithiatetrazocines (**VI-17**) discussed in Chapter 2 are demonstrative of this property. It has been remarked that these electron rich compounds, even when substituted with amino groups, show no alkaline properties when titrated with $HClO_4$ in AcOH-C_6H_5Cl.[11]

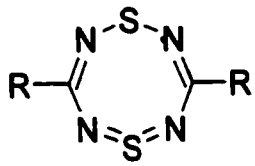

VI-17

Figure 6.9 General structure of a 1,5,2,4,6,8-dithiatetrazocine.

In order to facilitate the full appreciation of the scope of the issues involved in the **VI-5b**/ **VI-6** system, the entire redox manifold is presented in **Figure 6.10**. The geometry optimized energy of each of the compounds therein has been calculated at the B3LYP/6-31G** level and is discussed in due course. It is important to note that calculated electronic energy of a proton is zero,[†] and therefore the electronic energies of the protonated and unprotonated species can be compared directly.

[†] H^{+} has no electronic energy due the fact that it has no electrons.

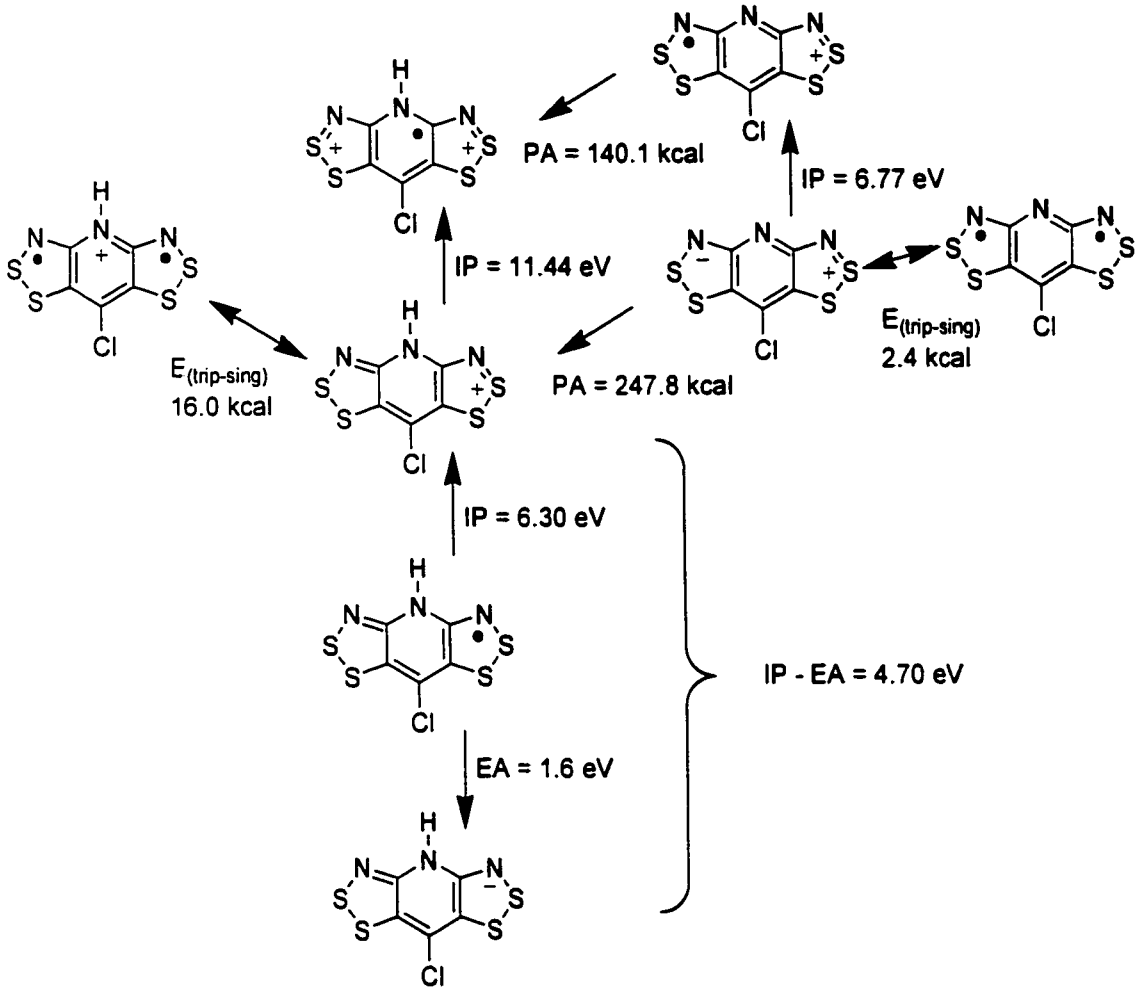

Figure 6.10 The redox manifold of the **VI-5b/VI-6** system.

Metathesis of [**VI-6**][Cl] to a number of other salts has been achieved. Treatment with either $AlCl_3$ or $GaCl_3$ affords microcrystals of [**VI-6**][X] (X = $AlCl_4$ and $GaCl_4$, respectively). The salts [**VI-6**][X] (X = BF_4, SbF_6) can be generated in crystalline form by reaction with the appropriate silver salt in sulfur dioxide. The iodide salt [**VI-6**][I] is easily prepared from [**VI-6**][SbF_6] and tetrabutylammonium iodide.

Gold, block-shaped crystals of [**VI-6**][SbF_6] of sufficient quality for structural

determination by X-ray diffraction were obtained by recrystallization from SO_2. Two important features of the [**VI-6**]$^+$ cation are revealed in the crystal structure. First, in likeness to the **VI-3c**, **VI-10**, and **VI-4b** systems, the pyridine carbon is chlorinated. There is no evidence of the unchlorinated species in the crystalline material or in the crude solid according to infrared analyses. Second, in the solid state, protonation occurs solely at the central nitrogen. No variation in the crystal morphology was observed that might indicate the presence of an asymmetrically protonated species. Furthermore, infrared analyses of the crude material confirm the presence of only one isomer in the solid state. The possibility that there is an equilibrium between the symmetric and the asymmetric species in solution cannot be ruled out from this evidence. As the less soluble symmetrically protonated salt drops out of solution, such an equilibrium, in as far as it exists, is maintained according to LeChetalier's principle, until the cation salt is fully recovered from solution as the symmetric isomer alone. As expected for a closed shell cation, solutions of purified [**VI-6**][SbF_6] in sulfur dioxide are EPR inactive.

We have made several attempts to isolate the neutral radical **VI-6**. Starting from a closed shell cation salt, we have taken three different approaches. The first was to sublime [**VI-6**][X] (X = Cl, I) in a temperature gradient under dynamic vacuum. Although a small quantity of black needle-shaped crystals were recovered from these experiments, they proved to be EPR silent. The second approach was the chemical reduction of the radical cation using a range of reducing agents in a variety of solvents. These, too, were largely unsuccessful. Finally, we employed cyclic voltammetry in an attempt to observe the formation of the neutral radical *in situ*. The results of this experiment are discussed at length in the following section.

6.3.1 Cyclic Voltammetry

The results of cyclic voltammetry performed on a solution of [**VI-6**][SbF_6] in acetonitrile

(0.1 M tetra-*n*-butylammonium hexafluorophosphate electrolyte, Pt electrodes, measured versus SCE) reveal a rich redox manifold. Of particular interest, is the neutral/cation redox process (0/+). A fully reversible wave, centered at $E_{1/2}$ = 0.01 V, is observed, provided the reduction sweep does *not* lower the potential of the working electrode to include the formation of the anion. The -/0 pair is characterized by a reduction peak of questionable reversibility. That is to say that the reduction sweep yields a large, relatively sharp peak at E_{pa} = -0.50 V, but the returning oxidation sweep uncovers a smaller, broader peak centered at E_{pc} = -0.33 V. Furthermore, the reversibility of the 0/+ wave is compromised on this returning oxidation sweep. The 0/+ oxidation (E_{pa} = 0.04 V in the reversible wave) is replaced by an irreversible oxidation at E_{pa} = 0.72 V.

The complex redox behaviour of this compound in solution militates against the generation of a stable neutral radical **VI-6** by chemical reduction of the salt. It is, therefore, not surprising that our many attempts have met with little success.

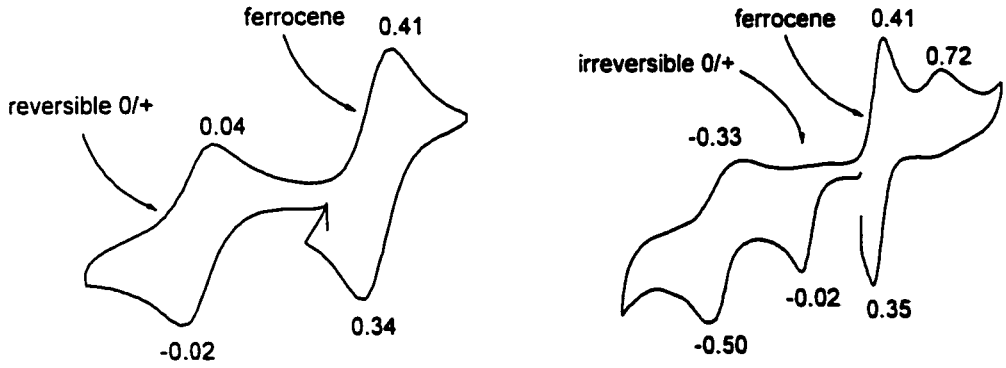

Figure 6.11 Cyclic Voltammogram for [**VI-6**][SbF_6] in CH_3CN.

One possible explanation for this cumulative behaviour is that upon reduction to the anion, there is a shift in the position of the H from the central nitrogen to one of the DTA nitrogens. The oxidation of this proton-shifted anion affords a different species of neutral radical and cation.

Hence, the disappearance of the anodic half of the 0/+ peak and the appearance of a new anodic peak is observed in the CV.

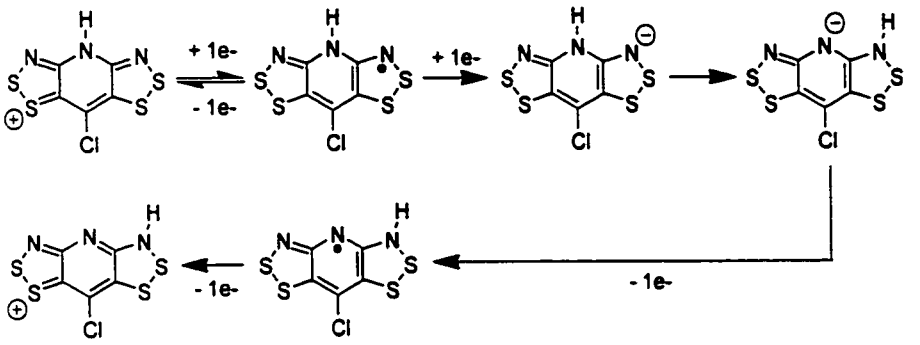

Figure 6.12 The shifting of the proton upon reduction of **VI-6**.

A second possible explanation for this behaviour is the breaking of a bond upon reduction to an anion. This harkens back to previous computational studies[6] on **VI-3a** wherein it was determined that reduction to **[VI-3a]**$^-$ places an electron in an orbital (b_g) that is stongly antibonding over the N-S linkage. A full geometry optimization predicts the cleavage of one of the N-S bonds, lowering the symmetry from C_{2h} to C_1. These results shed light on the irreversibility of the reduction peak in the CV of **VI-3b**. However, caution should be taken in equating the irreversibility of the (-/0) pair in **VI-3b** with that of the (-/0) pair in **VI-6** since the two are not electronically comparable. The comparison of the cation **[VI-6]**$^+$ with the neutral oxidation state of **VI-3b** has more validity.

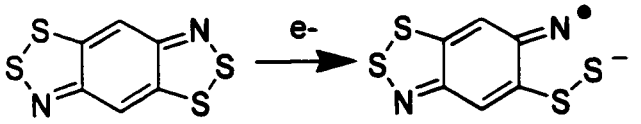

VI-3a

Figure 6.13 Breakage of an N-S bond upon reduction of **VI-3a**, according to calculations.

Electrochemical irreversibility with chemical reversibility (EI-CR) occurs when an electrochemical redox reaction alters the structure of a compound such that the reverse redox reaction does not regenerate the original compound. This phenomenon is described in a recent review[12] with respect to the -/0 redox couple of **VI-18**.[13] Upon formation of the anion **[VI-18]**$^{-}$, rapid cleavage of the S-S bond occurs to form a sulfido-thioketone. This species is further reduced to the dianion, but reoxidation to the now cleaved mono-anion occurs at a much more anodic potential. Hence the observed irreversibility of the -/0 redox process is due to a chemical change (S-S bond cleavage) occurring more rapidly than the cycling rate.

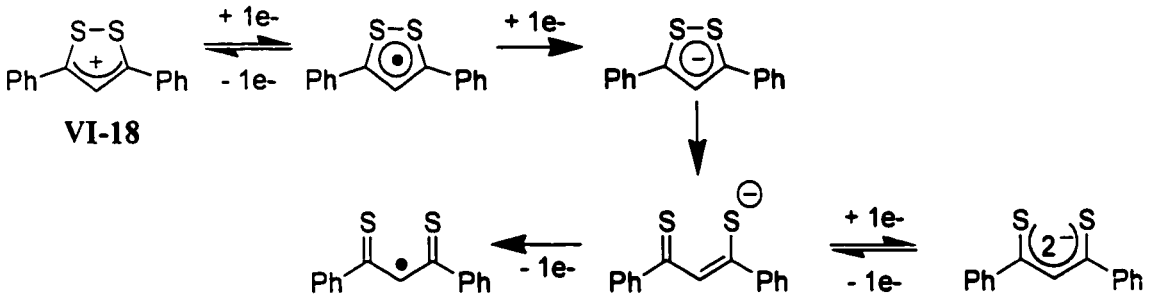

Figure 6.14 EI-CR observed for **VI-18**.

It is worth noting that, unlike **VI-18**, fused-ring dithioles such as **VI-19** and **VI-20** do not undergo S-S bond cleavage upon electrochemical reduction.[11,14] Both species display a fully reversible -/0 redox pair in their cyclic voltammograms. This has been attributed to the chemical rigidity imposed upon the dithiole rings by the naphthalene and phenalenyl groups. In the case that S-S bond cleavage were to occur in either of these systems, the sulfur atoms are held in such close proximity that there would be no great change in the thermodynamics of re-oxidation.[10]

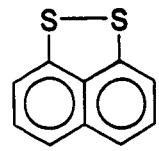

VI-19

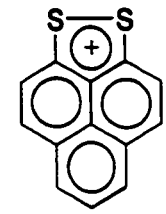

VI-20

Figure 6.15 Ring-fused 1,2-dithioles for which reversible -/0 reductions are observed in the CV.

6.3.2 Crystal Structure

[**VI-6**][SbF_6] crystallizes from a turquoise solution in SO_2 as gold blocks in the triclinic space group $P\bar{1}$. The [**VI-6**]$^+$ cations are planar to within 0.036 Å. A summary of the mean intramolecular bond distances for [**VI-6**]$^+$ is given in **Table 6.4** alongside the relevant bond lengths found for neutral **VI-11** and the [**VI-11**]$^+$ radical cation of [**VI-11**][ClO_4]. The electronic differences between **VI-11** and [**VI-6**]$^+$ are characterized by the inability to assign a quinoid formulation to the **VI-6** skeleton coupled with the fact that [**VI-6**]$^+$, although closed shell, bears a positive charge. These electronic differences predict that dissimilarities in the heterocyclic structures are also to be expected. The S-S and S-N bond distances for [**VI-6**]$^+$ are between those for **VI-11** and [**VI-11**]$^+$, although the S-S value is closer to that of the radical cation and the S-N to that of the neutral species. The more significant differences are seen in the S-C and (S)N-C bond lengths, which are shorter than those in either **VI-11** or [**VI-11**]$^+$. The contraction of these bond distances is indicative of a shifting of electron density off the central ring and into the π systems of the peripheral DTA rings.

The crystal packing arrangement consists of layers of [**VI-6**]$^+$ cations interspersed with SbF_6^- counterions affording a simple alternating cation/anion ionic structure. There is some degree of disorder within the anion arrangement. Additionally, there is evidence of hydrogen bonding

between the [**VI-6**]$^+$ cation and the fluorine F3 of the counterion, although antimony, the hydrogen, and said fluorine do not lie in a straight line but at a bond angle of 171.4°. The H···F distance is 1.906 Å. The N···H distance is 0.927 Å and the linear distance between N6 and F3 is 2.826 Å.

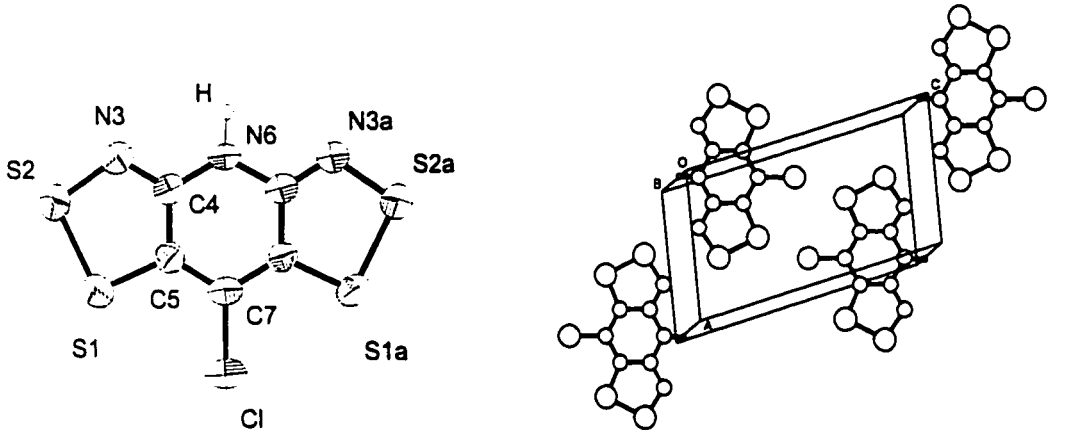

Figure 6.16 ORTEP and top view (x-axis) of [**VI-6**]$^+$ packing with anions removed for greater clarity.

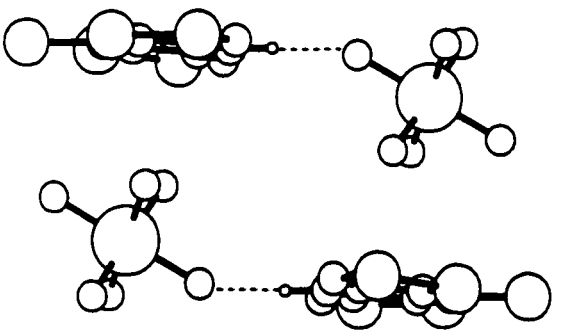

Figure 6.17 Ionic packing and H-bonding in [**VI-6**][SbF_6].

Table 6.4 Summary of Mean Intramolecular Distances (Å).

Compound	[VI-6][SbF_6]	VI-11	[VI-11][ClO_4]
Formal Charge	[VI-6]$^+$	VI-11	[VI-11]$^+$
S-S	2.0705(50)	2.096(5)	2.060(15)
S-N	1.6345(50)	1.646(7)	1.605(5)
S-C	1.6965(50)	1.744(8)	1.710(5)
(S)N-C	1.302(6)	1.305(6)	1.311(13)
(N)C-C(S)	1.433(10)		
(H)N-C	1.367(6)		
(S)C-C(Cl)	1.3815(60)		

The numbers in the parentheses represent the larger of the range and the ESD.

6.4 Continuation of this Research Project by Other Members of the Oakley Group.

In order to determine the origin of the irreversibility of the -/0 redox couple of **VI-6**, the methylated species **VI-21** was prepared and studied by cyclic voltammetry. [**VI-6**][SbF_6] was treated with proton sponge (1,8-diaminonaphthalene)[15] followed by $MeSO_3CF_3$ yielding [**VI-21**][SbF_6]. The cyclic voltammetry reveals a fully reversible redox couple -/0 at $E_{1/2}$ = -0.835 V. This indicates that bond cleavage is not occurring. Thus the irreversibility observed for **VI-6** is most likely due to proton shifting.

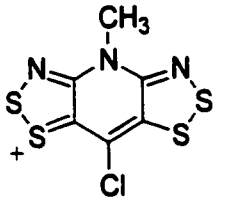

VI-21

Figure 6.18 Figurative representation of **VI-21**.

Two important features of the **[VI-21]**$^{+}$ redox manifold, in terms of the applicability of **VI-21** as a NRC, are presented in the cyclic voltammogram. The first is the potential difference between the -/0 redox wave and the 0/+ redox wave, and the second is the potential (*vs.* SCE) of that -/0 to 0/+ window. The successful design of a radical conductor depends on several factors, not the least of which is the potential barrier to conduction, given that the molecular radicals are able to interact electronically with one another in the solid state. Put simply, this is the ease with which an electron can be removed from one molecular radical site and added to a neighboring site. In the hopping model of conduction, this is the coulombic barrier to electron repulsion, which can be approximated by the gas phase dispersion enthalpy ($U \approx \Delta H_{disp}$ = IP - EA, where IP is the calculated gas phase ionization potential and EA is the electron affinity). Cyclic voltammetry provides solution measurements for the IP and EA of a material (the redox waves corresponding to the 0/+ and -/0 pair, respectively). Thus, the width of the -/0 to 0/+ window is effectively the solution IP - EA value and can be related to U for the solid neutral radical material. In the case of **VI-21**, this window is the narrowest of any neutral radical molecular material studied by the Oakley group to date. It is important to note that although the solution IP - EA value cannot be properly quantified for **VI-6** due to proton shifting, the *calculated* IP - EA value for **VI-6** is 4.70 eV. This is comparable to that of sodium metal (generally acknowledged as between 4.6 and 5.2 eV).[16,17]

The exploration of novel neutral radicals carried out by the Oakley group in the last decade has focused primarily on the design of potentially conducting materials. An important goal in this investigation, one that often guides the direction of the research, is the reduction of the IP - EA value. In the past, however, the narrowing of this gap has always been accompanied by a shift of the entire window to more anodic potentials. Ultimately, this seemed to be leading to materials for which the coulombic barrier to repulsion might be small, but the material itself is becoming more

electronegative.[18†] A representative sample of such neutral radicals is shown in **Figure 6.18** along with the measured -/0 to 0/+ cyclic voltammetry windows. As can be easily seen from this diagram, the second remarkable feature of the solution IP - EA for **VI-21**, apart from the narrowing of the window, is the position of the window. Not only is the coulombic barrier to repulsion predicted to be smaller for this material, the electronegativity of the material is expected to be closer to that of traditional metals, such as sodium.

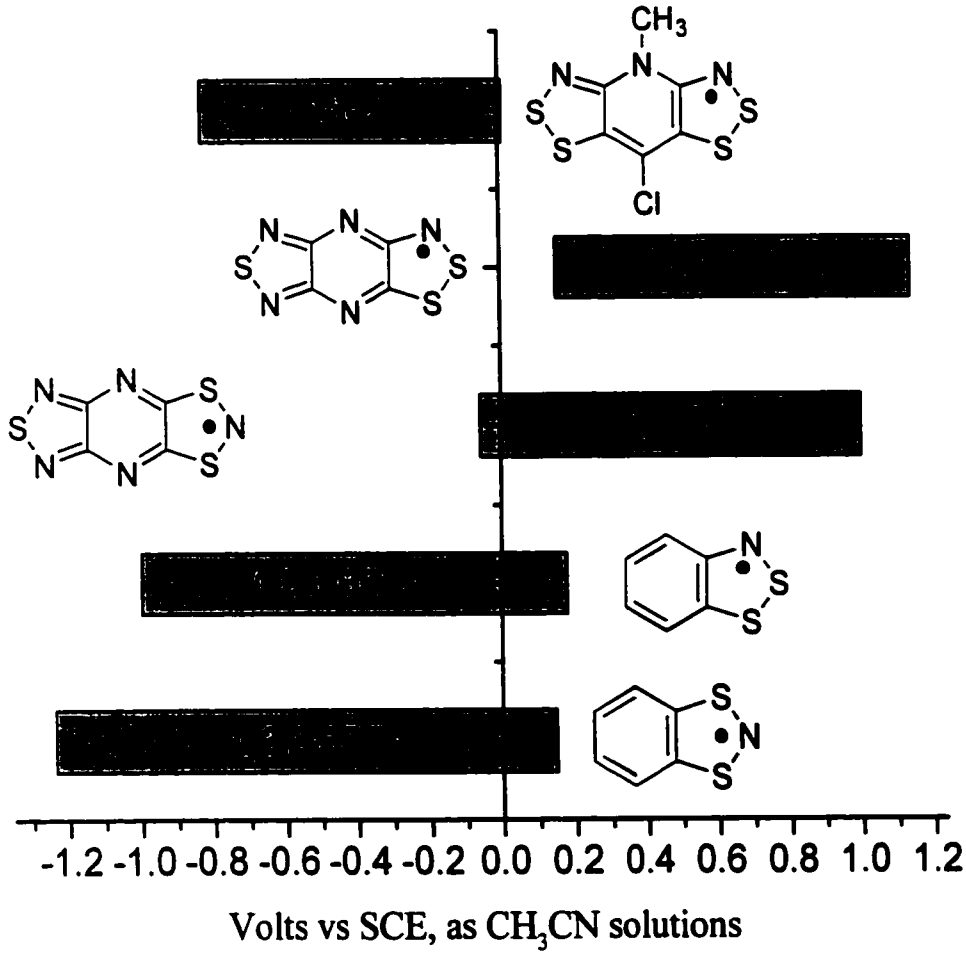

Figure 6.19 Comparison of the IP-EA values of a series of neutral radical dithiazoles by cyclic voltammetry.

---

† This is not a problem in terms of designing a conductor. Electronegative metals, such as $(SN)_x$, are known. The potential difficulties lie in the stability and ease of handling such materials.

To summarize Chapter 6, a ring-fused benzo-bis-(1,2,3-DTA) for which a quinoid-like closed shell ground state is not possible in the neutral oxidation state has been prepared in the radical cation oxidation state, and characterized by ESR. Whether **VI-4** exists as a diradical or closed shell zwitterion in the neutral oxidation state has not been confirmed. Attempts to prepare the analogous pyridine-based ring system, **VI-5**, yielded the protonated closed shell cation [**VI-6**][Cl]. Calculations of the IP-EA values for the neutral radical **VI-6** suggest that this compound may be a promising design for a neutral radical conductor. Further work involving the synthesis of the methylated species, **VI-21**, shows encouraging solution IP-EA values according to cyclic voltammetry.

6.5 Syntheses

N, *N'*-Dichlorourea[19] was prepared according to literature procedure (see Appendix A).

6.5.1 Synthesis of 4,6-diamino-1,3-dithiocyanobenzene:[20, 21] Freshly prepared *N*, *N'*-dichlorourea (3.547 g, 27.51 mmol) dissolved in 35 mL glacial acetic acid was added, dropwise, to a solution of *m*-phenylenediamine (2.987 g, 27.62 mmol) and ammonium thiocyanate (4.225 g, 55.50 mmol) in 50 mL glacial acetic acid, maintaining a temperature within 12° - 18° C. The resulting dark green solution was stirred, warming to RT, for 30 m as a white precipitate formed. The reaction mixture was poured onto 500 mL ice-water and the grey precipitate was collected by filtration, washed copiously with water, and dried by suction in air for 2 h. Once the precipitate could be removed from the filter paper, it was recrystallized in 125 mL hot ethanol, generating white crystals; yield 3.998 g (17.99 mmol, 65 %); mp 168° - 174° C (lit. 172° C). IR: 3457 (m), 3360 (s), 2152 (s), 1620 (s), 1534 (m), 1480 (m), 1334 (w), 1307 (w), 1273 (m), 1007 (w), 915 (m), 843 (m), 747 (w), 710 (w), 667 (m), 550 (w), 484 (m) cm^{-1}.

6.5.2 Synthesis of 4-6-diaminobenzene-1,3-dithiol, VI-12:[17] A slurry of 4,6-diamino-1,3-dithiocyanobenzene (4.066 g, 18.29 mmol) and sodium sulfide nonahydrate (17.580 g, 73.195 mmol) in 50 mL degassed water was refluxed until a yellow/brown solution formed (*ca.* 30 m). This was then cooled on ice and 175 mL of degassed glacial acetic acid was added SLOWLY, keeping the temperature near 5° C. A pale yellow precipitate was generated from the vigorous, exothermic reaction. This was collected by filtration, washed with 15 mL cold, degassed methanol and dried *in vacuo*; crude yield 2.636 g (15.30 mmol, 84 %). IR: 3421 (m), 3321 (m), 2489 (m), 2050 (m), 1710 (w), 1598 (vs), 1544 (w), 1325 (w), 1292 (w), 1265 (m), 885 (w), 839 (s), 746 (w), 679 (w), 632 (w), 612 (w), 453 (m) cm^{-1}. MS (*m/e*): 172 (M^+, 19 %), 140 ($[M-N_2H_4]^+$, 49 %)

6.5.3 Synthesis of 3,6-dichlorobenzo[1,2-*d*:5,4-*d'*]bis(1,2,3-dithiazolylium) chloride, [VI-4c][Cl]: Sulfur dichloride (10 mL) was added, dropwise, to a slurry of **VI-12** (1.047 g, 6.078 mmol) in dry acetonitrile (20 mL), on ice, resulting in a highly exothermic reaction characterized by an almost immediate blackening of the mixture. This was left to stir for 90 m at RT before the black solid product was collected by filtration, washed with 20 mL of acetonitrile, and dried *in vacuo*; crude yield 0.908 g (2.71 mmol, 45 %). IR: 1607 (m), 1442 (s), 1268 (m), 1132 (m), 1056 (m), 889 (w), 830 (m), 797 (m), 768 (m), 746 (m), 700 (m), 659 (m), 532 (m), 491 (m) cm^{-1}.

6.5.4 Synthesis of 3,6-dichlorobenzo[1,2-*d*:5,4-*d'*]bis(1,2,3-dithiazolylium) tetrachloro-aluminate, [VI-4c][$AlCl_4$]: Crude **[VI-4c]**[Cl] (0.908 g, 2.71 mmol) and aluminum trichloride (0.402 g, 3.01 mmol) were stirred together in 7 mL of SO_2(l) for 30 m to afford bronze crystals of **[VI-4c]**[$AlCl_4$]. These were collected by filtration and dried *in vacuo*, whereupon the crystals became metallic green; yield 0.395 g (0.844 mmol, 31.1 %). IR: 1435 (s), 1408 (m), 1333 (s),

1264 (m), 1144 (w), 1075 (w), 962 (s), 843 (m), 804 (m), 769 (s), 709 (m), 662 (m), 578 (w), 534 (w), 509 (m), 477 (s), 470 (w) cm^{-1}. ESR (SO_2): g 2.0073; a_N 4.3, a_{35Cl} 0.9, a_{37Cl} 0.7 gauss.

6.5.5 Synthesis of 2,6-diamino-3,5-bis(thiocyano)pyridine, VI-14: A solution of freshly prepared *N,N'*-dichlorourea (15.009 g, 116.39 mmol) in 100 mL glacial acetic acid was added, dropwise over 15 m, to a solution of 2,6-diaminopyridine (12.782 g, 117.13 mmol) and ammonium thiocyanate (17.854 g, 234.55 mmol) in 250 mL glacial acetic acid maintained at 12° - 18° C. This mixture was stirred for 30 m at RT to afford a white precipitate, then poured onto 1.5 L ice-water. The resulting grey precipitate was collected by filtration, washed with 3 x 50 mL water, and dried in air. The product was recrystallized from hot ethanol as white flakes; yield 3.415 g (15.30 mmol, 13 %); IR: 3494 (m), 3429 (m), 3381 (m), 3325 (w), 3140 (m, br), 2152 (s), 1659 (s), 1629 (s), 1601 (s), 1561 (s), 1540 (s), 1249 (w), 953 (w), 756 (m), 663 (w), 573 (w), 490 (m), 458 (w) cm^{-1}. ^1H NMR (δ, DMSO): 7.87 (s, aromatic), 6.95 (s, amino). MS (*m/e*): 223 (M^+, 48 %), 197 ($[M-CN]^+$, 10 %), 165 ($[M-SCN]^+$, 86 %).

6.5.6 Synthesis of 2,6-diamino-3,5-dithiolpyridine, VI-15: A slurry of 2,6-diamino-3,5-bis(thiocyano)pyridine (3.120 g, 13.97 mmol) and sodium sulfide nonahydrate (14.88 g, 61.95 mmol) were warmed in 40 mL degassed water for 45 m. The resulting yellow-brown solution was cooled on ice, and to this was slowly added 50 mL degassed glacial acetic acid. The product 2,6-diamino-3,5-dithiolpyridine **VI-15** precipitated as a yellow solid and was collected by filtration, washed with 25 mL of cold methanol, and dried *in vacuo*; crude yield 4.88 g. IR: 3429 (m), 3325 (m, br), 2473 (w), 1694 (s), 1654 (s), 1613 (s, br), 1402 (s), 1329 (w), 1294 (m), 1255 (m), 655 (w), 637 (w), 611 (w), 453 (m) cm^{-1}. For the purpose of easy purification, the material was converted to the hydrochloride salt **VI-16** by stirring in 50 mL of 4 M hydrochloric acid. The

yellow product was recrystallized in 75 mL hot ethanol to afford yellow crystalline blocks; yield 1.667 g (6.771 mmol, 48 % based on the assumption that the product is, on average, the dihydrochloride salt†). IR: 3413 (m), 3269 (m), 3149 (m), 3021 (w), 2724 (w), 2436 (w), 2388 (m), 1642 (s), 1586 (s), 1325 (w), 1292 (s), 1265 (s), 1123 (w), 1044 (w), 964 (w), 852 (m), 756 (w), 634 (m), 559 (w), 507 (m, br), 435 (m) cm^{-1}. MS (*m/e*): 173 (M^+, 100 %).

6.5.7 Synthesis of 4-chloro-1-imidopyridine[2,3-*d*:6,5-*d'*]bis(1,2,3-dithiazolium) chloride, [VI-6][Cl]: 2,6-diamino-3,5-dithiolpyridine dihydrochloride **VI-16** (0.251 g, 1.02 mmol) and excess sulfur monochloride (2 mL) were refluxed overnight in 8 mL chlorobenzene, under inert atmosphere. The reaction mixture was cooled to RT and the resulting purple-black powder was collected by filtration, washed with 10 mL CH_2Cl_2, and dried *in vacuo*; crude yield 0.30 g (0.99 mmol, 97 % based on the assumption that the starting material is, on average, the dihydrochloride salt†); dec 186° C. IR: 3084 (vw), 2741 (vw), 1655 (w), 1624 (w), 1507 (m), 1328 (s), 1105 (m), 842 (vw), 831 (s), 761 (s), 721 (w), 708 (w), 665 (s), 630 (s), 519 (m), 501 (w), 480 (s) cm^{-1}. MS (*m/e*): 266 (M^+, 35 %), 265 ($[M-H]^+$, 92 %).

6.5.8 Synthesis of 4-chloro-1-imidopyridine[2,3-*d*:6,5-*d'*]bis(1,2,3-dithiazolium) hexafluoroantimonate, [VI-6][SbF_6]: Silver hexafluoroantimonate (0.487 g, 1.42 mmol) and [VI-6][Cl] (0.383 g, 1.27 mmol) were stirred in 10 mL of SO_2 for 2 h to afford a turquoise solution with white AgCl precipitate. The solution was filtered and from it grew gold crystalline blocks. More crystals, suitable for X-ray structural determination were grown by concentrating the solution by slow evaporation. These were collected by filtration and dried *in vacuo*; yield 0.434

† There are three possible positions for protonation available in this compound. For the synthesis of [VI-6][Cl] it is not necessary to know the exact formula weight of this salt since a large excess of sulfur monochloride is employed.

g (0.864 mmol, 68 %). IR: 3259 (w), 1660 (w), 1548 (w), 1329 (s), 1103 (m), 1030 (w), 949 (w), 841 (s), 725 (w), 716 (w), 668 (s), 653 (s), 637 (m), 558 (w), 522 (m), 472 (s) cm^{-1}. MS (*m/e*): 266 (M^+, 5 %), 265 ($[M-H]^+$, 34 %). Anal. Calcd. for $C_5HClF_6N_3S_4Sb$: C, 11.95; N, 8.36 %. Found: C, 12.16; N, 8.50 %.

6.5.9 Synthesis of 4-chloro-1-imidopyridine[2,3-*d*:6,5-*d'*]bis(1,2,3-dithiazolium) iodide, [VI-6][I]: Tetra-*n*-butylammonium iodide (0.390 g, 1.06 mmol) and **[VI-6]**[SbF_6] (0.508 g, 1.01 mmol) were stirred in 10 mL of dry acetonitrile to get an almost instant colour change of the solution from blue to pale green and of the gold/copper **[VI-6]**[SbF_6] to a black powder. This was stirred for 30 m, then the black solid was collected by filtration, washed with 20 mL acetonitrile, and dried *in vacuo*; crude yield 0.266 g (0.767 mmol, 76 %); dec > 150° C. IR: 3077 (vw), 2722 (vw), 1632 (w, br), 1515 (m), 1318 (s), 1095 (m), 836 (m), 760 (s), 720 (m), 659 (w), 628 (m), 517 (w), 471 (m) cm^{-1}.

6.5.10 Synthesis of 4-chloro-1-imidopyridine[2,3-*d*:6,5-*d'*]bis(1,2,3-dithiazolium) tetrachloroaluminate, [VI-6][$AlCl_4$]: **[VI-6]**[Cl] (1.316 g, 4.369 mmol) and aluminum trichloride (0.660 g, 4.95 mmol) were stirred in 10 mL thionyl chloride for 1 h to afford a deep green solution and a microcrystalline precipitate. The latter was collected by filtration and dried *in vacuo*; yield 1.771 g (4.066 mmol, 93 %). IR: 3181 (w), 3055 (vw), 1671 (m), 1518 (w), 1345 (s), 1118 (s), 842 (s), 768 (s), 722 (w), 679 (m), 638 (s), 532 (w), 495 (s, br) cm^{-1}.

6.5.11 Synthesis of 4-chloro-1-imidopyridine[2,3-*d*:6,5-*d'*]bis(1,2,3-dithiazolium) tetrachlorogallate, [VI-6][$GaCl_4$]: **[VI-6]**[Cl] (0.601 g, 1.99 mmol) and gallium trichloride (0.416 g, 2.36 mmol) were stirred in 10 mL sulfur dioxide for 1 h to afford a microcrystalline

precipitate. The latter was collected by filtration, washed with SO_2, and dried *in vacuo*; yield 0.650 g (1.36 mmol, 68 %). IR: 3187 (w), 3055 (vw), 1661 (vw), 1534 (w), 1349 (s), 1121 (s), 840 (s), 771 (s), 712 (w), 681 (m), 633 (s), 527 (m), 470 (s) cm^{-1}. MS (*m/e*): 266 (M^+, 6 %)

References for Chapter 6

1. Genin, H.; Hoffman, R.; *Macromolecules*, **1998**, *31*, 444.
2. Frisch, M. J.; Trucks, G. W.; Schlegel, H. B.; Scuseria, G. E.; Robb, M. A.; Cheeseman, J. R.; Zakrzewski, V. G.; Montgomery Jr., J. A.; Stratmann, R. E.; Burant, J. C.; Dapprich, S.; Millam, J. M.; Daniels, A. D.; Kudin, K. N.; Strain, M. C.; Farkas, O.; Tomasi, J.; Barons, V.; Cossi, M.; Cammi, R.; Mennucci, B.; Pomelli, C.; Adamo, C.; Clifford, S.; Ochterski, J.; Petersson, G. A.; Ayala, P. Y.; Cui, Q.; Morokuma, K.; Malick, D. K.; Rabuck, A. D.; Raghavachari, K.; Foreman, J. B.; Cioslowski, J.; Ortiz, J. V.; Stefanov, B. B.; Liu, G.; Fox, D. J.; Keith, T.; Al-Laham, M. A.; Peng, C. Y.; Nanayakkara, A.; Wong, M. W.; Andres, J. L.; Gonzalez, C.; Head-Gordon, M.; Repogle, E. S.; Pople, J. A.; *Gaussian 98*, Revision A:6. Gaussian, Inc.: Pittsburg, PA, **1998**.
3. Hutchison, K.; Srdanov, G.; Hicks, R.; Yu, Huinan; Wudl, F.; Strassner, T.; Nendel, M.; Houk, K. N.; *J. Am. Chem. Soc.*, **1998**, *120*, 2989.
4. Hutchison, K. A.; Hasharoni, K.; Wudl, F.; Berg, A.; Shuali, Z.; Levanon, H.; *J. Am. Chem. Soc.*, **1998**, *120*, 6362.
5. Hoffmeyer, R. E.; Chan, W.-T.; Goddard, J. D.; Oakley, R. T.; *Can. J. Chem.*, **1988**, *66*, 2279.
6. Boeré, R. T.; Fait, J.; Larsen, K.; Yip, J.; *Inorg. Chem.*, **1992**, 1417.
7. Barclay, T. M.; Cordes, A. W.; Goddard, J. D.; Mawhinney, R. C.; Oakley, R. T.; Preuss, K. E.; Reed, R. W.; *J. Am. Chem. Soc.*, **1997**, *119*, 12136.
8. Barclay, T. M.; Cordes, A. W.; Oakley, R. T.; Preuss, K. E.; Reed, R. W.; *Chem. Mater.*, **1999**, *11*, 164.
9. Huestis, L. D.; Walsh, M. L.; Hahn, N.; *J. Org. Chem.*, **1965**, *30*, 2763.

10. Unpublished work by G. W. Patenaude, Oakley group, University of Guelph, **1996**.

11. Jorgensen, J.; Ph.D. Thesis, University of Wisconsin-Madison, **1981**. (As cited in Wellman, D. E.; Lassila, K. R.; West, R.; *J. Org. Chem.*, **1984**, *49*, 965.)

12. Boeré, R. T.; *Coord. Chem.*, in press, **2000**.

13. Bechgaard, K.; Parker, V. D.; Pedersen, C. Th.; *J. Am. Chem. Soc.*, **1973**, *95*, 4373.

14. Haddon, R. C.; Wudl, F.; Kaplan, M. L.; Marshall, J. H.; Cais, R. E.; Bramwell, F. B.; *J. Am. Chem. Soc.*, **1978**, *100*, 7629.

15. Staab, H. A.; Saupe, T.; *Angew. Chem. Int. Ed. Engl.*, **1988**, *27*, 865.

16. Lide, D. R. Ed.; *CRC Handbook of Chemistry and Physics*, CRC Press, **1992**, 10 -211.

17. Hotop, H.; Lineberger, W. C.; *J. Phys. Chem. Ref. Data*, **1985**, *14*, 731.

18. (a) Kertész, M.; Vonderviszt, F.; *J. Am. Chem. Soc.*, **1982**, *104*, 5889. (b) Bolton, B. A.; Prasad, P. N.; *Mol. Cryst. Liq. Cryst.*, **1981**, *76*, 309. (c) Marks, T. J.; Kalina, D. W.; *Ext. Linear Chain Cmpds 1*, **1982**, 197.

19. Chattaway, F. D.; *Chem. News*, **1908**, 285.

20. Lochon, P.; Méheux, P.; Néel, J. *Bull. Soc. Chim. Fr.*, **1967**, *11*, 4387.

21. Okada, M.; Marvel, C. S.; *J. Polym. Sci., Pt A-1*, **1968**, *6*, 1259.

Appendix A. General Experimental Section

A.1 Source of Starting Materials

A.1.1 Purchased chemicals that were used as received

acetic acid, glacial	(Fisher)
acetic anhydride, reagent grade	(Fisher)
acetone, reagent grade	(Fisher)
Adogen®464	(Aldrich)
aluminum trichloride, 99 %	(Aldrich)
aminothiophenol, 2- , 99 %	(Aldrich)
ammonia gas	(Matheson)
ammonium hydroxide	(Fisher)
ammonium thiocyanate	(Fisher)
argon gas	(Praxair)
benzyl cyanide, 98 %	(Aldrich)
bithiophene, 2,2'-	(Aldrich)
bromine	(Fisher)
N-bromosuccinimide	(Fisher)
n-butyllithium, 1.6 M in hexane	(Aldrich)
carbon disulfide	(Fisher)
carbon, decolorizing neutral	(Fisher)
chlorine gas	(Matheson)
chloroacetonitrile	(Aldrich)
chloroform, reagent grade	(Fisher)

chloroform-*d*	(Isotec)
chlorotrimethylsilane, 98 %	(Aldrich)
chloropyrazine, 2-	(Acros)
cyanogen bromide	(Aldrich)
cyanophenol, *p*-	(Aldrich)
cyanothiophene, 2-	(Aldrich)
diaminopyridine, 2,6-	(Aldrich)
dibromoethane, 1,2-	(Aldrich)
dimethylformamide, reagent grade	(Fisher)
dimethylsulfoxide-*d*	(Isotec)
ethyl acetate, reagent grade	(Fisher)
ethanol, 95 %	(Fisher)
ferric chloride, anhydrous	(Fisher)
gallium trichloride, anhyrdous, beads, -10 mesh, 99.99%	(Aldrich)
hexamethyldisilazane	(Petrarch)
hexanes	(Fisher)
hexylthiophene, 3-	(Aldrich)
hydrazine, 35 % in water	(Aldrich)
hydrazine, anhydrous, 98 %	(Aldrich)
hydrochloric acid, 12 M	(Fisher)
hydroxylamine hydrochloride	(MCB)
iodine trichloride	(Aldrich)
iodobenzene	(Aldrich)
lithium bis(trimethylsilyl)amide, 97 %	(Aldrich)

methanol	(Fisher)
methylthiophene, 3-	(Aldrich)
nitrogen gas	(In-house supply)
nitrosonium hexafluoroantimonate	(Strem)
nitrosonium hexafluorophosphate	(Strem)
nitrosonium tetrafluoroborate	(Strem)
oxygen gas	(Matheson)
pentafluorobenzonitrile, 2,3,4,5,6-	(Aldrich)
pentane, reagent grade	(Fisher)
phenol	(Aldrich)
phenylenediacetonitrile, 1,4-	(Aldrich)
phenylenediamine, 1,3- , pellets, 99+ %	(Aldrich)
phenylenediamine, 1,4- , flakes, 97 %	(Aldrich)
phosphorous pentachloride	(Aldrich)
phosphorous pentoxide	(Fisher)
potassium hydroxide, pellets, 99.99 %	(Aldrich)
potassium phthalimide	(Aldrich)
pyridine	(Fisher)
selenium powder, -100 mesh, 99.5+ %	(Aldrich)
silica gel 60, 230 - 400 Mesh	(Mallinckrodt)
silver hexafluoroantimonate	(Aldrich)
silver hexafluorophosphate	(Aldrich)
silver tetrafluoroborate	(Aldrich)
sodium	(BDH laboratories)

sodium acetate trihydrate	(Fisher)
sodium bicarbonate	(Fisher)
sodium carbonate	(Fisher)
sodium hydrogen sulfite	(Aldrich)
sodium sulfate	(Aldrich)
sodium sulfide nonahydrate	(Aldrich)
sulfur dioxide, anhydrous gas	(Matheson)
sulfur monochloride	(Aldrich)
tetra-*n*-butyl ammonium chloride, 96 %	(Aldrich)
tetra-*n*-butyl ammonium fluoride, 1.0 M in THF	(Aldrich)
tetra-*n*-butyl ammonium iodide, 98 %	(Aldrich)
tetracyanoethyleneoxide	(Aldrich)
triethylamine, 99 %	(Aldrich)
triphenylantimony, 99 %	(Aldrich)
urea	(Fisher)

A.1.2 Purchased chemicals that were purified prior to use

acetonitrile (Caledon) - distilled from P_2O_5

benzonitrile (Alrich) - distilled from P_2O_5

chlorobenzene (Fisher) - distilled from P_2O_5

dichloroethane, 1,2- (Fisher) - distilled from P_2O_5

dichloromethane (Fisher) - distilled from P_2O_5

tetrachloroethane, 1,1',2,2'- (Aldrich) - distilled from P_2O_5

tetrahydrofuran (Caledon) - distilled from lithium aluminum hydride

thionyl chloride (Aldrich) - distilled from linseed oil

toluene (Fisher) - distilled from sodium

A.1.3 Commonly used chemicals that were synthesized "In-House"

A.1.3.1 Lithium bis(trimethylsilyl)amide monoetherate, $LiN(SiMe_3)_2 \cdot Et_2O$

Lithium bis(trimethylsilyl)amide (250 g, 1.49 mol) was dissolved in 600 mL of warm hexanes under inert atmosphere. Dry diethyl ether (250 mL, 2.4 mol) was added *without* stirring, over a 45 m period, taking care to keep the exothermic reaction controlled. The reaction mixture was cooled to RT and large, white, hexagonal crystals precipitated. The mixture was cooled at -10 °C for a further 18 h. The solid was collected by filtration, washed with hexanes, and dried *in vacuo*; yield 85 - 90 %; mp 108 - 110 °C. ^{1}H NMR (δ, C_6D_6): 3.40 (q, CH_2O), 0.98 (t, CH_3CH_2), 0.27 (s, CH_3Si). Anal. calcd. for $C_{10}H_{28}LiNOSi_2$: C, 49.75; H, 11.69; N, 5.80 %. Found: C, 49.58; H, 11.90; N, 6.00 %.

A.1.3.2 Sulfur Dichloride, SCl_2

Chlorine gas was bubbled through 50 mL of sulfur monochloride, containing approx. 250 mg of iron trichloride, on ice, for 15 m. The reaction mixture was stirred, cold, for a further 1 h, then it was allowed to warm to RT. The product sulfur dichloride was distilled from the reaction mixture under inert atmosphere; yield 40 - 50 mL; bp 55 -60 °C. The red liquiud product was stored at -10 °C and used within 4 days of preparation.

A.1.3.3 Selenium Tetrachloride

Selenium powder (22.0 g, 0.28 mol) was slurried in 250 mL of dry acetonitrile, cooled on ice. Chorine gas was passed over, but not into, the slurry eventually yielding a white precipitate. The product was collected by filtration, washed well with acetonitrile, and dried *in vacuo*; yield 50 - 55 g (81 - 89 %). This air-sensitive solid was stored in the dry box and stable for over a year.

A.1.3.4 Iodobenzene Dichloride

Chlorine gas was bubbled through a solution of iodobenzene (8.9 g, 44 mmol) in 40 mL of dry methylene chloride, on ice, for 15 m. The reaction mixture was allowed to warm to RT to drive off the excess dissolved chlorine gas. It was then cooled again to 0 °C to precipitate yellow needle-like crystals. The product was collected by filtration under inert atmosphere, washed with 1 x 15 mL of cold methylene chloride, and dried *in vacuo*; yield 9.8 g (35 mmol, 81 %). The product was stored at -10 °C and used within 4 days of preparation.

A.1.3.5 *N,N'*-Dichlorourea

Urea (20 g, 0.33 mol) was dissolved in 40 mL of water and cooled in an ethanol / ice bath to -15 °C. Chlorine gas was bubbled rapidly through the solution, kept cold, for 30 m. The white precipitate was collected by filtration, washed with 2 x 20 mL of cold water, and immediately dried *in vacuo* for 24 h; yield 3.547 g (27.50 mmol, 8.3 %).

A.1.3.6 Phenylcyanate[1]

A solution of phenol in a 2:5 mixture of anhydrous ether and *n*-pentane was cooled in an ice bath. A molar equivalent of cyanogen bromide was added, with stirring. A molar equivalent of triethylamine was then added, dropwise, with vigourous stirring, taking care not to let the

temperature of the reaction mixture rise above 30 °C. The reaction mixture was then stirred for 1h at 0 °C. The white precipitate was collected by filtration. The phenylcyanate product was separated from the triethylamine hydrobromide byproduct by extraction with *n*-pentane. The product was distilled from the combined extracts. The literature yield is 80 %; bp 60 °C at 4 torr. The product must be stored at - 20 °C.

A.2 Procedures and Techniques

A.2.1 General

Many of the reactions and manipulations were performed under an inert atmosphere of either nitrogen or argon gas. Those reactions carried out in solution were handled by standard or modified Schlenk techniques using a double-manifold glass vacuum line (nitrogen / vacuum) with an Edwards E2M series rotary vacuum pump. Air sensitive solids were handled and stored in an argon- or nitrogen- filled Braun MB-150M drybox.

A.2.2 Handling of Sulfur Dioxide

Sulfur dioxide, used as a solvent for many of our reactions, must be transferred into the reaction vessel by condensation of SO_2 gas using liquid nitrogen. In order to keep the SO_2 liquid, the reaction vessel must be sealed under the solvent's vapour pressure at room temperature (ca. 3 atm.). Furthermore, it is often desirable to be able to filter the reaction mother liquor away from the solid product and to subsequently wash this product with clean solvent. The thick glass h-cells used for all our SO_2 reactions permit these manipulations (**Figure A.1**).

The reagents can be loaded into either arm of the h-cell. The SO_2 is condensed into the permanent arm of the evacuated cell and the rotoflo valve is closed. The SO_2 thaws as it is warmed to room temperature and the cell is now under pressure. The cell may be safely warmed to

approximately 60°C at which point the SO_2 vapour pressure is ca. 5 atmospheres. The glass frit between arms permits filtering of the reaction mixture. This is generally accomplished by slightly warming one cell arm with one's hand and slightly cooling the other in liquid nitrogen in order to create a pressure difference. Clean SO_2 can be condensed from one cell arm to another by vigourously cooling one side with liquid nitrogen. In this manner, desired precipitates may be washed with clean solvent multiple times. Finally, the removable arm of the h-cell permits various manipulations during the course of a reaction given that the SO_2 is either frozen or removed prior to opening the reaction vessel.

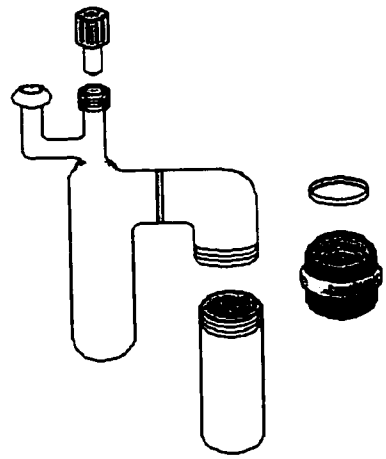

Figure A.1 Schematic representation of an h-cell.

A.2.3 Gradient Furnace Sublimations

In order to obtain X-ray diffraction structures of many of the products presented herein, it is necessary to obtain high quality single crystals. Vacuum sublimation in a three temperature zone programmable tube furnace yields well-formed crystals of many of these compounds (**Figure A.2**).

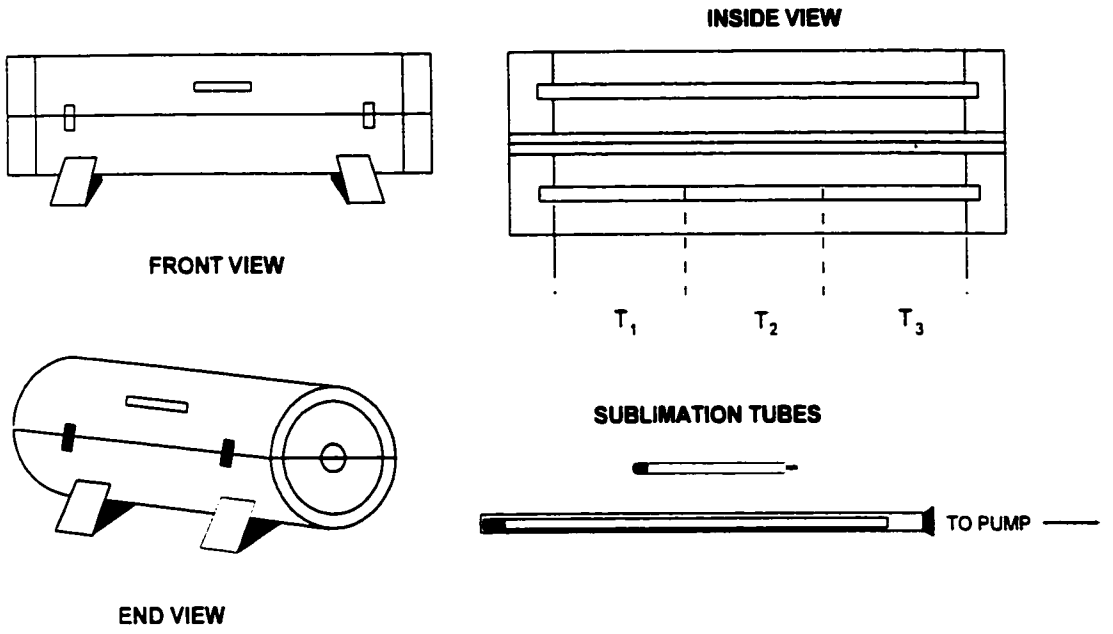

Figure A.2 Three-zone temperature gradient furnace.

A.2.4 Electrocrystallization

Many of the charge transfer salts we have synthesized are best obtained by electrocrystallization. A closed circuit containing an adjustable constant current supply (0.1 to 20 μA), a solution of the neutral material plus an electrolyte, and a solution of electrolyte alone can be employed to this end. The solvent must be chosen such that the neutral material is sufficiently soluble that it is in contact with the anode and that the product radical cation salt be insoluble allowing crystal growth. The electrolyte provides the counterion for the radical cation salt and therefore must be chosen judiciously. The H-cell design for this electrosynthesis is shown in **Figure A.3**. A fine glass frit connects the anodic and cathodic compartments allowing for solvent and ion diffusion. The two compartments are also bridged near the top of the H-cell to allow pressure equilibration. A rotoflo valve permits flushing of the cell with an inert gas. The electrodes are platinum wires that extend through a glass tube such that contact can be made on the outside

by dropping a steel rod down the tube while the other end of the wire sits immersed in the solution. The charge transfer salt crystals grow on the anodic platinum electrode.

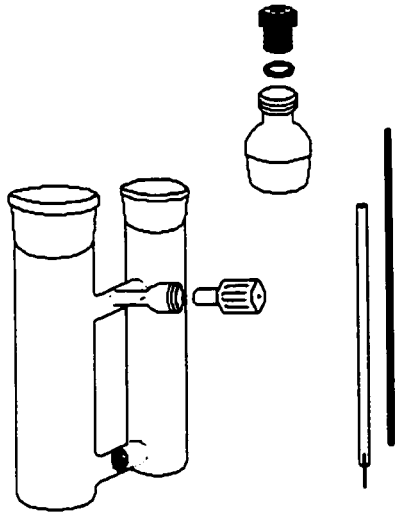

Figure A.3 Schematic representation for an electrosynthesis H-cell.

A.3 Instrumentation

X-ray data were collected by A. W. Cordes *et al.*, at the University of Arkansas, on an ENRAF-Nonius CAD-4 diffractometer with monochromated Mo $K\alpha$ radiation. Crystals were mounted on glass fibers with silicone or epoxy. Data were collected using a $\theta/2\theta$ technique. The structures were solved using direct methods and refined by full-matrix least squares which minimized $\Sigma w(\Delta F)^2$.

Magnetic susceptibility and conductivity measurements were performed by R. C. Haddon *et al.*, at the University of Kentucky. The magnetic susceptibilities were measured over the temperature range 5 - 350 K on a George Associates Faraday balance operating at 0.5 T. Conductivities were measured in a helium variable-temperature probe using a LakeShore 340 temperature controller. A Keithley 236 unit was used as a voltage source and current meter, and

two 6517A Keithley electrometers were used to measure the voltage drop between the potential leads in a four-probe configuration.

Ab initio calculations were run on a Pentium II workstation using the B3LYP DFT method available in the Gaussian 98W suite of programs[2]. Geometries were optimized using a 6-31G** basis set, within the constraints of appropriate symmetry.

Cyclic voltammetry was performed on dry acetonitrile or dichloroethane solutions containing 0.1 M tetra-*n*-butylammonium hexafluorophosphate. The two instruments employed were a PAR 273A electrochemical system (EG&G Instruments) and a PINE Bipotentiostat, Model AFCBP1. Scan rates of 50 - 100 mV s^{-1} were employed. Potentials were scanned from -2.5 to 2.0 V with respect to the quasireference electrode in a single compartment cell fitted with Pt electrodes and referenced to the ferrocenium / ferrocene couple at 0.38 V *vs.* SCE in CH_3CN (0.48 V *vs.* SCE in CH_2Cl_2).[3]

Elemental analyses were performed by MHW Laboratories, Pheonix, AZ.

Infrared spectra were recorded (at 2 cm^{-1} resolution) as Nujol mulls on KBr plates, unless otherwise specified. A Nicolet Avatar infrared spectrometer was employed.

Low resolution mass spectra (70 eV, EI, DEI and CI, DCI) were run on the following machines: a Finnigan 4500 quadrupole mass spectrometer at the McMaster Regional Centre for Mass Spectrometry, a Kratos MS 890 instrument using the MASPEC system [msw/95D5] at the University of Guelph, and a VG Analytical 7070E at the University of Waterloo.

The X-band ESR spectra were recorded using a Varian E-109 spectrometer with DPPH as a field marker.

UV-visible spectra were recorded on a Perkin-Elmer Lambda 6 spectrometer.

References for Appendix A

1. Zweifel, G.; Murray, R. E.; *Synthesis*, **1980**, 150.

2. Frisch, M. J.; Trucks, G. W.; Schlegel, H. B.; Scuseria, G. E.; Robb, M. A.; Cheeseman, J. R.; Zakrzewski, V. G.; Montgomery Jr., J. A.; Stratmann, R. E.; Burant, J. C.; Dapprich, S.; Millam, J. M.; Daniels, A. D.; Kudin, K. N.; Strain, M. C.; Farkas, O.; Tomasi, J.; Barons, V.; Cossi, M.; Cammi, R.; Mennucci, B.; Pomelli, C.; Adamo, C.; Clifford, S.; Ochterski, J.; Petersson, G. A.; Ayala, P. Y.; Cui, Q.; Morokuma, K.; Malick, D. K.; Rabuck, A. D.; Raghavachari, K.; Foreman, J. B.; Cioslowski, J.; Ortiz, J. V.; Stefanov, B. B.; Liu, G.; Fox, D. J.; Keith, T.; Al-Laham, M. A.; Peng, C. Y.; Nanayakkara, A.; Wong, M. W.; Andres, J. L.; Gonzalez, C.; Head-Gordon, M.; Repogle, E. S.; Pople, J. A.; *Gaussian 98*, Revision A:6. Gaussian, Inc.: Pittsburg, PA, **1998**.

3. Boeré, R. T.; Moock, K. H.; Parvez, M. Z.; *Anorg. Allg. Chem.*, **1994**, *620*, 1589.

Appendix B: Crystallographic Data

compd.	**II-4g**	**II-28**
formula	$C_{10}H_6N_4S_4$	$C_{16}H_3BrN_8S_4$
f.wt.	310.42	515.42
space group	$P2_1/c$	$P\bar{1}$
Z	2	2
V, Å^3	622.80(13)	955.48
d_{calc}, g·cm^{-3}	1.66	1.791
R	0.035	not fully refined
R_w	0.059	not fully refined
a, Å	6.9888(10)	9.1154
b, Å	5.6836(5)	10.3767
c, Å	16.019(2)	10.5985
α, deg	90.0	101.83
β, deg	101.822(11)	101.53
γ, deg	90.0	93.75
temp, K	293	293
mean d(SN), Å	1.5555(30)	1.56(1)
mean $d(NC)_{ring}$, Å	1.3265(40)	1.31(2)
mean $d(C_{ring}C)$, Å	1.466(4)	1.47(1)
mean ∠(NSN), °	126.60(16)	125.6(4)
mean ∠(SNC), °	141.65(30)	141.1(7)

compd.	**III-15b**	**III-16b**	**[III-16b][PF_6]**
formula	$C_{10}H_4N_4S_4Cl_2$	$C_4N_4S_4Cl_2$	$C_4N_4S_4Cl_2PF_6$
f.wt.	379.34	303.24	448.21
space group	$P2_1/n$	*Pbca*	*C2/c*
Z	2	4	4
V, Å^3	692.74(16)	975.4(3)	1445.4(9)
R	0.027	0.023	0.062
R_w	0.034	0.047	0.086
a, Å	3.9477(6)	5.1469(15)	11.699(4)
b, Å	23.790(3)	13.343(2)	12.753(5)
c, Å	7.3769(9)	14.203(17)	10.461(4)
α, deg	90.0	90.0	90.0
β, deg	90.793(12)	90.0	112.17(1)
γ, deg	90.0	90.0	90.0
temp, K	293	293	293
mean d(CS), Å	1.7859(18)	1.7402(16)	1.713(4)
mean d(SS), Å	2.0780(7)	2.0865(7)	2.0391(17)
mean d(SN), Å	1.6577(16)	1.6467(16)	1.616(4)
mean $d(NC)_{ring}$, Å	1.2708(24)	1.2690(21)	1.305(6)
mean $d(C_{ring}N_{bridge})$, Å	1.2691(25)	1.2994(20)	1.325(5)
mean d(NN), Å	n/a	1.381(3)	1.330(7)
mean ∠(SSN), °	97.58(6)	98.12(5)	99.04(16)
mean ∠(SNC), °	116.71(13)	115.77(12)	115.3(3)
mean ∠(NNC), °	n/a	111.44(13)	112.7(3)

compd.	**III-17b**	**[III-17b][BF_4]**	**[III-17b][ClO_4]**	**[III-17b][FSO_3]**
formula	$S_4Cl_2N_2C_4$	$S_4Cl_2F_4BN_2C_4$	$S_4Cl_3O_4N_2C_4$	$S_5Cl_2FO_3N_2C_4$
f.wt.	275.20	362.00	374.65	358.26
space group	$P2_1/c$	$P2_1/n$	$P2_1/n$	$P2_1/n$
Z	2	4	4	4
V, Å^3	425.76(14)	1107.6(5)	1132.6(4)	1143.8(3)
d_{calc}, g·cm^{-3}	2.15	2.17	2.20	2.08
R	0.046	0.039	0.044	0.047
R_w	0.048	0.046	0.049	0.054
a, Å	3.9795(10)	7.2873(17)	7.3684(14)	7.3774(11)
b, Å	8.9447(14)	13.992(2)	14.0572(19)	14.1757(18)
c, Å	11.973(2)	10.872(4)	10.942(2)	10.942(2)
α, deg	90.0	90.0	90.0	90.0
β, deg	92.537(17)	92.45(2)	91.937(17)	91.732(15)
γ, deg	90.0	90.0	90.0	90.0
temp, K	293	293	293	293
mean d(CS), Å	1.768(4)	1.726(4)	1.727(5)	1.730(7)
mean d(SS), Å	2.0759(15)	2.050(5)	2.059(14)	2.045(8)
mean d(SN), Å	1.657(4)	1.622(5)	1.615(5)	1.622(10)
mean d(NC), Å	1.276(6)	1.286(14)	1.303(7)	1.290(19)
mean d(C5C5'), Å	1.383(7)	1.410(5)	1.405(7)	1.401(7)
mean ∠(SSN), °	97.05(13)	97.44(24)	97.505(275)	97.62(17)
mean ∠(SNC), °	116.0(3)	115.85(25)	116.1(4)	115.75(40)
mean ∠(NC4C5), °	123.6(3)	122.3(4)	121.7(5)	122.4(14)

compd.	**IV-6a**	**[IV-6a][Cl]**	**V-7**	**[V-7][$AlCl_4$]$_2$**
formula	$ClS_2F_5NC_8$	$Cl_2S_2F_5NC_8$	$C_6Cl_2N_2S_4$	$C_6Cl_{10}Al_2N_2S_4$
f.wt.	304.66	340.11	299.22	636.81
space group	$I\bar{4}2d$	$P2_1/n$	$P2_1/c$	$P\bar{1}$
Z	16	4	2	1
V, Å^3	4041.2(4)	1123.4(4)	473.11(14)	543.09(9)
d_{calc}, g·cm^{-3}	2.00	2.01	2.10	1.95
R	0.029	0.044	0.038	0.041
R_w	0.033	0.050	0.032	0.054
a, Å	13.8634(8)	12.334(2)	3.8496(10)	7.2015(6)
b, Å	13.8634(8)	6.0917(17)	7.9577(7)	7.2286(9)
c, Å	21.0268(4)	15.947(3)	15.5280(18)	11.2841(10)
α, deg	90.0	90.0	90.0	104.746(9)
β, deg	90.0	110.382(16)	95.963(14)	100.965(8)
γ, deg	90.0	90.0	90.0	99.638(8)
temp, K	293	293	293	293
mean d(CS), Å	1.724(2)	1.673(4)	1.737(2)	1.724(4)
mean d(SS), Å	2.0717(8)	2.0284(4)	2.0904(9)	2.0285(18)
mean d(SN), Å	1.639(2)	1.605(4)	1.638(2)	1.567(4)
mean d(NC), Å	1.317(3)	1.309(5)	1.306(3)	1.349(6)
mean dS(CC)Cl, Å	1.390(3)	1.393(2)	1.356(3)	1.349(6)
mean ∠(SSN), °	98.88	97.59	98.23(7)	101.12(16)
mean ∠(SNC), °	112.99	115.54	116.51(17)	116.0(3)
mean ∠(NC4C5), °	122.82	119.58	119.61(20)	117.0(4)

compd.	**[V-7]$_2$[GaCl$_4$]**	**V-10**	**[V-10][AlCl$_4$]$_2$**	**V-15a**
formula	$S_4Cl_4Ga_{0.5}N_2C_6$	$Se_2S_2N_2C_6Cl_2$	$Se_2S_2N_2C_6Cl_{10}Al_2$	$S_4N_2C_6H_2$
f.wt.	404.99	393.02	730.61	230.33
space group	*C*2/*c*	$P2_1/n$	$P2_1/c$	$P2_1/c$
Z	8	2	2	4
V, Å^3	2563.0(12)	471.7(4)	1082.8(3)	809.8(2)
d_{calc}, g·cm^{-3}	2.10	2.76	2.24	1.89
R	0.043	0.089	0.057	0.045
R_w	0.049	0.216	0.071	0.048
a, Å	8.6809(19)	7.478(4)	9.1189(13)	3.9033(8)
b, Å	14.606(3)	3.9733(17)	12.0258(19)	14.8321(18)
c, Å	20.496(6)	15.875(9)	9.8823(10)	14.068(2)
α, deg	90.0	90.0	90.0	90.0
β, deg	99.53(2)	90.33(4)	92.368(10)	95.835(14)
γ, deg	90.0	90.0	90.0	90.0
temp, K	293	293	293	293
mean *d*(CS), Å	1.728(5)	1.727(13)	1.702(14)	1.744(8)
mean *d*(SE), Å	2.0758(19)	2.248(4)	2.136(5)	2.096(5)
mean *d*(EN), Å	1.6195(40)	1.783(11)	1.735(11)	1.646(7)
mean *d*(NC), Å	1.3155(60)	1.300(16)	1.356(18)	1.305(6)
mean *d*S(CC)Cl, Å	1.3645(70)	1.346(19)	1.40(2)	n/a
mean *d*S(CC)S, Å	n/a	n/a	n/a	1.356(6)
mean ∠(SEN), °	98.77(21)	92.7(4)	97.6(4)	98.775(140)
mean ∠(ENC), °	116.3(4)	117.6(8)	113.0(10)	115.85(30)
mean ∠(NCC)S, °	119.05(45)	120.79(10)	119.9(12)	119.8(4)

compd.	**[V-15a][ClO$_4$]**	**[V-15a]$_3$[ClO$_4$]$_2$**		**[V-15a]$_{1.5}$[FSO$_3$]·H$_2$O**	
formula	$S_4N_2C_6H_2ClO_4$	$S_{12}N_6C_{18}H_6Cl_2O_8$		$S_7N_3C_9H_5FO_4$	
f.wt.	329.78	889.90		453.59	
space group	*Pcab*	$P2_1/n$		*C*2/*c*	
Z	8	4		8	
V, Å^3	2239.7(7)	3079.9(15)		3039.5(16)	
d_{calc}, g·cm^{-3}	1.96	1.92		1.94	
R	0.056	0.066		0.055	
R_w	0.059	0.096		0.072	
a, Å	11.8155(19)	12.618(2)		16.448(3)	
b, Å	13.456(3)	18.282(3)		18.322(2)	
c, Å	14.087(2)	13.564(6)		10.534(5)	
α, deg	90.0	90.0		90.0	
β, deg	90.0	100.16(2)		106.77(2)	
γ, deg	90.0	90.0		90.0	
temp, K	293	293		293	
formal charge	**[V-15a]$^+$**	**V-15a**	**[V-15a]$^+$**	**V-15a**	**[V-15a]$^+$**
mean d(CS), Å	1.710(5)	1.731(13)	1.72(3)	1.735(6)	1.719(15)
mean d(SS), Å	2.060(15)	2.108(17)	2.066(18)	2.108(2)	2.071(15)
mean d(SN), Å	1.605(5)	1.648(11)	1.62(4)	1.640(5)	1.599(16)
mean dS(NC), Å	1.311(13)	1.302(12)	1.32(2)	1.308(8)	1.322(12)
mean dS(CC)S, Å	1.379(8)	1.3849(12)	1.38(3)	1.372(12)	1.390(8)
mean ∠(SSN), °	98.9(2)	97.8(4)	98.6(4)	98.4(4)	97.8(2)
mean ∠(SNC), °	116.5(4)	116.55(70)	116.9(12)	117.5(4)	116.9(4)
mean ∠(NCC)S, °	118.3(5)	119.45(80)	118.2(1.8)	117.6(6)	119.1(5)

compd.	**[VI-6][SbF_6]**
formula	$C_5HClF_6N_3S_4Sb$
f.wt.	502.53
space group	$P\bar{1}$
Z	2
V, Å^3	696.36(9)
d_{calc}, g·cm^{-3}	2.397
R	0.0355
R_w	0.0972
a, Å	7.7963(6)
b, Å	8.4268(7)
c, Å	11.9330(9)
α, deg	92.806(5)
β, deg	103.646(4)
γ, deg	112.317(4)
temp, K	293
mean d(CS), Å	1.6965(50)
mean d(SS), Å	2.0705(50)
mean d(SN), Å	1.6345(50)
mean dS(NC), Å	1.302(6)
mean dCl(CC), Å	1.3815(60)
mean ∠(SSN), °	97.855(17)
mean ∠(SNC), °	115.45(40)
mean ∠(NCC)S, °	120.2(4)

Appendix C. List of Abbreviations

3-21G	a split valence basis set
6-31G	a split valence basis set
6-31G**	a split valence plus polarization basis set
6-31G++G*	a split valence plus polarization plus diffuse function basis set
a	crystallographic lattice repeat along *x* axis
A	acceptor
Å	Angstrom
AcOH	ethanol
Anal.	analysis
b	broad (IR peak descriptor)
b	crystallographic lattice repeat along *y* axis
B3LYP	hybrid B3 including an HF exchange term and the LYP correlation functional
BLYP	Becke's gradient-corrected exchange functional with LYP correlation functional
bp	boiling point
BEDT-TTF	bis(ethylenedithio)tetrathiafulvalene
c	crystallographic lattice repeat along *z* axis
calcd.	calculated
CDW	charge density wave
CI	configuration interaction
cm^{-1}	reciprocal centimeters
CO	crystal orbital
CT	charge transfer

CV	cyclic voltammetry
d	doublet (NMR peak descriptor)
d	interatomic distance
D	donor
DBU	1,8-diazabicyclo(5.4.0)undec-7-ene
dec.	decomposition
deg	degrees
DFT	density functional theory
DMF	dimethylformamide
DMSO	dimethylsulfoxide
DOS	density of states
DT	dithiole
DTA	dithiazole
DTDA	dithiadiazole
e	electron; charge of an electron
E	sulfur or selenium
E	energy
EA	electron affinity
E_F	Fermi level
E_g	energy gap
EHMO	extended Hückel molecular orbital
EPR	electron paramagnetic resonance
ESD	estimated standard deviation
ESR	electron spin resonance (also EPR)

Et	ethyl
ET	bis(ethylenedithio)tetrathiafulvalene
eV	electron volt
FMO	frontier molecular orbital
FT	fourier transform
g	gram
GTO	Gaussian-type orbital
h	hour
h	Planck's constant
Hex	*n*-hexyl
HF	Hartee-Fock
HOMO	highest occupied molecular orbital
Hz	Hertz
IP	ionization potential
IR	infrared
J_{AB}	first order ^{1}H NMR coupling constant
k	Boltzmann constant
k	reciprocal space number
K	Kelvin
kcal	kilocalorie
L	litre
LANL2DZ	an effective core potential plus valence double zeta basis set for heavier elements
LUMO	lowest unoccupied molecular orbital
LYP	Lee, Yang, Parr gradient-corrected correlation functional

m	minute; medium (IR peak descriptor); multiplet (NMR peak descriptor)
m	mass
Mbar	millibar
MCD	magnetic circular dichroism
MCPBA	*m*-chloro-peroxybenzoic acid
Me	methyl
m/e	mass to charge ratio
mL	millilitre
mmol	millimole
MNDO	modified neglect of differential overlap
MO	molecular orbital
mol	mole
mp	melting point
MP	Møller-Plesset
MS	mass spectrometry
n	number of charge carriers
NBS	*N*-bromosuccinimide
nm	nanometer
NMP	*N*-methylphenazinium
NMR	nuclear magnetic resonance
NRC	neutral radical conductor
ORTEP	Oak Ridge thermal ellipsoid parameter
Ph	phenyl group
ppm	part per million

R	general substituent group
RT	room temperature
s	strong (IR peak descriptor); singlet (NMR peak descriptor)
S	Siemen ($1S = 1\ \Omega^{-1}$)
SCE	saturated calomel electrode
SCF	self-consistent field
SN	sulfur and nitrogen
$(SN)_x$	polythiazene
SOMO	singly occupied molecular orbital
STO	Slater-type orbital
STO-3G	a basis set using 3 GTOs to approximate an STO
STP	standard temperature and pressure
t	triplet (NMR peak descriptor)
T	temperature; trimethylsilyl group in chemical formulae
TCNE	tetracyanoethylene
TCNEO	tetracyanoethylene oxide
TCNQ	tetracyano-*p*-diquinomethane
THF	tetrahydrofuran
T_{MI}	metal to insulator transition temperature
TMPD	*N,N,N′,N′*-tetramethyl-*p*-phenylenediamine
Torr	unit of pressure = mmHg = 133.32 Pa
TREPR	time resolved EPR
TTF	1,1',3,3'-tetrathiafulvalene
V	volt

VOIP	valence orbital ionization potential
vs	very strong (IR peak descriptor)
vw	very weak (IR peak descriptor)
VWN3	Vosko, Wilk, Nusair local correlation functional
w	weak (IR peak descriptor)
X	halogen group
x	crystallographic axis
y	crystallographic axis
z	crystallographic axis
°	degree
α	crystallographic axis angle; coulombic parameter
β	crystallographic axis angle; resonance integral
γ	crystallographic axis angle
δ	chemical shift in ppm
μ	charge carrier mobility
μA	microamperes
ν	frequency
ρ	electrical resistivity
σ	electric conductivity; orbital type
ϕ	one electron atomic orbital wavefunction symbol
ψ	one electron molecular orbital wavefunction symbol
Ψ	many electron state wavefunction symbol
Ω	Ohm